THE UNIVERSITY
of EDINBURGH

THE UNIVERSITY *of* EDINBURGH

The role of misfolded prion protein in neurodegeneration

James Alibhai

2014

Doctor of Philosophy (PhD)

The University of Edinburgh

Abstract

Chronic neurodegenerative diseases, such as Alzheimer's disease, prion diseases and many others are unified by the aberrant folding of a host encoded protein to a disease-associated isoform and the predictable cell-to-cell spread of disease-associated misfolded proteins via a putative prion-like mechanism. Prion diseases, for example, are associated with the aberrant folding of host encoded prion protein (PrP^{C}) to a disease-associated isoform, which acts as a seed for the further conversion of PrP^{C} to misfolded protein species.

The role of misfolded prion protein in neurodegeneration remains unclear. Accumulation and spread of misfolded prion protein is typically slow and progressive, correlating with neurodegeneration. A number of studies show that mice are susceptible to prion disease with characteristic hallmarks of prion pathology but in the presence of little detectable misfolded prion protein (e.g. the GSS/101LL model). In this thesis I test the hypothesis that detectable species of misfolded prion protein correlate with neurodegeneration and spreads in a predictable, progressive fashion from one anatomically distinct brain region to the next.

Using the GSS/101LL model, misfolded prion protein was detected as mostly PK-sensitive isoforms (PrP^{sen}). The progression and pathological presentation is comparable to other prion diseases with larger quantities of PK resistant prion isoforms. A highly sensitive *in vitro* assay system (the QuIC assay) was subsequently used to establish the extent that misfolded protein was present within the brain.

Amyloidogenic prion seeds were found to be widespread throughout the brain from an early stage and spread rapidly throughout the brain. Absence of neurodegeneration in certain brain regions is not due to differing quantities of prion seeds between regions or time exposed to prion seeds, as unaffected regions are exposed to comparative quantities of prion seeds for the same time-period as regions of the brain which eventually succumb to neurodegeneration.

These results indicate a clear dissociation between prion seeds and neurotoxicity. They highlight the need to understand regional host responses to prion seeds that may evoke neurodegeneration in some but resilience in others. To test this, transcriptomic analysis was carried out on brain samples from regions undergoing neurodegeneration and unaffected regions. A gene profile signature of hybrid pro- and anti-inflammatory response was observed in regions undergoing neurodegeneration. However, large cohorts of genes were down-regulated across all regions tested, including pro-inflammatory genes and a large proportion of genes involved within transcriptional and translational regulation and function. These results highlight the possible molecular pathways in response to the presence of misfolded protein.

In summary, misfolded prion protein accumulates rapidly across the CNS but only specific brain regions undergo neurodegeneration. In the presence of the misfolded protein, the host elicits a robust molecular response. The additional activation of glial cells within regions undergoing neurodegeneration highlights their importance in

disease. It is therefore proposed that misfolded prion protein, alone, is not sufficient to trigger neurodegeneration. This gives rise to a “multi-hit” hypothesis whereby two or more factors, for example the accumulation of misfolded protein and glial cell response, are required to trigger neurodegeneration.

Acknowledgements

In contrast to other PhD candidates whom write their acknowledgement page in their pants at stupid o'clock at night, eating hot dogs straight from the can whilst watching 'Apocalypse Now'…you know who you are…the time is 11:47am on Sunday 7th September, I am fully dressed and quickly realising just how many people I have to thank for helping me get to this stage!

I must thank Jean Manson and Hugh Perry for firstly giving me the opportunity to pursue a PhD but also for the invaluable supervision and encouragement you have both given throughout my studies. I hope you remain not only colleagues, but good friends for many years to come.

In addition, there are many people without whom; I wouldn't have even gotten close to completing this PhD – Pedro, Debbie, Dot, Aileen, Kayleigh, Boon Chin, Lita, Sandra, Barry, Chris, Sonya and so many more. A special thanks also goes out to Richard who has helped in every step of the way both in the lab but as a friend, to Claire as a good friend who also committed some late nights and early mornings to help in the lab with some quite queasy experiments to say the least, and to Abi for her strict regimented work ethic which has quite literally dragged me kicking and screaming through some of the low points of this PhD…but she has also made doing this PhD the best choice I have made in a lifetime.

Outside of the Neurobiology Division, there have been many and more people instrumental throughout my studies. Bob Fleming has exhaustively helped with all my imaging needs. Charis Hogg, the unsung hero of the 1st floor west wing. The staff at the CSU, the unsung heroes of the entire building. All the staff in the BRF, especially Kris, Becky, Sally and Simon. Gillian, Dawn and Sandra who have processed and cut much of the tissue which was used for pathological analysis in this study. The IT guys, particularly Laurie, Barry and Matt.

Thank you also to Byron Caughey for welcoming me into your lab and Andy Hamilton, Jason Wilham and Christina Orru for then allowing me to learn the QuIC assay. Also thank you to Tom Freeman for all the help you have given with the microarray analysis, particularly for your help with using BioLayout *Express*3D.

Final thanks go to the biggest contributors of all, my parents. You have brought me up through the tantrums and tears (I am sorry to admit both of which still persist today) to grow into a, sort of, respectable man. Also my brother, who even as an adult, I seem to be copying everything you do as a little brother should. I thank you for everything you have done and continue to do for me, and I therefore dedicate this thesis to all my family.

Author Declaration

I certify:

that the thesis has been composed by me, and either that the work is my own, or, where I have been a member of a research group, that I have made a substantial contribution to the work, such contribution being clearly indicated, and that the work has not been submitted for any other degree or professional qualification except as specified.

James Alibhai

Contents

Figure contents

Abbreviations

101LL – A transgenic mouse model with a Proline to Leucine alteration at codon 101 in murine *Prnp*

ACDP – Advisory Committee for Dangerous Pathogens

AD – Alzheimer's Disease

ALS – Amyotrophic Lateral Sclerosis

ATF – activating transcription factor

ATP – adenosine triphosphate

Aβ - Amyloid-Beta

BBB – blood brain barrier

BSA – Bovine Serum Albumin

BSE – Bovine Spongiform Encephalopathy

CC – Corpus Callosum

CDI – Conformation Dependent Immunoassay

CFCA – Cell-Free Conversion Assay

CJD – Creutzfeldt-Jakob Disease. Derivatives of this could be variant CJD (vCJD), sporadic CJD (sCJD), familial CJD (fCJD) or iatrogenic CJD (iCJD)

CNS – Central Nervous System

CSF – Cerebral spinal fluid

CWD – Chronic Wasting Disease

dH_2O – distilled water

dpi – days post inoculation

ER – Endoplasmic Reticulum

FFI – Fatal Familial Insomnia

GABA – gamma-aminobutyric acid

GFAP – Glial fibrillary acidic protein

Gi – Gigantocellular reticular nuclei

GM – grey matter

GO – Gene ontology

GPI – Glycosylphosphatidylinositol anchor

GSS – Gerstmann-Sträussler-Scheinker syndrome

GSS/101LL – 101LL mice inoculated with GSS infected tissue

Ham/Shp – Hamster and sheep chimeric recPrP

HD – Huntington's Disease

HG – Hazard group. Refers to containment levels according to ACDP guidelines. In this study HG2 and HG3 conditions are used

HO – Home Office

Iba1 – ionized calcium-binding adaptor molecule 1. Also known as allograft inflammatory factor 1 (AIF1)

i.c. – intracerebral inoculation

IHC – Immunohistochemistry

KO – Knock-out

LPS- lipopolysaccharide

LTP – Long Term Potentiation

MAP2 – microtubule-associated protein 2

MCL – Markov Clustering algorithm

miRNA – microRNA

mlf – medial longitudinal fasciculus

mRNA – messenger RNA

NB – Nuclear Body

NBH – Normal Brain Homogenate

NBH/101LL – 101LL mice inoculated with normal brain homogenate

NMR – Nuclear Magnetic Resonance Spectroscopy

PCA – Principal Component Analysis

PCR – Polymerase Chain Reaction

PD – Parkinson's Disease

PK – Proteinase K

PMCA – Protein Misfolding Cyclic Amplification

PMSF - phenylmethylsulfonyl fluoride

PNS – peripheral nervous system

Prnp – The prion protein gene

PrP* - A sub-population of disease-associated PrP^{Sc} which is theorised to be the infectious agent

$PrP^{-/-}$ - Prnp KO

PrP^{C} – Cellular prion protein (not associated with disease)

PrP^{D} – Disease associated conformation of prion protein (also referred to as PrP^{Sc})

PrP^{res} – Proteinase K resistant isoform of PrP^{D}

PrP^{sen} – Proteinase K sensitive isoform of PrP^{D}

PVDF - polyvinylidene difluroride

QuIC – Quaking Induced Conversion. Further developments include Real-Time QuIC (RT-QuIC) and Enhanced QuIC (eQuIC)

recPrP – Bacterially expressed recombinant Prion Protein

ROb – Raphe Obscurus

RSGc – Retrosplenial Granular Cortex

SNc – Substantia nigra, pars compacta

SNr – Substantia nigra, pars reticularis

ThT – Thioflavin-T

TSE – Transmissible Spongiform Encephalopathy

UPR – unfolded protein response

UV – Ultraviolet

VM thalamus – ventral-medial thalamus

WM – white matter

WT – Wild-type

1. Introduction

Chronic neurodegenerative diseases of the Central Nervous System (CNS) represent a range of heredity and sporadic conditions which are characterised by progressive degeneration of the nervous system. These include Alzheimer's disease (AD), Huntington's disease (HD), Parkinson's disease (PD), Amyotrophic Lateral Sclerosis (ALS), Transmissible Spongiform Encephalopathies (TSEs or prion diseases), and others.

The mechanisms of neurodegeneration within such diseases are unclear and few therapeutic targets have been identified to date. As a result, few therapies can treat these diseases, with those that are available offering only modest relief from symptoms with limited or no impact on disease progression. These diseases therefore represent a substantial socioeconomic burden.

Particularly well-studied are fatal degenerative disorders of the CNS associated with aberrantly folded, host encoded proteins. These encompass intracellularly misfolded proteins, for example; α-synuclein in PD [1] or extracellularly misfolded proteins, for example; amyloid-β (Aβ) in AD [2] or the prion in TSEs [3]. That such a clinically and etiologically diverse range of diseases are associated with aberrant protein folding suggests that impaired protein homeostasis is a likely factor within the mechanisms of neurodegeneration.

1.1. Prion Diseases

Amongst the range of neurodegenerative diseases, Transmissible Spongiform Encephalopathies (TSE), or prion diseases, represent a distinctly unique group. This is namely due to the infectious nature of the disease [3-5], which is hypothesised to be a result of the aberrantly-folded protein acting as a template for the further conversion of cellular prion protein (PrP^{c}) to a disease-associated conformation (PrP^{Sc} or PrP^{d}) [6].

Prion diseases typically present in four ways: (i) sporadic, (ii) familial, as a result of a mutation in the prion protein gene (*PRNP*), (iii) infection from a host to a recipient or (iv) iatrogenic infection from contaminated substances or instruments used in surgery.

1.1.1. Prion Diseases: Background & History

Human prion diseases include a sporadic form of Creutzfeldt-Jakob disease (sCJD) and its variant form (vCJD), familial forms Gerstmann-Sträussler-Scheinker syndrome (GSS) and Fatal Familial Insomnia (FFI) and Kuru. Animal prion diseases include scrapie in sheep, Bovine Spongiform Encephalopathy (BSE) in cattle, and Chronic Wasting Disease (CWD) in elk and deer, amongst others [7, 8]. Scrapie is the archetypal prion disease which has been endemic within the UK sheep flock for around 200 years. Scrapie was experimentally found to be transmissible to other sheep and rodents in the 1930s and 40s [9]. A remarkable instance of human to human transmission of a progressive disease with clinical symptoms of cerebellar

ataxia [10] was described shortly after in 1957 [11]. This disease, termed Kuru, was caused by ritual cannibalism practiced by people of the Fore Linguistic tribe, Papua New Guinea, and was quickly identified to share similarities with scrapie in epidemiology, clinical symptoms and pathological characteristics [12]. Kuru was subsequently demonstrated to be transmissible to non-human primates via a variety of routes [13, 14].

In the 1980/90s, UK agriculture suffered an epidemic of BSE, followed by the identification of a novel form of CJD, vCJD, in the UK in 1996. It was quickly established that vCJD was likely contracted by the consumption of BSE-infected food produce [15]. Between October 1996 and November 2013, there have been 177 reported cases of vCJD in the UK and a further 51 cases worldwide, spanning across 11 different countries (www.cjd.ed.ac.uk).

Efforts to comprehend the nature of the transmissible agent led to the understanding that these diseases are not caused by conventional infectious agents. The transmissible agents displayed unusual resistance to ionising radiation, heating and acetylethyleneimine exposure, suggesting the infectious entity may be devoid of nucleic acids [16]. Specific conserved properties of these diseases – for example, long incubation times, lack of immunogenicity and high heat inactivation curves, alongside continued scrapie transmissions, allowed researchers to categorise prion diseases into definable groups, termed ‘strains’ [17-20].

Later studies examining the infectivity of the transmissible agent used LD_{50} tests to evaluate the dilution at which 50% of recipients succumb to disease. The fact that the proteinaceous entity was partially protease resistant due to the protein conformational state [21] led to the isolation of the proposed transmissible agent, which was termed prion, for proteinaceous infectious particles [6, 22]. This was followed by the cloning of PrP cDNA, which identified the prion protein gene [23]. Subsequent structural analysis [24] and the identification that scrapie associated fibrils (later accepted to be PrP^{d}) and PrP^{c} are both encoded by the same gene, *Prnp* [25], led to the acknowledgement that the host cellular protein, PrP^{c}, is misfolded into a disease specific conformation, PrP^{d}.

More recently, the establishment of transgenic mice strengthened the link between PrP and disease. Prusiner *et al.* 1990 [26] demonstrated that introducing the prion gene from the Syrian Hamster into mice and subsequent inoculation of hamster scrapie, which is not normally transmissible to wild-type (WT) mice, resulted in disease. This study, amongst others [27], indicates that sequence homology of *Prnp* is fundamental for susceptibility to infectivity, neuropathology and incubation time. Furthermore, introducing amino acid alterations within the mouse prion gene can render mice susceptible to prion diseases to which they would otherwise be resistant [28, 29]. This indicates that specific changes in protein conformation can influence the capacity of disease-associated conversion of PrP^{c} to PrP^{d}. Knockout of *Prnp* in mice imposed resistance to prion infection [30, 31], reinforcing the necessity of PrP in disease.

1.1.2. Prion Diseases: Nomenclature

The prion protein, PrP, is commonly referred to as either the cellular prion protein (PrP^{c}) or an abnormal, infectious form of the protein, PrP^{Sc}. As described in further detail in *1.14. Prion Diseases: The Prion Protein*, PrP^{c} is a predominantly α-helical structure and in the context of this study refers to any conformation of PrP which is found in uninfected, healthy individuals.

The term prion describes a protein species which can act as an infectious entity, commonly designated PrP^{Sc}. However, PrP^{Sc} contains a number of differing protein conformations. For example, the conformational rearrangement of PrP^{c} to an abnormal isoform has been shown to produce PrP conformations which are partially protease resistant [21], termed PrP^{res}. Subsequent studies identified protease sensitive isoforms of abnormally folded PrP, PrP^{sen}, which retain their infectious properties [32, 33]. Alternate forms of PrP, such as cytoplasmic [34, 35] and transmembrane PrP [36] have also been linked with disease. Whether PrP^{Sc} or a subset of conformations is responsible for neurodegeneration is unknown. As discussed in *1.4.1. The role of PrP in neurodegeneration*, conflicting studies argue the toxic role of oligomeric, protofibril and fibrillar forms of misfolded PrP. It is unclear how such protein aggregates fit within the definition of PrP^{Sc} and therefore the term PrP^{Sc} may not be suitable when discussing potential toxic isoforms of PrP. To circumvent this, any detectable conformations of PrP within a known, prion-infected individual will be termed disease-associated PrP, or PrP^{d}, in this study.

Recent studies have developed *in vitro* techniques which measure conformational rearrangement of PrP^c substrate to abnormal conformations using PrP^d as a seed (see *1.1.5. Prion Diseases: Misfolding of PrP^c to PrP^d*). This effectively measures the capacity of a specific sample to misfold PrP^c, or act as a "prion seed". Whether the prion seeds detected using these assays represent the detection of all species of PrP^d present in a sample is unknown. However, previous publications have shown these assays can detect prion seeds to a far greater sensitivity compared to other techniques, such as immunohistochemistry (IHC) or Western blot analysis. Therefore, in this thesis, PrP^d is an operational term referring to detectable forms of misfolded prion protein using IHC or Western blot analysis. Conversely, a prion seed refers to the detection of misfolded prion protein which may or may not be detectable using IHC or Western blot analysis but is capable of generating fibrils from recombinant PrP (recPrP) which can be detected using Thioflavin-T (ThT).

1.1.3. Prion Diseases: The Infectious Agent

The prion hypothesis states that the infectious agent is composed solely or primarily of protein. This is supported by; (i) the fact that prion disease infectivity has been demonstrated to co-purify with abnormal PrP [37, 38], and (ii) the prion protein is essential for disease susceptibility. Despite strong evidence implicating an abnormal conformation of PrP as the infectious agent, there are some animal models of disease which question this hypothesis [28, 29, 39-41]. Furthermore, a component/isoform of PrP from misfolded prion protein fractions can be separated from infectivity using

differential detergent treatments [42-44]. One study demonstrated that nearly all detectable PrP was solubilised after detergent treatment of an infected brain homogenate; however the sediment still remained infectious [44]. The infectivity of some prion strains, demonstrated to inactivate (i.e. at the point LD_{50} cannot be measured) at relatively low temperatures, do not show any alterations in protease resistance of PrP^{d} upon exposure to inactivating levels of heat [45]. These data combined suggest, at the structural level, the majority of detectable abnormally-folded protein can be separated from infectivity, and thus is likely independent of infectivity. This has led to alternate theories regarding the infectious agent. Most prominently, it has been hypothesised that only a proportion of the total PrP^{d} is infectious, termed PrP* [46]. This has been built upon by others, who suggest that intermediate species in the conversion process from PrP^{c} to misfolded isoforms could represent the infectious entity [47]. Indeed, such a theory could go some way to explaining the results of previous experiments. For example, the denaturing conditions of high temperatures, demonstrated to diminish infectivity, could have a substantial impact upon the intermediate forms (or PrP*) of the prion conversion, but have little or no impact upon the β-sheet rich and highly stable fibril and amyloid aggregates of PrP. In accord with this, other studies have indicated that larger aggregates are likely not infectious [48-51], and, instead, oligomers could serve as more probable templates of prion conversion and infectivity [51, 52].

Despite the wide acceptance of the prion hypothesis, it is important to note this concept is not universally accepted. Primarily as a result of the huge diversity of identified strains occurring both naturally and experimentally, some investigators

suggest that the protein-only element of the prion hypothesis is inaccurate - instead, hypothesising that the infectious agent in prion diseases consists of two major constituents: the host encoded prion protein and an unidentified disease-specific genetic element [53, 54]. It is hypothesised that small viruses [55-58], or viroid's [59, 60] (non-coding, single-stranded RNA molecules lacking a protein shell) could constitute the proposed genetic element. A theoretical species, termed virino, has also been proposed, which consists of a genetic element wrapped in a coat of host-encoded proteins, such as PrP [61, 62]. Despite reports of identified disease-specific nucleic acids [63-69], there is little independently-replicated published data to suggest a nucleic acid component. For this reason, this document reflects the balance of literature implicating the prion hypothesis as the most likely explanation for the infectious nature of prion diseases.

1.1.4. Prion Diseases: The Prion Protein

The mammalian prion protein is an N-glycosylated, glycosylphosphatidylinsitol (GPI)-anchored protein (figure 1.1) typically found on the cell surface within detergent insoluble membranes, termed lipid rafts [70-73]. The 'normal' conformation of PrP^{c} has been characterised using recPrP expressed within prokaryotic cells and folded under specific acidic pH conditions. The atomic-level structures of a variety of prion proteins have been elucidated using Nuclear Magnetic Resonance (NMR) spectroscopy [74-80] and X-Ray Crystallography [81, 82]. The prion protein consists of an N-terminal flexible domain and a C-terminal globular domain. The N-terminal domain comprises 4-5 glycine-rich octapeptide repeats which have been shown to bind copper ions [83] and mediate the binding of

polyanionic compounds [84]. The N-terminal region is present in the majority of misfolded prion protein isolated from infected brains [85], however, is not essential for disease progression as mice lacking the N-terminal domain of PrP^c are susceptible to disease [86]. The C-terminal of prion protein is a structured, globular domain consisting primarily of α-helices, with two short β-sheet strands (figure 1.1). This domain contains a disulphide bond and two sites of glycosylation – the latter of which has been shown to be differentially glycosylated in prion infected brains [87, 88].

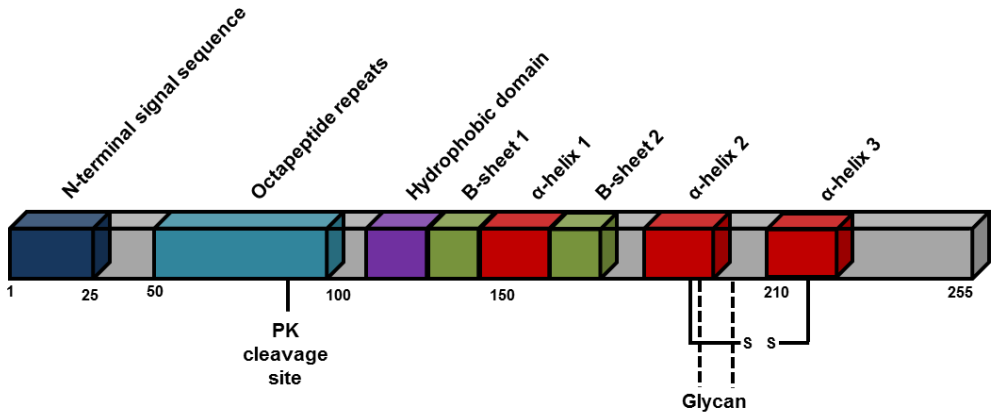

Figure 1.1 – Schematic diagram of prion protein indicating structural features of PrP^c as a function of primary sequence. All residue numbers are approximate.

Treatment of prion infected brain homogenates with proteinase K (PK) digestion results in the degradation of approximately 90 amino acid residues of the N-terminus. This is in contrast to PrP^c, which is completely degraded upon PK digestion. This resistance of disease related PrP is indicative of a significant alteration in

conformation of the prion protein and is a phenotype specific to prion-infected individuals. The fact that the C-terminus remains intact upon PK digestion suggests this region is involved in the misfolding process. Due to the insolubility of PrP^d, defining the tertiary structure has been challenging. Several low-resolution techniques suggest PrP^d is a β-sheet rich protein, with some retention of the original α-helix folding [89-92]. On the other hand, recent hydrogen/deuterium exchange studies indicate a lack of α-helices within PrP^d [93]. It is unclear whether such controversy within the literature is due to differences in PrP^d conformations being detected or due to a simple lack of atomic-level resolution. Ultimately, without high resolution descriptions of PrP^d it is challenging to define the prevalence of different PrP^d conformations in (i) different regions of the brain, and (ii) between different prion strains.

1.1.5. Prion Diseases: Misfolding of PrP^c to disease-associated isoforms

The underlying principle of the prion hypothesis is that misfolded prion protein can act as a template for the auto-catalytic conversion of PrP^c to disease-associated conformations. An important study to demonstrate this was performed by Caughey *et al.* [94]. By adding enriched preparations of PrP^d from prion-infected brain homogenates to recPrP *in vitro,* Caughey and colleagues were able to identify the formation of small quantities of PK-resistant aggregates as a result of cell free *in vitro* conversion. Thus, as a result of PrP^d exposure, the conformation of PrP^c misfolds to an abnormal entity. This technique is termed the Cell-Free Conversion Assay (CFCA), and has also been demonstrated to replicate specific phenotypes of disease. For example, hamster recPrP exhibits a relatively inefficient conversion rate

in the CFCA in comparison to murine recPrP in response to murine strains of scrapie, a phenotype generally observed *in vivo*. Conversely, murine recPrP was highly resistant to strains of hamster scrapie within the CFCA, again replicating *in vivo* findings [95] and in accord with earlier findings using a similar approach [96].

A development upon CFCA was the introduction of the Protein Misfolding Cyclic Amplification (PMCA) assay [97]. The PMCA assay differs from CFCA in two principle ways; (i) it uses uninfected brain homogenate as a source of PrP^{c} substrate rather than recPrP, and (ii) it uses sonication to drive conversion. Sonication theoretically breaks down larger aggregates of misfolded protein into smaller particles, providing additional surface area for further misfolding events. The detection of a conformational rearrangement of PrP^{c} to an abnormal species is thus determined by the gain of protease resistance of PrP. By sonicating and replenishing the PrP^{c} substrate, this approach allows for the use of extremely small quantities of misfolded prion protein as a 'seed' for the conversion process. This gave scope for a sensitive diagnostic test to be developed. It is important to note, however, that PMCA is also capable of generating *de novo* PrP^{res} in the absence of an initial misfolded prion protein seed [98, 99]. Similarly to 'seeded' PMCA reactions [100], the *de novo* generation of prions was also infectious. Such findings demonstrate that under specific conditions, the prion protein is capable of spontaneously misfolding to disease-associated conformations. Such a finding, however, questions the feasibility of using this approach as a potential diagnostic due to the inability to define differences between misfolded prion protein 'seeded' conversion and *de novo*

conversion. It is thought that the sporadic and spontaneous formation of *de novo* prions was the result of inconsistent physical conditions generated during sonication.

To avoid the use of sonication other laboratories have developed vigorous shaking methods to drive conversion. This method is known as the Quaking Induced Conversion (QuIC) assay [101]. Similar to CFCA, the QuIC assay uses purified recPrP as the PrP^{c} substrate. As a result, the reaction conditions of the QuIC assay are tightly controlled and consistent across larger numbers of samples, allowing the assay to be run on multi-well plates for higher throughput. The misfolding of recPrP was similarly detected by the appearance of PK resistant isoforms of PrP when the QuIC product was examined on a Western blot [101, 102]. As a result of the reaction conditions of the QuIC assay, the converted products are prone to form fibrils. This allows the QuIC assay to use a fluorescent compound, ThT, as a real-time detection method. ThT is a benzathiole dye which selectively binds to fibrils and exhibits a dramatic increase in fluorescence. As a result, this allowed the visualisation of fibrillar formation within the assay in real-time. This new protocol was thus termed Real-Time QuIC (RT-QuIC) [103, 104]. Figure 1.2 shows diagrammatic representation of the protein misfolding/aggregation in the QuIC assay, highlighting the tools used to detect the misfolded recPrP. Further developments have integrated an immunoprecipitation step using a PrP^{d}-specific antibody (15B3) to isolate PrP^{d} 'seeds' prior to addition to the recPrP substrate. This step was introduced due to an unknown inhibitory factor within blood which acted to prevent seeded conformational rearrangement of recPrP. This was termed enhanced-QuIC (eQuIC) [105].

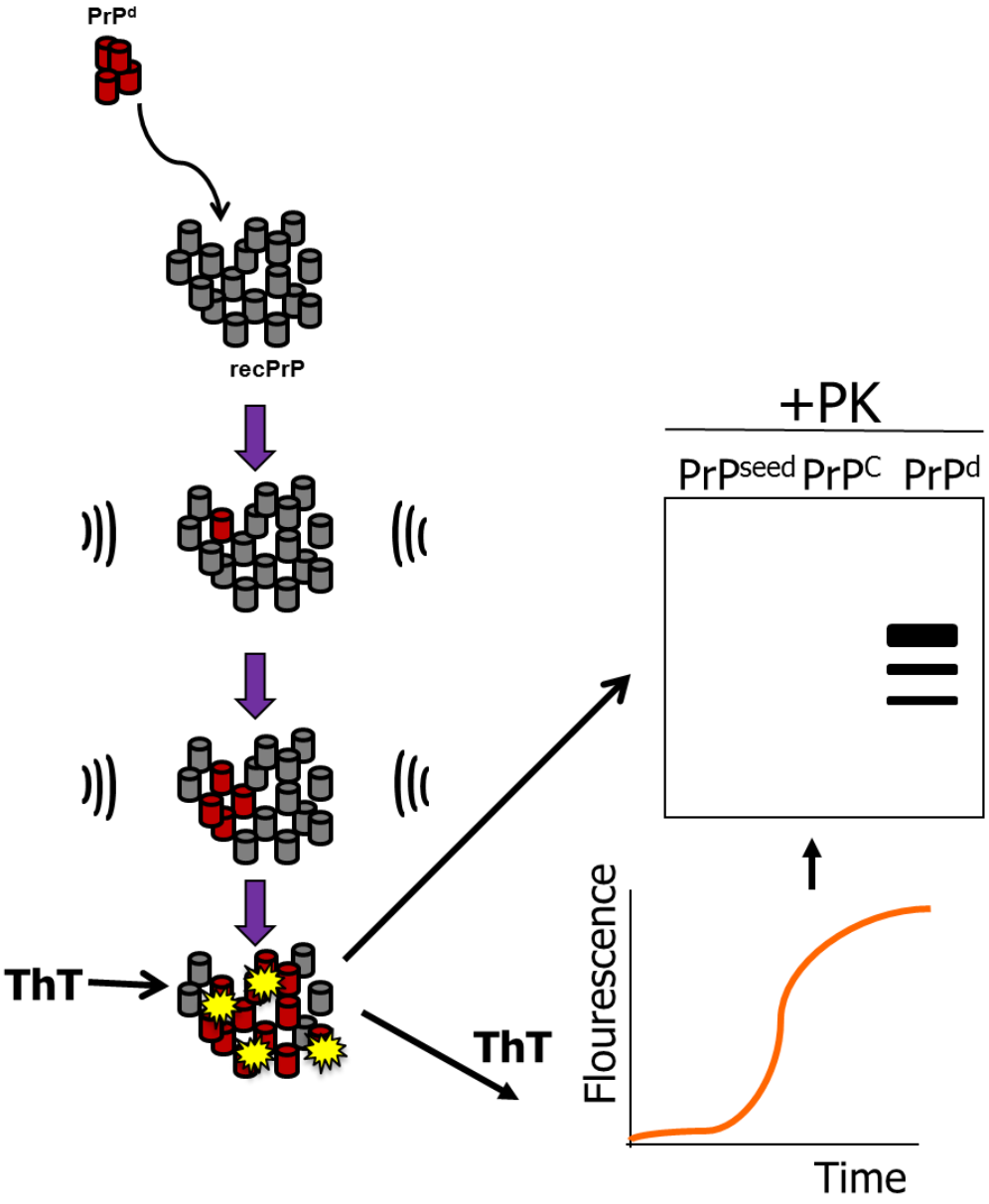

Figure 1.2 – RT-QuIC. Sample which may or may not contain misfolded prion protein is added to recPrP substrate. The reaction mixture undergoes cycles of intense shaking to break aggregates down followed by rest, whereby recPrP aggregates into fibrils which are detectable via ThT binding and fluorescence or by Western blot analysis using PK digestion to identify the altered conformation of recPrP.

The amino acid sequence and alterations within the *Prnp* gene have shed light on the regions of the protein critical for misfolding. Homology between PrP^c and PrP^d in the central region of the prion protein plays a critical role in determining whether a host is susceptible to disease [106, 107]. Similarly, there are a number of polymorphisms which confer resistance to prion disease, the archetypal example being the influence of *Prnp* polymorphisms on sheep scrapie [108-110]. In humans, a host of mutations in the *PRNP* gene are associated with onset of heredity prion diseases [111-117]. Post-translational processing of the prion protein may also play a significant role in protein folding. Three main areas of investigation are; (i) the disulphide bridge, (ii) glycosylation and (iii) the GPI-anchor. It was established that two cysteines in the C-terminal globular domain of the prion protein were oxidised (i.e. were in a disulphide bond) [118]. This bond confers a strong influence upon 'normal' protein folding and stability. It was thus suggested that, during the conversion process, the disulphide bond is reduced, which leads to higher flexibility of the protein and potential unfolding of the α-helical structure(s). Upon re-oxidation of the cysteines (re-forming the disulphide bond), the protein may take on a stable β-sheet-rich structure [119]. The mechanism enforcing reduction of the disulphide bond could be of critical importance when considering the mechanism of conversion. In contrast, other studies show that upon conversion from PrP^c to PrP^d, this bond is not broken down [120]. This highlights the need for further study to decipher the role of the disulphide bond in the conversion mechanism.

Glycosylation and the GPI-anchor of the prion protein have been extensively studied. Glycosylation of the prion protein occurs at two sites [121] (figure 1.1). The state of

glycosylation has been shown to significantly affect the binding interactions of PrP^c and PrP^d [122]. A number of laboratories have generated gene-targeted mice lacking the specific glycosylation sites *in vivo* [123, 124]. These studies demonstrated that glycosylation is essential for the efficient and correct trafficking of the prion protein, as knock out (KO) of glycosylation sites results in uncharacteristic incubation periods and pathological targeting of well-defined and robust prion strains. Further study of PrP glycosylation-deficient mice demonstrated that upon infection with different prion strains the efficacy of infection is markedly influenced by the degree of glycosylation of the host PrP^c [125]. It has been long established that the glycan structure binding the asparagine is highly variable in both PrP^c and PrP^d [126] and there is little understanding of the role that specific glycoforms could have within the mechanism of misfolding and progression of disease.

The role of the GPI-anchor within the mechanism of conversion has been studied by gene-targeted deletion of the GPI-anchor site. $GPI^{-/-}$ transgenic mice express the prion protein but it cannot tether to the cell membrane and is thus secreted from cells. When the $GPI^{-/-}$ mice are experimentally infected with a prion disease, large accumulations of extracellular amyloid plaques are observed in the absence of overt neurodegeneration [127]. This highlights the requirement of PrP^c expression on the cell surface for prion-associated neurodegeneration to occur. It is also important to note, however, these mice are also glycosylation deficient, therefore the results could, at least in part, be due to glycosylation deficiency.

A number of other non-prion protein determinants have also been identified that contribute to the conversion mechanism. One such study added polyanionic compounds (e.g. RNA) to purified PrP^{c} within the PMCA assay. Remarkably, in the absence of misfolded prion protein as a seed, *de novo* generation of PK-resistant PrP was observed. Moreover, when experimentally inoculated into mice, this *de novo* generated PrP^{res} initiated a prion-like disease [128-130]. A further study has demonstrated high levels of infectivity as a result of amplifying recPrP in the presence of synthetic lipids and RNA purified from murine liver [131]. Notably, this suggests that the prion protein is capable of misfolding provided the conditions meet the minimal molecular requirements – critically, without the need for a misfolded prion protein template. It may be that *in vivo*, the molecular requirements for conversion are not readily reached and misfolded prion protein can act to lower this requirement for conversion. Despite determining, *in vitro*, what specific species of co-factors are minimally required for conversion, the identities of such entities *in vivo* represents a far more challenging prospect. Of course, understanding the localisation of the prion protein, and thus, what potential co-factors the prion protein will come into contact with is important. Some preliminary studies to identify co-factors *in vivo* have identified that non-prion, proteinacious species co-purify with PrP^{d} aggregates [132, 133]. More specifically, one study identified the Na^{+}/K^{+}-ATPase protein as commonly co-purifying with scrapie associated fibrils extracted from infected murine scrapie brains and this appears to increase conversion efficiency in the CFCA [134].

1.1.6. Prion Diseases: Cell Biology of the Prion Protein

After expression of the prion protein and post-translational modifications are added, the prion protein migrates to the cell surface, where it resides for the majority of its lifetime on the cell surface. Here it is found enriched in detergent-insoluble membranous fractions, termed lipid rafts [70]. The prion protein then moves out of these rafts and undergoes endocytosis, primarily by clathrin-mediated endocytosis [135], but other methods of re-entry have also been proposed [136]. A large fraction of the internalised prion protein is thus degraded by proteolytic processing. The remainder is thought to recycle back to the cell surface [137]. It is hypothesised that the most likely sites of conversion take place on the cell surface or within membranous intracellular compartments, such as endosomes. There are a number of studies which support this hypothesis [134, 138-141]. Recent studies detecting the trafficking of PrP^{d} in neurons have shown similar cellular trafficking as identified with PrP^{c} [142]. Figure 1.3 shows the normal intracellular trafficking of PrP and the hypothetical misfolding pathways within the cell. The majority of these studies have taken place within *in vitro* cell cultures or primary neuronal cultures. In spite of yielding a good understanding of the cellular processing of the prion protein within *in vitro* cell and primary cultures of neurons, the cellular processing of the prion protein in other cell types or *in vivo* is unknown. Certainly, in different microenvironments, unique co-factors may interact with the prion protein, influencing the cellular processing/trafficking of the prion protein.

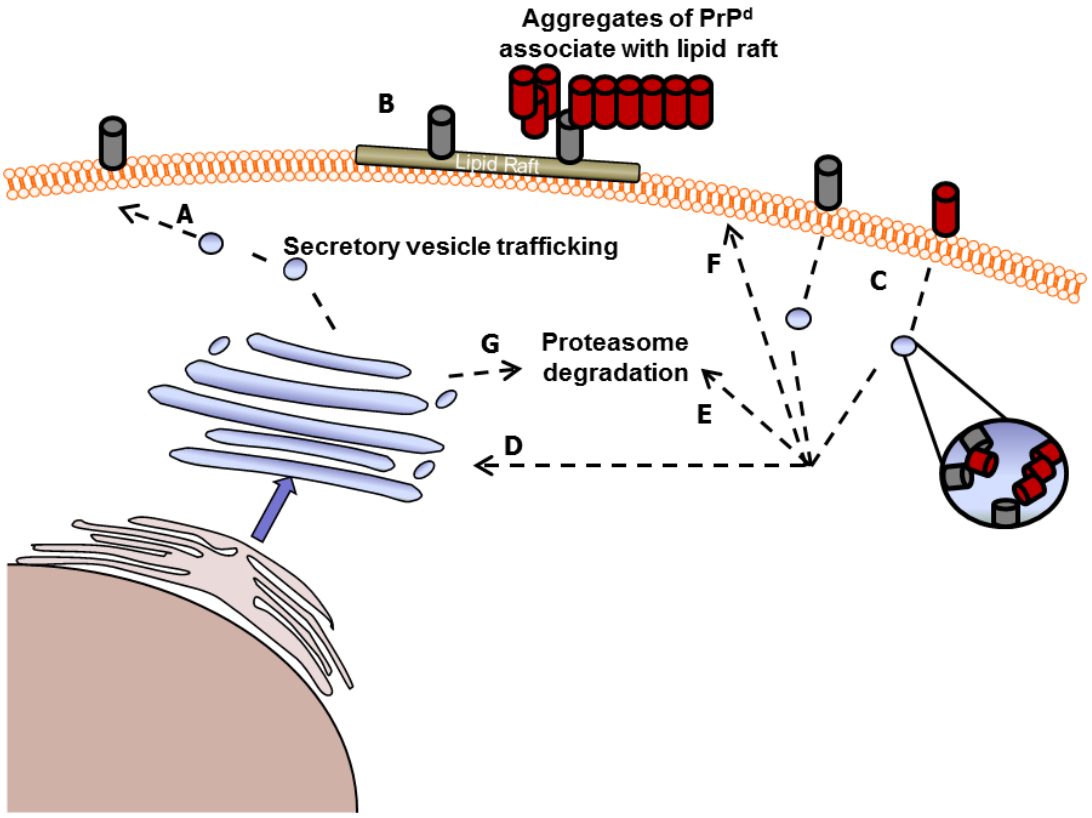

Figure 1.3 - Cell biology of the prion protein. After transiting the ER and Golgi apparatus, the protein is secreted to the cell surface (A), where it resides in lipid rafts for the majority of time (B). The protein leaves the lipid rafts to undergo endocytosis (C). Both the cell surface and the endosomal pathway are the major candidates for prion protein misfolding. PrP is then either trafficked to the Golgi (D) where it is then shown to be trafficked to lysosomes for degradation (G), or migrates directly to lysosomes to be degraded (E) or recycled back to the cell surface (F). Grey cylinders represent PrP^{c} whereas red cylinders represent PrP^{d}.

1.2. Other Chronic Neurodegenerative Diseases and the Prion Protein

Similar to the key role that the prion protein appears to play in prion diseases, misfolded proteins are associated with a number of different chronic neurodegenerative diseases, which migrate between one neuroanatomical distinct region to another [143, 144]. Traditionally, prion diseases have been considered to be distinct from these other diseases, primarily due to the infectious nature of the prion. Recent advances show there is an increasing understanding of 'prion-like' spread of non-prion, disease-associated proteins in other chronic neurodegenerative diseases

[145-155]. Although no epidemiological evidence exists for the inter-individual transmission of other non-prion diseases, this data highlights that cell-to-cell transmission in a prion-like mechanism is a fundamental phenomenon shared amongst many, if not all, chronic neurodegenerative diseases associated with a misfolded protein [156].

Despite the diverse structural and etiological nature of disease-associated proteins, there are some consistencies and overlap between such diseases. For example, as discussed previously, the prion protein appears to readily misfold to a disease-associated state both *de novo* and in the presence of a misfolded prion protein 'seed'. The wealth of conformations that are hypothesised to occur are thought to give rise to strains, a concept mostly foreign in other chronic neurodegenerative diseases. A recent study however has shown the distinct groups of tau lesions aggregating within *in vitro* cultured neurons. These subsequently were inoculated into mice and produced distinct pathologies which were consistent across multiple inoculations in mice. The tau then reforms its original pathology when returned *in vitro*, showing the characteristics of the tau was not altered [157]. This study subsequently showed *in vitro* neurons exposed to human tissue exhibiting characteristically distinct tau-lesions caused specific tau lesions in neurons, which were distinct between diseases [157]. Other studies have shown similar strain-like properties of non-prion misfolded proteins [158-162]. Some insights into the potential for strain establishment in other disease associated protein have also been hypothesised due to the structural diversity of detectable Aβ [163, 164] and α-synuclein [165] isoforms.

1.3. Prion Diseases as models for studying neurodegeneration

Prion diseases manifest as fatal neurodegenerative diseases in a range of animals and are most commonly associated with the formation and aggregation of PrP^{d}. The structure of PrP^{c} and the post-translational modifications which contribute to conformational alterations of PrP^{c} have been well characterised. However, due to the insolubility of PrP^{d}, its precise structure remains unknown and this compromises the ability to assess the role that PrP^{d} may play within the mechanism of neurodegeneration. Conversely, due to the infectious nature of prion diseases, experimental study of these diseases *in vivo* represents a significant advantage over other models of chronic neurodegeneration. For example, animals can be experimentally infected with a prion disease - this represents the 'start-point' of disease. Other neurodegenerative diseases typically rely on transgenic animal models which carry a human mutant form of the protein which is usually expressed at higher levels than the respective host gene. Furthermore the researcher cannot reliably elucidate the 'start-point' of disease since the transgene is expressed during development even in the prenatal period. In addition prion diseases are invariably fatal and exhibit predictable incubation periods of disease. Models of other neurodegenerative diseases usually only recapitulate limited components of human pathology, and often will not succumb to neuronal loss or death of the animal. As a result, the progression of pathology can be robustly and predictably dissected from start-point to death of the animal (see *1.4.3. Temporal pathological progression of prion disease*). This highlights the benefit of using prion diseases as models for studying the evolution of neuropathology associated with a misfolded protein.

1.4. Mechanisms underlying neurodegeneration

It is unclear what role misfolded PrP has within the mechanism of neurodegeneration. There are numerous avenues of study to elucidate this role. These include; (i) identifying what misfolded prion protein conformations are toxic to neurons, (ii) studying whether loss of PrP^c function, as a result of its conversion to a misfolded isoform, plays a role and (iii) whether the mechanistic conversion of PrP^c to misfolded prion protein compromises neuronal homeostasis.

1.4.1. The role of PrP in neurodegeneration

PrP^c has a critical role within prion disease since PrP^c deficient mice are resistant to prion disease [30, 31]. It is hypothesised that the conversion process of PrP^c to misfolded isoforms and the presence and accumulation of aggregates are essential for neuronal loss. However, it remains unclear whether misfolded prion protein is directly toxic to neurons; whether the conversion of PrP^c to misfolded isoforms compromises neuronal homeostasis or even if loss of PrP^c function contributes to the toxic events associated with prion diseases.

In order to answer whether PrP^d would act as a direct toxic entity, Brandner *et al.* grafted PrP^c-rich normal brain tissue into cerebral ventricles of mice which lacked the *Prnp* gene. Upon prion infection of these mice, the grafted tissue degenerated, however the host $PrP^{-/-}$ tissue remained unaffected. This was in spite of PrP^d being

detectable within the $PrP^{-/-}$ host tissue [166]. This demonstrated that, *in vivo*, PrP^{d} cannot act as a direct toxic entity to neurons in the absence of PrP^{c}.

Additionally, studies in GPI-anchorless mice show that when PrP cannot bind to the cell membrane the development of disease is substantially impacted. This indicates that PrP is required on the cell surface, or within intracellular membranous compartments, for prion-associated pathology to occur [127]. When GPI-anchorless PrP is overexpressed in mice, a spontaneous late-onset of neurodegeneration and eventual death of the animal is observed [167]. This suggests the PrP^{d} generated in this model did exhibit some level of toxicity but this was perhaps impacted by the lack of PrP^{c} on the cell surface and/or the inability of PrP^{d} to bind to the cell surface and migrate into the cell. This highlights the importance to understand the intracellular and intercellular trafficking and processing of PrP in disease.

Whether PrP^{d} is directly toxic to neurons in the presence of host expressed PrP^{c} is a critically unanswered question. This is a challenging concept to study but it would be assumed that PrP^{c} on the cell membrane and in the presence of PrP^{d} would result in the conformational rearrangement of PrP. This makes it impossible to discriminate between toxicity as a result of direct exposure of PrP^{d} and toxicity as a result of the mechanistic conversion of PrP^{c} to PrP^{d}. Certainly, the location of conversion will play a critical role in any potential toxicity, as aforementioned, PrP^{d} is not toxic to neurons in the extracellular space unless exposed at high levels [127, 167]. Nevertheless, a study which can implicate or refute either of these concepts as the

toxic entities would be a substantial advancement in our understanding of the role that misfolded protein plays within the mechanism of neurodegeneration.

In general, investigating toxicity of the misfolded protein has been challenging *in vivo* due to the diversity of PrP monomers and aggregates in prion infected animals. Many researchers use recPrP preparations which have been experimentally aggregated into oligomers, proto-fibrils and fibrils of differing sizes. A number of such studies have implicated small oligomeric protein species as highly neurotoxic within prion diseases and other neurodegenerative diseases [168-172]. As a result, there is a growing consensus that such oligomers disrupt cellular membranes, which result in a dysregulation of calcium levels within the cell [171-173]. How this occurs is unclear, however, some researchers suggest oligomers insert into the phospholipid bilayer of the cell membrane [174]. Alternatively, oligomers may form within the lipid bilayer [175]. As a consequence, the presence of oligomers in the membrane renders it relatively porous, thus affecting ionic homeostasis and consequently resulting in apoptosis of the cell.

In contrast, when determining the toxicity of fibril aggregations *in vitro* some studies indicate that fibrils are not toxic to cells [171], whereas others have determined fibrils to be equally toxic as oligomers [170]. Another study also exposed cells to fragmented Aβ fibril structures which possess a high level of toxicity to cells and cause hyperphosphorylation of Tau in mice [176]. It is generally considered that fibrils represent the ‘end-point’ of the misfolding or aggregation pathway [51, 169] –

whereby monomeric PrP^c is converted to PrP^d. This consequently forms dimers and oligomers which develop into proto-fibrils. Finally, these aggregations form fibrils and in some cases, large amyloid plaques.

Ultimately, there is an ongoing debate about the nature of the toxic proteinaceous species (reviewed by Haass and Selkoe [177]). As mentioned earlier, there are several studies demonstrating that levels of PrP^d and neuronal loss are poorly correlated [28, 29, 39-41]. Nevertheless the underlying foundation that expression of PrP^c is required for the pathological events associated with prion disease highlights the importance of PrP in neurodegeneration.

1.4.2. Possible links between loss of PrP^c function and neurodegeneration

The understanding that PrP^c is essential for pathogenesis and the current ambiguity regarding the role that misfolded prion protein has within neurodegeneration led to some theories that the loss of PrP^c function may be toxic. It is clear that the loss of PrP^c does not elicit the toxic effects observed within prion disease since mice lacking the prion protein gene develop normally [31, 178]. Subsequently, some subtle phenotypes were observed in these mice including abnormal morphology of mitochondria [179], defects in long term potentiation (LTP) [180, 181], an abnormal circadian rhythm [182] and age-related loss of myelin sheath surrounding peripheral neurons [183]. As a result, there are suggestions that the prion protein plays subtle roles in neuronal homeostasis and/or may exhibit some level of neuroprotection [184]. However, conditional knock-down of PrP^c in neurons during prion disease

progression appears to protect neurons and demonstrate a recovery [185, 186]. Further studies have proven mice with conditional *Prnp*$^{-/-}$ in neurons will eventually die of a prion disease, but only after a significantly extended incubation period (Manson, personal communication). In this latter study, although neurons appear to be protected from the degenerative effects of the disease, it appears the astrocytes accumulate PrP^{d} demonstrating a substantial shift in prion-pathology which eventually results in death of the mouse.

Earlier studies generated mice devoid of murine-PrP^{c} but which express hamster-PrP^{c} only in astrocytes. Upon prion infection with 263K hamster scrapie, these mice exhibited a highly infectious, invariably fatal disease [187]. These studies show that PrP^{c} expression is not required in neurons for disease to occur, and also show that astrocyte pathology may play a role in the disease process. This study also used mice which expressed hamster-PrP^{c} on astrocytes alongside endogenously expressed murine-PrP^{c}. Mice appeared to resist disease but accumulated PrP^{d}, which when inoculated into WT hamsters and mice was capable of producing a prion disease in hamsters but not mice, and therefore retained its prion strain characteristics [187]. Thus, the mice accumulate hamster PrP^{d} on murine astrocytes, but in the presence of murine-PrP^{c} the animal was protected, suggesting PrP^{c} acted as a protective entity. Indeed when considering how astrocytes interact with neurons within the tri-partite synapse and the fact that the synapse is amongst the earliest targets of pathogenesis (see *1.4.3. Temporal pathological progression of prion disease*) – it is unsurprising that astrocyte pathogenesis could have such severe effects in the absence of direct putative PrP^{d}-neuronal toxicity.

1.4.3. Temporal pathological progression of prion disease

An understanding of the pathophysiological progression of chronic neurodegenerative diseases is of critical importance for understanding how and why an abnormally folded protein may cause disease. In prion diseases, the pathological progression within the ME7 model of murine scrapie has been extensively characterised. Experimental infection of C57BL/6 mice with ME7 results in a consistent incubation period of approximately 24 weeks [188-193] (figure 1.4). The mice exhibit clinical symptoms of piloerection and urinary dysfunction – symptoms indicative of an autonomic nervous system failure. Mice also have a hunched posture with an abnormal gait – typically splayed hind legs. Autonomic neurons remain intact and appear 'unaffected' – despite numerous studies implicating this pathway as a probable route in the spread of infection from the periphery to the CNS [194-196]. Autonomic failure has been identified in a number of human prion diseases [197, 198], but such phenotypes have been attributed to thalamic degeneration of the CNS rather than direct pathology of the neurons of the autonomic nervous system [199, 200].

Neuronal loss in ME7/C57BL/6 animals is widespread across the CNS – including pyramidal neurons of the hippocampus. This is of significance as the hippocampus is central to cognitive function and loss of hippocampal neurons results in dementia, a key clinical feature in human prion diseases [201, 202]. The CA3 neurons of the hippocampus project axons along the Stratum Radiatum which synapse with

dendrites of CA1 neurons in this region - this is termed the Schaffer-Collateral pathway. Upon ME7 infection, synaptic deficits are observed early, typically identified by the loss of synaptic vesicle proteins, such as synaptophysin [189, 191, 192]. Electron microscopy of the Stratum Radiatum at this time-point shows loss of synaptic vesicle integrity and a darkening of the presynaptic element [192]. Such pathological phenotypes suggest significant functional impairments of the synapse at early stages in disease. Indeed, further studies identified deficits in LTP of synapses in this region [203], findings which also temporally correlate with behavioural abnormalities in mice [188, 189]. Morphological changes including swelling and hypertrophy in pre-synaptic boutons has also been reported [204] (figure 1.4). These investigations demonstrate that synaptic degeneration is an early target of prion-associated pathology. A schematic of behavioural and pathological (hippocampal) events occurring in the ME7/C57Bl/6 murine model of prion disease is shown in figure 1.4.

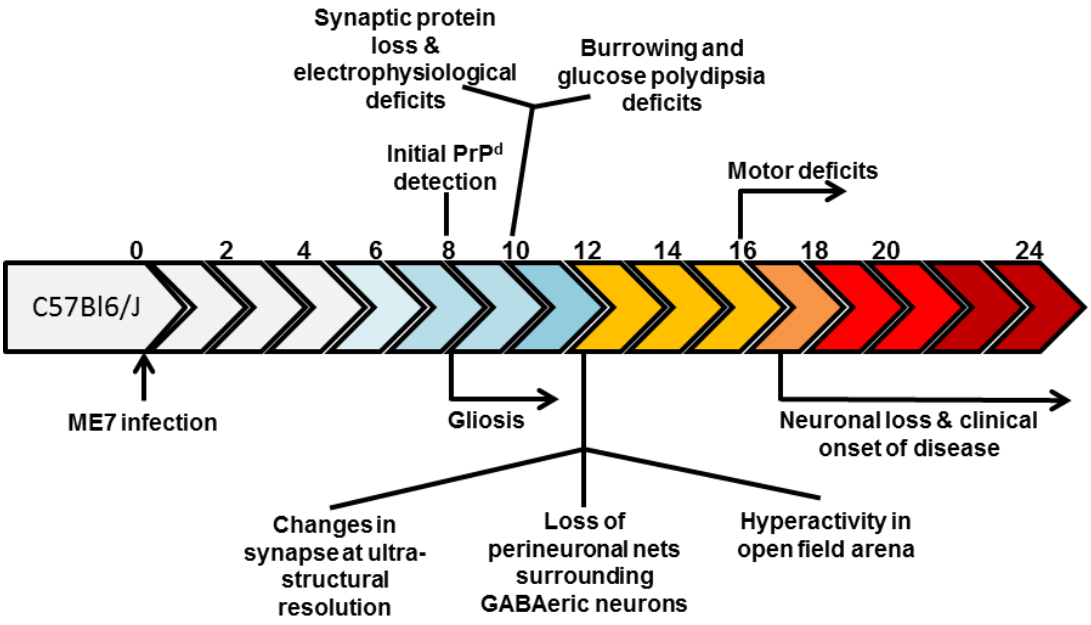

Figure 1.4 - Hippocampal pathology in the ME7/C57BL/6 murine model of prion disease. Total incubation period is around 24 weeks. Initial detectable deposits of PrPd are identified around 8 weeks of age which approximately coincides with the appearance of activated microglia and astrocytosis. Synaptic protein loss, electrophysiological deficits and hippocampal-dependent behavioural deficits are subsequently observed. Ultrastructure resolution images taken at EM then show morphological changes to the synapse. This coincides with a loss of perineuronal nets surrounding the GABAergic interneurons of the hippocampus and a hyperactivity behaviour observed in the open field test. Neuronal loss is observed substantially after synaptic degeneration in the CA1 pyramidal neurons. All data in this figure is obtained from [188, 189, 191, 192].

Synapses are also highlighted as a critical target of pathology and for therapeutic intervention in a range of diseases (reviewed in [205-208]). It is unknown how misfolded protein can cause/contribute to synaptic degeneration. Synapses are rich in PrP^c [209], however synaptic vesicles have been demonstrated to be almost completely devoid of PrP^c [210]. Based on our understanding that PrP^d is not directly toxic in the absence of PrP^c [166], it may be argued that PrP^d plays no direct toxic role on synaptic vesicles, which at early stages of disease are shown to undergo ultra-structural abnormalities and synaptic vesicle protein loss [189, 191, 192]. Instead, synaptic vesicles may be affected as a result of upstream deficits, for example endoplasmic reticulum (ER) stress or loss of neuronal/synaptic activity. Studies by

Sudhof and colleagues in a transgenic model of neurodegeneration, by KO of CSPα, an important synaptic vesicle co-chaperone, demonstrate that CSPα KO leads to decreased SNAP25 levels. SNARE-complex assembly is consequently disrupted which is correlated with the neurodegenerative phenotype in this model [211]. This demonstrates that loss of synaptic function may therefore lead to neurodegeneration. It has also been suggested that neurons with higher metabolic/functional activity could play a role in defining the severity of synaptic degeneration. However, a recent study using *Botulinum toxin* to silence synapses has indicated that loss of activity in synapses does not result in the loss of the synapse. Therefore, alterations in synaptic activity as a result of disease may not contribute to the loss of synapses during disease [212].

Using other models of murine prion disease, Mallucci *et al.* have indicated that synaptic degeneration can be halted when PrP^{c} is removed from the neuron during the progression of disease [186, 213]. This led to the amelioration of cognitive behavioural tasks, suggesting the mice somewhat adapt or even recover from the initial degenerative impacts of disease when PrP^{c} is knocked out of neurons during disease progression. As mentioned above, other studies have demonstrated in a number of murine prion strains, mice which exhibit a conditional KO of PrP will eventually succumb to disease (Manson, personal communication). Therefore synaptic degeneration may play a critical role in driving early pathology possibly leading to neurodegeneration, but animals are still vulnerable to disease even upon neuronal preservation.

The post-synaptic density of the dendrites of neurons also represents an important early target of disease. Numerous studies implicate dendritic spine loss/abnormalities as amongst the earliest morphological changes of affected neurons [214, 215]. It is also found at the electron microscopic level that the post-synaptic density curves around degenerating pre-synaptic elements [192]. What part of the synapse is targeted initially is an interesting debate and could deliver a vital understanding in the role of misfolded prion protein in synaptic degeneration. Previous conflicting studies have been performed in different regions of the brain in different prion models. The route of infection, the area of study and the dose of infection are all variable factors in these studies. One investigation assessed neurons in the cortex of mice and found the dendrites, and more specifically the post-synaptic densities are the initial targets of neuronal degeneration [215]. Similarly, it was also shown that dendritic spine loss was an early pathological alteration [214], however this study did not address the pre-synapse. Furthermore, functional abnormalities associated with deficits of the post-synaptic density have been implicated as early markers of disease [216]. In contrast, a number of studies assessing synapses of the Schaffer-Collateral pathway show presynaptic degeneration preceding post-synaptic deficits [186, 189, 191, 192, 217].

Studies by Booth *et al.* have generated whole genome transcriptional profiles from cell bodies of the CA1 pyramidal neurons of the hippocampus [218]. These neurons are eventually lost as a result of disease and are the origin of the dendritic spine

projections which form post-synaptic densities with the axons of CA3 neurons. Such an approach identified a number of previously unidentified mRNAs and miRNAs being up- or down-regulated as the result of disease. At the earliest stages of disease there was a striking down-regulation of genes associated with synaptic structure and function, which correlates with previous findings of a loss of synapse-associated proteins [189, 191]. A number of ryanodine receptors and genes associated with calcium binding were also down-regulated. This is a notable finding when comparing to *in vitro* studies which suggest oligomeric aggregates of prions could affect calcium regulation of cells and therefore impact upon neuronal homeostasis [171-175], such as activation of the endoplasmic reticulum (ER) stress pathways. Dysregulation of calcium signalling and/or the accumulation of misfolded proteins are capable of initiating the Unfolded Protein Response (UPR) which acts to restore ER homeostasis [219]. In the instance that ER homeostasis does not return, the cell up-regulates apoptotic pathways [220]. In prion diseases, it has been shown that ER stress-associated pathways may be induced [218, 221-227]. It is important to note that the specific ER stress pathways highlighted by Moreno *et al.*[225] do not show any observable alteration in gene expression profile in a number of microarray studies of prion diseases [218, 228-230]. Moreno *et al.* however demonstrate that inhibition of critical proteins in the pathways involved in translation [225, 226] or dephosphorylation [222] have been shown to ameliorate neurodegeneration. How the misfolded prion protein could cause such a phenotype is of significance for understanding the role that it plays in neurodegeneration. It is suggested that misfolded prion protein comes into contact with bip-proteins on the surface of the ER. This then initiates the protein kinase-like endoplasmic reticulum kinase (PERK)-

signalling pathway which eventually results in the repression of translation [225]. When considering the cellular biology of WT mice (see *1.1.6. Prion Diseases: the cell biology of the prion protein*), the prion protein is predominantly located either on the cell surface or within recycling endosomes. Therefore, it is unlikely that disease-associated misfolded proteins readily come into direct contact with bip-proteins on the surface of the ER. The cellular dysregulation of calcium as a result of oligomer attachment/formation on the cell surface represents a far more likely, upstream, role that misfolded protein has upon induction of ER stress. Moreno *et al.* have indicated that PrP^{d} interactions specifically with bip-proteins are activating only the PERK pathway; however there are certain caveats of this work that must be considered. Namely, the PERK pathway has been demonstrated to be activated as a result of Bip/Grp78 induction within mice overexpressing the prion protein by three-times the level of WT mice. It has been shown previously, mice overexpressing the prion protein exhibit an irregular distribution of the prion protein, including in the cytosol and mitochondria [210]. Therefore, prion infection in mice overexpressing PrP^{c} is likely to result in significant accumulations of misfolded prion protein in the cytosol, which perhaps does not represent the distribution of misfolded isoforms in WT animal or human prion diseases. Indeed it has been shown that the PERK pathway is not up-regulated in human prion disease patients [231]. In this study, mice showed subtle up-regulation of this pathway, but this does not appear to correlate with the severity of disease [231]. Activation of the PERK pathway is thus likely a contributing factor rather than integral driver of disease [231, 232]. Other studies have indicated the activation of phosphatases, such as calcineurin as drivers of pathological phenotypes associated with prion diseases [222]. For example,

dysregulation of calcium in cells leads to disruption of the calcium/calmodulin complex which in turn can lead to the hyperactivation of calcineurin [233]. Hyperactive calcineurin has been previously shown to reduce the phosphorylation of the apoptosis inducer BAD [234] which leads to the dissociation of BAD from the 14-3-3 protein scaffold and leads to the interaction of BAD with the Bcl-2 family of proteins in the mitochondria. Ultimately cytochrome C is released into the cytosol which leads to caspase pathway activation and apoptosis [234]. Hyperactivation of calcineurin also leads to the dephosphorylation of the transcription factor CREB, which is known to transcriptionally regulate a number of synaptic proteins, including synapsin-1 [235, 236], which are critically affected in prion diseases [189, 191, 218]. Inhibition of calcineurin within prion disease has been demonstrated to ameliorate disease phenotypes at the clinical stage of disease [222]. The effects of hyperactivation of calcineurin are insufficiently explored as this protein is known to regulate a number of critical cellular functions, such as; the ATF3 and NFAP transcription factors; calcium channels, such as Inositol 1,4,5-triphosphate and ryanodine receptors; and GABA and glutamate receptors. In addition, a relatively unexplored function of hyperactive calcineurin is the disinhibition of Protein Phosphatase 1 (PP1). PP1 is expressed throughout the CNS and plays a significant role in many CNS functions as a serine/threonine phosphatase. The hyperactivation of calcineurin therefore may play an important role in neurodegeneration. It is important to note, however, that further work is required as a number of CREB-regulated proteins are found up-regulated in a transcriptional array analysis on the CA1 neurons of the hippocampus discussed earlier [218]. This suggests other

processes may also be activated which combat the effects of calcineurin hyperactivation.

In addition to synaptic deficits/loss, a significant loss of perineuronal nets surrounding GABA-ergic interneurons of the hippocampus has also been identified at early stages of disease [237]. Furthermore, recent studies have temporally and spatially dissected different gross morphological, disease-associated changes in different neuronal populations in the brain [238]. These data suggest that distinct neuronal populations may undergo neurodegeneration in unique patterns – a result that may indicate different mechanisms of neurodegeneration in different regions of the brain. Thus, although synapses may represent a critical early target within prion disease, the pathological targeting is not restricted to the synapse.

A recent study on human prion patients demonstrated severe thalamic pathology in the absence of detectable PrP^{d} deposition in the thalamus. Instead, PrP^{d} was detected in the somatosensory cortex of these patients [239], which is well established to be connected to the degenerating thalamic neurons in these patients [240, 241]. A likely explanation is the PrP^{d}-targeting of neurons in the cortex resulted in pathology in both the cortex and in interconnected regions. The spatial and temporal distribution of PrP^{d} could therefore provide fundamental insights into the progression of disease.

In the ME7 model of murine scrapie, the distribution of PrP^d has been extensively mapped within the hippocampus. Initial detectable deposits of PrP^d accumulate within the hilus of the dentate gyrus and subsequently spread to encompass the CA3 pyramidal cell layer. This suggests the spread of PrP^d along the Mossy-Fibre pathway. As discussed earlier, the pre-synaptic components of the CA3 projections along the Schaffer-Collateral pathway degenerate, and this pathology correlates with the apparent spread of PrP^d to the CA1 region [188, 189, 191]. However, different prion disease models exhibit different spatial and temporal distributions of misfolded protein, and some models do not appear to correlate with misfolded prion protein. For example, in models which exhibit a highly infectious prion disease with vacuolation in the presence of little or no detectable PrP^d [28, 39, 41]. Within these models, only vacuolation pathology has been assessed to determine degeneration. Further studies will therefore be required to study the correlation of misfolded prion protein with neurodegenerative phenotypes, such as neuronal loss or synaptic protein loss. Additionally, time-course studies have not been performed to dissect out the earliest pathological events. This would be essential to establish whether the appearance and accumulation of misfolded prion protein does or does not correlate with neurodegeneration.

1.4.4. Astrocytes and prion disease

Astrocytes are an abundant glial cell type in the CNS and are crucial regulators of CNS development, function and health. Astrocytes are morphologically categorised into two forms; *protoplasmic* and *fibrous*. *Protoplasmic* astrocytes are typically localised to grey matter regions of the CNS and exhibit a small cell body and

numerous fine processes which make contact with synapses to form the tri-partite synapse [242] and have specific 'end-feet' structures abutting the cerebral endothelial cells forming part of the blood-brain barrier (BBB). *Fibrous* astrocytes on the other hand are predominantly found in white matter regions of the CNS and have long, thin fibre-like processes. It is unclear whether different morphological categories of astrocytes produce different functions.

As mentioned above, astrocytes have a role in a number of critical functions in the CNS, including CNS development, BBB formation and maintenance, synaptogenesis, neurotransmission and metabolic regulation (reviewed in [243-245]). Astrocytes are exquisitely sensitive to changes in homeostasis and injury to the CNS and undergo a complex response, morphologically characterised by hypertrophy of the cell body and shortening/thickening of processes [246, 247]. Glial Fibrillary Acidic Protein (GFAP), an intermediate filament protein, also exhibits significant up-regulation which mediates the substantial morphological changes observed in astrocytes [248]. Therefore GFAP is typically utilised as a marker of astrocyte responses to changes in CNS homeostasis/injury.

The specific stimuli driving astrocyte responses can range from degenerating axons and their dying terminals [249], BBB breakdown [250, 251], cytokines [252], changes in neuronal homeostasis [253-255], overexposure to purines, such as ATP [256], reactive oxygen species, such as Nitric Oxide [257], hypoxia and glucose deprivation [258] and misfolded proteins [259]. In prion diseases, astrogliosis is a

well-documented pathological response in humans [260, 261] and other animals [189, 262]; however what stimulates the astrocytic response, or how the astrocytic response impacts disease progression is unknown. During disease, it has been reported that PrP^d accumulates in the astrocyte [263] and therefore it could be argued that astrocyte dysfunction during disease could potentially contribute to or drive neurodegeneration as a result of loss of astrocytic function. Genetic KO of GFAP does not impact upon prion disease progression [264]. Whether GFAP plays an important role in reactive astrocytes is unknown, but further studies are required to address whether functional deficits of the astrocyte contribute to disease.

During prion disease, astrogliosis is observed prior to functional synaptic deficits and concurrently with the appearance of detectable PrP^d [189]. These observations indicate that astrocytes are more likely responding to the presence of misfolded protein than the functional deficits of synapses. More work is required, however, to establish the true relationship between astrocytes, PrP^d and neurodegeneration. Nevertheless, by mapping the response of the astrocyte, using GFAP as a marker, early events of pathology can be elucidated prior to the appearance of neurodegenerative features.

1.4.5. Microglia and prion disease

Microglial cells are the predominant resident macrophage of the CNS parenchyma. These cells are constantly monitoring their local microenvironment and can rapidly respond to neuronal signals and damage [265]. For example, one study created

highly focal cortical lesions using a laser and visualised microglia directing their processes towards the site of damage [266]. At a structural level, microglia have a highly plastic morphology. Within a 'healthy' CNS, microglia exhibit a ramified morphology, typically consisting of a small cell body with long thin processes. Upon exposure to CNS injury, foreign material and/or changes in CNS homeostasis the microglia undergo substantial structural and morphological alterations, typically exhibiting a hypertrophied cell body and short, thick processes.

Microglia have recently been implicated to have a role in synaptic phagocytosis [267, 268] and function [269-271]. Such studies have led to the proposition of a 'quad-partite synapse' with microglia constantly surveying the synaptic and astrocytic connections of the tri-partite synapse [272]. During neurodegenerative disease, however, the true role microglia play remains unknown. A review by Block *et al.* hypothesise that microglia could have a neurotoxic role in neurodegeneration [273]. This is thought to be due to a potential release of pro-inflammatory cytokines, reactive oxygen species, proteases and complement proteins. However, others suggest microglia could play a neuroprotective role [274]. Ultimately, whether a pro-(or anti-) inflammatory, response would act as a protective or toxic entity within chronic neurodegenerative diseases is unclear. Recent advances in our understanding of microglial function, notably with synapses, would indicate that changes in microglial function during disease could play a significant role.

During prion disease, a remarkable activated morphological response by microglia is observed. This morphological response does not appear to be solely associated with a pro-inflammatory response [275]. Instead, a concurrent anti-inflammatory response, driven by TGFβ-1 appears in the CNS as a result of ongoing pathology [275, 276]. Further studies exposed prion-infected mice peripherally with the bacterial endotoxin, lipopolysaccharide (LPS), at focal time-points to induce a systemic inflammatory event during the prion disease incubation. Following exposure to LPS, a rapid systemic pro-inflammatory response is observed, initially by increases in IL-1β [190, 277]. Further, systemic inflammation induced with bacterial (LPS) or viral (poly I:C) mimetics were demonstrated to impact upon the progression of disease [278, 279]. This data indicates that a switch in the innate immune response, which is likely driven primarily by microglial activation, may play a substantial role in disease. Recent studies have shown that the local proliferation of microglia in prion disease has a detrimental effect on disease severity as by reducing the numbers of microglia present in the CNS by inhibiting cellular proliferation the prion disease incubation period increases [280].

Whether microglia respond to PrP^d or neurodegeneration is unclear. Morphological microglial activation is observed prior to the earliest behavioural and neuropathological events, and concurrently with appearance of PrP^d. As a result, many studies use proteins that are solely expressed within microglia in the CNS, such as Allograft Inflammatory Factor 1 (AIF1 or Iba1), as markers of activated microglia and thus as markers of the initial pathological events within the CNS.

1.4.6. Spread of PrP^d via neuroanatomical connections

Spread of pathological lesions in neurodegenerative diseases is a precise and predictable process which appears in a pattern resembling neuronal connectivity [281]. In AD and PD, the spread and distribution of specific pathological lesions has been mapped extensively [143, 144]. It is well established that the infectious and toxic agent(s) of prion disease are capable of spreading via neurons. This was originally demonstrated using the extensive anatomical understanding of the visual pathway in mice. Around 90% of axons from retinal ganglion cells to the superior colliculus send projections to the contralateral hemisphere of the brain [282]. Prion-infected brain homogenate was injected into one eye of mice and both the propagation of infectivity and the pathological lesions were initially observed in the contralateral superior colliculus [283]. Microglial activation and an increased T-lymphocyte infiltration has further been described as the earliest pathology in the contralateral superior colliculus using the same approach [284]. This demonstrated that the infectious and toxic agent(s) of prion disease had spread specifically via the neuron. It has also been shown that PrP is capable of migrating throughout the CNS and PNS via fast axonal transport [285].

A number of studies have presented convincing evidence of a "prion-like" propagation mechanism associated with a number of different non-prion disease-associated proteins, such as Aβ [146, 286, 287], Tau [161, 288, 289], α-synuclein [290-292] and others [154, 293]. Minute quantities of misfolded Tau fibrils in one

study has been shown to be sufficient to induce the propagation of further misfolded Tau species, suggesting a self-perpetuating template-conversion mechanism [153]. *In vivo*, the injection of inoculums known to contain protein aggregates have demonstrated the spread of protein aggregates from the site of injection to neuro-anatomically connected regions of the brain [161, 286, 288, 290-292].

Defining the correlation of misfolded proteins with neurodegeneration and the mechanism of spread is therefore of critical importance for understanding the role that the misfolded protein may have within neurodegeneration.

1.5. Thesis aims and outline

The correlation between detectable misfolded prion protein and neurodegeneration remains unclear. For example, it is known that PrP^d species can accumulate without any observable neurodegeneration [40]. This highlights the need to understand the relationship between spread and distribution of misfolded prion protein, the mechanism by which this spread occurs and neurodegeneration. This study will use a highly infectious animal model of prion disease, GSS/101LL, which has been previously demonstrated to accumulate extremely small quantities of detectable PrP^d [28, 41]. Whether the detectable PrP^d in this model is solely the required entity for neurodegeneration to occur is therefore important to answer. The aim of this thesis is to test the correlation between the small quantities of PrP^d detected in GSS/101LL animals and neurodegeneration. If the correlation is upheld, further studies will aim to understand the mechanism that PrP^d utilises to migrate between specific regions of

the CNS and how such mechanism relate to neurodegeneration. Demonstration that PrP^{d} and neurodegeneration do not correlate however, draws a question mark over current detection methods for the toxic agent within prion diseases.

The content of this thesis will be split into four results chapters (chapters 3, 4, 5 and 6). Chapter 3 tests a number of pathological phenotypes in GSS/101LL mice at clinical onset of disease to evaluate whether such observations correlate with the detection of PrP^{d}. The major finding in this chapter was the detection of larger quantities of PrP^{d} comparative to previous publications using this model. The predominant species of PrP^{d} detected were mostly sensitive to proteinase K digestion (PrP^{sen}), as determined by Western blot analysis and correlate with neurodegeneration. Other PrP^{d} isoforms were also detected, such as PrP^{res}, but these did not correlate with neurodegeneration.

Chapter 4 thus uses a time-course study to further test the correlation of IHC detectable PrP^{d} and neurodegeneration and the temporal and spatial spread of PrP^{d} between one neuroanatomical distinct region to another. PrP^{d} is initially detected associated with specific neurons of the midbrain, such as the interpeduncular nuclei and substantia nigra, pars compacta. This is followed by microglial activation and astrocytosis. Spread of PrP^{d} is observed correlating with pathological spread in a fashion resembling anatomical connections in a selective manner.

Chapter 5 uses the QuIC assay to detect the presence of prion seeds within GSS/101LL brain regions. A widespread distribution of prion seeds was observed in both regions undergoing neurodegeneration and regions which appear pathologically "unaffected". This data represents a critical dissociation between IHC detectable PrP^d, prion seeds and neurodegeneration. Therefore it is predicted that understanding the host response to prion seeds will elucidate how some regions of the brain remain resilient to neurodegeneration whilst others are susceptible.

Chapter 6 uses microarray as a tool to characterise the host transcription profile of regions undergoing neurodegeneration and regions which appear unaffected. A mixed pro- and anti-inflammatory response is found to predominate in regions undergoing neurodegeneration. Stress responses were observed across all regions of the brain tested, suggesting prion seeds are potentially detrimental, however this response was not sufficient to trigger neurodegeneration. An additional group of genes, predicated to be microglial-specific, were observed down-regulated across all regions of the brain.

Chapter 7 discusses the correlation of misfolded prion protein and neurodegeneration and the paradoxical lack of correlation between prion seeds, PrP^d and neurodegeneration. Finally, based on the host response to prion seeds across all brain regions tested and the specific innate immune response restricted to regions of neurodegeneration, a "multi-hit" hypothesis will be proposed, whereby prion seeds, alone, are not sufficient to trigger neurodegeneration, instead two or more factors

(e.g. prion seeds and microglial activation) may be required to trigger neurodegeneration.

2. Materials & Methods

2.1. Ethics statement

All experiments were approved by the Roslin Institute Ethical Review committee and in accordance with the United Kingdom Home Office Regulations [Animals (Scientific Procedures) Act of 1986]. Ethical consent for the use of human materials for research was obtained and approved by the Lothian National Health Service Board Research Ethics Committee (reference: 2000/4/157).

2.2. Animal husbandry

The "101LL" transgenic mouse line contains an amino acid alteration from Proline to Leucine at codon 101 of the 129/Ola (129/OlaHsd, Harlan, UK) murine prion gene by gene-targeting [28]. 129/Ola mice homozygous for the targeted allele were crossed and bred over multiple generations to generate progeny homozygous for the *Prnp*^{L101L} (101LL) allele which can be used for experimental purposes. All mice were bred at the Roslin Institute in derogated containment level 3 (CL3) conditions, according to Advisory Committee to Dangerous Pathogens (ACDP) guidelines and under a temperature controlled, 12 hour light/12 hour dark cycle. Mice were housed with wood-chip bedding and a wood chew stick for environmental enrichment. Food and water were available *ad libitum*.

All experiments henceforth are performed under derogated CL3 conditions according to ACDP guidelines, with exception of work not using animal material or using ME7/C57BL/6, 87V/VM or 263K in Syrian hamsters, which are performed at containment level 2 (CL2) according to ACDP guidelines.

2.3. 101LL genotyping

2.3.1. DNA extraction

To confirm the presence of the targeted allele alteration, mice were genotyped before and after studies. Prior to inoculation of animals, DNA extraction was performed using DNeasy Blood and Tissue kit (Qiagen) on ear clips. After the study, DNA extraction was performed by lysing tail tissue (10mM Tris-HCl pH 7.6, 10mM EDTA, 0.5% sarcosyl, 10mM NaCl and 100µg/mL PK) overnight at 37°C. Phenol was then added, followed by chloroform (1:1) and DNA was precipitated with isopropanol and pellet resuspended in nuclease-free water at 4°C until use.

2.3.2. PCR analysis

Presence of the 101LL mutation was determined by PCR analysis using primers specific for positions 107-130 and 871-848 of the prion protein gene; the 5' primer used was (5'-ATGGCGAACCTTGGCTACTGGCTG–3'; DDBJ/EMBL/GenBank accession number M18070) and the 3' primer used was (5'–TCATCCCACGATCAGGAAGATGAG–3'; DDBJ/EMBL/GenBank accession

number M18070). PCR was set up using a Type-it mutation detection kit (Qiagen) with 2µL extracted DNA added to the provided master-mix. PCR cycle conditions were: 94°C for 3 minutes, followed by 30 cycles of 94ºC for 30 seconds, 62ºC for 30 seconds, 72ºC for 1 minute. A final extension phase of 72ºC for 10 minutes was performed and samples were subsequently stored at 4ºC. The induced alteration of proline to leucine in 101LL mice forms a DdeI restriction enzyme cut site, which allows for identification of 101LL homozygous mice. The PCR product was incubated for 3 hours at 37°C with DdeI restriction enzyme (Promega) before being run on a 1.5% agarose gel (Invitrogen) for 1 hour 30 minutes at 125V prior to imaging.

2.4. Prion disease inoculum and challenge

Human frontal cortex brain material (Tissue ID: RU13/2006), which was pathologically identified as positive GSS carrying the *PRNP*^{L102L} mutation, was obtained from the CJD Brain and Tissue Bank (Edinburgh Brain and Tissue Banks). The GSS brain tissue was obtained from a snap frozen half brain, therefore it is not possible to define the precise region of the frontal cortex that was dissected. However, in clinical cases of GSS, the cortex suffers from a heavy burden of misfolded prion protein, in the form of diffuse and amyloid plaque staining [294]. The tissue was homogenised in 0.9% sterile saline (Martindale Pharmaceuticals) to a 10% (w/v) homogenate, aliquots made and stored at -80°C until used. The homogenate was checked for sterility prior to inoculation by spreading an aliquot of the homogenate on blood agar cultures and incubating both at aerobic and anaerobic conditions at 37°C for 7 days. No visible growth was observed confirming the

sterility of the tissue for inoculation. The 10% GSS brain homogenate was then further diluted 1:10 in 0.9% sterile saline and 101LL mice were injected intracerebrally (i.c.) into the right hemisphere with 20µL of 1% homogenate under anaesthesia. Animals were monitored and any that did not recover were culled (Home Office Schedule 1) and excluded from experimental analysis. Due to the difficulty in obtaining uninfected human tissue as a negative control, an i.c. injection of 20µL uninfected hamster normal brain homogenate (NBH) (1% w/v in saline) was performed instead. These form the GSS/101LL and NBH/101LL groups respectively, which hereafter will be referred to throughout the text. All animals were aged-matched and were injected between 10-14 weeks of age.

2.4.1. TSE clinical scoring

All animals were assessed daily from approximately 100 days post inoculation (dpi) by an independent researcher to this study using parameters that have been previously described [295]. At latter stages of the disease incubation period, mice were found to exhibit clinical symptoms of ataxia and symptoms typical of an autonomic failure, such as piloerection and weak bladder control. Other causes of death were defined as intercurrent and therefore animals were excluded from the study. A time-course analysis was set up in this study, ranging from 150dpi (n=24), 200dpi (n=24), 220dpi (n=12), 240dpi (n=12) and upon clinical symptoms of disease (n=24) (figure 4.1). The groups of animals at each time-point were halved, and 12 (or 6 for groups of 12) 101LL animals were inoculated with 1% GSS inoculum and 12 (or 6 for groups of 12) 101LL animals were inoculated with 1% NBH inoculum. All

mice were killed by CO_2 asphyxiation according to Schedule 1 of the [Animals (Scientific Procedures) Act of 1968].

2.5. Preparation of brain tissue for pathological analysis

The brains of 101LL mice were removed and halved along the midline between the right and left brain hemispheres. The left hemisphere was flash frozen in liquid nitrogen and stored at -80°C for later use. The right hemisphere, which contains the injection site, was immersion fixed in 10% formaline saline for 48 hours, before being exposed to 98% formic acid for 90 minutes to minimise the infectious titre of the sample. The tissue was subsequently re-washed in 10% formaline saline for at least 24 hours to remove residual formic acid. The tissue was cut into five coronal sections for vacuolation scoring (figure 2.1) [296] which encompasses nine gray matter (GM) regions (medulla, cerebellum, superior colliculus, hypothalamus, thalamus, hippocampus, septum, retrospinal cortex, cingulate and motor cortex) and three white matter (WM) regions (cerebellar peduncle (CP), decussation of superior CP, basal cerebral peduncle). Tissue was then paraffin-embedded. Haematoxylin and eosin (H&E) staining of 6μm sections were taken for vacuolation (spongiform) severity scoring, scoring was performed on a scale of 1 to 5 for GM and 1-3 for WM [296]. Vacuolation scoring was performed blind by a researcher independent to this study. For further pathological analysis, serial 10μm sections were cut through the brain to encapsulate regions outlined in figure 2.1.

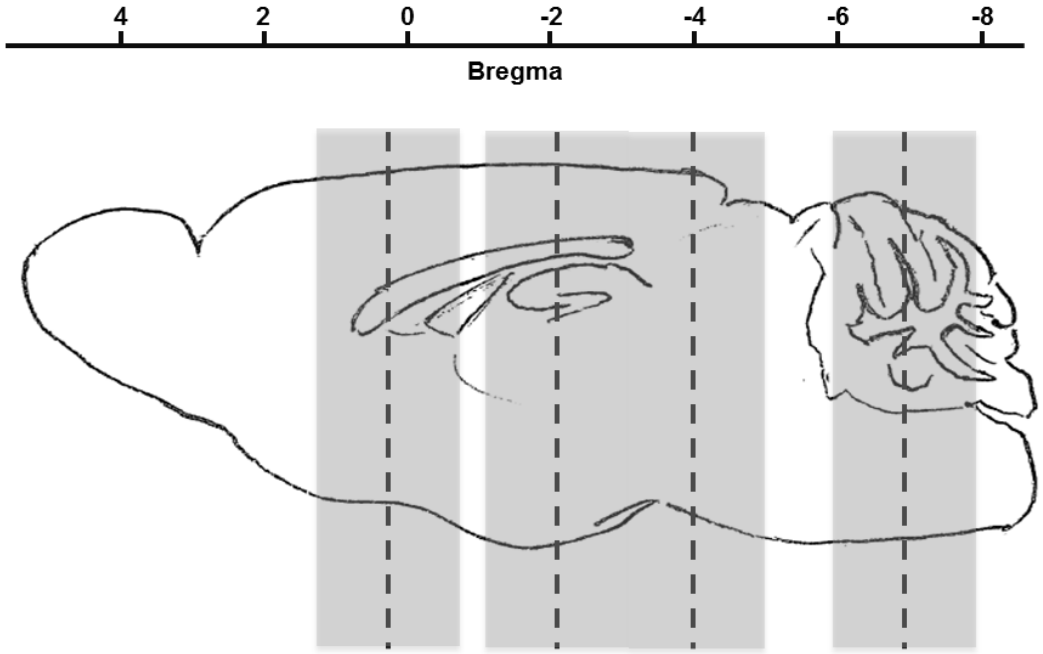

Figure 2.1 - Schematic of mouse brain viewed at sagittal plane of section. Black dashed lines represent each cut made when processing the brain, according to the parameters outlined in [296]. Grey scale areas surrounding dashed lines highlight the approximate areas of serial section performed for pathological analysis. *note* diagram and Bregma coordinates are an approximation.

2.6. Immunohistochemistry

Paraffin-embedded tissue was dewaxed by immersing in xylene and re-hydrated through a series of decreasing alcohol concentrations at room temperature. For PrP immunostaining, the slides was either immersed in distilled water (dH_2O), according to previously published protocols [41], or citric buffer (0.1M citric acid, 0.1M Sodium Citrate, pH 6.4) and autoclaved at 121°C for 15 minutes. Slides were then cooled in running water for 5 minutes before immersing in 98% formic acid for 10 minutes. Subsequently slides were thoroughly washed in running water for 20 minutes. To block for endogenous peroxidase, slides were immersed in 1% H_2O_2/methanol before washing in running water for 5 minutes followed by PBS/1% BSA wash buffer for 5 minutes. Sections were subsequently incubated with Normal

Goat Serum (Stratech) for 20 minutes before application of either BH1 ([297] used at 0.02µg/mL) or 6H4 (Prionics used at 3µg/mL) anti-prion protein antibodies. The primary antibodies were incubated overnight before washing with PBS/1% BSA wash buffer. Goat anti-mouse secondary antibody (Jackson ImmunoResearch) was applied for 1 hour at room temperature, washed with PBS/1% BSA and Vector ABC Elite kit (Vector Laboratories) was applied for 30 minutes then washed. Peroxidase activity was visualised using diaminobenzidine (DAB):H_2O_2 and slides were counterstained in Harris' haematoxylin.

For the immunohistochemical detection of other proteins, sections were either given no antigen-retrieval step (e.g. GFAP) or immersed in citric buffer (pH 6.0) and autoclaved for 15 minutes at 121°C. The protocol replicated that of prion protein detection, with exception of 10 minute incubation in 98% formic acid. All antibodies used in this study are shown in table 2.1.

Antibody	Source	Use	Conc.
BH1	Roslin Institute [290]	IHC (citric pre-treatment) and WB	See chapter 2
6H4	Prionics	IHC (citric pre-treatment)	3µg/mL
GFAP	Dako	IHC (no pre-treatment)	4.5µg/mL
Iba1	Wako	IHC (citric pre-treatment)	1µg/mL
MAP2 a+b	Abcam	IHC (citric pre-treatment)	9µg/mL
Piccolo	Synaptic Systems	IHC (citric pre-treatment)	2.5µg/mL
Tyrosine Hydroxylase	Abcam	IHC (no pre-treatment)	1µg/mL
Parvalbumin	Synaptic Systems	IHC (citric pre-treatment)	1µg/mL
Drebrin	Synaptic Systems	IHC (citric pre-treatment)	1µg/mL
VAMP2	Abcam	WB	0.125µg/mL

Table 2.1 – All primary antibodies used in this study and the methods and concentrations each was used at

2.7. Cell counts

To interpret neuronal cell loss in GSS/101LL animals throughout the disease incubation, ten serial sections from three GSS/101LL and three NBH/101LL mice at each time-point (150dpi, 200dpi, 220dpi, 240dpi and clinical stage pathology (see figure 4.1 for details) were used. These encompass neuronal populations from two anatomically distinct brain regions; the gigantocellular reticular (Gi) nucleus of the brain stem and the retrosplenial granular cortex (RSGc). These regions represent the cell counts of figure 3.3 and were performed at approximately Bregma -6mm (brain stem) and Bregma -1.8mm (cortex).

Images of Gi nuclei were taken at x20 magnification using a Nikon E800 bright-field microscope. To ensure minimal variability in cell counts between sections, the midline below the medial longitudinal fasciculus (mlf) and the 4th ventricle was used as a landmark with the image adjacent to the midline. An example of MAP2 IHC staining of an uninfected murine brain stem [Bregma -6.1mm] is given in figure 2.2A. This demonstrates the approximate area of cell counting performed. In some animals, sections were omitted from the study due to tissue damage and adjacent sections were used. In these instances, the raphe obscurus nucleus (ROb) was present along the midline [Bregma -6.25mm] but does not compromise the standard parameters set out here.

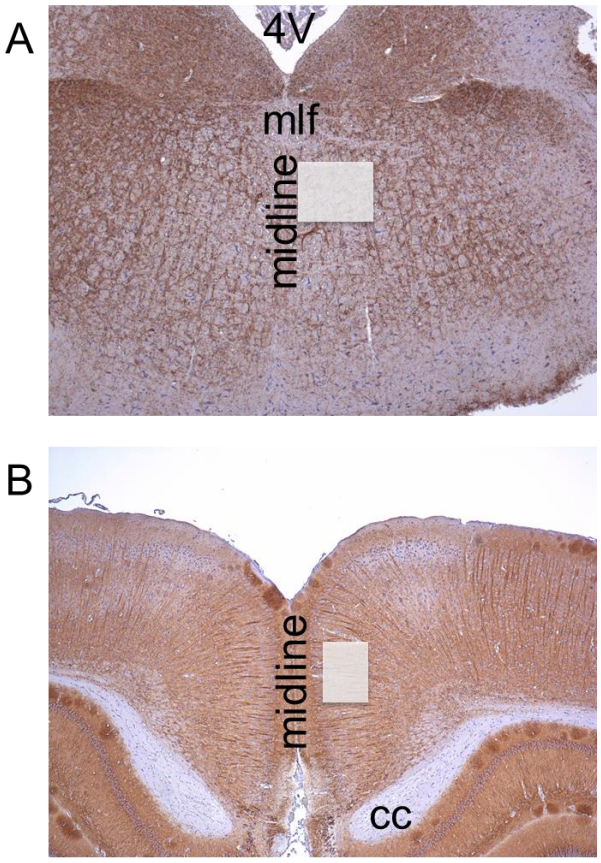

Figure 2.2 – immunohistochemical staining of (A) brain stem [Bregma -6.1mm) and (B) cortex [Bregma -1.8] using anti-MAP2 antibody. White boxes represent area where cell counts were undertaken. *mlf* = medial longitudinal fasciculus. *4V* = 4th Ventricle. *cc* = corpus callosum.

Similarly images of the RSGc were taken at x20 magnification. Due to the proximity of this cell population to the midline and the corpus callosum, these were used as landmarks to minimise variability in cell counts between sections. Each section was stained with anti-MAP2 antibody and counterstained with haematoxylin to allow visualisation of neurons. Cell counts were performed on layer III of the RSGc. Figure 2.2B shows an example of uninfected murine cortex [Bregma -1.8] stained with anti-MAP2 antibody, highlighting the area of cell counting performed.

Counts of Iba1 positive cells which identify microglial cells were performed in clinical stage mice in the substantia nigra, pars compacta (SNc) and substantia nigra, pars reticularis (SNr). To do this, five serial sections from three GSS/101LL animals and three NBH/101LL animals taken from 200dpi group at approximately Bregma -3.5mm. Slides were stained with Iba1 and images taken at x20 magnification using the medial lemniscus as a landmark to minimise variability in cell counts between sections. Cells positive for Iba1 were counted regardless of cellular morphology.

All quantification was performed by the researcher, but sections were blinded using only mouse reference numbers to discriminate between sections. Furthermore, during disease, tissue atrophy may occur due to cell loss – therefore the overall tissue size was quantified in GSS/101LL and compared to NBH/101LL for each brain region tested.

2.7. Biochemical analysis of brain material; Western blot

The flash frozen tissue was dissected in artificial cerebrospinal fluid (CSF; 125mM NaCl, 26mM $NaHCO_3$, 25mM Glucose, 2.5mM KCl, 1.25mM NaH_2PO_4, 1mM $CaCl_2$, 4mM $MgCl_2$) into broadly four anatomically distinct brain regions (brain stem, cerebellum, thalamus and cortex) (figure 2.3). As highlighted, the term 'brain stem' refers only to tissue obtained between the coordinates Bregma -6mm to Bregma -8mm. Due to the distinctive tissue morphology of the cerebellum, the brain stem and cerebellar can be defined easily. Similarly, the cortex sample refers only to mouse brain coordinates Bregma -1mm to Bregma -3mm. For simplicity, each region herein will be referred to as brain stem, cerebellum, thalamus and cortex.

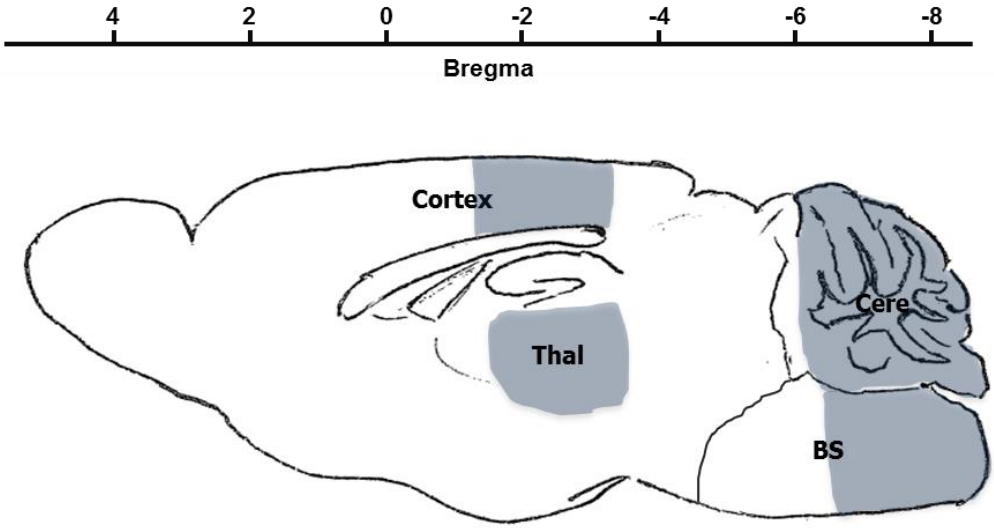

Figure 2.3 - Schematic of mouse brain viewed at sagittal plane of section. Highlighted areas represent approximate regions for tissue dissection. *note* diagram and Bregma coordinates are an approximation.

2.7.1. Total protein measurement

The total protein was assessed for each sample used for Western blot using a bicinchoninic acid assay (BCA; Pierce). This uses bicinchoninic acid to detect the reduction of copper ions which typically occurs in the presence of proteins. A standard protein curve was created using known protein concentrations of bovine serum albumin (BSA) diluted in the same buffer as the samples ranging between 20-2000µg/mL. The experimental homogenate samples were diluted to give a 1:10 (1% of the tissue mass w/v) dH_2O and a 1:100 (0.1% of the tissue mass w/v) before addition of the copper/BCA solution. The resultant change in spectrometric read-out at 564nm was then detected using a PolarStar Omega (BMG Labtech) plate reader Final absorbance was calculated by subtracting the blank reading and the 1:10 and 1:100 concentrations were plotted against the spectrometric read-out from the standard curve to work out total protein concentration in each sample.

2.7.2. Sample preparation and Proteinase K treatment

Samples were exposed to 25U/µL Benzonase (Merck) and 25mM $MgCl_2$ for 30 minutes at 37°C. A 4% (w/v) Sarcosyl/PBS solution was added 1:1 to the sample and incubated for 10 minutes at 37°C. For detection of PrP^{res}, samples were further exposed to 20µg/mL PK (Sigma) for 1 hour 15 minutes at 37°C. The PK digestion reaction was stopped by addition of 10µL 100mM phenylmethylsulfonyl fluoride (PMSF).

2.7.3. Protein denaturing and separation

Samples were diluted to a total protein concentration of 15µg and mixed with sample loading buffer and sample reducing agent (Invitrogen) before denaturing at 80°C for 15 minutes. Samples were run in MES running buffer (Life Technologies) on 10% Bis/Tris polyacrylamide gels (Invitrogen) with see blue pre-stained protein standard (Life Technologies).

After separation, proteins were transferred onto a polyvinylidene difluroride (PVDF) membrane by wet transfer electroblotting (Invitrogen) at 25V for 60 minutes. The PVDF membrane was subsequently blocked using 1% Western Block Solution (Roche) for 60 minutes at room temperature. Antibodies specific to the protein of choice were thus added to the blocking solution and incubated overnight at room temperature under constant shaking. Unbound primary antibody was subsequently washed off with TBS-Tween before incubating in secondary HRP antibodies for one hour at room temperature, before washing with TBS-Tween. The protein of interest was detected using West Dura ECL substrate (Pierce). All primary antibodies used in this study are summarised in table 2.1. As see blue pre-stained protein standard (Life Technologies) was used as markers, which do not show up after immunoblotting onto film, the markers in this text are superimposed onto the Western blots to show molecular weight.

2.8. Recombinant prion protein purification

2.8.1. Inclusion body preparation

Prnp DNA sequences encoding Syrian hamster residues 23 to 137 followed by sheep residues 141 to 234 of the R154 Q171 polymorph [accession number AY907689] (Ham/Shp chimeric PrP) were previously amplified and ligated into the pET41 vector (EMD Biosciences). After transforming the plasmids into *E. coli* Rosetta cells (EMD Biosciences) the bacteria were frozen in a glycerol stock and stored at -80°C. This was performed at the NIH Rocky Mountain Laboratories, USA, by researchers independent of this study, as described previously [298, 299]. The glycerol stocks were transported to our laboratories. Kanamycin culture plates were subsequently streaked with the glycerol bacterial stock and incubated overnight at 37°C. Colonies were picked from this plate and further grown at 37°C with shaking in 3mL media (LB-M Broth, 50mg/mL Kanamycin and Chloramphenicol 34mg/mL in 100% ethanol) for 5-6 hours. The recPrP was expressed using the Overnight Express Autoinduction system (EMD Biosciences). Cell pellets from 0.25L cultures were frozen at -20°C. The cell pellet was then lysed using 1x BugBuster master mix (EMD Biosciences). The lysed cells were centrifuged at 16,000 x g for 20 minutes at 4°C followed by resuspension of the pellet in 1x BugBuster and repeating the 16,000 x g centrifugal step. A 0.1x BugBuster solution was then added before centrifugation at 7,900 x g for 15 minutes at 4°C to pellet the inclusion bodies. The inclusion bodies were then frozen at -20°C prior to recPrP purification.

2.8.2. recPrP purification

The inclusion body pellet was denatured in 8M GuHCl (pH8) and centrifuged at 16,000 x g for 5 minutes at 4°C. The denatured protein present in the supernatant

was then bound to Ni-NTA superflow resin (Qiagen) that had been equilibrated in denaturing buffer (100mM $NaPO_4$, 10mM Tris, 6M GuHCl [pH 8]) and mixed at 10 rpm for 1 hour at room temperature. The resin was loaded into a column and, using an AKTA Explorer system (GE Healthcare), further denaturing buffer was run through the column for 25 minutes before the denatured protein was refolded on the column using a linear gradient of denaturing buffer to refolding buffer (100mM $NaPO_4$, 10mM Tris [pH 8]) over 200 minutes at a flow rate of 1mL/minute. After this gradient was complete, 100% refolding buffer was run through the column for a further 30 minutes. To elute the protein from the column, a linear gradient from refolding buffer to elution buffer (500mM Imidazol-HCl, 100mM $NaPO_4$, 10mM Tris [pH 5.8]) was performed at a flow rate of 1mL/minute for 60 minutes. Protein concentration being released from the column was determined by measuring UV absorbance at 280nm. Upon an increase in 280nm absorbance, protein fractions were collected and diluted 1:1 in dialysis buffer (10mM $NaPO_4$ [pH 5.8]). Each protein fraction was then run on 10% Bis/Tris gels and total protein detected using Instant Blue coomassie staining (Expedeon) to ensure purity. Figure 2.4 shows an example protein purification with protein detected most intensely with the first and second elutes. These were then dialysed in snakeskin dialysis tubing (Pierce) overnight in dialysis buffer (10mM $NaPO_4$ [pH5.8]) at 4°C. RecPrP preparations were then portioned into aliquots and stored at -80°C.

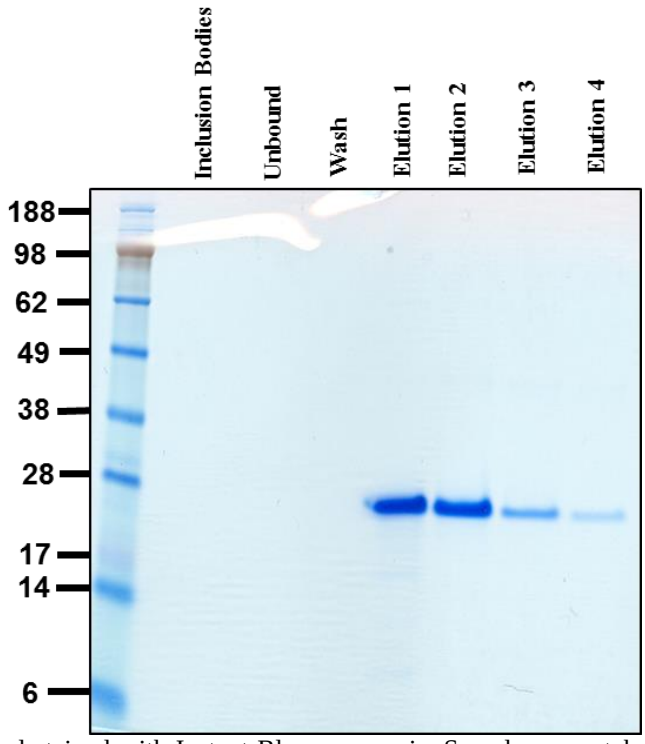

Figure 2.4 - Bis/Tris gel stained with Instant Blue coomassie. Samples were taken at several points during recPrP purification. Bands represent total protein observed which corresponds with expected recPrP size.

2.9. RT-QuIC

A RT-QuIC master mix is composed as follows: 10mM phosphate buffer [pH 7.4], 130mM NaCl, 10µM Thioflavin T [ThT], 10µM EDTA and a final concentration of 0.1mg/mL recPrP. 98µL of this master mix were loaded onto black 96-well clear bottom plates (Nunc). The 10% brain homogenates described in section 2.7 were serially diluted in 0.1% SDS in PBS containing 130mM NaCl with N2 media supplement (Gibco). Reactions were then seeded by addition of 2µL diluted brain homogenate sample or with dH_2O as a negative control. All reactions contained a final concentration of 0.002% SDS. Plates were then sealed with a plate sealer film (Nalgene Nunc International). A PolarSTAR Omega (BMG Labtech) plate reader was used to incubate the samples at 42°C for 60 hours with cycles of 1 minute rest

and 1 minute 700 rpm double orbital shake. ThT fluorescence was then measured (450nm excitation/480 emission) every 15 minutes during the 60 hour incubation.

2.10. RNA extraction

Brain stem, thalamus, cerebellum and cortex were dissected from six GSS/101LL animals at terminal illness and from six NBH/101LL aged matched mice as described in figure 2.3. The tissue was weighed then homogenised in 1mL Trizol (Life Technologies) per 100mg of tissue. Trizol is a monophasic solution of phenol and guanidinium isothiocyanate that solubilises biological material and denatures protein. The homogenate was thus centrifuged at 11,500 x g for 10 minutes at 4°C. The pellet was discarded. Choloform (0.2mL/mL Trizol) was then added to cause phase separation, whereby protein constitutes the organic phase, DNA the interphase and RNA the aqueous phase after a 11,500 x g centrifugal step for 15 minutes at 4°C. The aqueous phase was transferred to fresh RNase free tubes (Life Technologies). Isopropanol (0.5mL/mL Trizol) was added and incubated for 10 minutes at room temperature. The RNA sample was then centrifuged for 10 minutes at 11,500 x g at 4°C. The RNA pellet was washed in 75% ethanol (1mL/mL Trizol) then centrifuged for 5 minutes at 8,000 x g at 4°C. The RNA pellet was then resuspended in Nuclease Free dH_2O (Life Technologies), aliquoted and stored at -80°C.

2.11. Microarray

RNA was extracted from individual animal brain regions. To remove non-disease specific inter-animal variation, each sample consisted of a pool of two animals for an

individual brain region. This resulted in 24 arrays, as highlighted in table 6.1. A minimal RNA concentration of 180ng/μL was required for microarray analysis, which as exemplified in table 6.1, all RNA samples exceeded. The microarray was performed by Edinburgh Genomics (www.genomics.ed.ac.uk) using an Affymetrix Mouse Gene 2.0 array (Affymetrix) and transcript intensity analysed using Affymetrix GeneTitan instrument (Affymetrix). Samples were then returned to our laboratories with raw array data. The data was normalised using Affymetrix Expression Console software. Data was saved as an '.expression' file containing a unique identifier for each transcript (gene annotation concatenated to probe ID). In subsequent columns, the gene and gene ontology (GO) annotations were included for assigning class-sets for the analysis of information contained in the network graph. Finally, the normalised raw data were included in following columns, which each column representing a single sample. The '.expression' output file is subsequently loaded into the network analysis tool, Biolayout Express 3D [300]. Each transcript had pairwise Pearson correlations calculated as a measure of similarity between transcripts where $r \geq 0.7$. A modified Fruchterman-Rheingold algorithm [301] was used to create a graph, whereby each node represents a single transcript which are connected by weighted, undirected edges which represent the correlation. Groups of highly correlated transcripts were then 'clustered' using the Markov cluster algorithm [302]. To confirm the changed expression of transcripts between GSS and NBH/101LL brain regions, two-tailed t-test analysis was used to compare within a region. A p-value cut-off of 0.05 was selected as the significance threshold by which significantly differentially expressed genes were identified.

3. Characterisation of GSS/101LL clinical stage pathology

Chapter aim: To define the pathology in the GSS/101LL model to establish if the apparent lack of accumulated PrP^d leads to differences in prion disease-associated pathology.

3.1. Introduction

Models of murine prion disease exhibit a range of measurable pathological phenotypes within the CNS. These include vacuolation [296, 303], gliosis [262, 263, 304], neuronal loss [305, 306], synaptic degeneration [189, 191-193, 204, 214, 217] and cell/tissue atrophy [191]. It is well established that the neuropathology observed in animal models of prion disease recapitulates that seen in human prion diseases (reviewed in [307]). Expression of PrP^c is essential for susceptibility to prion disease [30, 31]. The accumulation of misfolded prion protein appears to correlate with pathology. In animal models of prion disease, the accumulation of PrP^d has consistently been observed a number of weeks prior to initial detectable neuronal deficits [189, 191, 214]. Other pathological observations appear to occur concurrently with the accumulation of PrP^d, such as gliosis [191].

Antibodies specific for detection of PrP are the most commonly used detection method for PrP; however these cannot differentiate between PrP^c and disease-associated forms, PrP^d. To solve this, different sample pre-treatments are performed

which enables the detection of PrP^d isoforms which are distinct from PrP^c. This distinctiveness of these PrP^d species could be the result of protein misfolding, aggregation (e.g. dimer, oligomer, fibril), other unidentified co-factors, or a combination of these. Figure 3.1 shows a diagrammatic representation of different hypothetical PrP^d species and their methods of detection.

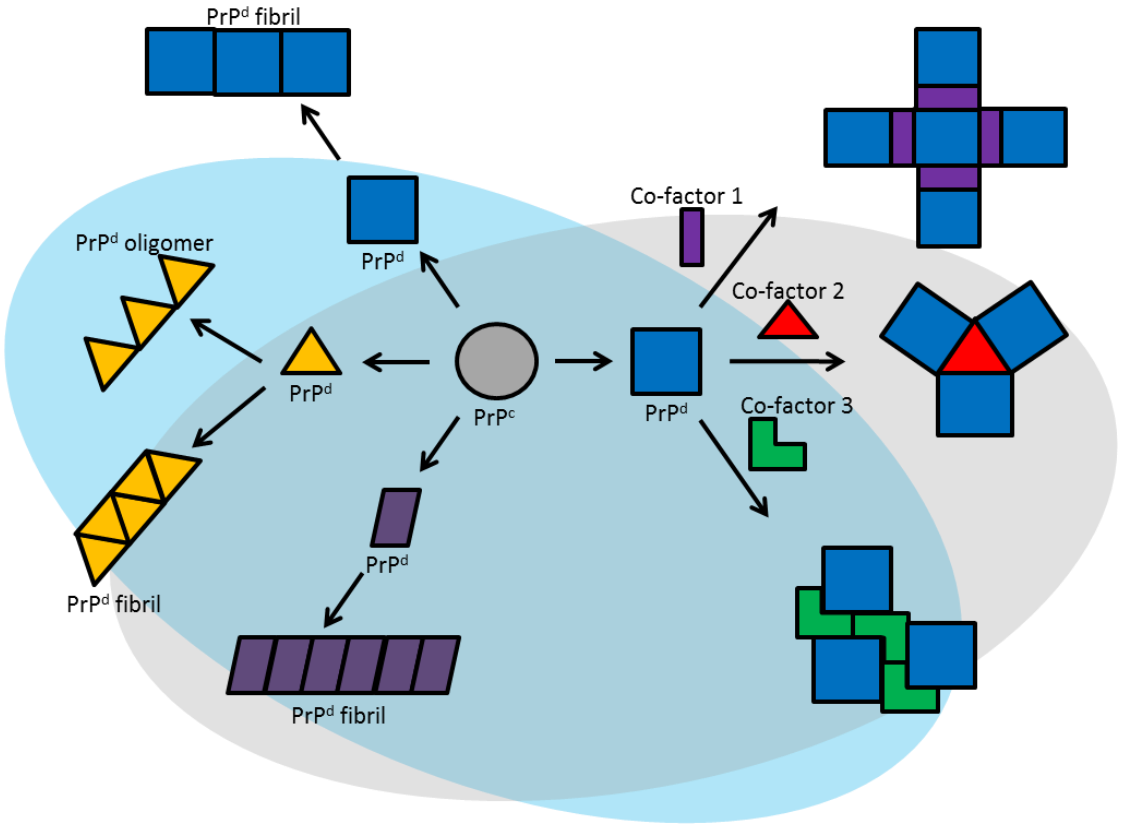

Figure 3.1 - Diagrammatic representation of different conformations of PrP^d which are distinct from PrP^c. These can aggregate, either PrP^d autonomously or potentially with co-factors. Different aggregates may be morphologically similar, but require specific techniques for their detection. For example, the hypothetic blue and grey shading may represent forms which can be identified in Western blot (blue) or IHC (grey). Although both detection systems can detect many similar species of PrP^d, some techniques may identify specific isoforms which others cannot. Moreover, other species of PrP^d may yet remain undetected.

Immunohistochemistry (IHC) typically relies on using specific conditions, for example formic acid, trypsin or PK exposure, prior to the application of the prion-specific antibody. These conditions are thought to destroy PrP^c epitopes within CNS

tissue. As a result, when applying PrP specific antibodies to uninfected tissue, no PrP is detected. Application of these same antibodies to known prion-infected samples, however, results in IHC detection of PrP. This PrP is likely the result of a conformational alteration, rendering the increased resistance of PrP to such conditions, and therefore represents PrP^{d}. The advantage of using IHC is the ability to localise PrP^{d} detection to specific regions of the CNS. The limitation is the inability to define the isoform of PrP^{d} that is being identified. For example, it is known PrP^{d} can consist of both PK-resistant and sensitive isoforms [21, 308].

PrP^{c} is PK-sensitive, and therefore detection of PK-resistant isoforms of PrP, PrP^{res}, in prion disease is indicative of a disease-associated isoform, PrP^{d}. Western blots are commonly used to detect PrP^{res} as a diagnosis of the presence of PrP^{d} [21]. In humans and animals with prion disease, for example, PrP^{res} isoforms are commonly observed [3]. However, PK-sensitive isoforms have also been recognised in some prion strains exhibiting high PrP^{res} levels [308]. In contrast to IHC, Western blot analysis allows the interpretation of the species of PrP^{d} present in a sample, but cannot effectively define localisation of PrP^{d}. As a result, using Western blot analysis to detect the species of PrP^{d} present and IHC to identify the targeting of PrP^{d} represents an appropriate approach to further correlate PrP^{d} with neurodegeneration.

It is unclear what role either PrP^{res} or PrP^{sen} have within neurodegeneration. It has been shown previously that smaller aggregates of PrP^{d} represent the most infectious species of PrP^{d} [51]. Due to the size of these aggregates, it is assumed these fractions

of PrP^{d} consist predominantly of oligomers. As discussed in *1.4.1 The role of PrP in neurodegeneration* there is much conflict regarding whether such oligomers or fibrils represent the toxic entity within prion disease. There is, however, little data to define whether oligomers, for example, are predominantly PrP^{sen} or PrP^{res}, or both. What role all/any isoform of PrP^{d} has within neurodegeneration has also been brought into question due to models which exhibit little or no detectable PrP^{d} [28, 39, 41]. In one such study, only extremely small quantities of PrP^{d} could be identified by both IHC and Western blot analysis which correlated with high infectivity levels, vacuolation and a robust and predictable incubation period [41]. This study incorporated a proline to leucine mutation at codon 101 of murine *Prnp*. This mutation is the equivalent to the disease-associated P102L mutation in human GSS but unlike humans, does not cause spontaneous disease in mice [28]. Upon experimental infection with human GSS, these mice exhibit the disease phenotype described above (briefly low PrP^{d}, high infectivity) [41]. This model is henceforth abbreviated as GSS/101LL.

In order to assess the apparent low quantities of PrP^{d} in the GSS/101LL model, a range of mono- and polyclonal antibodies across the length of the protein were previously used. These detected only extremely small levels of PrP^{d} via IHC and no detectable PrP^{d} using Western blot. Denaturing techniques to expose epitopes that may not be presented due to the PrP protein conformation in this model were also used [32]. For example, increasing concentrations of guanidine hydrochloride were used to denature the protein, and subsequently the samples were analysed using conformation dependent immunoassay (CDI). This involves measuring the ratio of native vs. denatured protein present in a sample (d/n ratio) via a sandwich ELISA.

An increase in d/n ratio would indicate the presence of PrP^d, due to the increase in antibody binding to denatured product (i.e. a higher level of exposed epitope). In the GSS/101LL model, the d/n ratio was equivalent to uninfected 101LL mice [41].

The GSS/101LL model therefore indicates a critical dissociation between the large accumulation of PrP^d detected in many prion disease models and pathology. The limited PrP^d accumulation observed in this model may therefore represent the sole toxic species of PrP^d or suggest a minimal role of PrP^d in neurodegeneration. Prior studies, however, only examine the relationship between deposited PrP^d and vacuolation and show no clear correlation. Conversely, PrP^d may be associated with other aspects of pathology, such as neuronal loss, microglial activation or astrocytosis.

To determine the pathology of GSS/101LL mice compared to NBH/101LL animals, most interpretation in this chapter will be performed as a descriptive pathological analysis. Where possible, quantitative or semi-quantitative analysis will be performed, such as neuronal counts or vacuolation scoring. In all instances, it is important for quantitation to be performed blind and if possible, by a researcher independent to the study. Vacuolation scoring in this thesis is performed by a researcher independent to this study and who is scoring the samples blinded and according to parameters which have been outlined previously [296]. To quantify the number of neurons present, in order to interpret whether neuronal loss is occurring in one brain region and not another, one must not only consider counting the number of

cells within a well-defined brain region of the brain using multiple sections for counting. This is because the tissue being studied is a 3D structure, but the sections that are being counting are a 2D representation of the structure. Therefore it is important to include measurements which take into account the measurements of the tissue within which the neuronal counts are being performed. This is especially important in this study, as disease-specific brain regions are being compared to region matched uninfected controls. It is therefore possible that brain regions undergoing neurodegeneration may also be undergoing gross brain region atrophy. As a result the neuronal cell counts will need to take this into account to prevent any possible bias as a consequence of differences in total tissue size [309].

This chapter thus examines a number of pathological phenotypes in GSS/101LL mice at terminal illness and aims to test whether such observations may be associated with the detection of PrP^{d}.

3.2. Results

To assess the different parameters of the neuropathology at clinical stages of disease, paraffin-embedded tissue from previous studies was available and used. Due to limited availability of tissue for biochemistry analysis (such as Western blot), a further cohort of GSS/101LL and NBH/101LL animals was set up to examine other aspects of the disease at late stages of disease progression, namely clinical onset.

The paraffin-embedded tissue from nine GSS/101LL and three NBH/101LL animals used in previous studies [28] was serially sectioned throughout the brain. This tissue

was then used to assess the pathology at clinical stages of disease. The brains from 12 GSS/101LL and 12 NBH/101LL animals set up for biochemical analyses were halved and four regions were dissected (brain stem, cerebellum, thalamus, cortex; see chapter 2 for details). The regional dissection is based upon the vacuolation profile from previous studies (figure 3.2) to incorporate regions of targeted pathology and unaffected regions. This tissue was used to assess what isoforms of PrP^{d} exist in GSS/101LL animals.

3.2.1. Incubation period and vacuolation severity scoring in "archive" and "recent" GSS/101LL animals

Prion diseases produce remarkably consistent incubation periods. Alongside this, the disease appears to target predictable, specific regions of the brain and traditionally, this regional vulnerability has been scored by the presence of disease-specific vacuolation [296, 303]. In this study, two cohorts of GSS/101LL animals were used; nine "archive" GSS/101LL animals and twelve "recent" GSS/101LL animals. The average incubation period of the archive group was 286.66 ± 2.95 days compared to 291.11 ± 5.29 days in recent GSS/101LL animals.

The vacuolation severity scoring was performed blind by a researcher independent to this study. Vacuolation severity was scored according to the parameters outlined in chapter 2, which are based upon previously published standards [296, 303]. The vacuolation severity in GSS/101LL mice is relatively minor compared to other prion diseases [296, 303, 310] (figure 3.2). The vacuolation scores are highest at four areas

of grey matter in archive tissue. These are medulla, superior colliculus, hypothalamus and thalamus. In the recent group, however, a relatively high level of vacuolation is observed in the medulla but is lower in all other regions but still represents a similar pattern (i.e. higher levels of vacuolation in medulla, superior colliculus, hypothalamus and thalamus, but also in the septum) (figure 3.2). Within white matter, there is a difference between high vacuolation severity scores in archive tissues and low vacuolation scores in recent GSS/101LL tissues. Increased vacuolation cannot be attributed to differential aging as all animals in the recent GSS/101LL group were injected at a similar age to those in the archive GSS/101LL group. Ultimately, the similar incubation period and consistency of vacuolation scoring in neuronal-rich grey matter tissue demonstrate the conserved properties of this model. Due to the low levels of vacuolation, however, little can be made of the importance of this as a pathological feature.

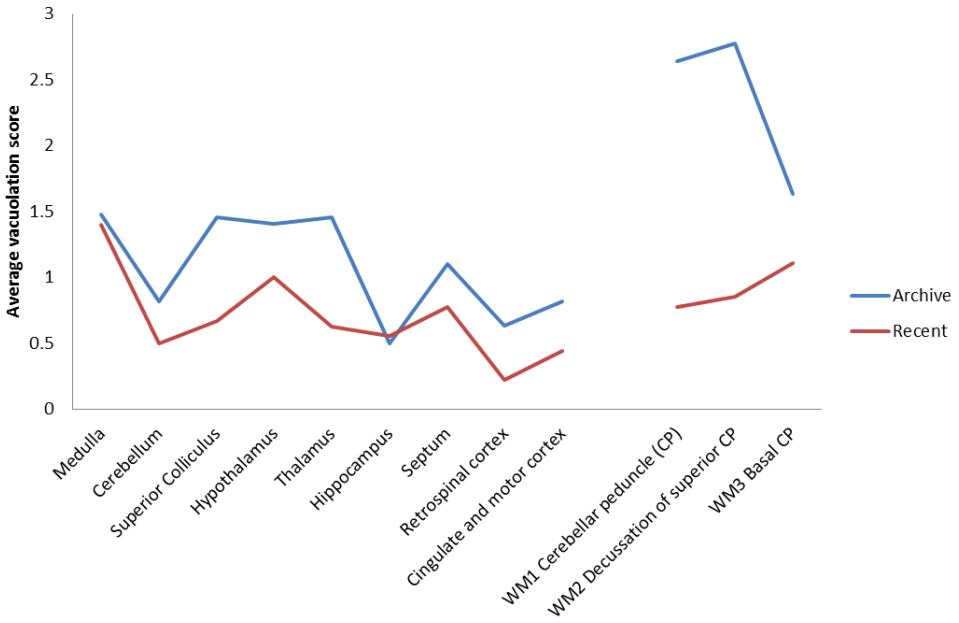

Figure 3.2 – Vacuolation profile of "archive" and "recent" groups of GSS/101LL clinical stage animals. Grey matter scores (medulla [brain stem], cerebellum, superior colliculus [midbrain], hypothalamus, thalamus, hippocampus, septum, retrospinal cortex and cingulate and motor cortex) are

scored blind on a scale of 0-5, whereby 5 represents severe vaculation and 0 represents no vacuolation. Blue line indicates archive tissue, red line indicates recent tissue.

3.2.2. Neuronal loss is restricted to specific regions of the brain

Neuronal degeneration and loss is thought to be the fundamental causal factor behind the establishment of overt clinical symptoms and subsequent death of the animal. Within chronic neurodegenerative diseases, selective vulnerability of specific neuronal populations is well established (reviewed in [311]). When considering the extremely small quantities of PrP^{d} present in GSS/101LL animals, it will be important to precisely define the extent of neuronal loss to determine whether neurodegeneration progresses to similar cell loss fate as demonstrated in previous studies examining different murine prion strains [189, 225].

To identify whether neuronal loss occurs in GSS/101LL mice, neuronal cell counts were performed in two areas; brain stem and cortex. This allowed for the comparative analysis of cell loss in regions exhibiting a higher vacuolation score (brain stem; medulla) against regions showing minimal vacuolation (cortex). The specific neuronal populations counted were the gigantocellular reticular nuclei of the brain stem (Gi) and layer III of the retrospinal granular cortex (RSGc). To do this, a series of ten sections were taken throughout a coronal-section tissue slice. Each section was stained with anti-MAP2 antibody, to detect microtubule-associated protein 2 (MAP2) which is commonly observed in dendrites and cell bodies of neurons in the CNS. The number of neurons within a specific pre-defined neuronal

population were then counted and averaged according to the mean number of neurons per section.

Figure 3.3 shows the average number of neurons per section in the Gi and RSGc from ten serial sections of three GSS/101LL and three NBH/101LL animals. The Gi exhibits significant neuronal loss compared to NBH/101LL controls (t-test; p=<0.001). The RSGc does not appear to suffer any discernible neuronal loss in GSS/101LL animals comparated to NBH/101LL controls. To ensure that these cells counts were performed accurately and are compared to NBH/101LL region and aged matched controls appropriately, the total brain region was measured to test for any changes, such as tissue atrophy. Results are presented as the percentage size of GSS/101LL brain regions compared to the respective region and aged matched NBH/101LL controls. No significant changes in either brain region tested were observed compared to NBH/101LL controls, although there appeared to be a general decrease in total tissue size in GSS/101LL brains compared to NBH/101LL controls – but this was not statistically significant.

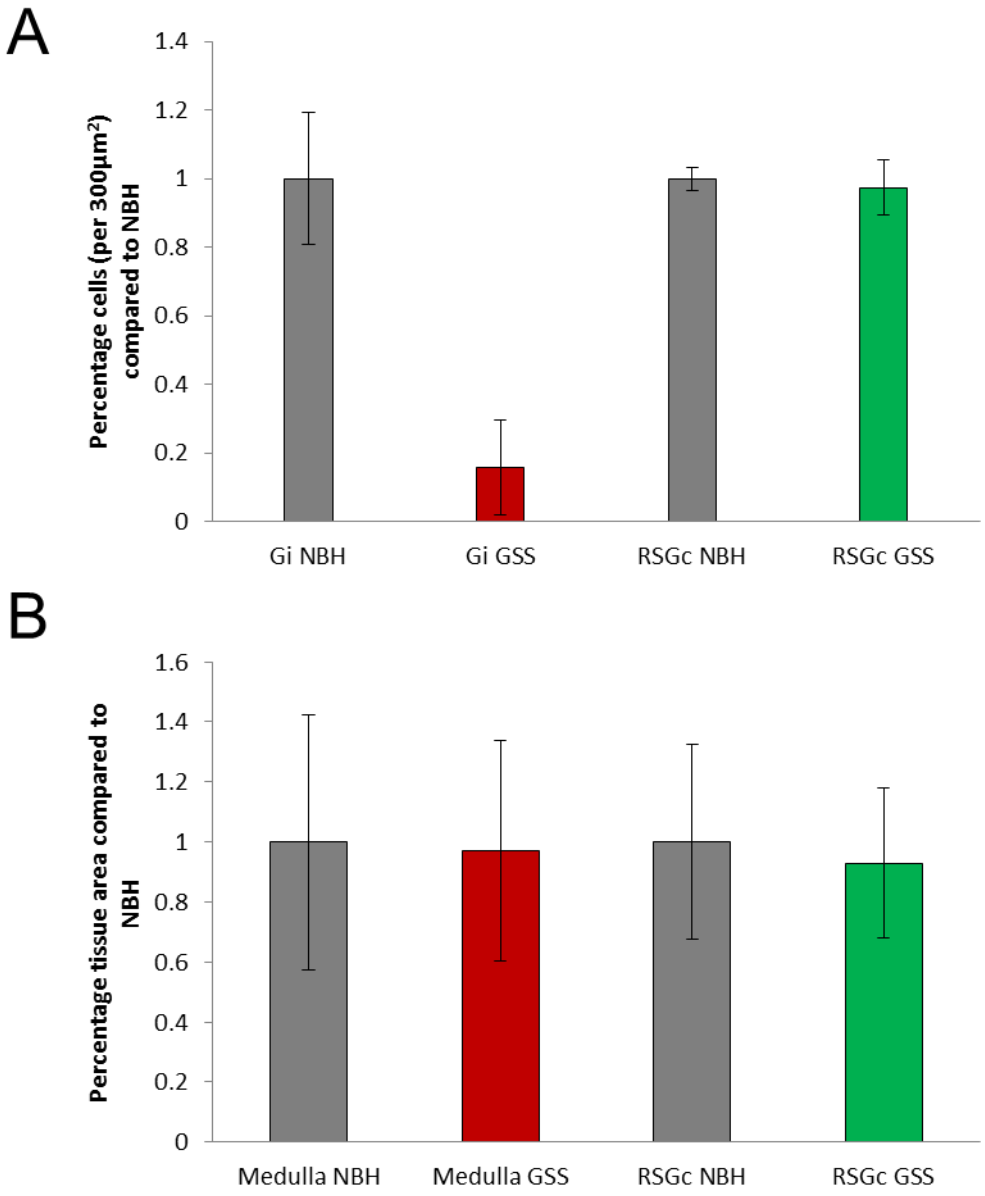

Figure 3.3 - Neuronal cell counts. (A) Each bar represents average number of neurons per section (n=10) per animal tested (n=3). Gigantocellular reticular nuclei (Gi) of the medulla are lost at clinical onset of disease, compared to NBH/101LL animals (t-test, p = <0.001). Retrosplenial granular cortex (RSGc) nuclei showed no statistically significant change in neuronal number compared to NBH/101LL controls (t-test, p = >0.05). (B) No change in tissue area could be observed in GSS/101LL brain regions compared to the respective region and aged matched NBH/101LL controls.

3.2.3. Synaptic degeneration is observed only in regions of neuronal loss and vacuolation

Synapses are known to degenerate early in prion disease, long before loss of the neuronal cell body occurs [189, 191-193, 204, 214, 217]. Within regions of neuronal

loss it will therefore not be surprising to observe synaptic degeneration. Detection of synaptic degeneration in other regions may, however, indicate earlier stages of pathology. The integrity of the post-synaptic structure was assessed using the actin-binding protein drebrin. This protein exists predominantly within the dendritic processes of neurons and thus is a useful probe to detect the post-synaptic structure, which has been shown to degenerate early in prion diseases [193, 214]. Drebrin only appeared significantly expressed in NBH/101LL animals within specific neuronal populations within the brain stem, such as the facial nuclei, and the hippocampus. Repeated attempts to optimise the antibody to detect post-synaptic structure in additional regions were unsuccessful. Nevertheless, this antibody was used to define the post-synaptic structure of neurons in a region exhibiting neuronal loss and pre-synaptic degeneration (brain stem facial nuclei), compared to neurons which do not (hippocampus). Figure 3.4A shows the loss of drebrin staining in brain stem neuronal populations in GSS/101LL animals. Within the facial nuclei, it is clear the neuronal cell bodies have not been lost (see green and red arrows in NBH and GSS – figure 3.4A) but the neurons in GSS/101LL have atrophied. To quantify this, Image J was used to measure the cell area in GSS/101LL and NBH/101LL facial nuclei. Figure 3.4B shows the significant cell shrinkage of GSS/101LL facial nuclei (t-test; $p<0.001$). In the hippocampus, drebrin staining intensity or morphology does not appear to differ between GSS/101LL or NBH/101LL animals, see figure 3.4C.

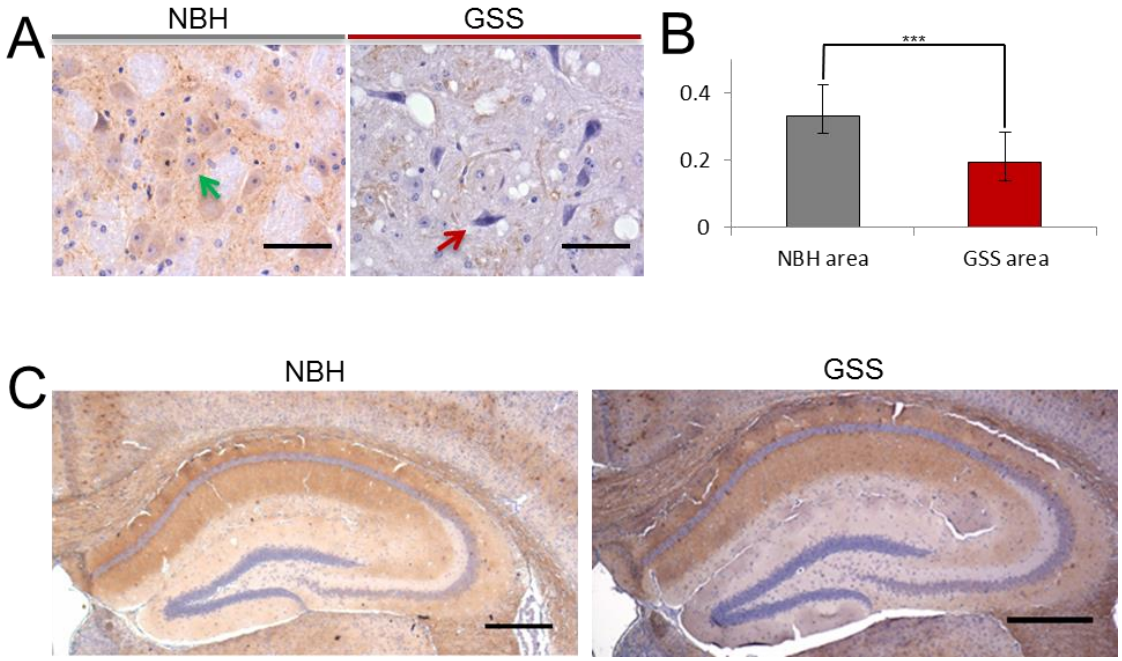

Figure 3.4 – Drebrin staining of facial nuclei and hippocampal nuclei. (A) Facial nuclei stained with anti-drebrin antibody shows highly structured morphology of post-synaptic densities which is lost in GSS/101LL facial nuclei. Green arrows show neuronal cell bodies in NBH/101LL facial nuclei but red arrows show significant cell shrinkage (atrophy) of these nuclei in GSS/101LL facial nuclei. Scale bars = 50µm. (B) Quantification of cell body area using Image J software. The cell bodies of facial nuclei are significantly reduced in GSS/101LL animals comparative to NBH/101LL facial nuclei (t-test; p=<0.001). (C) Drebrin staining in hippocampus shows significant level of staining in CA1 hippocampus which is unchanged in NBH or GSS/101LL animals. These results were observed in all animals used in this study. Scale bars = 200µm.

Taken together, this data shows that both pre- and post-synaptic deficits occur in GSS/101LL animals in regions which also show neuronal loss. No synaptic deficits could be observed in regions not exhibiting neuronal loss, such as the cerebellum or cortex.

3.2.4. Neuronal specific structural proteins are compromised only in regions of neuronal loss

Neuronal atrophy is a common neuropathological feature of chronic neurodegenerative disease [312, 313], and figure 3.5 demonstrates atrophy in

GSS/101LL animals. This suggests a deficit or loss of proteins involved in maintenance of neuronal structure. Microtubule-associated protein 2 filaments (MAP2a and MAP2b) are expressed specifically within the dendrites and cell body of neurons. Detection of MAP2a, MAP2b (hereby referred to as MAP2) is thus an ideal approach to study the structure of the neuronal cell body and dendritic processes. Antibodies specific to MAP2 strongly stained numerous neuronal populations throughout the CNS. Figure 3.5 demonstrates the substantial loss of MAP2 within the thalamus of GSS/101LL animals. High magnification shows that some neurons remain with MAP2 staining in the cell body. This indicates the neurons remaining in the thalamus do not lose MAP2 proteins, and therefore are perhaps structurally intact. Within the cortex and cerebellum however, the staining intensity of MAP2 appear increased comparative to NBH/101LL region matched controls.

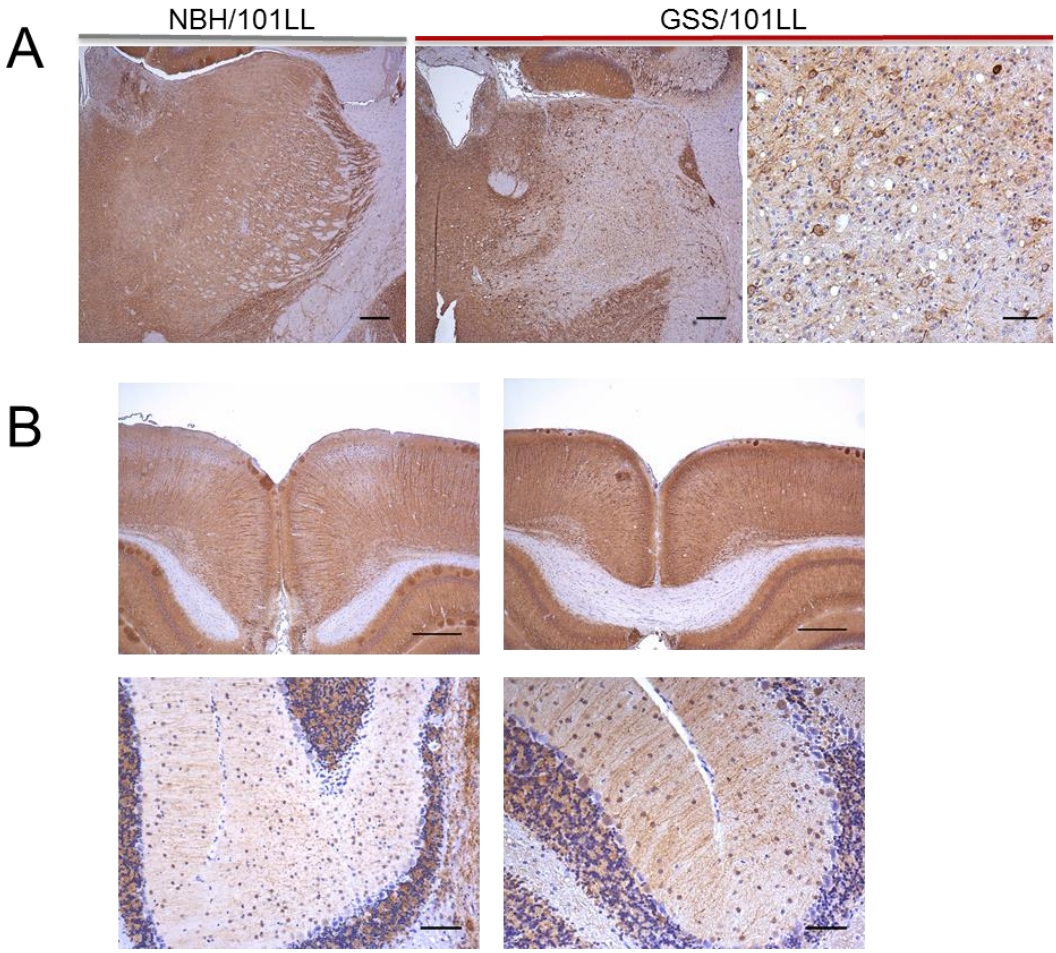

Figure 3.5 – MAP2 staining of thalamus (A) and cortex and cerebellum (B). (A) Significant loss of MAP2 staining is observed in the ventral-lateral thalamus. This represents a loss of neurons, although neurons which remain in these regions are still positively stained for MAP2. Low magnification scale bars = 100μm. High magnification scale bar = 50μm. (B) Left panels represent NBH/101LL cortex and cerebellum, right panels represent GSS/101LL cortex and cerebellum. An increase in staining intensity in both cortex and cerebellum is observed in GSS/101LL regions. This does not correlate with vacuolation, neuronal loss or synaptic protein loss. These results were observed in all animals used in this study. Cortex scale bar = 200μm. Cerebellum scale bar = 100μm.

To further test this, antibodies to parvalbumin were used. Parvalbumin is highly expressed in the Pukinje cells of the cerebellum which project dendrites into the cerebellar molecular layer. This therefore is an ideal method to detect the structural morphology of a major cell type in the cerebellum. No change in the staining quality was observed in parvalbumin positive cells in GSS/101LL animals compared to NBH/101LL (figure 3.6). Overall, this data confirms the neurodegeneration is

observed in specific regions, such as the brain stem and thalamus. Conversely, increased protein expression of MAP2 was observed in both the cerebellum and cortex of GSS/101LL animals.

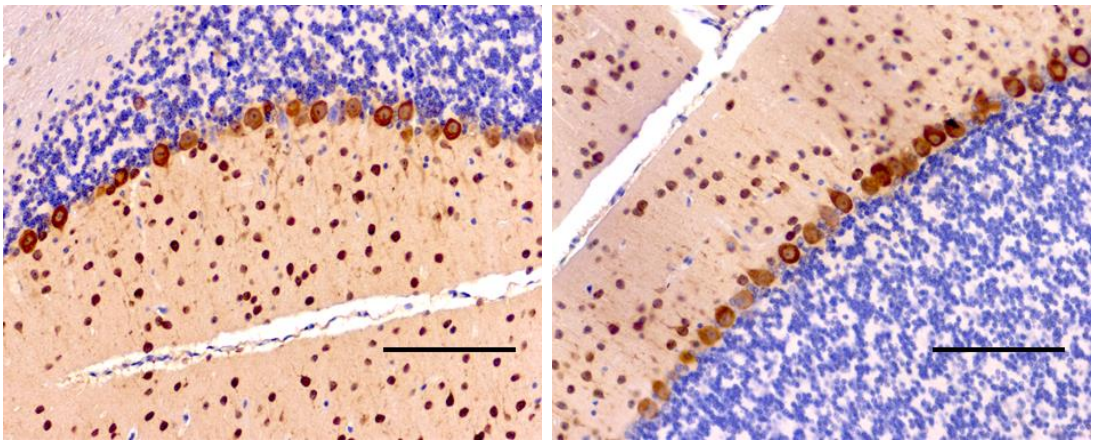

Figure 3.6 – Parvalbumin staining of GSS and NBH/101LL cerebellum. Left panel represents cerebellum from GSS/101LL animal, right panel represents cerebellum from NBH/101LL animal. No change in staining intensity, quality or morphology could be observed. These results were performed in three GSS/101LL and three NBH/101LL mice from the 'recent' group. Scale bars = 50μm.

3.2.5. Glial responses are restricted to regions undergoing neurodegeneration

Two glial cells of the CNS are known to be consistently morphologically and functionally altered within a range of chronic neurodegenerative diseases, these are microglia and astrocytes. The functions of both cell types have been discussed previously (see *1.4.4. Astrocytes and prion disease* and *1.4.5. Microglia and prion disease*). Both cell types are known to exhibit substantial morphological responses in prion disease, typically by hypertrophy of the cell body and shortening/thickening of cell processes. This morphological response has been shown to be associated with initial detectable deposits of PrP^d and neurodegeneration [189, 191].

Ionized calcium-binding adapter molecule 1 (Iba1), also known as allograft inflammatory factor 1 (AIF1), is a protein expressed specifically within macrophages, including microglia [314]. Antibodies to detect this protein can thus be used as a tool to study microglial phenotype within different regions of the brain. Figure 3.7 shows the GSS/101LL cortex and cerebellum do not exhibit any changed microglial morphology in comparison to region matched NBH/101LL mice. In the GSS/101LL brain stem and thalamus, the microglial morphology is characteristic of disease-associated activated microglial morphology, i.e. hypertrophied cell body and short, thick processes. This is in stark contrast to NBH/101LL brain stem and thalamus which exhibit quiescent microglial morphology.

Astrocytes are known to express low levels of GFAP within a healthy brain. Upon alterations to neuronal homeostasis astrocytes undergo a morphological alteration, as described above. GFAP, an intermediate filament protein, is up-regulated within morphologically “reactive” astrocytes [248, 315]. This allows antibodies specific to GFAP to be used as tools to assess the morphological change of astrocytes in response to prion-disease [262]. Figure 3.8 shows GFAP staining in a characteristic astrocytic morphology (small cell body, long thin processes) in GSS/101LL cortex. This is comparable to NBH/101LL astrocyte morphology. Very little GFAP staining is observed in the molecular layer of the cerebellum in GSS/101LL mice. Some positive staining can be observed in the granular cell layer, but this is also seen in NBH/101LL animals. GFAP staining in GSS/101LL brain stem and thalamus was indicative of reactive astrocytes, both in up-regulation of GFAP and their cellular

morphology. This was a disease specific phenotype, as these phenotypes are not observed in NBH/101LL brain stem or thalamus.

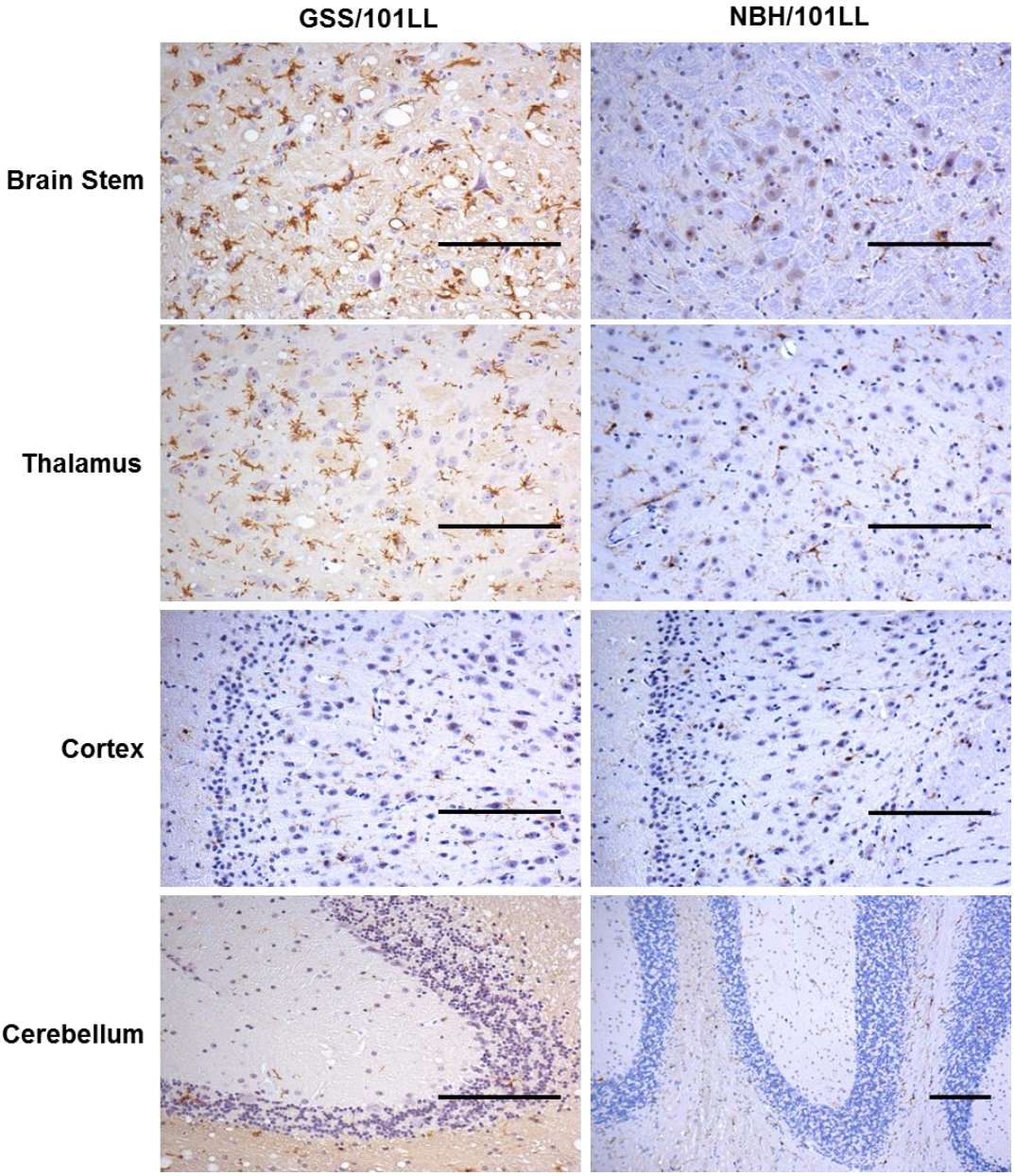

Figure 3.7 – Microglial morphology in brain stem, thalamus, cortex and cerebellum. Iba1 staining shows the microglial morphology is altered in GSS/101LL brain stem and thalamus comparative to NBH/101LL. No change in microglial morphology could be detected in cortex or cerebellum. These results were observed in all animals used in this study. Scale bars = 50μm.

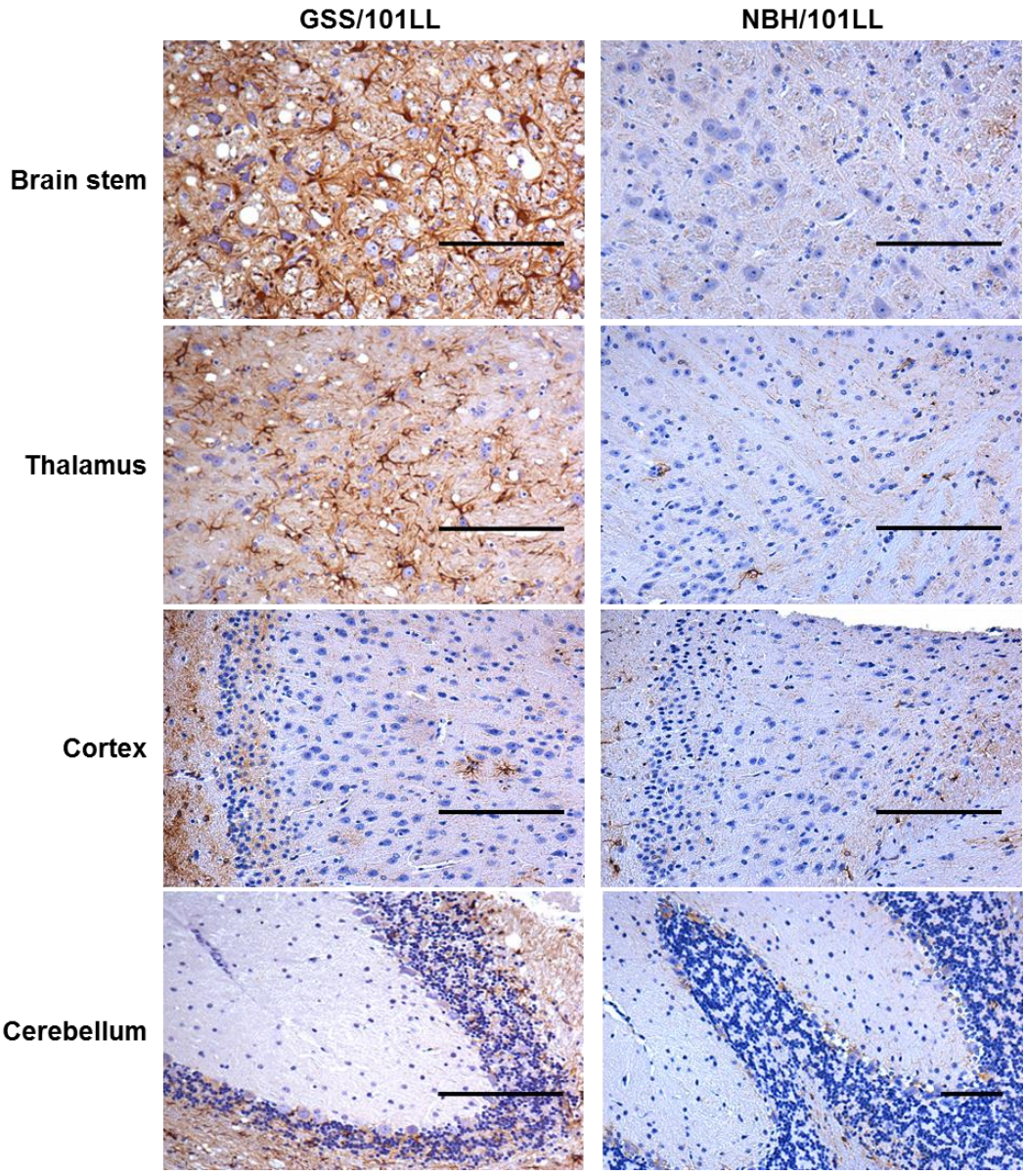

Figure 3.8 – Astrocyte morphology in brain stem, thalamus, cortex and cerebellum. GFAP staining shows an increased number of GFAP positive astrocytes in GSS/101LL brain stem and thalamus comparative to NBH/101LL. No observable changes in the number of GFAP positive astrocytes could be observed in cortex or cerebellum. These results were observed in all animals used in this study. Scale bars = 50μm.

3.2.6. Comparatively larger quantities of PrP^d observed in GSS/101LL animals than previously identified

There has traditionally been an association between the accumulation of PrP^d and neurodegeneration in prion diseases, with a few exceptions, including the

GSS/101LL model [28, 39-41]. To confirm that only the extremely small quantities of PrP^d are detected in regions shown here to undergo neurodegeneration; IHC and Western blots were performed. Using a PrP-specific antibody, BH1 [297] in an IHC protocol described in previous studies [41], very small quantities of PrP^d were detected in some GSS/101LL animals (figure 3.9). At high magnification, small aggregates of granular PrP^d staining could be observed in the thalamus and midbrain, but not in every animal tested. No PrP staining could be detected in NBH/101LL animals or using an isotype (IgG1) control antibody on GSS/101LL tissue. This indicates the PrP staining observed in a subset of GSS/101LL animals is disease-associated, or PrP^d. Mice infected with ME7 or 87V were used as positive controls to confirm the staining protocol was effective. Large quantities of PrP^d were identified in these prion strains under these experimental conditions (figure 3.9).

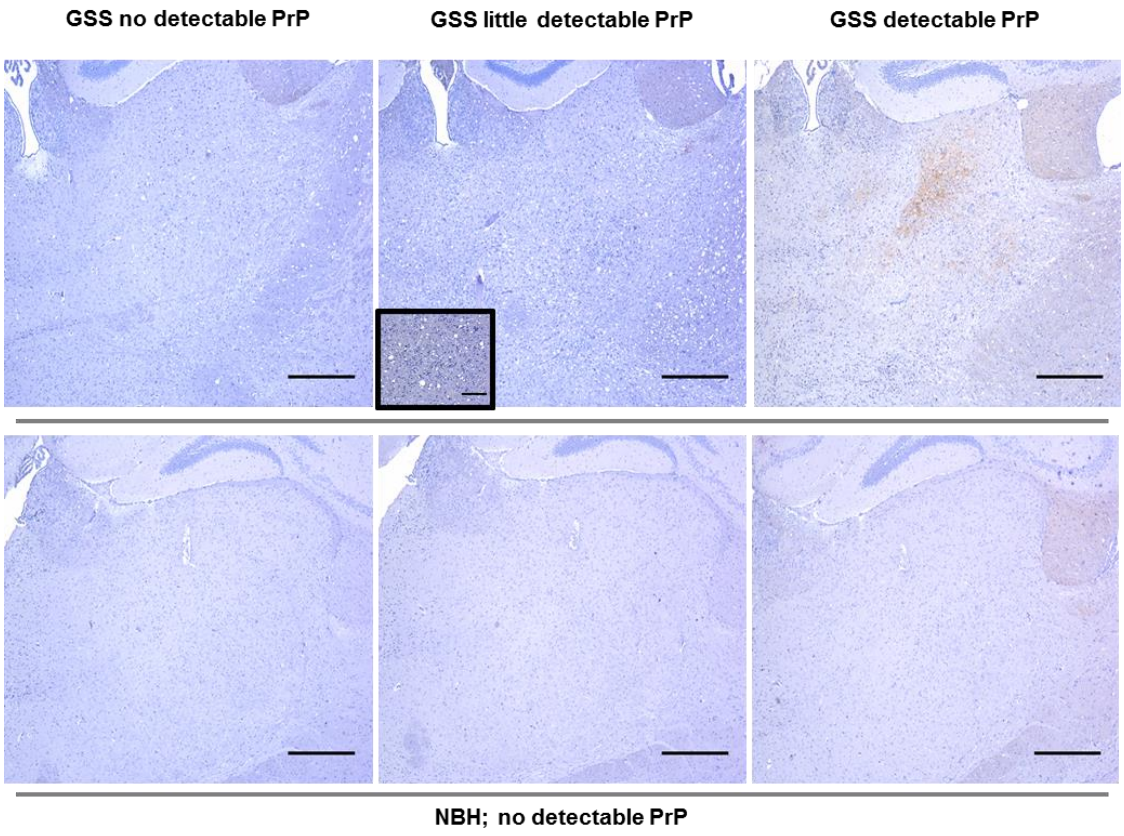

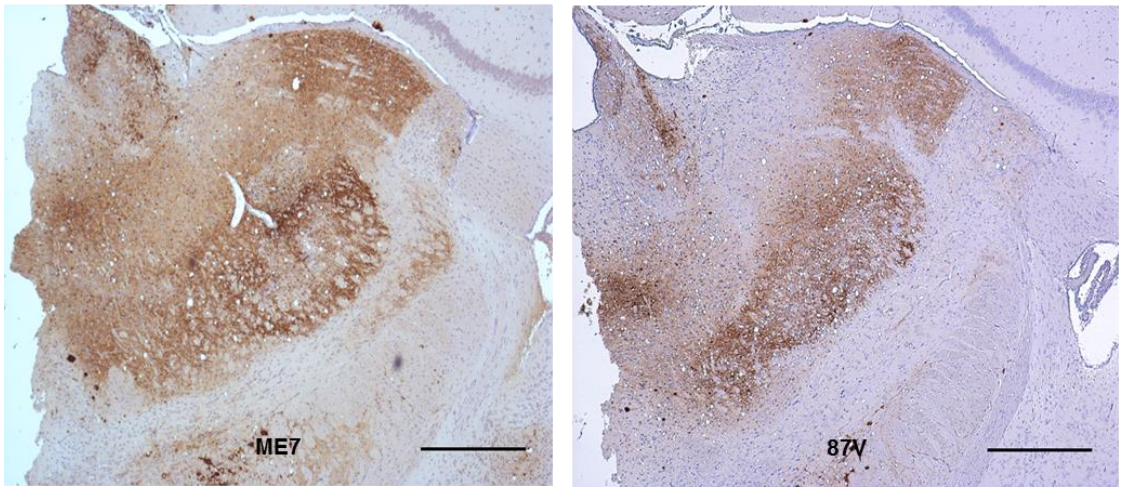

Figure 3.9 – PrP staining using previously defined protocol [41]. Some GSS/101LL mice present no detectable PrP^d, whereas others present some small quantities of PrP^d. When using this protocol on ME7 or 87V clinical stage material as positive controls, these clearly show large quantities of PrP^d staining. Low magnification scale bars = 200μm. High magnification scale bar = 50μm.

To investigate the influence of the staining protocol and in particular the pre-treatment steps on the detection of PrP^d, other immunohistochemistry protocols were

tested using BH1. It was found upon changing the water autoclave step in the previously published protocol [41] to an autoclave step using citric acid buffer in place of water, comparatively larger quantities of PrP^d could be detected in GSS/101LL animals. Figure 3.10 shows the "citric acid protocol" in the same IHC experiment as the "water protocol". The now detectable PrP^d did not appear morphologically different from the smaller quantities identified previously, with the same appearance of granular aggregates of PrP^d. No detectable PrP could be observed in NBH/101LL animals and no non-specific staining could be identified when using an isotype (IgG1) control. The detectable PrP^d using the altered IHC conditions showed PrP^d widespread in the brain stem, midbrain and thalamus (figure 3.11A), but none could be detected in the cortex or cerebellum (figure 3.11B).

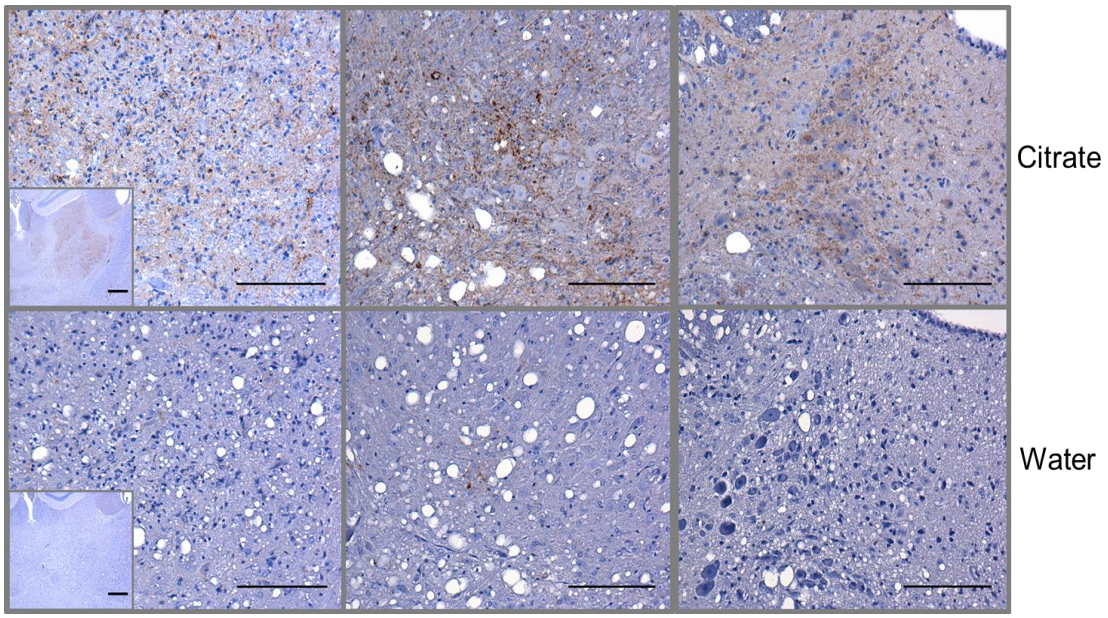

Figure 3.10 – PrP staining using modified IHC conditions (citric) comparative to previously published IHC conditions (water). Left panel shows GSS/101LL VM thalamus, middle panels show hypoglossal nuclei of brain stem and right panels show locus coeruleus nuclei of the pons. Substantially larger quantities of PrP^d could be detected using modified IHC conditions. Scale bars = 50µm. Low magnification scale bars = 100µm.

To identify whether the additional conformations of PrP^{d} detected using immunohistochemistry with a citric acid buffer–autoclave step exhibit a protein conformation that is PK-resistant, homogenates of different brain regions (brain stem, thalamus, cortex and cerebellum) were exposed to PK (see chapter 2 for detailed methods). Western blots were then used to detect whether any PrP^{res} isoforms of PrP^{d} exist. Figure 3.12 shows Western blots using BH1 antibody demonstrates that PrP^{res} isoforms could not be identified in brain stem, cerebellum or thalamus from GSS/101LL animals. A very faint band was observed in GSS cortex, thereby suggesting small quantities of PrP^{res} present in this region. This however was only observed in two of nine GSS/101LL animals tested. In all other cases, no PrP^{res} was detectable in any brain regions. In comparison, PrP^{res} could be identified in every animal tested under these same conditions in 79A murine prion disease (n=3). This data indicates the presence of IHC detectable PrP^{d} in GSS/101LL animals, which correlates with regions of neurodegeneration, but is not PrP^{res}. Conversely, an extremely small quantity of PrP^{res} was observed in the cortex of some GSS/101LL mice, which is not associated with neurodegeneration identified in this chapter.

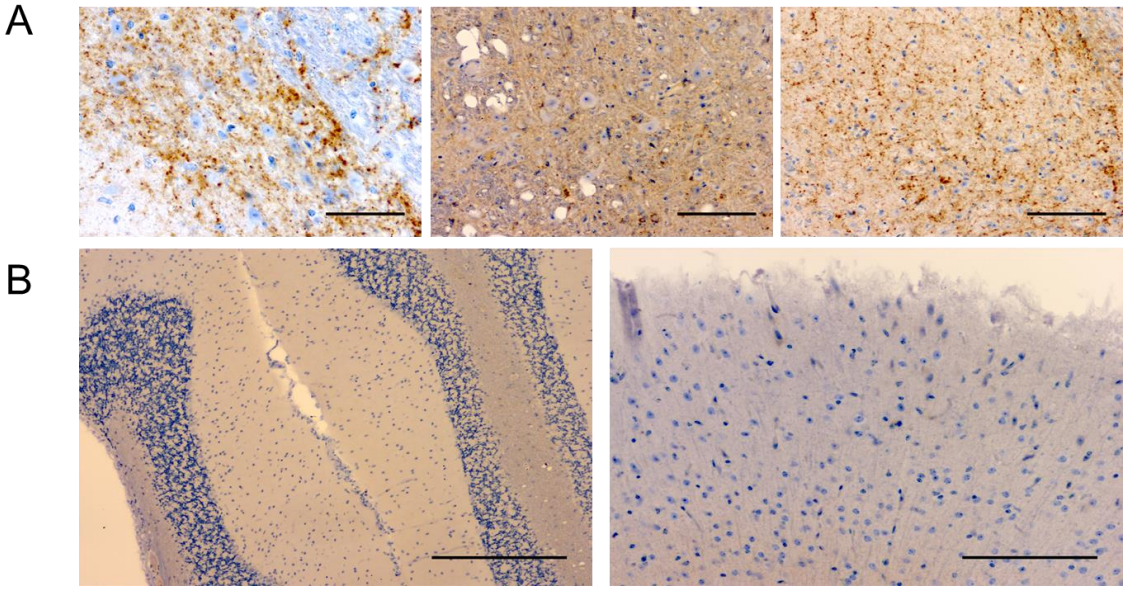

Figure 3.11 – PrP staining in regions of neurodegeneration (A) but none observed in regions of no overt neurodegeneration (B). (A) Left panel shows substantia nigra, pars compacta, middle panel shows medial raphe nuclei and right panel shows ventral-lateral thalamus. Scale bars = 50μm. (B) Left panel shows representative images of cerebellum and right panel shows representations of cortex of GSS/101LL animals. Scale bars = 100μm.

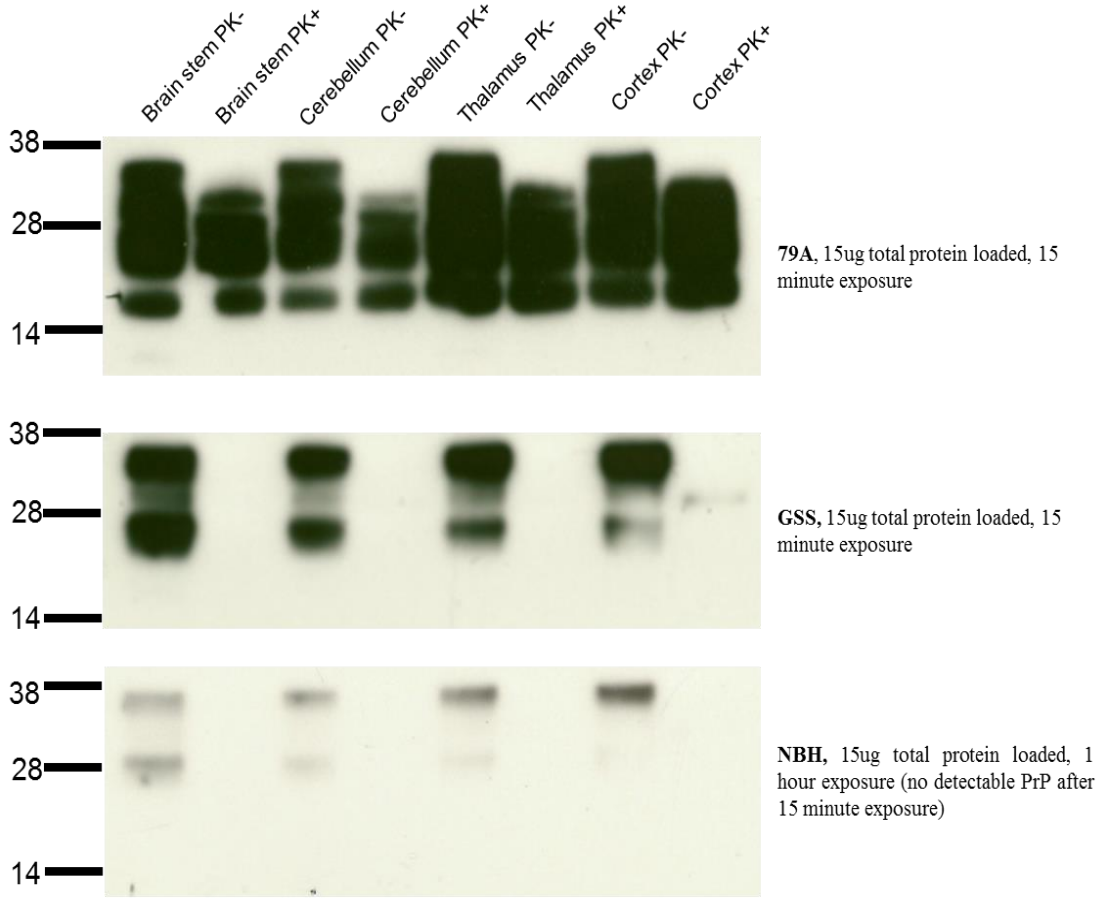

Figure 3.12 – Western blot for PrP. 79A shows large quantities of PrP, even after PK exposure, indicating PrP^{res} present in every brain region tested. GSS/101LL shows PrP staining but no PrP^{res} present in all brain regions with exception of a faint band in GSS/101LL cortex. This result occurred in two out of four animals GSS/101LL tested, the remain two samples did not show PrP^{res} detection in any brain region tested. NBH/101LL shows small quantities of PrP present and no PrP^{res}.

3.3. Results summary

- No significant changes in incubation period or in grey matter vacuolation in past and present models of GSS/101LL.
- Neurodegeneration, including neuronal loss, atrophy and synapse loss is observed in specific regions of the brain, such as: brain stem and thalamus
- Astrocytosis and microglial activation were restricted to regions of neurodegeneration

- Larger quantities of PrP^{d} identified in GSS/101LL animals compared to previous studies [41] using a modified IHC protocol
- No PrP^{res} isoform of PrP^{d} could be identified in regions of neurodegeneration
- Extremely small detection of PrP^{res} in cortex which does not correlate with neurodegeneration
- IHC detectable PrP^{d} is restricted to regions of the brain undergoing neurodegeneration

3.4. Discussion

In prion diseases PrP^{d}, as defined by IHC detection of PrP isoforms resistant to specific denaturing conditions and Western blot detection of PrP^{res}, is generally associated with regions of the brain undergoing neurodegeneration and glial cell responses. The establishment of animal prion disease models which provide exceptions to this are therefore useful platforms to further study and identify the species of PrP^{d} that are necessary and sufficient to cause neurodegeneration [28, 39-41]. The GSS/101LL model has previously been characterised to exhibit a highly infectious, invariably fatal neurodegenerative prion disease, but in the presence of extremely small quantities of PrP^{d} after infection with human GSS inoculum [41]. This model, however, does not show spontaneous disease associated with the human-like mutation at codon 101 either in this study or in previous studies [28, 41]. Further, in human GSS, a vast majority of the cortex suffers from heavy misfolded prion protein burdens and associated neurodegeneration. In this study, we show that the cortex does not suffer from such neuropathology. Therefore, this model is used as

a tool to study the association between PrP^d and neurodegeneration, but not necessarily as a model of human GSS.

The brains of GSS/101LL mice at clinical stages of disease were assessed for signs of previously described prion-associated pathology [189, 191-193, 204, 214, 217, 262, 263, 296, 303-307]. Loss of proteins the post-synapse (Drebrin) and in the dendrites of neurons (MAP2) in brain stem and thalamus, alongside neuronal loss concurs with previously defined pathology in murine models of prion disease [189, 191-193, 204, 214, 217, 262, 263, 296, 303-307]. No overt neurodegeneration could be detected in other regions, such as the cortex and cerebellum.

In prion diseases, changes in both astrocyte and microglial morphology occur concurrently with appearance of PrP^d, and prior to overt neurodegenerative phenotypes [189, 191]. In clinical stages of GSS/101LL animals, microglia and astrocytes change morphology to a phenotype typical of an activated cell. The absence of activated microglia or astrocytosis in other regions, such as cortex and cerebellum, is indicative that these regions remain pathologically "unaffected", as defined by neurodegeneration and glial cell responses.

There appears to be a difference in severity of vacuolation scoring in white matter tracts of archive and recent groups of GSS/101LL mice. The reason for these differences in the two cohorts used in this study is unclear. Vacuolation can occur as

a phenotype of ageing [316], however GSS/101LL animals from both cohorts (archive and recent) of mice used in this study were of comparable age. The human GSS inoculum used was from the same region of the same GSS brain used previously. The human GSS is sourced from the Edinburgh Brain Bank (see chapter 2) and tissue is obtained as a dissection of frozen tissue. It is feasible different quantities of PrP^{d} may be present between GSS tissue used in archive and recent experiments. If this were the case, it might be assumed the incubation periods between archive and recent experiments would differ significantly. However, previous studies have shown vacuolation lesion profiles are unaffected by dose of the agent [317] and furthermore the incubation periods of the two cohorts of animals were very similar. Therefore, the reasons for this difference in WM tracts are not known but importantly, the vacuolation severity appeared similar in grey matter regions of the brain between both groups.

To test whether the presence of extremely small quantities of PrP^{d} identified previously [41] is associated with pathology outlined in this chapter, IHC and Western blots were used to identify PrP^{d}. Following a previously published IHC protocol, very small quantities of PrP^{d} were identified – in accord with previous results [41]. Altering the protocol to autoclave in citric acid buffer instead of water revealed the presence larger quantities of PrP^{d} in GSS/101LL animals. The detection of PrP could not be identified in NBH/101LL animals and thus is a disease-specific conformation of prion protein, PrP^{d}. Moreover, the presence of IHC detectable PrP^{d} is associated with brain regions undergoing neurodegeneration. Western blot analysis however shows a small quantity of PrP^{res} in two of nine GSS/101LL tested cortex

samples. The cortex wasn't found to exhibit any overt neurodegeneration in this study, therefore suggesting the PrP^{res} species that are observed in the cortex in the two out of nine GSS/101LL animals is not associated with neurodegeneration. This demonstrates the requirement to study the GSS/101LL model in further detail to question the relationship between IHC detectable species of PrP^{d} and neurodegeneration.

In the brain stem and thalamus, which show IHC detectable PrP^{d}, but no PrP^{res}, the predominant species of PrP^{d} present is likely PrP^{sen}. It is becoming increasingly evident in many prion stains; both PrP^{res} and PrP^{sen} isoforms comprise total detectable PrP^{d} [308]. These results show that PrP^{sen} isoforms, rather than PrP^{res}, are directly, or perhaps indirectly, involved in driving neurodegeneration in prion diseases.

In summary this chapter shows PrP^{sen} isoforms of PrP^{d} are related to prion-associated pathological phenotypes. This data indicates that PrP^{sen} isoforms of PrP^{d} may represent the toxic species, however further elucidation of the temporal progression of disease is required to strengthen this association. In order to study the role of a predominantly PrP^{sen} isoform during disease, a time-course study of GSS/101LL animals was set up (see chapter 4). This will allow the comparison of progressive disease in GSS/101LL animals exhibiting predominantly PrP^{sen} isoforms of PrP^{d} to other models exhibiting both PrP^{sen} and PrP^{res} isoforms [308].

4. Time-course analysis of the GSS/101LL model

Chapter aim: To define the progressive pathology of the GSS/101L model from the perspective of understanding the relationship between PrP^d, neurodegeneration and glial cell responses. Multiple brain regions will be examined along a time-course to additionally assess spread of pathology.

4.1. Introduction

Chronic neurodegenerative diseases occur over extended periods of time; in some human prion disease cases the incubation period can be as long as 50+ years [318]. Long incubation periods also exist in murine models of prion disease, relative to their expected life-time [319]. This allows the study of the spread and progression of pathology using animal models of disease. Studies in animal models have indicated a predictable sequential and progressive set of events, beginning with detection of disease-associated misfolded protein concurrently with morphological glial cell responses [189, 191, 320-325]. Synaptic degeneration [186, 189, 191, 192, 204, 217, 238, 320, 326-331] and perineuronal net breakdown [237] are subsequently observed. Synaptic degeneration coincides with the onset of the behavioural [188] and electrophysiological deficits in mice [203]. As disease continues, pathology spreads to different regions of the brain [143, 144]. Finally, neuronal loss occurs followed by death of the animal [189, 216, 320]. This robust picture of progressive neurodegeneration provides a platform for further studies to compare and contrast models of chronic neurodegeneration.

The progression of neurodegeneration has been best defined in the hippocampus, due to its well-defined anatomy and functional role. These studies have demonstrated that synapses degenerate prior to neuronal cell loss [189, 191, 217, 320, 328, 329]. It is important to note, however, that different regions of the brain appear to exhibit different neuronal targets – for example, pre-synaptic vesicles correspond to the earliest observable neurodegenerative phenotype in the hippocampus of two murine models of prion disease [189, 191, 192], but the post-synaptic density appears to be the initial target in the cerebellum [238]. Nevertheless, morphological glial cell responses and PrP^{d} deposition occur prior to detectable neurodegeneration. Therefore, the identification of these events is indicative of the initiation of a pathway leading to neurodegeneration, prior to overt signs of neurodegeneration.

The spread and distribution of pathological lesions throughout the incubation of a number of chronic neurodegenerative diseases has been extensively mapped [143, 144, 303]. This occurs in a pattern suggesting spread along neuronal pathways [281, 283, 284]. The precedence of the transmissible properties in prion diseases has led to the notion that disease-associated misfolded proteins can spread in a "prion-like" mechanism [146, 154, 161, 286-293]. The association between misfolded proteins and neurodegeneration in multiple models of chronic neurodegeneration has led to the hypothesis that preventing the spread of disease-associated proteins may be an important therapeutic target [332].

Murine models of prion disease, particularly those studied in extensive detail such as ME7 or RML [186, 188, 189, 191, 192, 203, 204, 217, 237, 238, 326], demonstrate the association between detection of accumulated PrP^{d} and neurodegeneration. In all cases, a morphological glial cell response occurs concurrently or immediately after detection of PrP^{d}. The PrP^{d} is commonly detected using IHC or Western blot. In the instance of Western blot, the PrP^{res} isoform is the desired conformation of interest. As mentioned previously, it is becoming increasingly evident that PK-sensitive isoforms of PrP^{d}, PrP^{sen}, are present in prion diseases known to accumulate large quantities of PrP^{res} [308]. These studies highlight a probable relationship between PrP^{d} and neurodegeneration but are not sufficient to establish whether limited subsets of isoforms are responsible for progressive neurodegeneration. Results outlined in chapter 3 highlight the presence of a predominant PrP^{sen} species of PrP^{d} in region of the brain undergoing overt neurodegeneration in the GSS/101LL model. Although very limited amounts of PrP^{res} were detected in some GSS/101LL cortex samples, this was not associated with neurodegeneration or glial cell responses. As a result, understanding the sequential order of pathological events will be important for understanding the relationship between the PrP^{sen} isoforms detected in GSS/101LL animals and neurodegeneration. Similarly important is whether the spread of lesions between brain regions takes place in a sequence related to neuronal connectivity.

4.2. Results

As described in chapter 3, the incubation period of previous studies using the GSS/101LL model is approximately 286.66 ± 2.95 days (archive group). Therefore, a study to examine pathology at a number of stages during disease progression was set

up. Since previous studies examining murine prion strains have demonstrated initial signs of pathology from between 40-50% incubation period, this study examined five time-points. These were 150dpi, 200dpi, 220dpi, 240dpi and clinical stages (terminal) – see figure 4.1B. The incubation period measured in GSS/101LL animals progressing to clinical stages of disease was 291.11 ± 5.29 days. All mice were genotyped to ensure the P101L alteration appears within the mice in the study (figure 4.1A) [28].

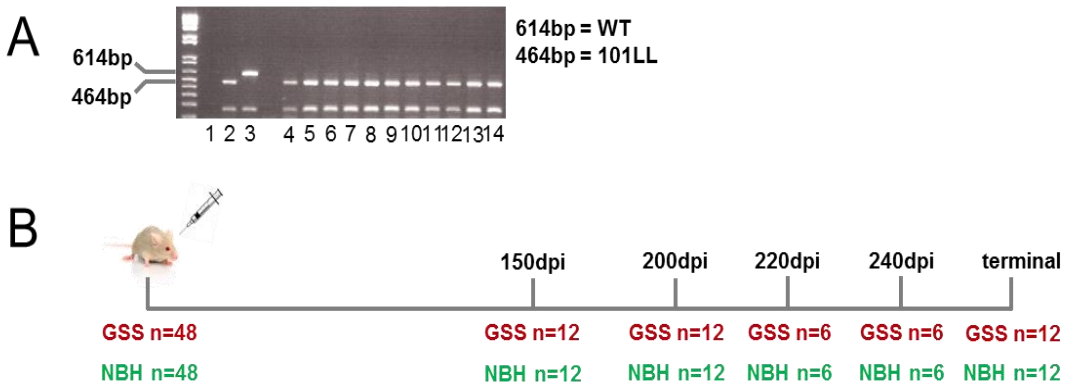

Figure 4.1 - Time-course of GSS/NBH transmission. A total of 96 101LL mice were bred and genotyped. A – 1 = water (no DNA). 2 = 101LL positive control. 3 = WT control. 4-14 = experimental animals. All animals were found to exhibit the proline to leucine alteration at codon 101. B – animals were either injected with 1% human GSS frontal cortex homogenate or 1% uninfected hamster brain homogenate. All animals were between 6-8 weeks of age at time of injection. Mice were subsequently culled at 150, 200, 220 and 240 days post inoculation and another group was left to progress to overt clinical stages (terminal), at which point animals were culled for ethical considerations.

4.2.1. PrP^d is observed at 150dpi in GSS/101LL animals

The same IHC protocol with citric acid buffer-autoclave and BH1 antibody, as described in chapter 3 was used to assess the targeting of PrP^d at early stages of disease. GSS/101LL animals at 150dpi were stained and compared to NBH/101LL. Non-specific antibody isotype control (IgG1) was used to determine whether non-

specific staining is occurring. Serial sections through numerous regions of the brain were used, including; medulla, pons, cerebellum, midbrain, hippocampus, thalamus, hypothalamus, cortex (Bregma -1 to -3) and striatum, as described in chapter 2.

Figure 4.2A shows PrP staining within midbrain. This was observed in five of twelve GSS/101LL mice in this group. No other detectable PrP could be identified across all other regions; figure 4.2B shows typical examples of medulla and thalamus sections with no PrP staining. The PrP staining observed is not present in region matched sections of NBH/101LL animals. Additionally, the isotype control does not demonstrate staining. This shows the accumulation of PrP^d restricted to the midbrain at 150dpi in GSS/101LL animals. The staining observed is associated with neurons of the midbrain, such as the interpeduncular nuclei which innervate the medial lemniscus and substantia nigra, pars compacta (SNc).

PrP^d was not observed in the surrounding medial lemniscus, despite the relatively large number of axons which comprise this white matter tract from affected neurons. This could either be a result of restricted targeting of PrP^d to the neuronal soma which does not allow the axonal migration of the agent, or a technical inability to identify PrP^d in axons. Nevertheless, these results demonstrate the initial targeting of PrP^d to the midbrain.

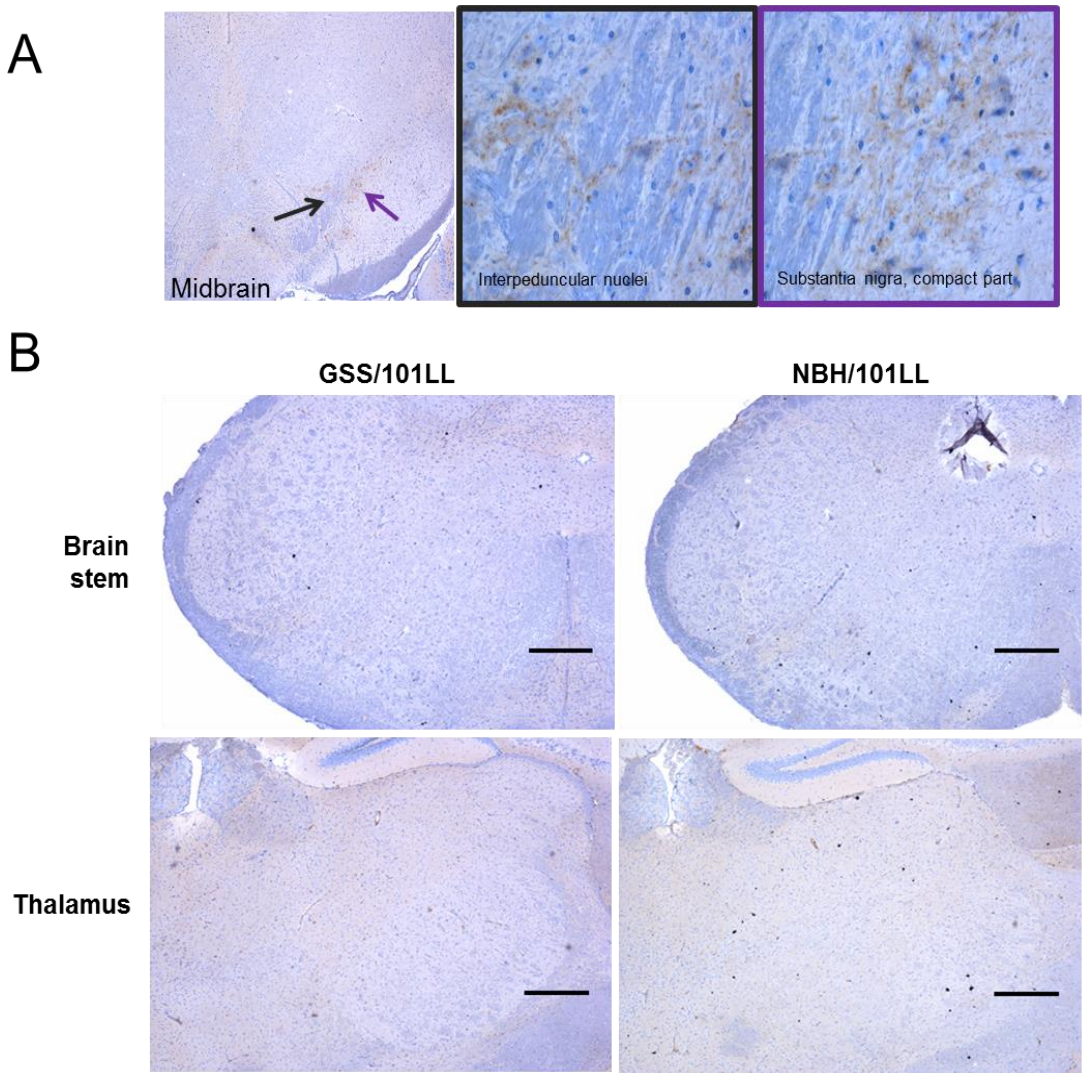

Figure 4.2 - PrP staining at 150dpi in 101LL mice. A – PrP is detected in the midbrain. Specifically, this appears to be associated with the interpeduncular nuclei innervating the medial lemniscus (purple arrow and box) and also in the substantia nigra, compart part (black arrow and box). (B) No PrP staining could be observed in other regions of the brain, including the medulla and thalamus (left panel). No PrP deposition could be detected in NBH aged matched controls (right panel). Scale bars = 200μm.

4.2.2. No glial cell responses are detected at 150dpi

Previous studies have shown glial cell responses occur concurrently, or shortly after initial detection of PrP^d [189, 191, 325]. This glial cell activation phenotype is also observed association with deposits of misfolded protein in other neurodegenerative diseases [321, 322]. The morphological alterations of both microglia and astrocytes can therefore be indicative of early pathological events in the incubation period (see

1.4.4. Astrocytes and prion disease and *1.4.5. Microglia and prion disease*). To assess the possible morphological activation of glial cells at 150dpi, antibodies against GFAP were used.

The neurons of the midbrain which are associated with PrP^d deposition at this stage do not concur with a morphological alteration of glial cells as determined by GFAP staining (figure 4.3B). An up-regulation of GFAP comparative to NBH/101LL controls does occur in the medial lemniscus. As these midbrain neurons, such as the interpeduncular nuclei, project axons in the medial lemniscus, this could possibly be indicative of down-stream effects of PrP^d detection associated with the neuronal cell bodies. The morphology of the astrocytes up-regulating GFAP is characteristic of fibrous astrocytes which are known to commonly up-regulate GFAP even in uninfected brains (see *1.4.4. Astrocytes and prion disease*). Nevertheless, this up-regulation comparative to NBH/101LL region matched controls appears to be a common phenotype across all GSS/101LL animals tested at this stage of disease. In regions which do not show any detection of PrP^d, such as the brain stem, there were no apparent differences in GFAP staining intensity or morphology of astrocytes (figure 4.3A). During prion disease, the number of GFAP positive astrocytes increases [262]. It is important to recognise that the increase in GFAP positive astrocytes may not reflect an increase in the absolute number of astrocytes but up-regulation of the expression of GFAP [280]. Overall, whether a glial cell response occurs as a result of the accumulation of PrP^d in the midbrain at 150dpi is inconclusive.

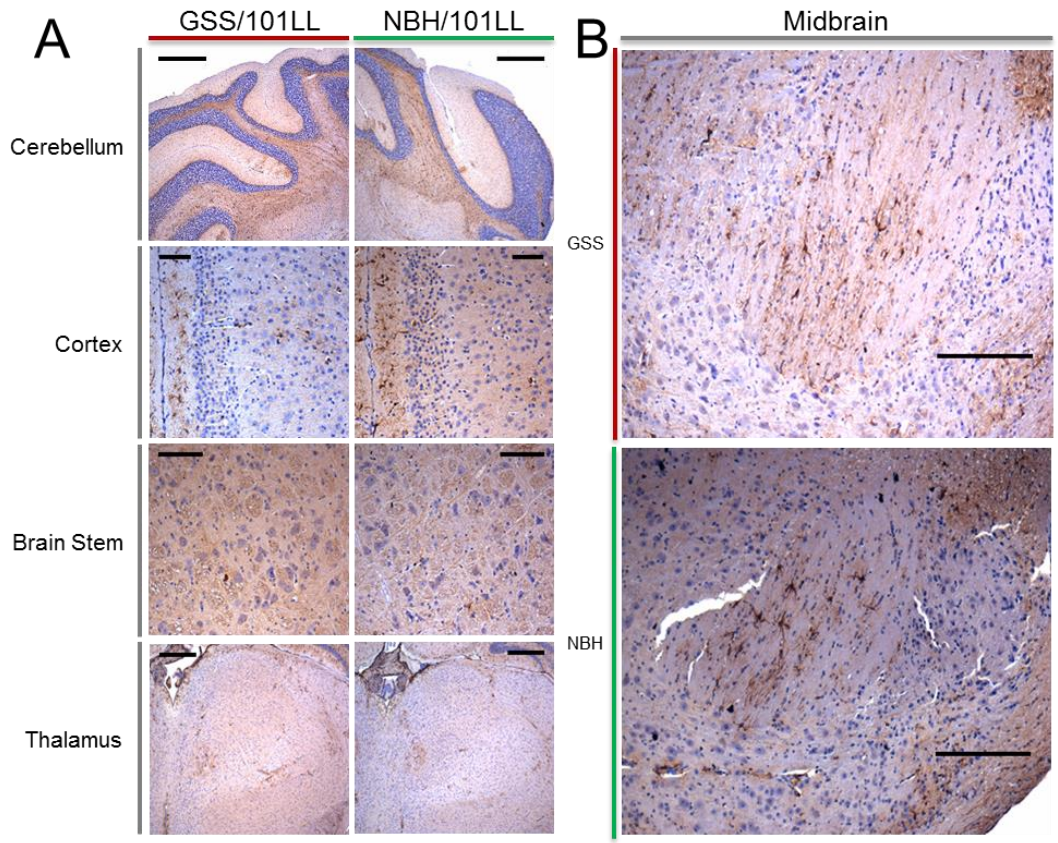

Figure 4.3 – GFAP staining at 150dpi. **(**A) GFAP staining in cerebellum, cortex, brain stem and thalamus. Cerebellum and thalamus scale bars = 100μm. Cortex and brain stem scale bars = 50μm. (B) GFAP staining midbrain where PrP^d has been detected. In cerebellum, cortex, brain stem and thalamus there is no observable GFAP up-regulation or astrogliosis. In midbrain, fibrous astrocytes appear to exhibit minor increases in GFAP but this is not extended to protoplasmic astrocytes and occurs in both GSS and NBH/101LL animals. Scale bars = 100μm.

4.2.3. No neuronal deficits are observed at 150dpi

The detection of PrP^d associated with the interpeduncular nuclei and SNc indicates possible neuronal deficits. To examine whether morphological or structural changes have arisen in association with the deposited PrP^d, antibodies to MAP2 were used to assess neuronal structure. Figure 4.4B demonstrates no detectable change in neurons associated with the GSS/101LL midbrain compared to NBH/101LL animals at 150dpi. Similarly, figure 4.4A shows no change in MAP2 staining pattern in any brain region examined.

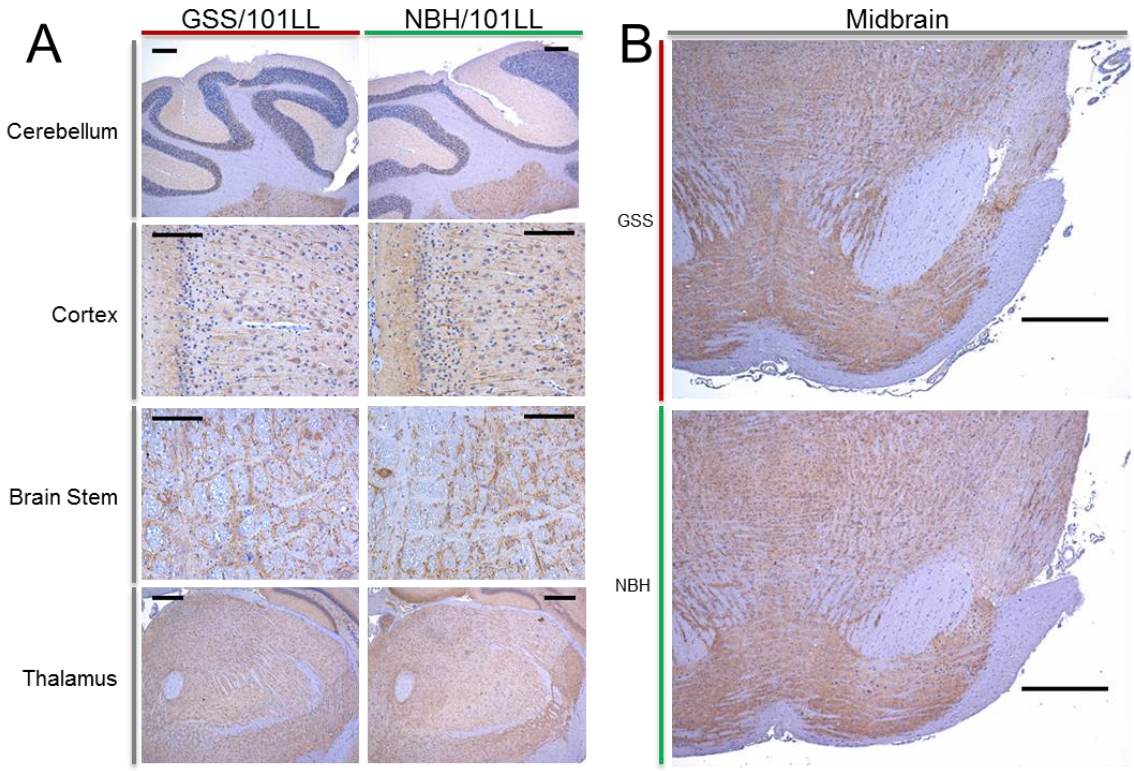

Figure 4.4 – MAP2 staining at 150dpi. (A) MAP2 staining in cerebellum, cortex, brain stem and thalamus shows no change in staining quality or intensity between GSS or NBH/101LL animals. Cerebellum, cortex and brain stem scale bars = 50µm. Thalamus scale bars = 100µm. (B) MAP2 staining in midbrain, which is where initial PrP^d accumulation is observed. No change in staining quality or intensity is observed between GSS or NBH animals. Scale bars = 200µm.

The neurons of the SNc are known to synthesise large quantities of dopamine for neurotransmission and express high levels of tyrosine hydroxylase. Using antibodies specific for this enzyme thus allows the level of expression of this critical enzyme and the number of neurons to be assessed. No detectable differences could be observed in the quality of staining in tyrosine hydroxylase positive neurons at this time-point (figure 4.5). Together, this data suggest that there are no structural or functional deficiencies in SNc or interpeduncular neurons, which are associated with PrP^d accumulation, at 150dpi.

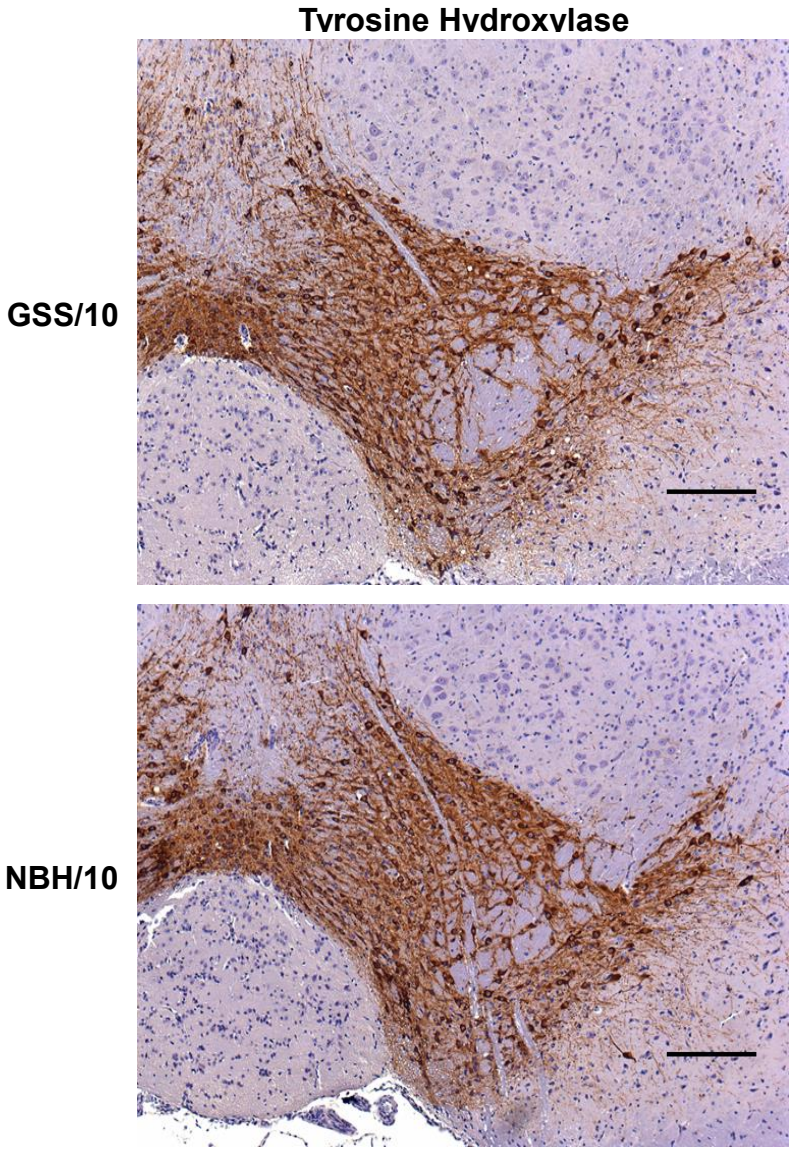

Figure 4.5 – Tyrosine hydroxylase staining at 150dpi of the midbrain nuclei. No change in staining quality or intensity could be observed between GSS or NBH/101LL animals at this stage indicating no loss of tyrosine hydroxylase staining in neurons associated with PrP^d at this stage. Scale bars = 100μm.

4.2.4. Glial cell responses are observed at 200dpi, prior to neuronal deficits

The neuronal-associated PrP^d observed in GSS/101LL animals at 150dpi exhibits a similar staining pattern at 200dpi in the midbrain (figure 4.6), but observed in a higher proportion of animals tested; in eight of twelve GSS/101LL mice. The detectable PrP^d remained restricted to the SNc and interpeduncular nuclei at this

time-point (figure 4.6). When using antibodies against GFAP and Iba1, the glial cells in GSS/101LL animals in the SNc had undergone cell body hypertrophy with shortening and thickening of cell processes (figure 4.8A). These morphological changes are typical of activated microglia and reactive astrogliosis. Five serial sections through the midbrain were used to count the number of microglia identified using Iba1 in the SNc. No increase in average number of microglial cells per tissue section could be detected at this time-point in GSS/101LL animals despite the morphological changes of these cells (t-test; p=0.26, figure 4.7). An increase in the number of microglia in the substantia nigra, pars reticularis (SNr) is observed (t-test; p=0.0196, figure 4.7). This is a region which does not exhibit detectable PrP^d at this stage (figure 4.6), but there is high connectivity between different parts of the substantia nigra [333]. No glial cell responses could be observed in medulla, thalamus, cortex or cerebellum (figure 4.8B). This demonstrates a glial cell response specifically in regions of the brain exhibiting PrP^d. Neuronal structure in the midbrain was assessed using antibodies specific to tyrosine hydroxylase (figure 4.9). No qualitative difference in staining between GSS/101LL animals and NBH/101LL could be observed. Together, this data indicates the initial detection of PrP^d, followed by glial cell responses – both occurring prior to detectable neuronal deficits.

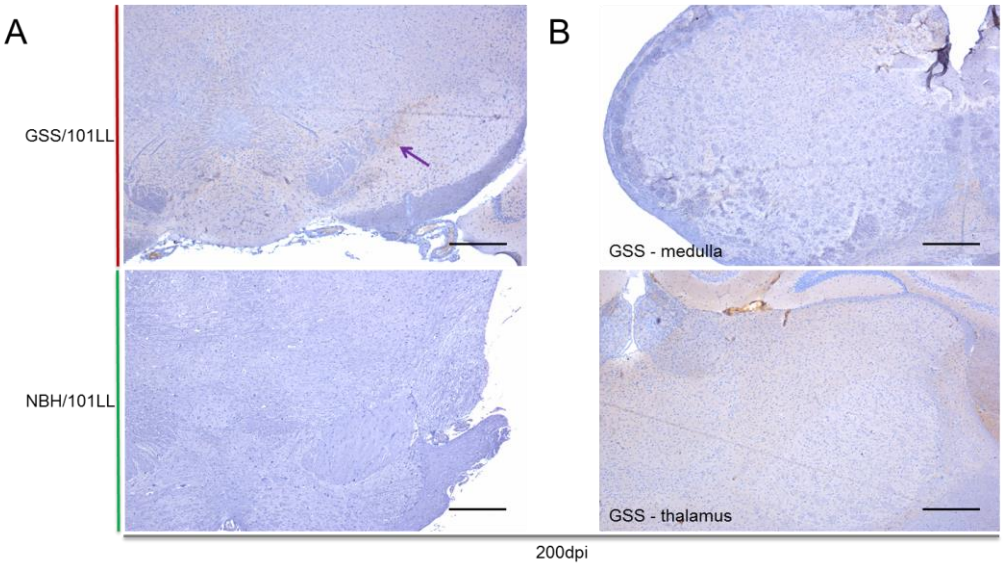

Figure 4.6 – PrP staining at 200dpi. (A) Staining was observable in midbrain neurons (indicated by arrow), similar to 150dpi but no staining could be observed in other regions, for example, medulla or thalamus (B).

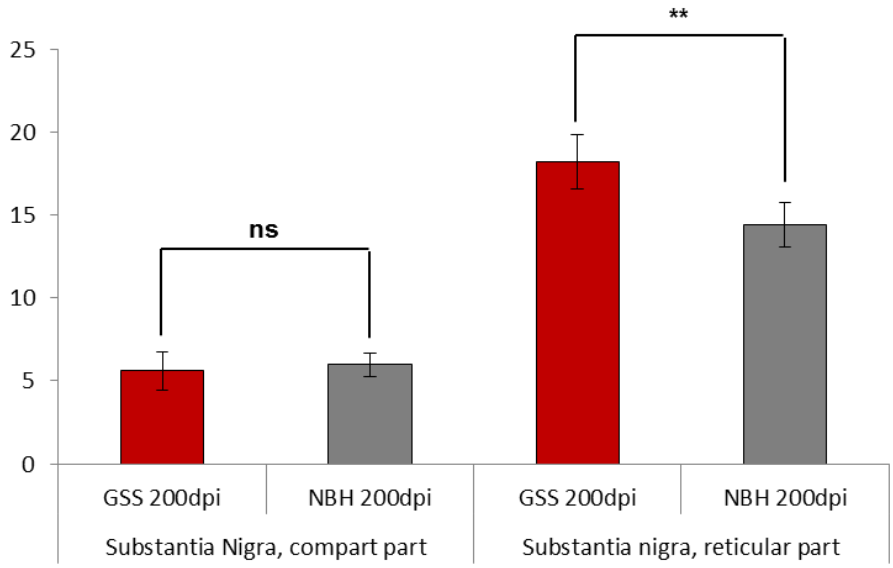

Figure 4.7 – Quantification of microglial cell number in SNc and SNr. No significant change could be observed in microglia cell number between GSS and NBH/101LL animals in SNc (t-test; p=0.26). A significant increase in number of microglial cells could be observed between GSS and NBH/101LL animals in the SNr (t-test; p=0.0196). SNc = substantia nigra, pars compacta. SNr = substantia nigra, pars reticularis.

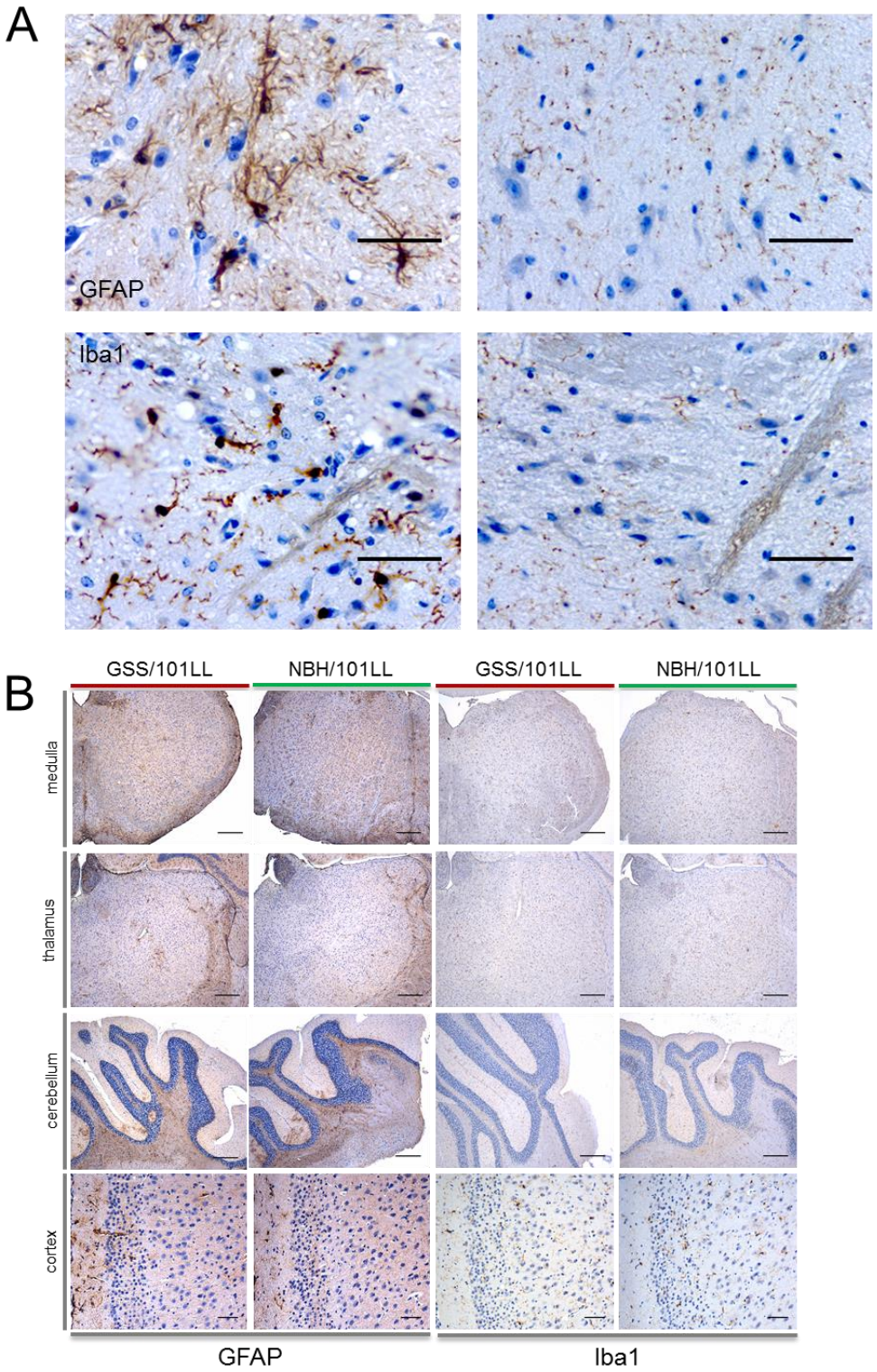

Figure 4.8 – Glial cell responses at 200dpi in SNc. (A) GFAP and Iba1 staining. Left panels represent GSS/101LL animals, right panels represent NBH/101LL animals. Significant morphological glial cell responses are observed using both glial cell markers. Scale bars = 50µm. (B) No glial cell changes in morphology could be observed between GSS and NBH/101LL animals in other regions of the brain, such as brain stem, thalamus, cerebellum or cortex. Cortex scale bars = 50µm. Medulla, thalamus and cerebellum scale bars = 200µm.

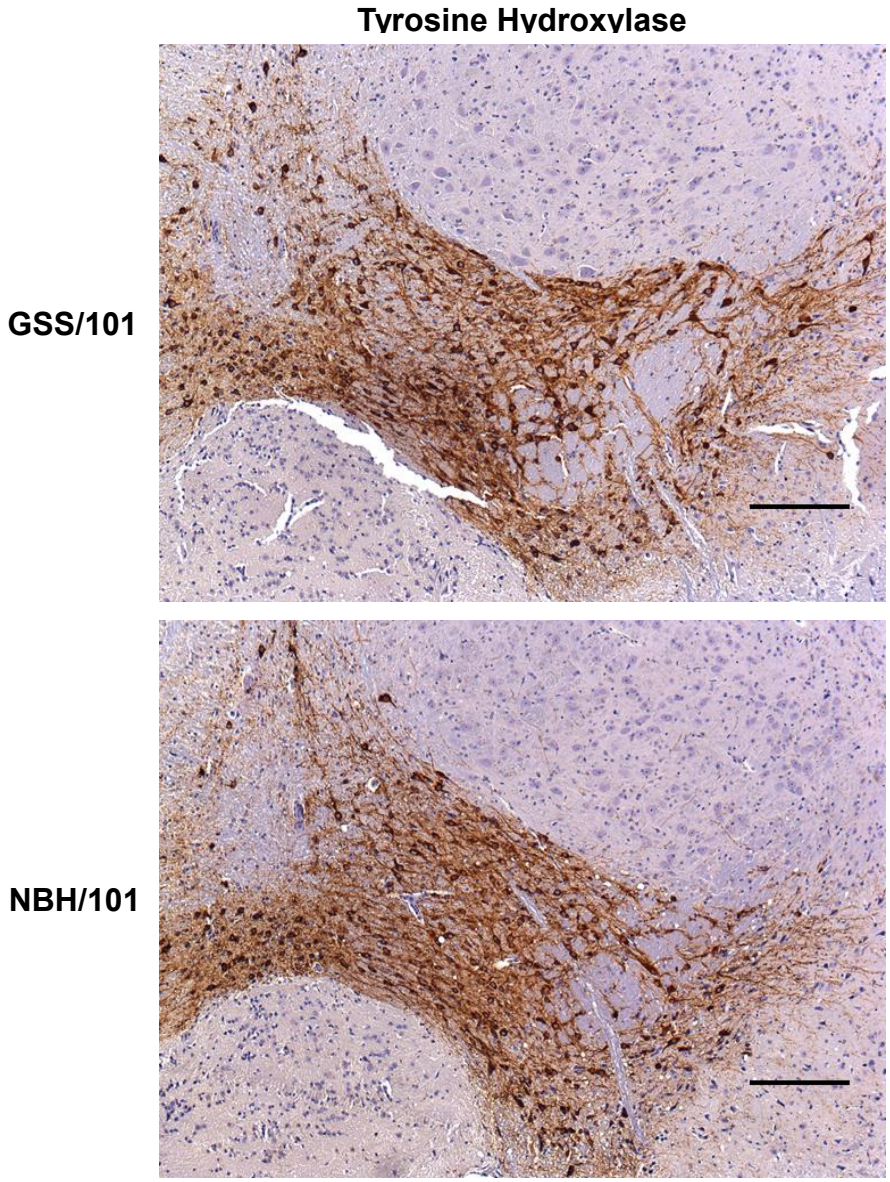

Figure 4.9 – Tyrosine hydroxylase staining at 200dpi of the midbrain nuclei. No change in staining quality or intensity could be observed between GSS or NBH/101LL animals at this stage indicating no loss of tyrosine hydroxylase staining in neurons associated with PrP^d and glial cell responses at this stage. Scale bars = 100μm.

4.2.5. PrP^d accumulation occurs in a pattern akin to neuronal connectivity

The spread of pathological lesions around the CNS in chronic neurodegenerative diseases is a well-established phenomenon [143, 144]. The detection of PrP^d associated with midbrain neurons raises the prospect that PrP^d and/or neurodegeneration/glial cell responses may follow a predictable pathway, based on

our understanding of neuroanatomy. The interpeduncular nucleus has been shown to be connected to neuronal populations of the brain stem, such as the medial and dorsal raphe nuclei [334, 335]. The dorsal raphe nuclei, for example, project axons to numerous regions of the brain, such as the striatum [336], the medial prefrontal cortex [337], the cerebellum [338, 339] and the paraventricular nucleus of the thalamus [340]. The interpeduncular nuclei also receive numerous innervations from the habenula [341]. The SNc exhibits extensive connectivity with other neurons of the midbrain, especially with the SNr [333]. The major thalamic projection of the SNr is to the ventromedial (VM) thalamus [342]. The SNc also has numerous afferent and efferent connections with the striatum [343]. This allows a platform to test the localisation of PrP^d accumulation along well-established neuronal pathways, which are highlighted in figure 4.10, and compare them to the development of neurodegeneration or glial cell responses.

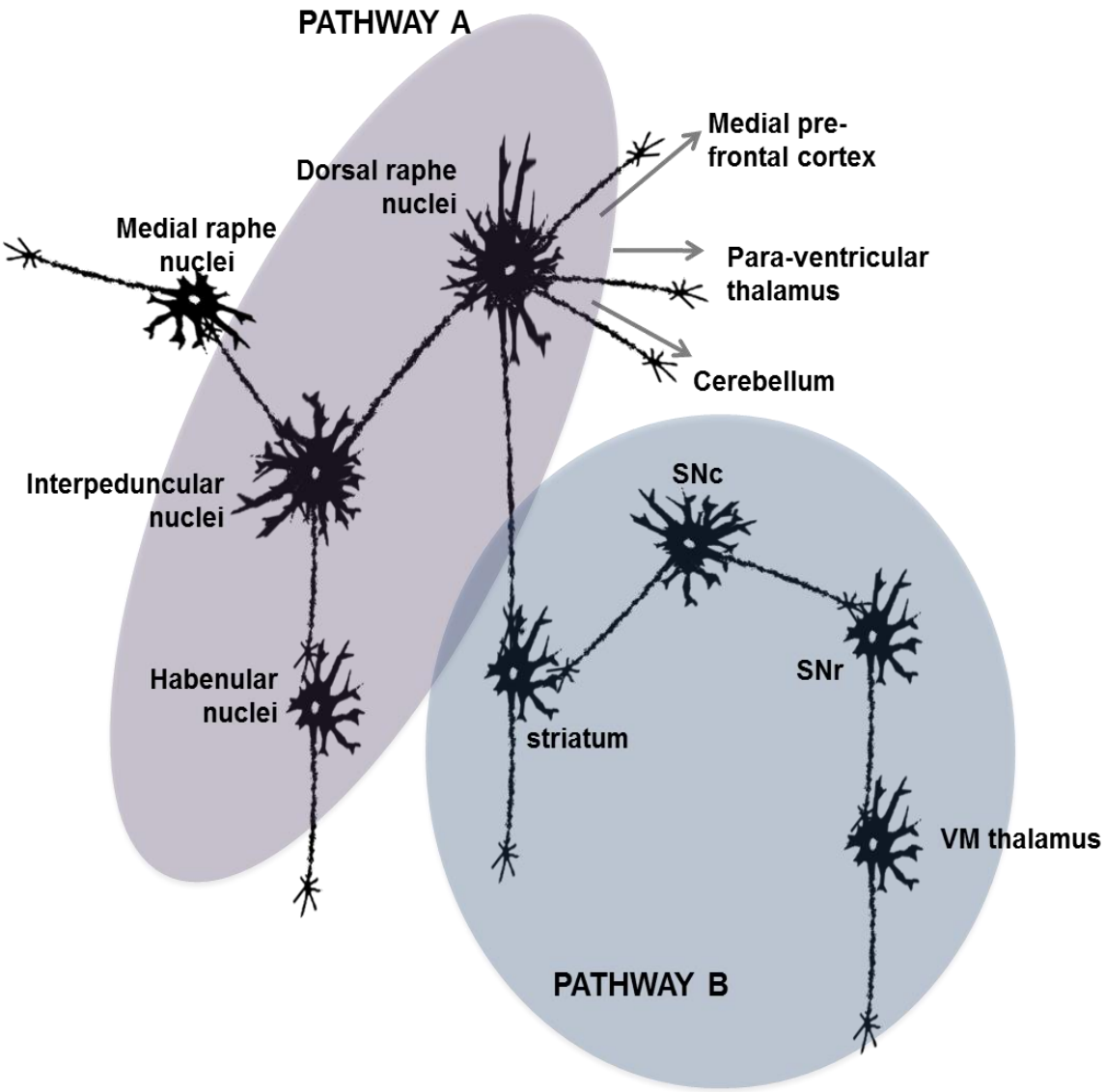

Figure 4.10 – Neuronal networks of the interpeduncular nuclei and SNc. Pathway A – This represents the neuronal connections of the interpeduncular nuclei. The habenula nuclei project axons to the interpeduncular nuclei. These nuclei then project axons to the dorsal and medial raphe nuclei. Further axons are then projected from the dorsal raphe nuclei to other regions such as medial pre-frontal cortex, paraventricular thalamus, cerebellum and striatum. Pathway B – This represents neuronal connections of the SNc. The SNc project most axons either to the SNr or striatum. Down-stream axons are then projected from the SNr to the VM thalamus.

Using PrP specific antibodies on GSS/101LL and NBH/101LL animals at 220dpi, PrP could be detected in brain stem regions such as the medial raphe nuclei and dorsal raphe nuclei specifically in GSS/101LL animals (figure 4.11). This is of interest as the interpeduncular nuclei and the brain stem exhibit known neuronal

connections [334, 335]. No PrP^d could be observed in the paraventricular thalamus or cerebellum, which are known to be connected to the dorsal raphe nuclei [339, 340], indicating a limited distribution of misfolded protein accumulation which is not associated with further down-stream brain regions at this stage. In addition, no PrP^d could be observed in the habenula, which is known to exhibit anterograde projections to the interpeduncular nuclei [341].

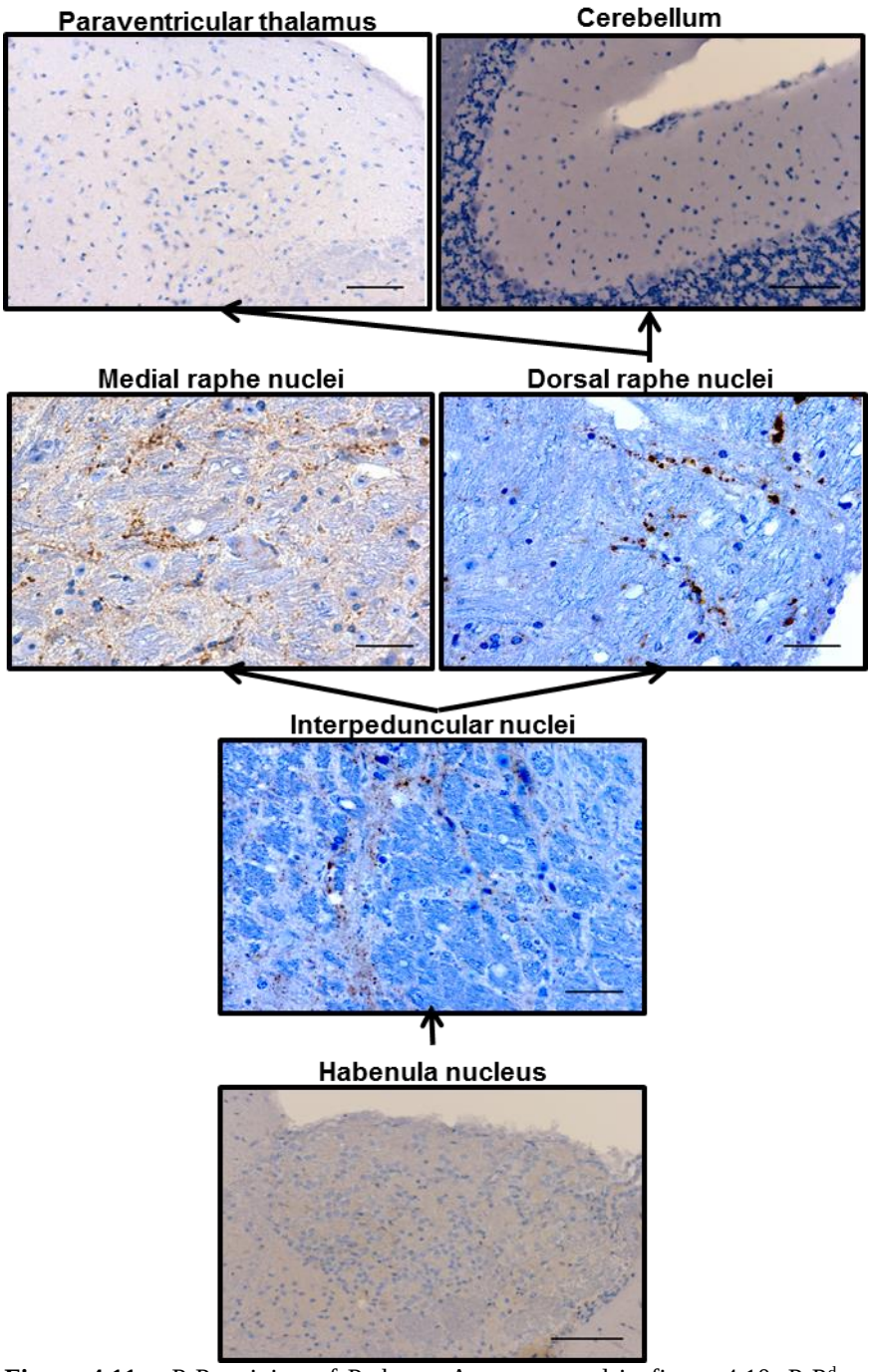

Figure 4.11 – PrP staining of Pathway A, represented in figure 4.10. PrP^d staining is observed in interpeduncular nuclei, dorsal raphe nuclei and medial raphe nuclei. No PrP staining could be observed in the paraventricualr thalamus, cerebellum or habenula nuclei. Cerebellum and habenula scale bars = 100µm. Thalamus, brain stem and midbrain scale bars = 50µm.

PrP^d could also be observed in the SNr neurons of the midbrain at this time-point (figure 4.12). This is of particular relevance due to the known connectivity between

the SNc and SNr [333]. No PrP^d could be observed in the VM thalamus or the striatum in GSS/101LL animals at this time-point (figure 4.12).

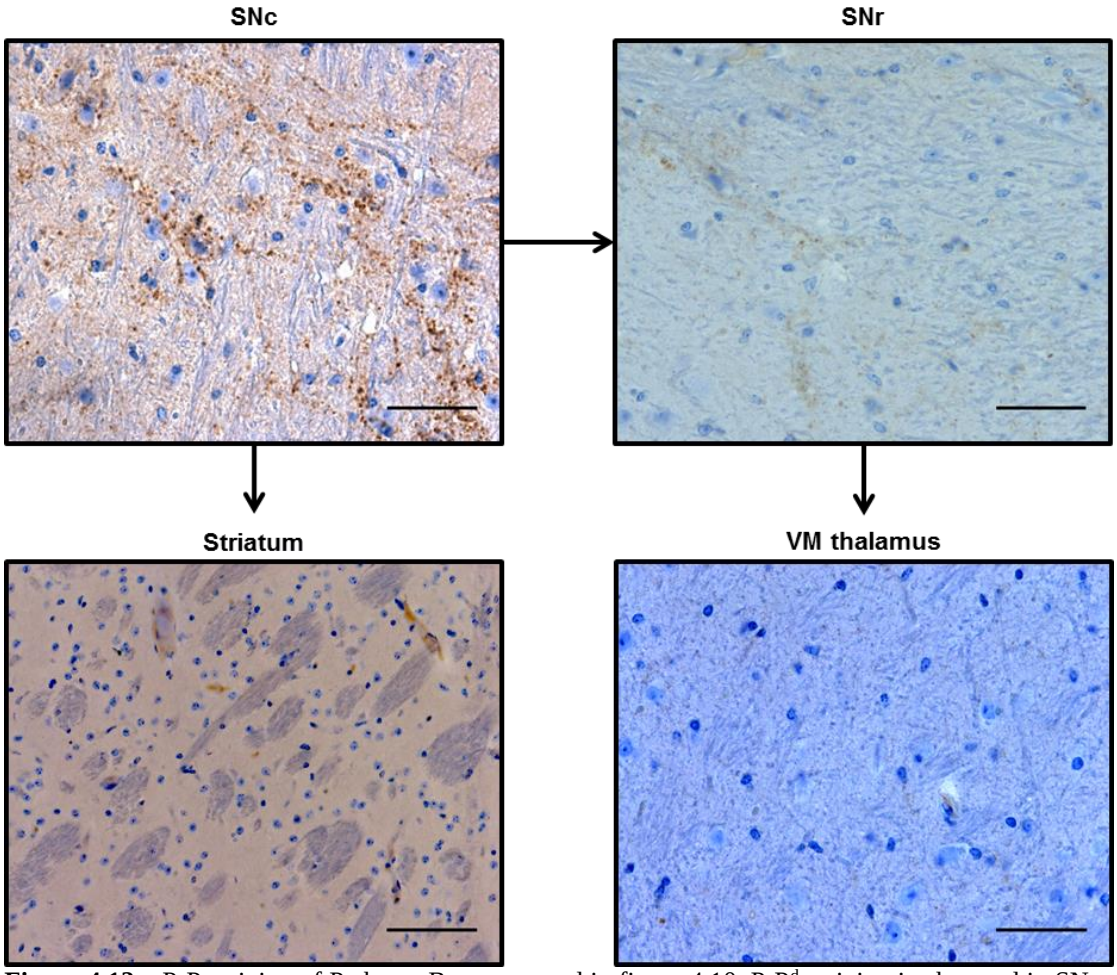

Figure 4.12 – PrP staining of Pathway B, represented in figure 4.10. PrP^d staining is observed in SNc and SNr. No PrP staining could be observed in the striatum or VM thalamus at this stage, indicating a spead of PrP^d along a specific neuronal pathway. Scale bars = 50μm.

4.2.6. Pathological spread is associated with regions of PrP^d accumulation

The distribution of PrP^d between midbrain and brain stem populations represents an ideal platform to study the association between PrP^d accumulation, the glial cell response and neurodegeneration between neuroanatomical distinct regions. Due to the sensitivity of glial cells as markers of neurodegeneration, these cells were assessed at 220dpi in the medial raphe nuclei of the brain stem. A notable alteration in cellular morphology of both astrocytes and microglia was observed in the medial raphe nuclei (figure 4.13). No glial cell response was observed in any part of the thalamus, striatum, cerebellum or retrosplenial granular cortex at this time-point (figure 4.13).

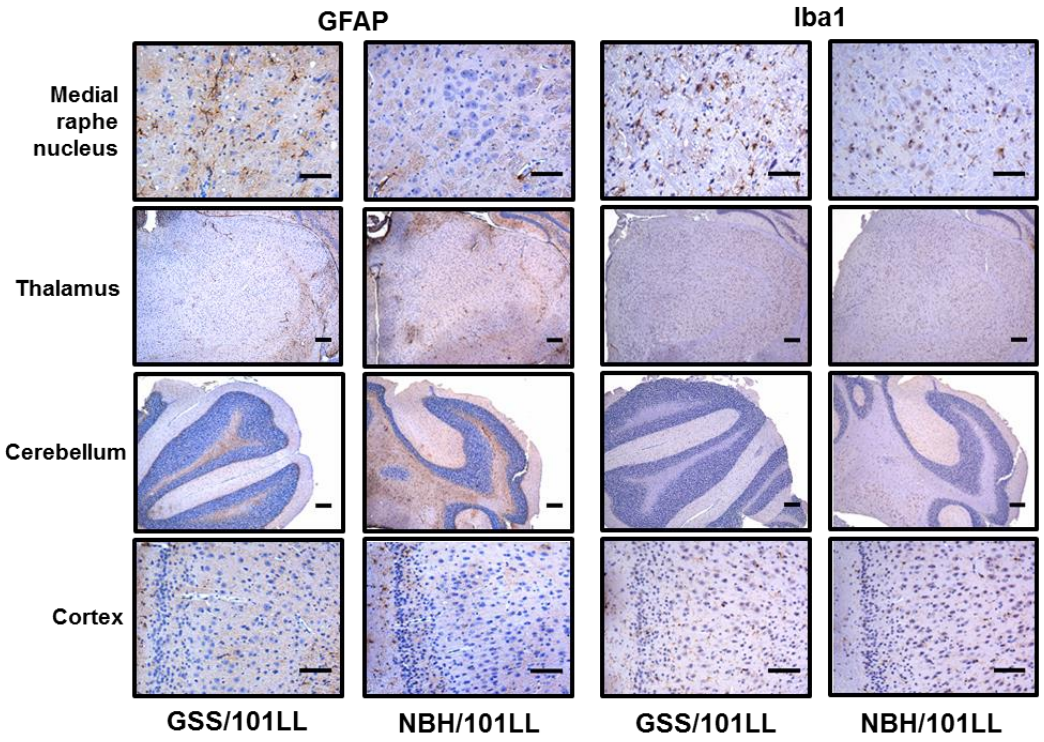

Figure 4.13 – Glial cell responses at 220dpi. GFAP and Iba1 show astrocytosis and activated microglia associated with the medial raphe nuclei of the brain stem at this stage. No other glial cell responses were observed in other brain regions such as thalamus, cerebellum or cortex at this stage. Scale bars = 50μm.

Due to limited tissue availability, the dorsal, medial raphe nuclei, SNc or interpeduncular nuclei were not available to be assessed for neuronal deficits. Alternatively, the neuronal structure was assessed in other parts of the brain stem, such as the Gi nuclei, which as shown in chapter 3, undergoes neurodegeneration. Using antibodies specific to MAP2, as described previously at 220dpi, the MAP2 staining quality was consistent with that of NBH/101LL brain stem (figure 4.14). At 240dpi, the Gi nuclei are present (figure 4.14A; green arrow), but have lost MAP2 staining. Hypertrophy of dendritic processes also occurs in this region (figure 4.14A; black arrow). This is a process known to occur in synaptic varicosities in other murine models of prion disease [204]. No change in MAP2 staining quality could be observed in other regions such as the retrosplinal cortex in GSS/101LL animals compared to NBH/101LL animals (figure 4.14B).

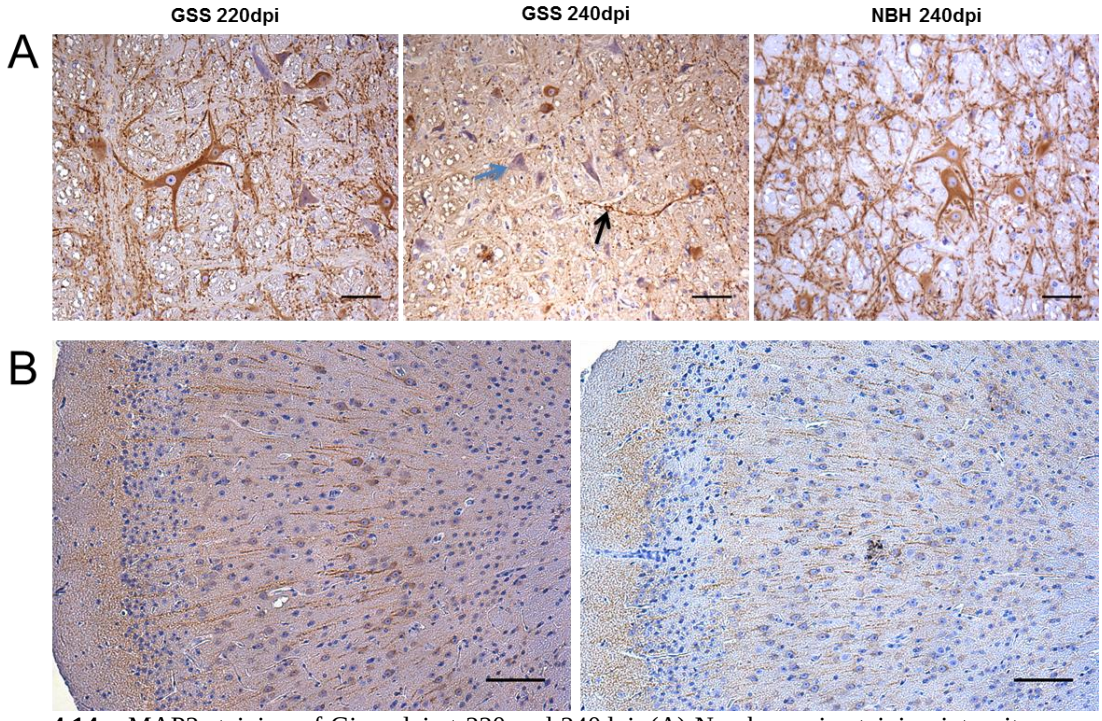

Figure 4.14 – MAP2 staining of Gi nuclei at 220 and 240dpi. (A) No change in staining intensity or quality could be observed in the GI nuclei at 220dpi compared to NBH. A significant loss of MAP2 staining is observed in the Gi nuclei at 240dpi in GSS/101LL animals. Neurons still remain at this stage in this neuronal population, green arrow, but have lost MAP2 staining. Hypertrophy of the dendritic process is also observed at this stage in MAP2 stained neurons, black arrow. Scale bars = 20μm. (B) No change in staining intensity or quality between GSS/101LL cortex (right) or NBH/101LL cortex (left). Scale bars = 50μm.

Upon clinical onset of disease, VM thalamic MAP2 staining appeared substantially reduced (figure 4.15). The neuronal deficits observed in the thalamus at clinical stages of disease are similar to those observed in chapter 3, whereby MAP2 staining is generally lost in the ventral-lateral parts of the thalamus, but some neurons remain with MAP2 positive staining. To confirm the presence of PrP^{d} spread to this region, PrP was assessed using IHC in GSS/101LL and NBH/101LL animals. PrP staining was observed in the thalamus of GSS/101LL animals at clinical stages of disease, but not in NBH/101LL animals (figure 4.16). In addition, the staining intensity of PrP^{d} in the midbrain, for example, appears substantially increased compared to earlier stages

of disease. This data reaffirms the association between the IHC detectable PrP^d and neurodegeneration.

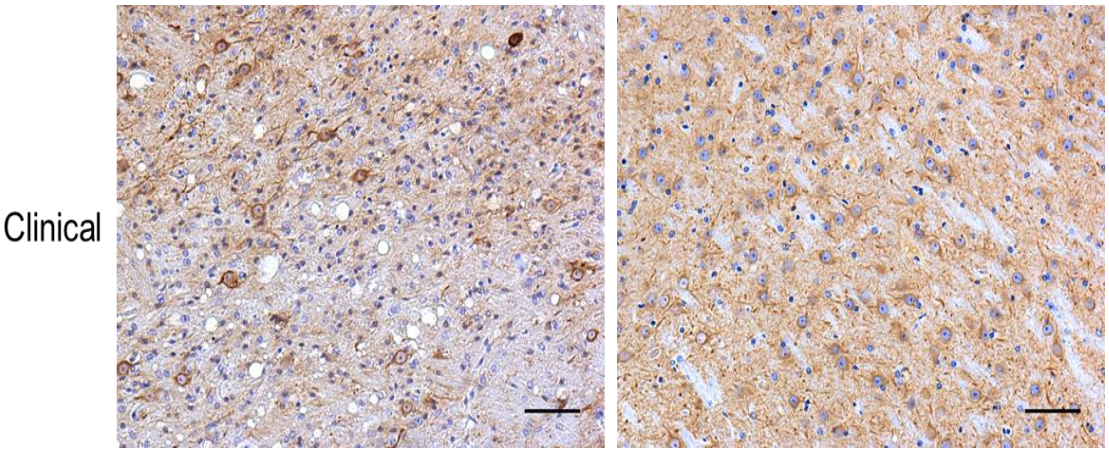

Figure 4.15 – MAP2 staining at clinical stage pathology in VM thalamus. Left panel represents GSS/101LL animals, right panel represents NBH/101LL animals. Significant loss of MAP2 staining is observed. Neurons which remain still retain MAP2 staining. Scale bars = 50µm.

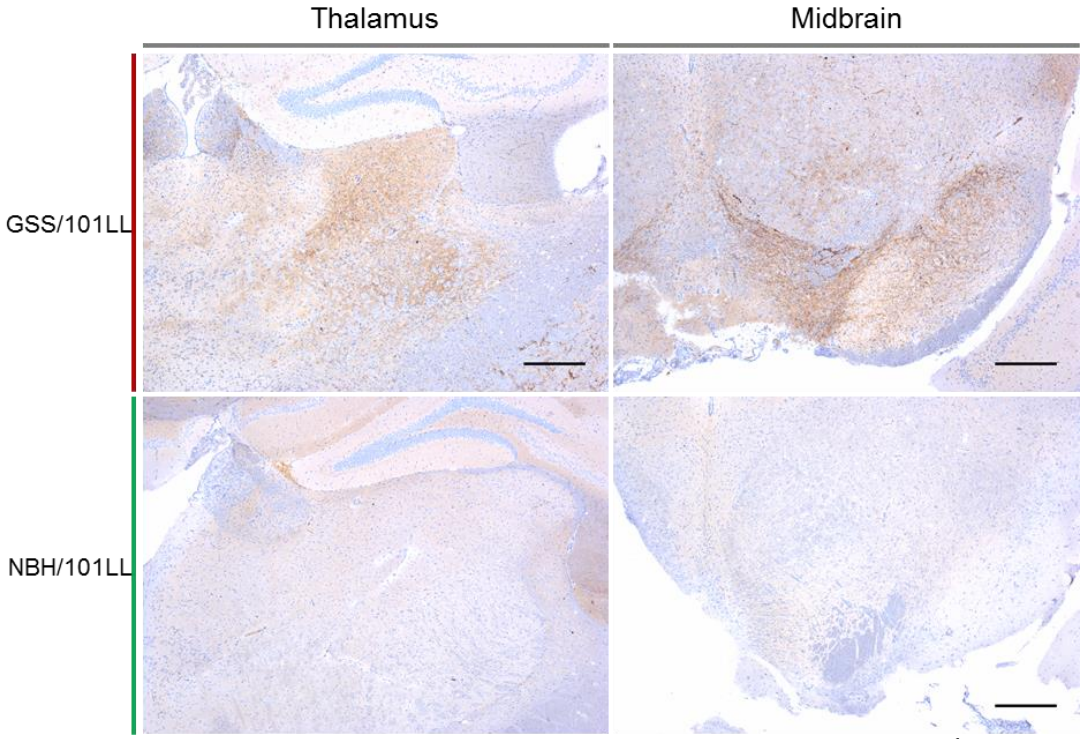

Figure 4.16 – PrP staining at clinical stage of pathology. Large quantities of PrP^d accumulate in thalamus at this stage. In midbrain, the PrP^d has increased from small quantities at 150dpi (see figure 4.2) to large quantities at clinical stage pathology. Scale bars = 200µm.

4.3. Results summary

- PrP^{d} is observed restricted to the midbrain at 150dpi, but no glial cell responses or neuronal deficits could be defined
- Glial cell responses are observed at 200dpi correlating with the same region of PrP^{d} targeting at 150dpi and 200dpi – this occurs prior to overt neuronal deficits
- Distribution of PrP^{d} accumulation in interpeduncular nuclei and dorsal and medial raphe nuclei and in SNc and SNr at 220dpi is associated with neuronal deficits and glial cell responses across both regions
- Accumulation of PrP^{d} occurs in a pattern which resembles neuronal connectivity, however other regions of physical connection do not exhibit PrP^{d} or pathology spread

4.4. Discussion

The results in chapter 3 highlighted the presence of a predominantly PrP^{sen} isoform of PrP^{d} which is associated with regions of the brain undergoing neurodegeneration and associated glial cell responses. It was therefore important to consider whether the general progression of disease, from detection of PrP^{d} to glial cell response to neurodegeneration, was present in the GSS/101LL model as has been described in some other prion diseases. Further, assessing the spread of pathology between regions could also strengthen the relationship between IHC detectable PrP^{d} and neurodegeneration. A final important question is whether PrP^{sen} isoforms accumulate in patterns resembling neuronal connectivity, as may expected from previous studies [143, 144, 281, 283, 284, 303], and whether this is associated with development of neurodegeneration and glial cell responses.

Using the IHC conditions that reliably detect PrP^d at terminal disease (chapter 3), PrP^d was observed at 150dpi in the midbrain of GSS/101LL animals. The detectable PrP^d appeared associated with the interpeduncular nuclei and SNc. No PrP^d could be identified in any other region of the brain. The exact sub-cellular localisation of detectable PrP^d was not tested due to tissue limitations, but could be of value in future studies to decipher how affected cells respond to PrP^d in early stages of disease. Using IHC with appropriate antibodies, no glial cell response or overt neuronal deficits could be defined at 150dpi. Given the known sensitivity of glial cells to changes in neuronal homeostasis, it is perhaps surprising no concurrent glial response is observed. This indicates either that: (i) there are no changes in neuronal homeostasis, (ii) the host is able to inhibit or 'dampen' the glial cell response or (iii) glial cell responses do occur, but assessing the morphology of the cells is insufficient to assess responses. In the first instance (i), no change in neuronal homeostasis would indicate that the detectable PrP^d is having limited or no effect on the cells associated with or in closest proximity to the PrP^d deposition. Similarly, the host could maintain neuronal homeostasis or inhibit the glial cell response from potentially exacerbating pathology, as hypothesised in scenario (ii). A likely option is (iii), whereby the markers being used in this study are simply not sensitive enough to identify a glial cell response. Further work is therefore required to elucidate the interaction of glial cells, neurons and PrP^d at the earliest stages of disease.

At later time-points, glial cell responses are observed in the midbrain where PrP^d was first detectable and sustained. These glial cell responses precede detectable neuronal deficits, a phenotype observed previously [189, 191, 320-325]. At later time-points, the specifically targeted regions of the midbrain exhibit overt neuronal deficits. These are exemplified by the intrinsic disorder and loss of MAP2 stained neurons. These neurodegenerative phenotypes are associated with the spread of PrP^d and glial cell responses from the interpeduncular nuclei to the medial and dorsal raphe nuclei. This data indicates an association between accumulation of IHC detectable PrP^d, glial cell responses and neurodegeneration – reaffirming results in chapter 3.

The accumulation of PrP^d and associated pathology in anatomical distinct brain regions which have known neuronal connections is of further importance due to its implications in understanding interaction of disease components. The prion-like mechanism of misfolded protein propagation traditionally relies on detection of increased levels of misfolded protein or spread of misfolded proteins from injection site to interconnected regions [146, 154, 161, 286-293]. Here, PrP^d is initially detected associated with specific neurons of the midbrain, namely the interpeduncular nuclei and SNc. The reasons for this initial targeting are unclear and will require further work. The subsequent observation of PrP^d in neurons of the brain stem (such as the dorsal raphe nuclei) and in the SNr shows accumulation of PrP^d in neuronal populations with known connectivity. The restricted observation of PrP^d along these pathways and not to other known connected neuronal populations, however, shows this distribution is selective. It is unclear why specific neuronal populations are associated with PrP^d accumulation whilst others are not. Selective

vulnerability is a well-established phenomenon in chronic neurodegenerative diseases (reviewed in [311]). The mechanism(s) for such selectivity is under considerable attention.

In this study, we performed an intracerebral (i.c) 20μL injection of 1% GSS brain homogenate. This will likely result in widespread dispersion of the homogenate which will be quickly degraded, becoming undetectable [344]. Of course a small but undetectable quantity of misfolded prion protein may remain localised or widespread in the brain. Therefore, it is important to consider that the accumulation of detectable PrP^{d} between brain regions may not be the result of a 'spread' along neuronal connections, although this is certainly a possibility. Alternatively, accumulation may result specifically due to physiological differences between brain regions, or other non-misfolded protein factors migrating in neurons which result from the initial deficits associated with protein misfolding.

In summary, in the presence of previously defined PrP^{sen} isoforms of PrP^{d}, the relationship between IHC detectable PrP^{d}, glial cell responses and neurodegeneration are reaffirmed in this chapter. This is particularly highlighted at 220dpi, where alongside the accumulation of PrP^{d} in distinct brain regions which have neuronal connections, glial cell responses, for example, can be observed restricted to the same regions. This indicates that isolation of a predominant PrP^{sen} isoform of PrP^{d} in the GSS/101LL model does not disrupt the association of PrP^{d} and neurodegeneration or alter the spread of pathology.

5. *In vitro* amplification of GSS/101LL CNS regions

Chapter aim: To evaluate the relationship between PrP^{d} and appearance of neurodegeneration using an assay with enhanced misfolded prion protein detection.

5.1. Introduction

The GSS/101LL model shows the same key features of vacuolation, activated microglia, astrogliosis and neurodegeneration as other murine prion diseases at clinical stages of disease, and in progression. However, the accumulation of a predominant species of PrP^{sen} in this model represents a disease-specific feature, without the requirement for PrP^{res} isoforms of PrP^{d}. The initial aggregates of PrP^{d} appear to be associated with neurons of the midbrain, for example the SNc, at early stages of disease. The deposited PrP^{d} at later stages then appears to spread specifically to interconnected regions alongside the establishment of overt neuronal deficits, although this only occurs selectively along some but not all neuronal pathways. This suggests an association between PrP^{d} and neurodegeneration. However, these results rely upon the detection of misfolded prion protein via IHC, which may not represent the full extent of PrP^{d} present. Therefore, it was considered important to use more sensitive measures of detectable misfolded protein to discover whether this correlation is upheld.

A number of methods to detect PrP^d exist, but highly sensitive techniques have been developed recently for the use as diagnostic tests for misfolded prion protein in samples. These are the PMCA [97] and the QuIC assay [101, 104]. Both techniques take advantage of the understanding of protein-template misfolding, using a small quantity of PrP^d "seed" to induce a conformational conversion of PrP^c "substrate" to a misfolded isoform. Originally, the CFCA was developed to encapsulate this reaction [94], but the PMCA was later published using periods of sonication to break down larger aggregates to form larger surface areas for additionally seeded conversion to take place. The *in vitro* misfolding is then measured using Western blots of the PMCA products with PK digestion. This experimental set up yielded extremely sensitive detection of PrP^d species [97] (see *1.1.5. Prion diseases: Misfolding of PrP^C to disease-associated isoforms* for details). The immediate benefit of this method was the prospect of developing an ultra-sensitive diagnostic assay for screening and detection of pre-clinical prion disease. Additionally, further studies have used PMCA to investigate important questions regarding the protein-only hypothesis and the prion hypothesis [99, 345]. Firstly, it was discovered that the conformationally re-arranged product of the PMCA was infectious to animals [100]. This demonstrated the importance of the assay's ability to propagate the unique properties of individual prion strains [346]. Important studies by Delault *et al.* demonstrated that polyanionic co-factors such as lipids and/or non-specific RNA products are required for propagation of PrP^d using recPrP as a substrate [99]. These results suggest that a minimal number of factors are required for the *in vitro* generation of PrP^d. However, these results also represent a limitation of PMCA, as a more recently developed technique, the QuIC assay [101, 104], requires only

misfolded prion protein in the presence of recPrP (and in the absence of polyanionic co-factors) for misfolded protein amplification. Other limitations of the PMCA are the batch effect of the assay. Due to the use of sonication to disrupt protein aggregates, only relatively small numbers of samples can be amplified at any one time. Furthermore, the individual variation between sonicators means it is unlikely that the reaction conditions in each sample remains consistent throughout. In this study, the *in vitro* amplification technique to be used will compare detection of misfolded prion protein between different regions of the same GSS/101LL brain. It is not known whether different isoforms of misfolded prion protein exist between anatomically distinct regions of the brain, but due to the distinct microenvironments present in individual regions, this would not be unexpected. Therefore, as a result of the potential batch effect, variability in sonication and the requirement for specific co-factors for aggregation/misfolding of recPrP (which may or may not be present in an isolated brain region), the PMCA has a limited capability for comparative analysis between different regions of the same brain.

The QuIC assay was subsequently developed, which uses a similar founding principle to the PMCA, with periods of disrupting protein aggregates and periods of rest for annealing and conformational rearrangement of recPrP to occur [101]. In contrast to PMCA, however, this assay uses a programmable and controlled intense shaking to disrupt aggregates rather than sonication. Furthermore, the shaking method allows the use of a shaking-incubator platform to be used. Importantly, shaking-incubators commonly hold 96-well plates and elicit a consistent shaking intensity across all wells of the plate. This development bypasses some of the

problems associated with PMCA by generating a sample-to-sample consistency which is also high-throughput. The conditions of the QuIC assay permit the misfolded recPrP to form fibrils. Initially, the detection of amplified PrP^{d} was performed using Western blot analysis to detect the formation of PrP^{res} isoforms [101], however, the fluorescent compound, ThT, can be used to identify fibril formation. This is due to the increased fluorescence of this compound when in contact with fibrils. The reasons for this increased fluorescence is unclear, but recent studies have begun to elucidate this enigmatic phenomenon (reviewed in [347]), and allowed the real-time detection of PrP fibril formation using a plate-reader, a technique termed the Real-Time QuIC, or RT-QuIC [104]. In recent studies, it has also been shown that RT-QuIC can propagate the strain properties of two distinct murine prion strains – including a comparable incubation period [348]. These results implicate the faithful propagation of conformations of misfolded prion protein using RT-QuIC.

The reproducibility of the QuIC assay, as a result of the 96-well shaking-incubator platform, allows the comparative analysis of the presence/absence of misfolded prion protein species between brain regions. In addition, the recent demonstration of conformational properties of misfolded prion protein resulting from the RT-QuIC propagating the original prion strains used, including infectivity [348], highlight the RT-QuIC as an ideal method to assess the presence/absence of misfolded prion protein between different brain regions of the same brain. A caveat of the RT-QuIC however, is that the species of misfolded prion protein being detected is unknown. It is highly likely a misfolded prion protein species is responsible for the

aggregation/misfolding of recPrP in the RT-QuIC. This is because the product from PrP immunoprecipitation [105] and PK-digestion [299] are both capable of seeding the QuIC assay (aggregating/misfolding recPrP). Further, recent studies show the aggregated/misfolded recPrP product from the QuIC assay retain the original "seed" prion strain properties, including the transmissibility to mice [348]. Whether QuIC detection represents the entire cohort of PrP^{d} or a subset is unknown. Due to a sample's capability to seed/propagate ThT positive product from a recPrP substrate, the term prion seed is used in this thesis as an operational definition of the agent in diseased (but not control) tissue that initiate the generation of a ThT-positive reaction with recPrP. Therefore the distinction between prion seeds and PrP^{d} is that PrP^{d} represents all detectable forms of PrP using IHC and/or Western blot analysis. Prion seeds may represent the same species of PrP^{d} as IHC or Western blot, or different misfolded prion protein species. Certainly, previous reports indicate the increased sensitivity of the RT-QuIC comparative to IHC or Western blot [101, 103, 104, 298]. Therefore other uncharacterised misfolded prion protein isoforms may also be identified using this method.

Data presented in chapters 3 and 4 of this thesis present the close association between IHC detectable PrP^{d} and neurodegeneration. To reaffirm this correlation, the QuIC assay will be utilised as a tool for ultra-sensitive detection of prion seeds between different brain regions of the same individual. It is known in some instances that different tissues within the same individual can influence the propagation of PrP^{c} to a misfolded isoform. For example, known prion-infected whole brain tissue can

show prion seeding in the QuIC assay, however that same infected brain homogenate cannot propagate the misfolding of recPrP when spiked into blood [105].

This study set out to test the distribution of prion seeds in GSS/101LL brain regions to determine whether the QuIC assay detects prion seeds correlating with neurodegeneration, similar to IHC detectable PrP^{d}, or not, such as PrP^{res} identified in the GSS/101LL cortex. Due to the prior understanding of different tissues inhibiting the propensity for recPrP aggregation/misfolding, this study will firstly test: (i) the propensity of brain homogenates from a range of murine prion strains to seed the QuIC assay; (ii) whether different brain regions propagate prion seeding with an equal capacity and (iii) whether prion seeds can be detected in GSS/101LL animals. Based on the results for the above questions, this study outlines stringent parameters to determine whether a sample can be classified as QuIC positive or negative. All QuIC positive samples will thus be interpreted as containing prion seeds.

5.2. Results

5.2.1. Set up of the QuIC assay

Previous work by Vascallari *et al.* demonstrated that murine prion strains could be detected via the QuIC assay using either murine recPrP or a hamster-sheep (ham/shp) chimeric recPrP substrate [299]. The ham/shp recPrP was used exclusively as a

substrate in this study and the QuIC protocol outlined in by Vascellari and colleagues was followed.

To confirm that the assay worked in our laboratories, 263K hamster scrapie was used as a positive control to seed the QuIC assay, as previous studies have demonstrated high sensitivity using 263K as a seed [101, 104]. Initial findings showed that the 263K brain homogenate used could be diluted to 10^{-6} concentration and continue to yield increased ThT fluorescent readings – indicative of recPrP misfolding fibril formation (figure 5.1). A 10^{-8} concentration of the original brain homogenate also showed an increased ThT fluorescent reading; however 10^{-7} did not. Therefore it is considered the reaction had a consistent sensitivity of 10^{-6} or 0.0001% of the original brain mass.

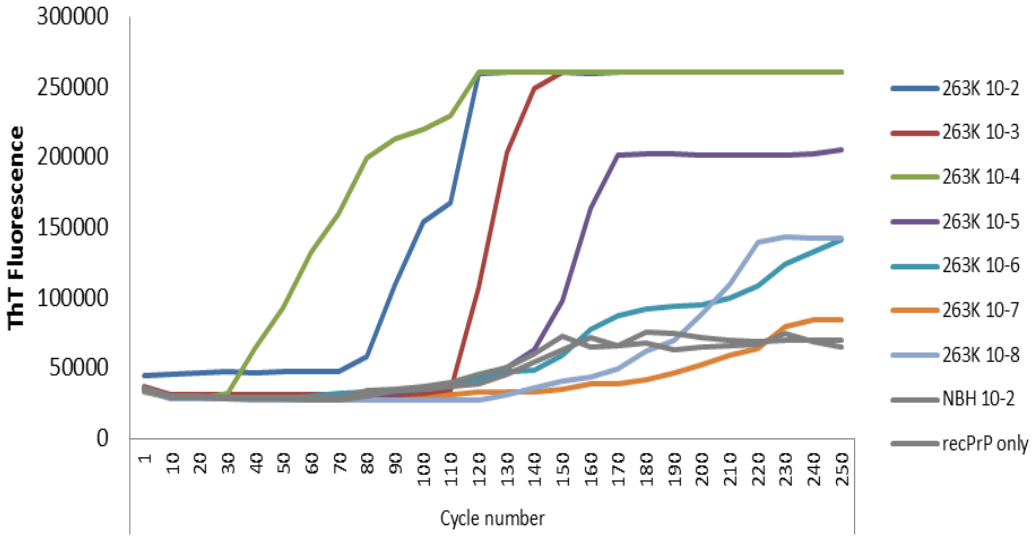

Figure 5.1 - RT-QuIC assay set-up using 263K as a seed for converting Hamster-Sheep chimeric recPrP^{c} to an abnormal conformation. Each line represents the mean Thioflavin-T fluorescence (n=8) within a log dilution series of an original 10% 263K hamster scrapie brain homogenate. The NBH and recPrP only (black lines) are used as negative controls to confirm that the seeding is disease-specific and not an entity within either an uninfected hamster brain or outwith the brain homogenate which is capable of seeding the assay.

5.2.2. Prion seed detection in various murine prion strains

An important consideration in the development of the QuIC assay for the use in these studies is the ability of the QuIC assay to detect prion seeds in murine prion disease brain. A previous study has reported that the QuIC assay can reliably and efficiently produce increases in ThT fluorescence of both murine and Ham/Shp recPrP when using murine prion disease tissue as a seed [299]. To establish whether murine prion seeds can be detected within the protocol presented here, brain homogenates from a number of murine prion strains (79A, ME7, 22A and 22L) were tested. This selection of strains was used to assess whether the QuIC assay could identify murine prion seeds which has been derived from the infection of a number of different original sources. For example, 79A is the result of a series of infections (sub-passages) of "Drowsy Goat" in mice with a *Prnp*^{A} allele. ME7 is the result of sub-passages of natural scrapie into mice, whereas 22A and 22L are different strains obtained from the sub-passages of SSBP-1 ovine scrapie in mice. The detection of prion seeds from such diverse strains, established from a variety of different sources gives some confidence that prion seeds can be detected in murine tissue, regardless of the original source. This is important when considering the GSS/101LL model which involves the primary passage of human tissue into mice.

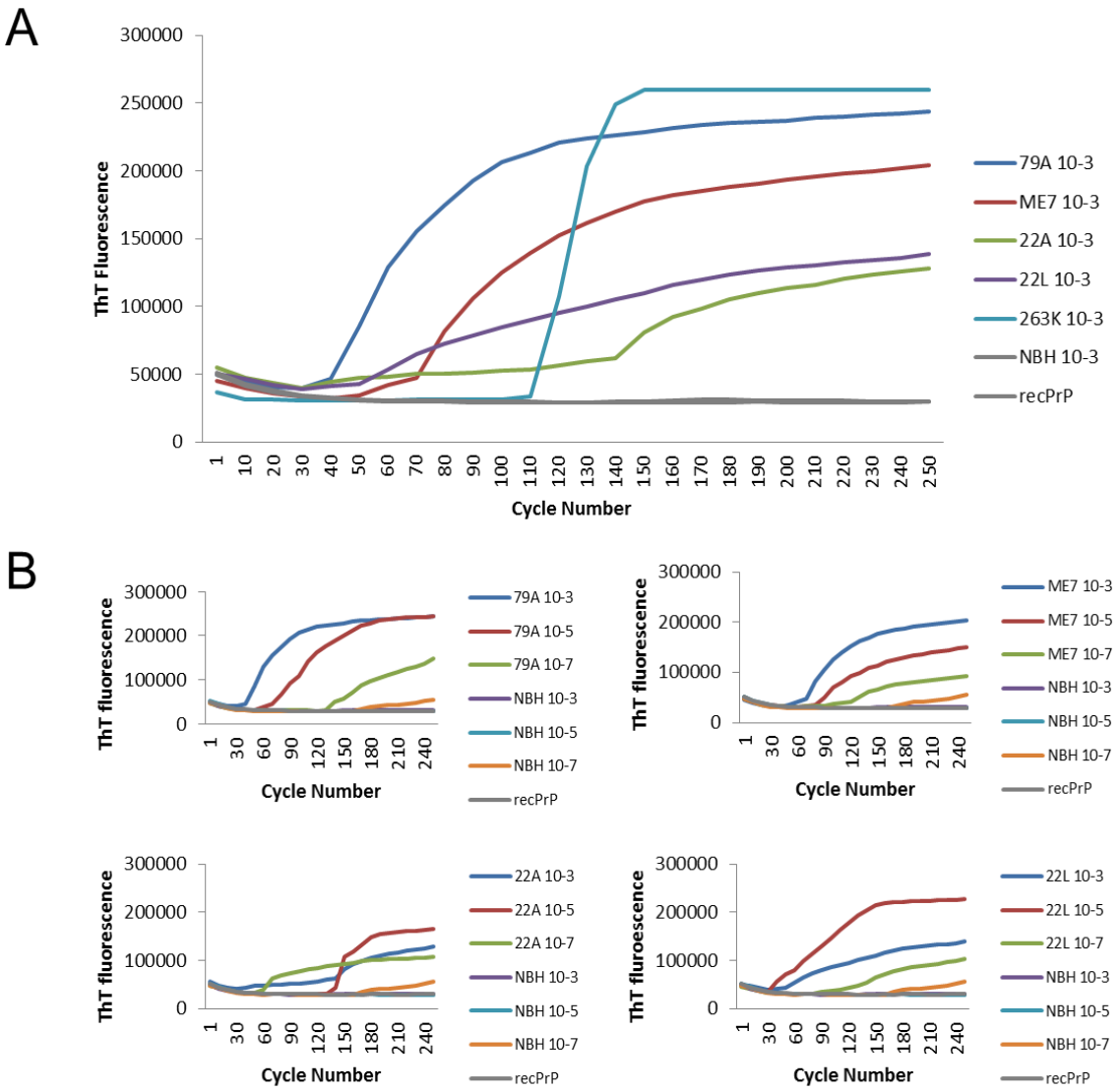

Figure 5.2 – (A) RT-QuIC assay seeds a number of different murine prion strains using Hamster-Sheep chimeric recPrP^{c}. Uninfected murine brain and recPrP (grey) are used as negative controls to demonstrate that neither brain homogenate or the reaction conditions alone are capable of seeding the assay. Each line represents the mean of 4 replicates. (B) Dilution series of each prion strain. The sensitivity of the QuIC assay was high in all strains tested as all gave increased ThT fluorescence even at 10^{-7} concentrations.

When testing each of these strains in the QuIC assay, all strains altered the ThT fluorescence above the baseline, as established by uninfected controls (figure 5.2A). This shows that misfolded protein species can be detected in all murine prion strains tested here. Interestingly, each strain exhibits a different lag-phase and altered plateau of ThT fluorescence. When considering only the ThT plateau, this phenotype

categorised the prion strains according to the original sources. A dilution series of each strain was performed to determine if the differences in ThT plateau were the result of potentially different quantities of prion seeds. In each murine prion strain, a dilution of 10^{-7} could be readily detected (figure 5.2B). Unexpectedly, within 22A and 22L strains a concentration of 10^{-5} showed a higher ThT plateau compared to a higher concentration of 10^{-3}. The reasons for this are unclear but suggest the plateau of ThT fluorescence may not necessarily represent the total quantity of misfolded prion protein originally added into the assay. Instead, the dilution series of the sample to be added into the QuIC assay likely provides a more accurate quantitation of prion seeds. Overall these results demonstrate that misfolded prion protein can be detected from murine brain homogenates from a multitude of different prion strains.

5.2.3. GSS/101LL infected brain tissue can be detected by the QuIC assay

In these studies, it is important to establish whether GSS/101LL animal tissue can seed the QuIC assay effectively. Previous studies have tested 263K infected 101LL animals (263K/101LL) and found detectable prion seeds without evidence of inhibition of the reaction or spontaneous false-positive prion seeding [299]. To test whether prion seeds could be detected in GSS/101LL animals, a dilution series of clinical stage GSS/101LL whole brain was performed. The animals (n=2) chosen had been previously demonstrated to exhibit no detectable PrP^d by IHC using protocols replicated from previous publications [41], but were found to express relatively larger quantities of PrP^d using optimised conditions with citric acid-buffer as detailed in chapter 3. It was found that in both animals, the brain homogenate could be diluted to a concentration of 10^{-5} and exhibit an increased ThT fluorescence (figure 5.3A).

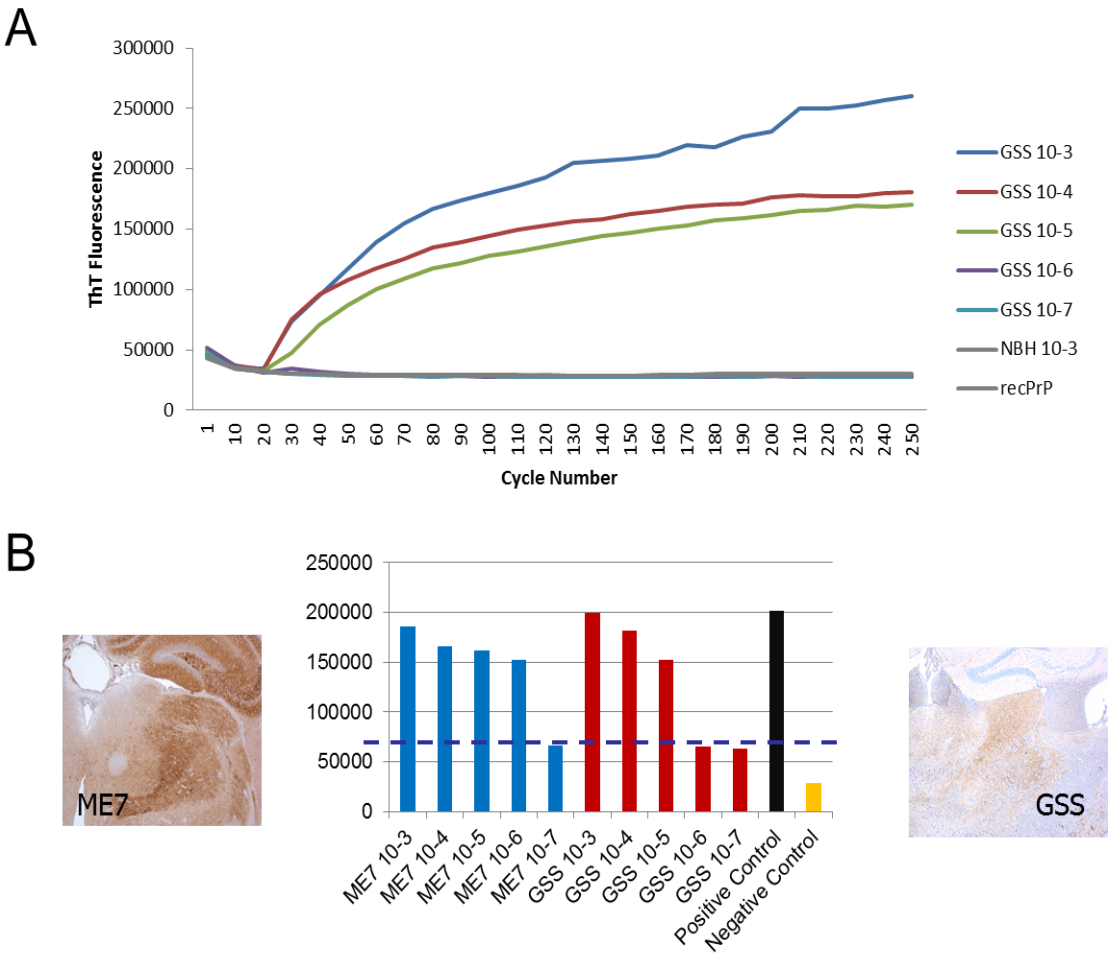

Figure 5.3 – (A) RT-QuIC is capable of seeding GSS/101LL infected material. NBH is an uninfected 101LL aged matched control and together with recPrP demonstrate that neither are capable of seeding the QuIC assay. (B) ThT fluorescence at 48 hours in the QuIC assay with ME7 or GSS dilutions. ME7 consistently dilutes to 10^{-6} concentration, whereas GSS consistently dilutes to 10^{-5}. Purple dashed line represents 10 standard deviations added to the negative control which is used as baseline.

As described in chapter 3 of this study, the PrP^{d} detected within the GSS/101LL models is predominantly PrP^{sen}, although some PrP^{res} isoforms are detected. To test the propensity of GSS/101LL brain homogenate to seed the QuIC assay versus a murine prion strain which exhibits large quantities of both PrP^{sen} and PrP^{res}, a dilution series of GSS/101LL material was tested comparative to ME7. The data presented in figure 5.3B show ThT fluorescence values after 48 hours of seeding in the QuIC assay. Despite the differing isoform ratios of PrP^{d} between ME7 and GSS/101LL animals, prion seeds could be detected within the QuIC assay in both

samples. ME7 could detect prion seeds to a concentration of approximately 0.0001% of the brain mass, whereas GSS/101LL could detect a concentration of 0.001%. This represents a quantitative difference in prion seed detection between ME7 and GSS/101LL animals.

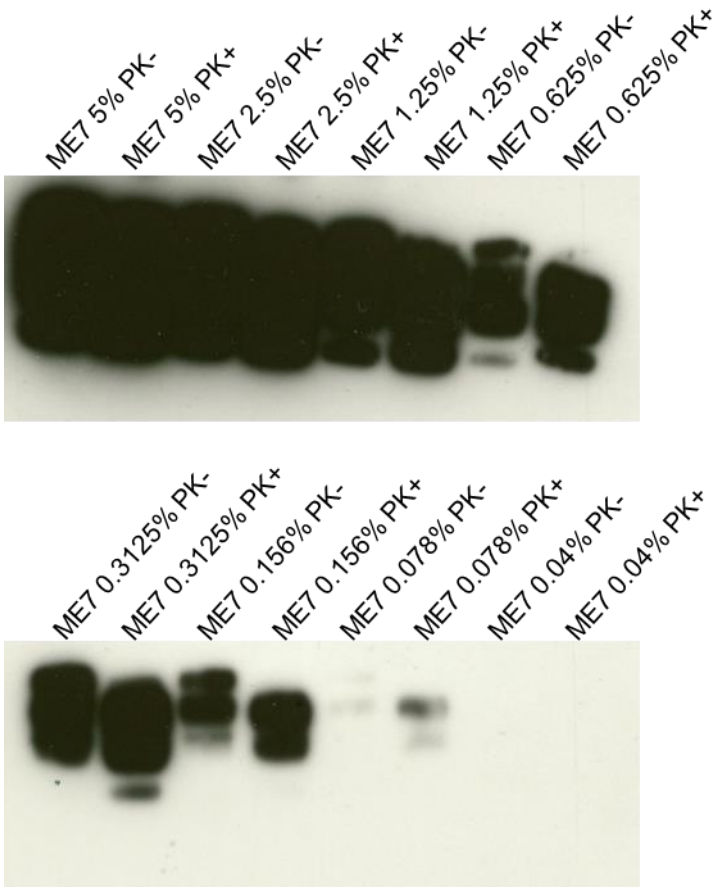

Figure 5.4 – Western blot of ME7 PrP levels. Dilution series ranging from 5% (w/v) of total brain mass to 0.04%. PrP and PrP^{res} can be detected to a concentration of 0.078% of total brain mass but no further.

To compare the sensitivity of prion seed detection to other biochemical methods of PrP^{d} detection, such as Western blot, a dilution series of ME7 brain homogenate was performed and tested using Western blot. To do this, a few adaptations were made to the Western blot protocol outlined in chapter 2. These were a 15µL brain homogenate of ME7 was diluted in 5µL of 4% sarcosyl, 5µL Western sample buffer (Invitrogen), 3µL sample reducing agent (Invitrogen) and 2µL dH_2O or PK was added. This generated a sample which was 5% (w/v) of the original brain mass. A dilution series from 5% to 0.04% (5%, 2.5%, 1.25%, 0.625%, 0.3125%, 0.156%, 0.078% and 0.04%) was then performed. Western blot detection using the PrP-specific BH1 antibody could identify overall PrP levels to a concentration of 0.078% of the original brain mass. PrP^{res} levels could also be detected to this level (figure 5.4). In comparison to the QuIC assay detection of 0.0001% of the original brain mass in ME7 or even 0.001% of the original brain mass in GSS/101LL demonstrates the increased sensitivity of the QuIC assay comparative to Western blot analysis.

5.2.4. No regional differences within an infected murine prion disease brain are observed

Previous reports of the QuIC assay have highlighted the fact that different tissues can have different propensities to seed the QuIC assay. Most notable is the difference in the ability to detect prion seeds within the brain versus known infected blood. For example, previous studies by Orru *et al.* have demonstrated that when "spiking" uninfected blood with a known prion infected brain homogenate, the QuIC assay detection appears to be compromised [105]. This data suggests that components of blood are capable of inhibiting the QuIC assay. To date, the majority of studies used

to identify prion seeds have tested whole brain or peripheral tissues. As a consequence, it is unknown whether anatomically distinct regions of the brain exhibit prion seeding with equal capacity.

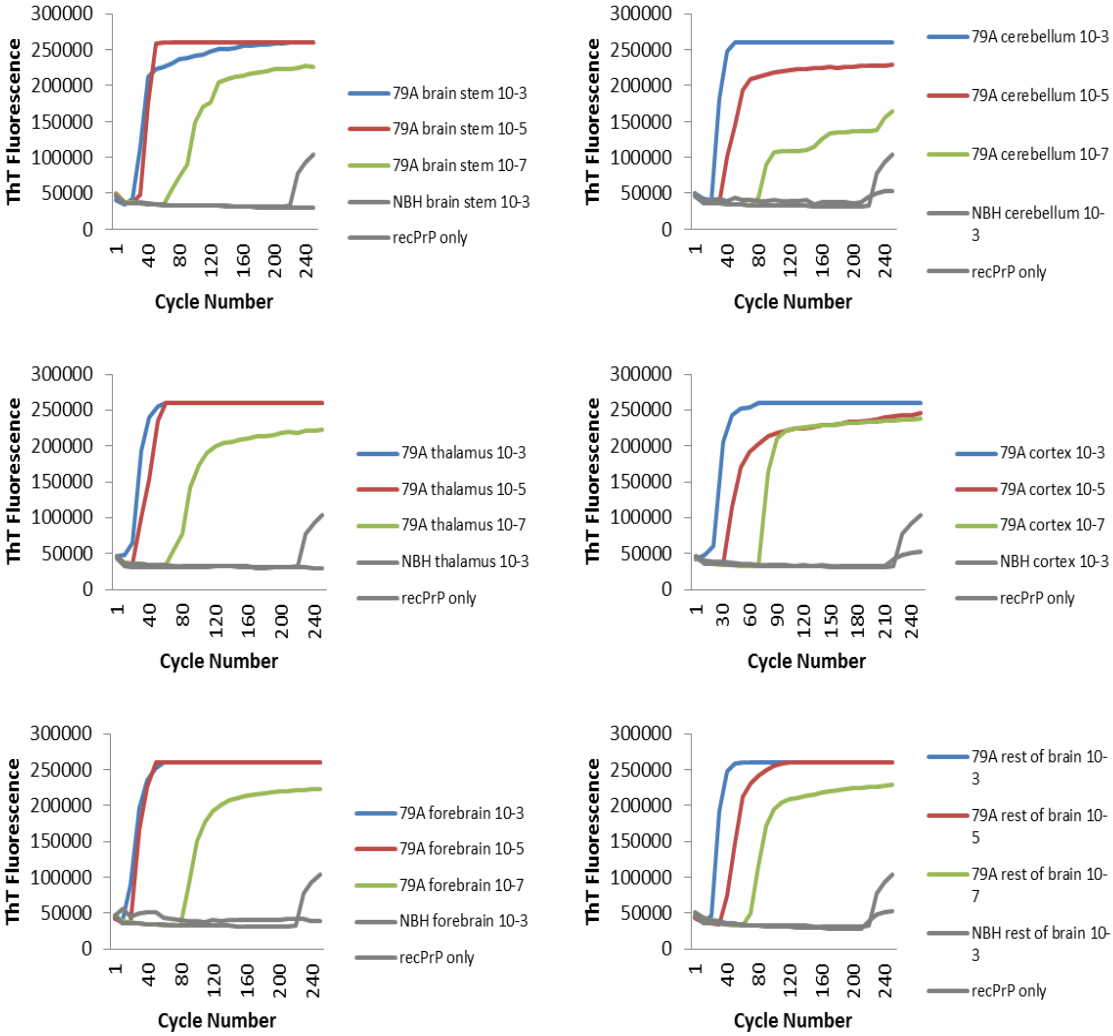

Figure 5.5 - QuIC assay detection of individual regions of 79A prion infected brain. All regions of the brain can readily and specifically seed the conformational conversion of recPrP at comparably sensitive levels.

To test this, 79A murine prion strain was regionally dissected into brain stem, cerebellum, cortex, thalamus, forebrain and rest of brain. In all these regions, it is known that PrP^{res} can be detected (figure 3.13). This therefore allowed the normalisation of misfolded protein across regions, therefore regional effects upon

QuIC assay seeding could be tested. No difference in prion seed detection was observed in any brain region (figure 5.5). This shows that despite different brain regions being used, there is no difference in the propensity of any brain region to seed the QuIC assay. Therefore, unlike blood components, it is unlikely any factor exists within any compartment of the brain which is an inhibitor to the QuIC assay.

5.2.5. Development of parameters to allow positive/negative reading of QuIC assay

The QuIC assay in this study, and in other published studies, is shown to be a sensitive detection system for the presence of prion seeds. A confounding factor, however, is the limited understanding whether the QuIC assay detects all misfolded prion protein species or a sub-set of conformations. It is therefore necessary to establish stringent parameters to allow a positive or negative read-out from the QuIC assay. Previous studies have used an approach to identify a sample as positive or negative based on whether it passes a threshold which is the baseline (as determined by the average ThT fluorescence of an appropriate negative control) plus 10 standard deviations of the baseline. Generally, at least 3 or 4 replicates per sample are run per QuIC assay, and a sample which tests positive in at least 50% of replicates is considered positive [298]. In order to establish a positive or negative read-out from the QuIC assay, this study used the same threshold parameters outline above (i.e. any sample which accumulates a ThT fluorescence which is over 10 standard deviations of a negative control sample).

In previous studies, the threshold parameters used are set up per assay. This is a useful tool to compensate for false-positive readings within an individual QuIC assay experiment. However, in this study it was found that different batches of purified recPrP exhibited different average ThT baselines (figure 5.6). Furthermore, between QuIC assay runs using the same samples, it was found that samples from uninfected animals had a random propensity to spontaneously increase ThT fluorescence over time (figure 5.7). Therefore, a system of generating a novel threshold for every assay would result in random *de novo* levels of spontaneous seeding being hidden amongst genuine, template-mediated conformational rearrangement. As a consequence, the levels of false-positive seeding are not recognised and thus compromise the comparison of results between QuIC assays, especially when using two different batches of purified recPrP. To overcome this, a standard threshold across all samples tested within and between batches of recPrP is important to establish.

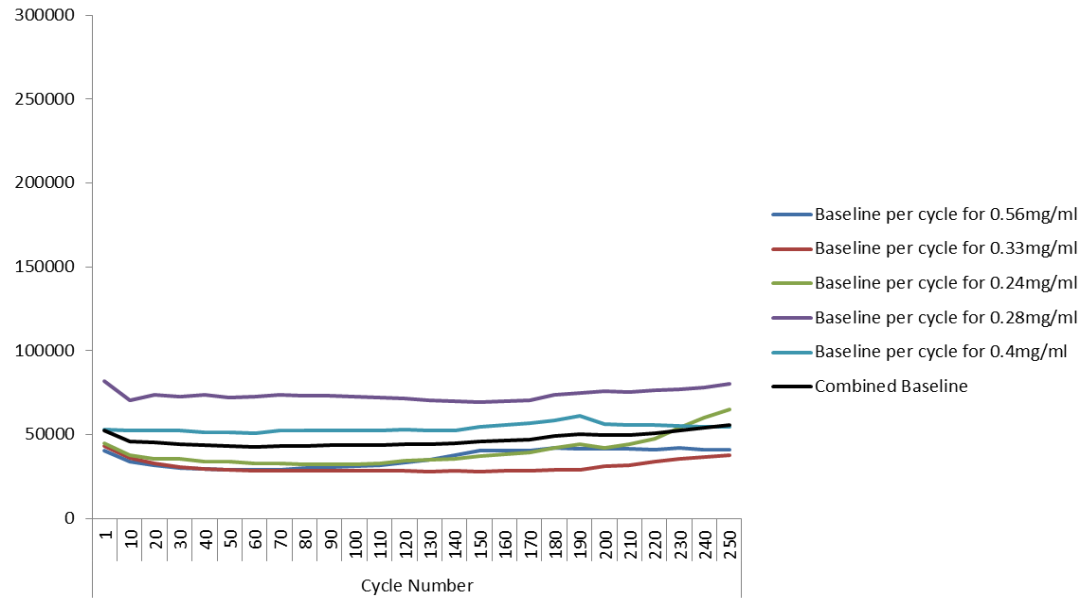

Figure 5.6 - The baseline of individual batches of hamster-sheep chimeric recPrP produced. Although the average baseline fluorescence is markedly different between batches, the average fluorescence in any recPrP batch does not appear to rise above 100,000 fluorescent units. The combined average baseline of all recPrP batches is shown in black.

This study accumulated all known-negative control samples run across all QuIC assays tested here using the Ham/Shp recPrP under consistent conditions. The ThT fluorescence for all negative control samples was averaged at each time-point within the QuIC assay, as depicted in figure 5.7.

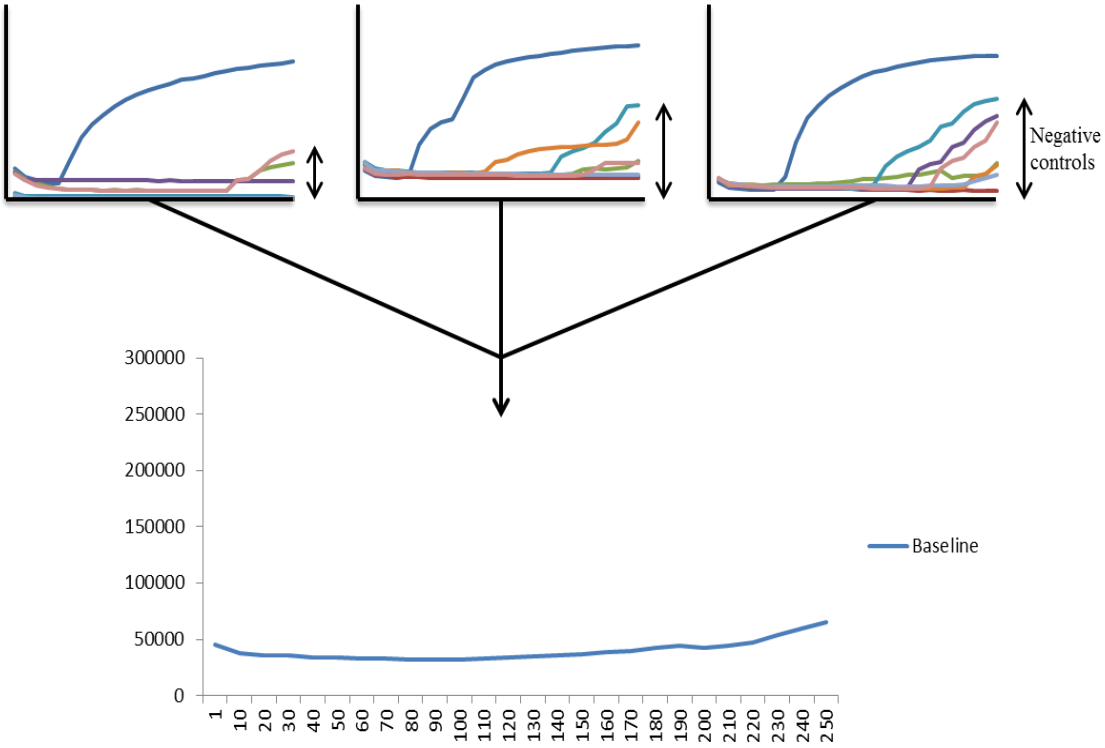

Figure 5.7 - All NBH controls corroborated in a single average ThT fluorescence line over time. This line can thus be referred to as the baseline ThT fluorescence.

Figure 5.8 shows the average 'combined baseline' of all negative samples across all QuIC assays performed in this study (n=127 – black line). The baseline remains consistent at all time-points throughout the assay. Around cycle 220 (approximately 50 hours), however, the standard deviation rises. When comparing data to average baselines for individual batches of recPrP, it is clear in some recPrP batches this is the time-point at which increased ThT "false-positives" are observed (figure 5.6; green line). This data suggests that *de novo* generation of a positive signal (a false-

positive) can occur after 50 hours, therefore a 48 hour time-point (figure 5.8; purple dashed line) was chosen as the determinant time-point at which to apply the above positive/negative parameters. The threshold according to the baseline plus 10 standard deviations is thus represented in figure 5.8 as the grey line. As a result, all samples will be adjudged according to whether the ThT fluorescence overcomes this standard threshold.

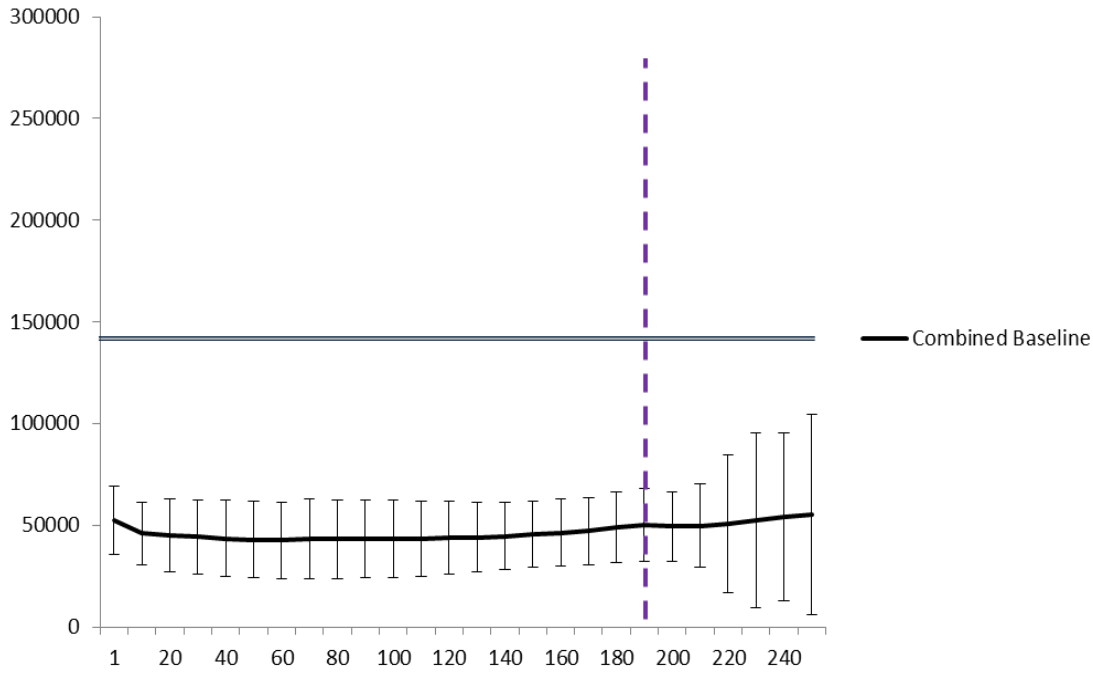

Figure 5.8 - The combined baseline with standard deviations. At 48 hours into the QuIC assay (purple dashed line) the standard deviation (SD) is 14910 arbitrary fluorescent units. 10 SDs are added to this to established a threshold (grey line). Any fluorescence reading below this threshold will be counted as a negative QuIC result and any reading above this line will be regarded positive.

5.2.6. Prion seeds are detected independent of neurodegeneration

Thus far this study has demonstrated that GSS/101LL brain tissue is capable of seeding the QuIC assay (figure 5.3) and different regions of the brain from other well established prion models appear to have no effect on the detection of prion seeds (figure 5.4). With this understanding and under the parameters outlined above,

different regions (brain stem, thalamus, cerebellum and cortex) of the GSS/101LL brain were tested. As described in chapter 3, the brain stem and thalamus are regions which have neuronal populations undergoing severe neurodegeneration; however the cerebellum and cortex appear 'unaffected'. It would be expected that prion seeds would be restricted to only those regions undergoing neurodegeneration. However, an increase in ThT fluorescence associated was observed in all regions of the GSS/101LL brain tested (figure 5.9A). The individual assay runs are shown in figure 5.9B to demonstrate the limited variability between assay runs. It was found that 100% of GSS/101LL animals tested at clinical stages of disease (n=4) surpassed the threshold, with the exception of a cortex sample of a single animal (figure 5.10). An individual NBH/101LL animal sample from cortex demonstrated a positive result, as did a NBH whole brain negative control. This demonstrates a low level of *de novo* seeding of recPrP. When comparing this data to findings in chapters 3 and 4 and what is currently understood of the correlation of PrP^{d} and neurodegeneration, this finding shows that prion seeds do not correlate with neurodegeneration.

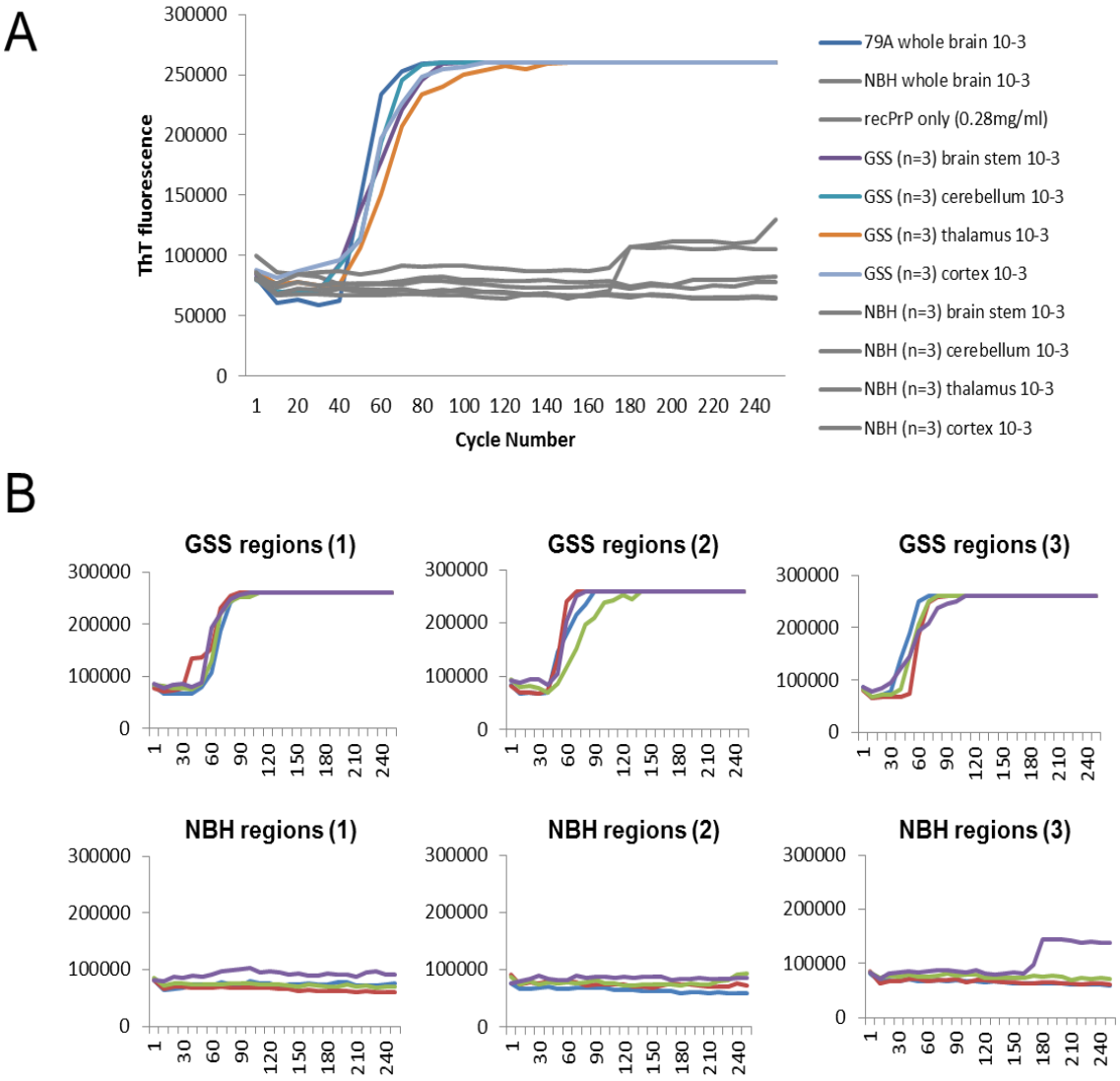

Figure 5.9 – (A) Average ThT fluorescence for each region of GSS/101LL 'terminal' tissue tested. All negative controls are marked as grey lines. (B) The plots of each region tested in the QuIC assay for individual animals. Brain stem = blue line. Cerebellum = red line. Thalamus = green line. Cortex = purple line.

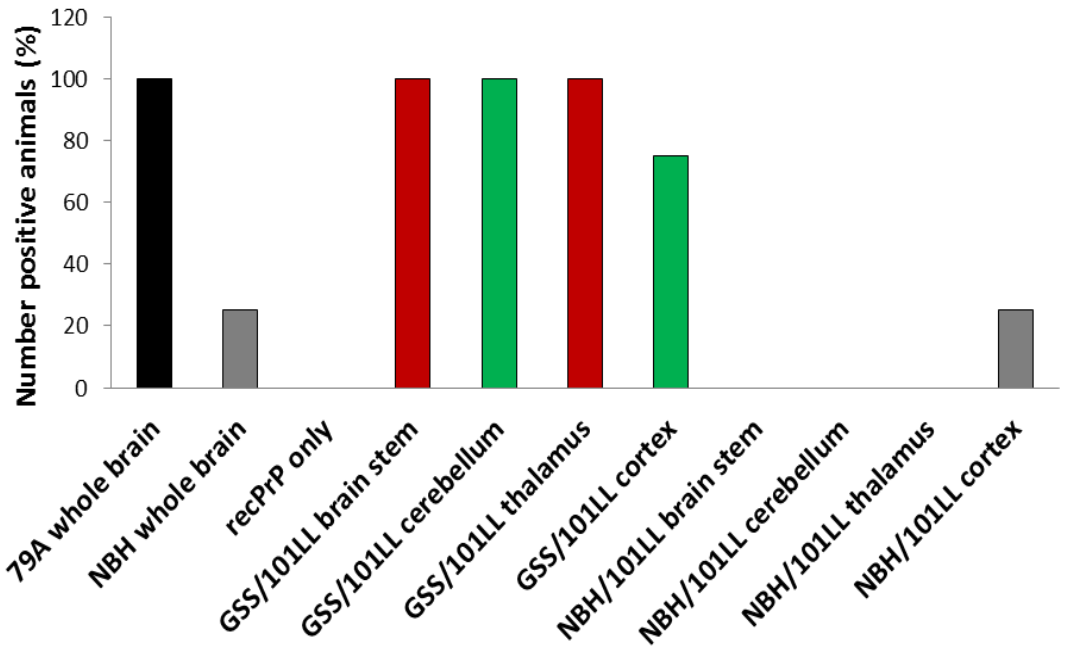

Figure 5.10 - Number of regions which surpass the threshold outlined in figure 5.8 at 48 hours in all animals tested (n=4). All regions tested within a GSS/101LL animal at clinical stage of disease are capable of seeding the conformational rearrangement of recPrP in the QuIC assay, with the exception of 1 animal which did not surpass the thresholds of ThT fluorescence within the cortex. The grey bars in 'NBH whole brain' and 'NBH/101LL cortex' demonstrated false positive results in 1/4 animals

5.2.7. Characterisation of prion seeds in GSS/101LL animals

The finding that 'unaffected' regions of the brain, with no detectable vacuolation, neurodegeneration or activated glia, are capable of seeding the QuIC assay is surprising. Although no PrP^{res} is detectable via Western blot with the exception of the GSS/101LL cortex, the QuIC assay has been demonstrated to be exquisitely sensitive. Therefore, samples from three GSS/101LL clinical stage animals were exposed to 20µg/ml PK for 90 minutes prior to protease inhibition. These conditions are sufficient to detect partially PK resistant isoforms of PrP^{d} in a number of different prion strains [349]. As demonstrated in chapter 3, these conditions reveal no detectable PrP^{res} in clinical stage GSS/101LL animals in all regions with the

exception of a small quantity observed in the cortex. When using identical conditions to seed the QuIC assay, all regions tested identified prion seeds (figure 5.11). These results indicate either the presence of small levels of PrP^{res} within multiple regions of the brain in GSS/101LL animals, or that prion seeds are indeed PrP^{res}, but are possibly a different isoform to those detectable on Western blot or IHC analysis.

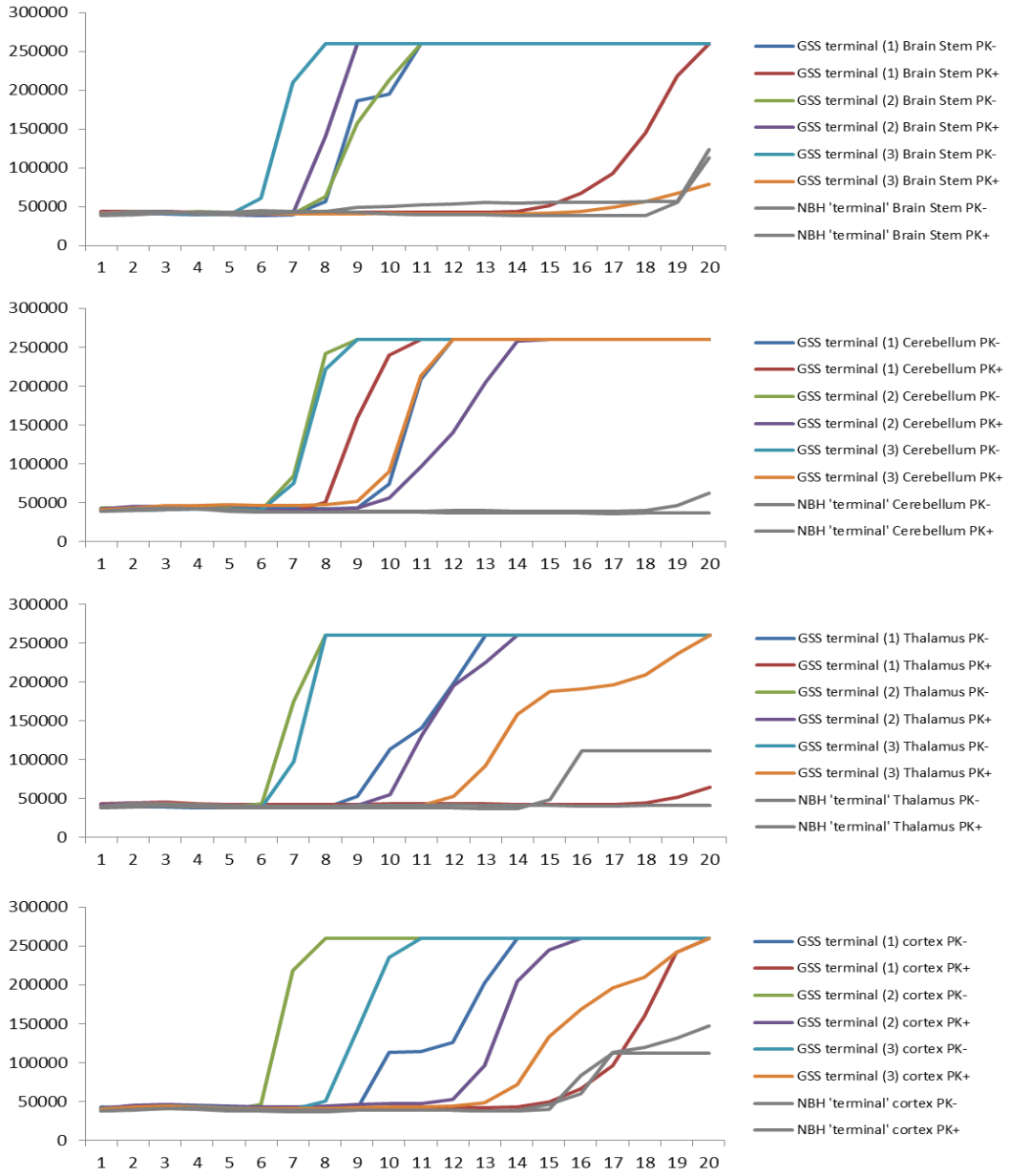

Figure 5.11 - ThT fluorescence in regional samples from clinical stage GSS/101LL animals. The samples are either exposed to proteinase K (PK+) or water (PK-) for 90 minutes prior to addition of the homogenate to the assay. All samples, regardless of PK- or PK+ within GSS/101LL animals surpass the threshold, with the exception of 'GSS terminal (1) thalamus PK+'.

5.2.8. The quantity of prion seeds does not differ between regions

The targeted neurodegeneration within the CNS of GSS/101LL animals, despite the detection of prion seeds in unaffected brain regions, could be explained by quantitative differences in prion seed accumulation and subsequent generation of neurotoxic species between regions of the brain. A region may accumulate larger quantities of prion seeds and as a result may be more susceptible to neurodegeneration. Therefore, the quantity of prion seeds was assessed in each region outlined above. Brain regions from GSS/101LL and NBH/101LL animals were diluted to a series of concentrations and added to the QuIC assay. It is hypothesised that as the concentration is lowered, samples containing small quantities of prion seeds will cease to give positive QuIC results before samples containing larger quantities of prion seeds.

Regions of GSS/101LL brains at clinical stage pathology were used. Concentrations used in the assay were 0.1% [10^{-3}], 0.01% [10^{-4}], 0.001% [10^{-5}], 0.0001% [10^{-6}] and 0.00001% [10^{-7}] of the original sample mass. In order to control the experiment, NBH/101LL aged matched brain regions were used at 10^{-3} and 10^{-7} concentrations in the same assay. The regional dissections from three terminally sick GSS/101LL and three aged matched NBH/101LL animals were used to test this hypothesis. Each sample within an assay used three replicates and each individual assay run was repeated twice (figure 5.12).

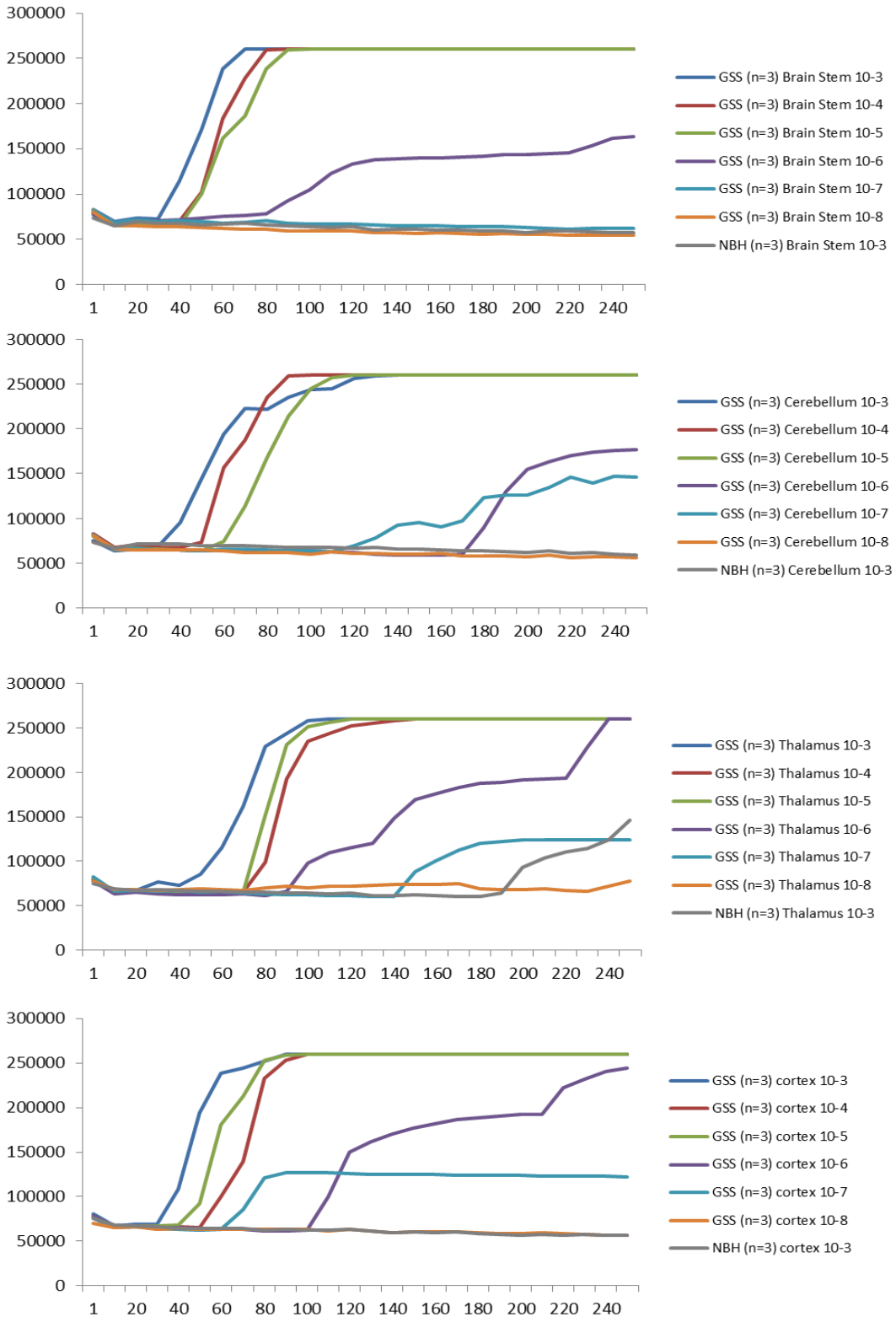

Figure 5.12 - Dilution series of regions within GSS/101LL animals. Each line represents the average ThT fluorescence of a particular homogenate concentration tested separately from 3 clinical stage animals.

It was found that each region had the propensity to seed the QuIC assay to at least 0.001% of the original sample mass (figure 5.12 and 5.13). The brain stem, thalamus and cortex samples exhibit a raised ThT fluorescence no further than 0.001% of the original tissue mass. The cerebellum on the other hand appears to dilute to a concentration of 0.0001% of the original tissue mass. Why there is a difference between cerebellar samples propensity to seed the QuIC assay is unknown. The results show that the quantity of prion seeds in each region studied bears no influence upon whether a region will succumb to neurodegeneration or remain 'unaffected'.

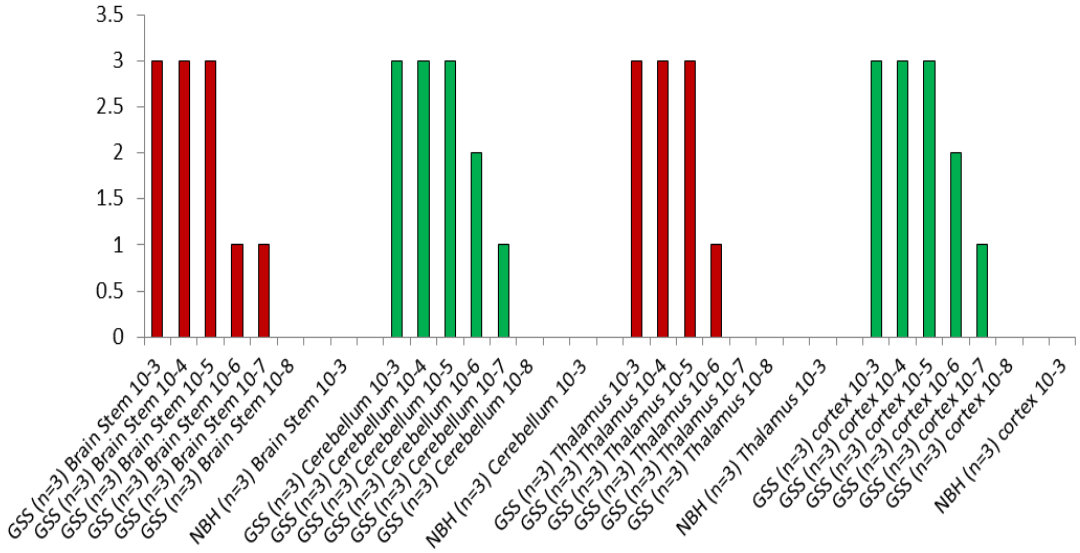

Figure 5.13 - Number of animals in dilution series from figure 5.12 which surpass threshold outlined in figure 5.8. At a concentration of 10^{-5}, all animals tested exhibited a ThT fluorescence higher than the threshold. No animals overcame the threshold when tested at a concentration of 10^{-8}.

5.2.9. Prion seeds accumulate in a similar time-frame in affected and 'unaffected' regions

In chronic neurodegenerative diseases, the incubation period prior to onset of overt clinical symptoms is relatively large. During this time period, it is known that many subclinical stages of neurodegeneration occur, the best elucidated are synaptic

deficits and degeneration [189, 191, 203, 204, 217]. Prior to such neurodegenerative phenotype, accumulation of PrP^d is detected – a finding recapitulated in this thesis (see chapter 4). These results hint that a region may only undergo neurodegeneration upon prolonged exposure to a misfolded protein. To test this, samples from the time-course outlined in chapter 4 were used (150, 200, 220, 240 dpi and upon clinical onset [figure 4.1]). We hypothesised that regions which are undergoing neurodegeneration likely accumulate prion seeds earlier in disease and are exposed to such prion seeds for relatively longer periods of time.

At each time-point (with exception of terminally sick animals), five GSS/101LL and five NBH/101LL animals were tested at a concentration of 10^{-3} of the original brain homogenate. In each individual QuIC assay, three replicates of a sample were used and every QuIC assay was repeated twice. At 150 dpi, two out of five (40%) of GSS/101LL animals tested were able to seed the QuIC assay in the brain stem (figure 5.14). In other regions tested, only one out of five (20%) of GSS/101LL animals were positive, therefore suggesting the initial targeted accumulation of prion seeds in the brain stem in a subset of animals. At 200dpi, three out of five (60%) animals exhibit prion seeds in brain stem, thalamus and cerebellum. Two out of five (40%) showed positive QuIC seeding in the cortex at this time-point. This demonstrates an exponential spread of prion seeds in a larger number of animals, which is not restricted to specific brain regions and independent of neurodegeneration (as defined in chapter 4). At later time-points, at least three out of five GSS/101LL animals exhibit QuIC positive seeding in all regions tested with four out of five (80%) testing positive in brain stem and cerebellum at 220dpi and in the brain stem, thalamus and

cortex at 240dpi. As described above, all terminally sick (onset of clinical symptoms) GSS/101LL animals show prion seeds accumulated in all regions tested, with exception of one GSS/101LL cortex sample.

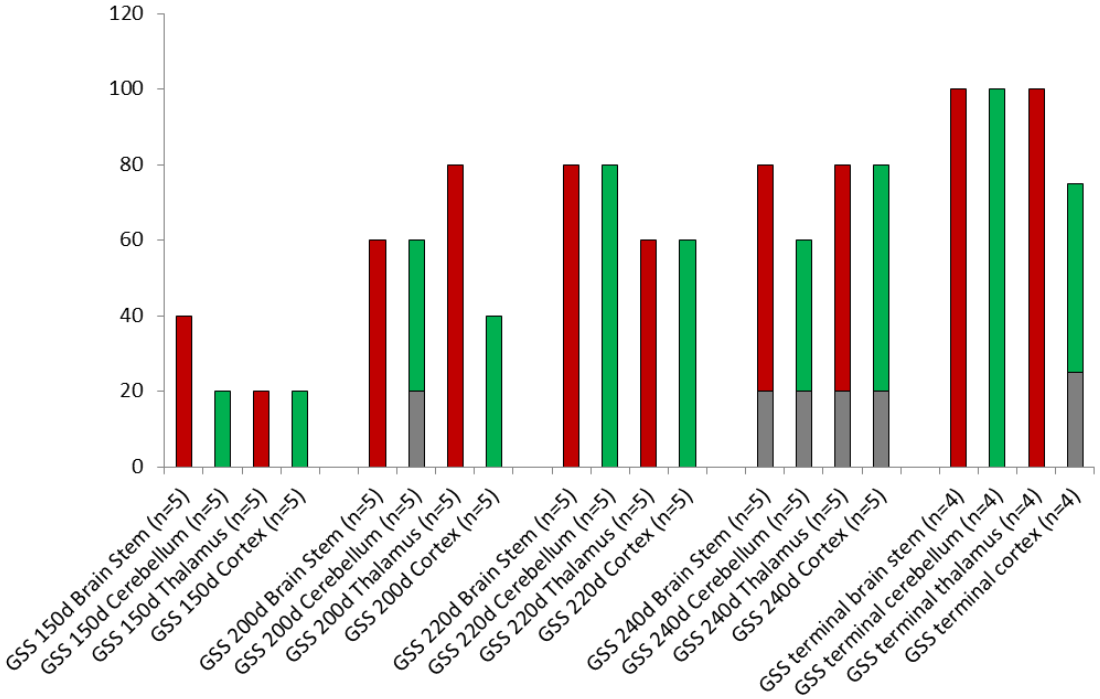

Figure 5.14 - Percentage number of animals positive in QuIC assay in each region at each time-point tested. Overlaid grey bars represent NBH time-point controls. Red bars represent GSS/101LL samples. Each positive is categorised based on the parameters outlined earlier in this chapter.

This data shows the accumulation of prion seeds at similar time-points in both brain regions which suffer neurodegeneration or are unaffected. For example prion seeds accumulate in the cerebellum and thalamus at similar time-points in a cohort of GSS/101LL mice at 200dpi. The thalamus will subsequently undergo neurodegeneration, whereas the cerebellum appears to remain pathologically unaffected (see chapter 3 and 4).

5.3. Results summary

- Multiple murine prion strains exhibit the property to seed the QuIC assay, including GSS/101LL
- Inherent differences in brain regions have no effect on the capacity of QuIC detection of prion seeds
- Prion seeds can be detected in regions with typical prion disease pathology and which appear to remain 'unaffected' in GSS/101LL animals
- The lack of neurodegeneration in unaffected regions is not due to (i) quantitative differences between the levels of expression of prion seeds in different brain regions or (ii) the time from disease initiation at which each region is exposed to prion seeds
- prion seeds detected in every region tested are PrP^{res}

5.4. Brief discussion

In this thesis, the term prion seed refers to the detection of misfolded prion protein species in a particular sample using the QuIC assay. Prion seeds are the operational definition given to the capability of a sample to propagate the aggregation and/or misfolding of recPrP to a fibril-species of recPrP. Such prion seeds are disease-specific and likely represent misfolded prion protein. However, what exact species of misfolded prion protein that prion seeds represent is, as yet, unknown.

To study the relationship between misfolded prion protein and neurodegeneration, no study to date has been performed using novel techniques developed for enhanced-

detection of prion seeds, such as the QuIC assay. It is unknown whether a possible association between prion seeds and neurodegeneration will be helpful in understanding the progress to neurodegeneration. In order to use the QuIC assay as a suitable protocol for the sensitive detection of prion seeds, a number of confirmatory experiments were required. The first step was to prove that prion seeds could be detected in murine prion strains, regardless of original source (including GSS/101LL animals) and that different regions of the infected mouse brain could seed the assay with equal propensity. As described above, all murine prions strains tested, including in the GSS/101LL model, could act as starting material for the QuIC assay and thus contained prion seeds. Furthermore, experiments with samples from 79A murine prion strain infected brain demonstrated that each region of the brain tested exhibited an equal capacity to identify prion seeds.

Prion seeds were identified in all regions of the brain tested (brain stem, cerebellum, thalamus and cortex) at clinical stage in GSS/101LL animals. This data shows the distribution and accumulation of prion seeds does not correlate with neurodegeneration. This data therefore refutes the hypothesis that misfolded prion protein is closely associated with neurodegeneration. As mentioned earlier, the exact species of misfolded prion protein that prion seeds represent is unknown, and may or may not overlap with IHC or Western blot detectable PrP^{d}.

The presence of prion seeds but absence of neurodegeneration could be explained in a number of ways. Firstly, different brain regions may be exposed to different

quantities of prion seeds, whereby a neuron belonging to a specific brain region, such as the brain stem, are exposed to larger quantities of prion seeds comparative to the cerebellum. This study addressed this question using a dilution series of the sample being used to seed the QuIC assay. Each brain region tested, independent of neurodegeneration, was consistently capable of being diluted to at least 0.001% (w/v) of the original brain mass before losing the ability to seed the QuIC assay. This showed no quantitative difference in levels of prion seeds between brain regions could be observed. Another possible explanation for the absence of neurodegeneration in regions exposed to prion seeds could be accounted for by the time-exposure of prion seeds to a specific brain region. For example, a particular brain region may suffer neurodegeneration as it was exposed to prion seeds for comparatively longer than a region which appears pathologically unaffected. To test this, a number of GSS or NBH/101LL animals were tested at all time-points set up in these experiments (namely 150dpi, 200dpi, 220dpi, 240dpi and at clinical onset). It was found that a region which eventually undergoes neurodegeneration (e.g. thalamus) was exposed to prion seeds at a comparative time-period as a region which appears pathologically unaffected (e.g. cerebellum). A small cohort of GSS/101LL animals accumulates prion seeds in the brain stem at 150dpi. This may explain the earlier pathology observed in the brain stem comparative to the thalamus, as shown in chapter 4.

Overall, prion seeds accumulate within the brain stem initially at earliest stages of disease. This coincides with the appearance of IHC detectable PrP^{d} at 150dpi associated with midbrain neurons. No IHC detectable PrP^{d} was detected in the brain

stem at this stage however. The interpeduncular nuclei and SNc of the midbrain which are associated with the IHC detectable PrP^{d} at this stage exhibit neuronal-connectivity with neurons of the brain stem, such as the dorsal and medial raphe nuclei [334, 335]. This could mean the prion seeds detected in the brain stem at 150dpi may be the result of neuronal-specific migration of prion seeds from midbrain neurons to the brain stem. This study was not set up to answer such specific questions, therefore future studies could study the spread of prion seeds between individual neurons by laser micro-dissecting specific neurons associated with IHC detectable PrP^{d}, such as the interpeduncular nuclei or SNc, and their respective interconnected neuronal populations before and around the 150dpi time-point. At later time-points, however, prion seeds are observed widespread across all brain regions tested, independent of neurodegeneration. This data indicates that prion seeds most likely spread in a non-disease-associated mechanism from one anatomical distinct brain region to another. How and why specific neuronal populations then undergo neurodegeneration is unknown. A possible explanation is the potential for different species of misfolded prion protein present in each brain region or a specific host response elicited from individual regions which renders one brain region susceptible to neurodegeneration, whilst others are resilient.

In this thesis, the species of PrP^{d} identified in regions of neurodegeneration are defined by the inability to detect PrP^{res} using Western blot analysis. Using the QuIC assay, PrP^{res} isoforms of misfolded prion protein can be detected in these regions however. This could either be due to the additional sensitivity of the QuIC assay to detect PrP^{res} isoforms which were not detectable using Western blot, or as a result of

not establishing optimal conditions for the detection of PrP^{res} species using Western blot on GSS/101LL brain regions. Certainly, the detection of small quantities of PrP^{res} specifically in the cortex of GSS/101LL animals using Western blot analysis but the comparative identification of PrP^{res} in cortex and other brain regions tested using the QuIC assay suggests the latter explanation is more likely correct. Future studies may therefore concentrate on defining the exact species of misfolded prion protein present between brain regions. A recent study by Choi *et al*. used sucrose gradients to separate aggregates of PrP in known prion-infected human brains [350]. Unique aggregates of PrP were separated in concentrations of sucrose between prion-infected brain regions in comparison to uninfected brain regions [350]. These differences therefore represent unique misfolded prion protein species detectable between different brain regions of the same individual. Future work could apply this approach to elucidate differences/similarities of PrP aggregates between brain regions in GSS/101LL animals which may explain the selective vulnerability of neuronal populations in specific brain regions. Another explanation for this selective vulnerability may be due to the host response to prion seeds, which may differ between brain regions. To test this, chapter 6 will use a microarray analysis to assess the transcriptome of regions exposed to prion seeds and undergoing neurodegeneration or remaining unaffected.

6. Genome-wide expression changes between different regions of GSS/101LL brains

Chapter aim: To evaluate the host response in multiple brain regions of clinical stage GSS/101LL brains using a microarray analysis.

6.1. Introduction

The appearance of prion seeds exposed to regions of the brain which appear pathologically unaffected, even at clinical stages of disease, led to the hypothesis that the host response is an important factor in determining neurodegeneration. There are a number of methods to study the molecular differences between specific brain regions, such as assessing the transcriptome, proteome or metabolome.

Genome-wide transcriptional analysis using a microarray is a well-established and widely used technique. In prion diseases, a number of microarray studies have been performed previously in mice [218, 228, 230, 351-354], sheep [355, 356], cattle [227, 357-361], non-human primates [362, 363] and humans [364-367]. Other studies assessed the transcriptome of *in vitro* murine infected neurons [368] and identified a number of differentially expressed genes with functions attributed to the cell structure, signal transduction, ribosome biogenesis amongst many others. In this study, differential gene expression was observed between prion infected cell lines, suggesting different neuronal backgrounds respond to the same prion strain in unique

mechanisms [368]. In whole brain analysis however, the predominant signature was represented by the glial cell response, specifically the innate immune response [228, 230, 351-353]. Differential gene expression associated with a number of molecular functions was also observed, for example, genes associated with transcription, RNA splicing, translation, cell proliferation, cell adhesion and signal transduction [228, 230, 351-353]. A more precise, mixed cell analysis was performed on dissected brain regions from ME7 and RML prion infected animals. These arrays concentrated on regions of the brain exhibiting overt neurodegeneration and, similar to whole brain analysis, a predominant glial cell response was also observed [354]. In other animal models of prion disease, the glial cell response is also observed as a predominant feature [227, 355, 356, 358-360] and is also observed in humans [365, 366]. Additionally, a number of other functions overlap with murine microarray studies, for example gene expression changes in genes associated with transcription, RNA splicing, translation and signal transduction [227, 355, 356, 358-360, 364-367]. A number of stress responses have also been identified using the microarray approach, such as ER stress [227, 355, 356].

A recent microarray analysis was performed on laser micro-dissected CA1 pyramidal neurons of the hippocampus of RML-prion disease mice over time. The findings from this study indicated that gene expression in neurons can be separated into distinct active phases [218]. Briefly, a set of genes associated with NMDA receptor signalling are up-regulated in pre-clinical stages of disease, but return to basal levels of expression upon clinical onset of disease [218]. The NMDA receptor signalling is hypothesised to be a neuroprotective response [369].

A number of proteomic and metabolomic studies on prion disease animal models have been performed. These have mostly concentrated on detecting differentially regulated compounds to use as biomarkers in readily available tissue or fluid samples from animals infected with prion disease, such as the blood or CSF [370, 371]. A recent study has assessed the hippocampal proteome [372]. Additionally, this study assessed the astrocyte specific response, identifying a set of proteins which potentially protects against protein misfolding, excitotoxicity and ROS production [372]. Other proteomic studies have assessed the phosphor-states of proteins in prion diseases to evaluate the post-translational modifications incurred during prion disease [373]. The metabolome (profile of endogenous metabolites such as amino acids, nucleic acids, fatty acids, sugars etc.) can be assessed using mass spectrometry or NMR spectroscopy. A recent metabolomics study on the blood of CWD infected elk was performed to test for key biomarkers in prion-infected samples and identified several metabolites potentially specific for prion disease cases [374]. Specific changes in metabolites have also been observed in the brains of AD patients compared to healthy controls [375]. It is likely that as a result of the vast changes in the proteome and transcriptome during disease, the metabolome will exhibit large alterations. What relevance these changes have in neurodegeneration remains unknown.

In the context of this thesis, a tool to assess the host response to prion seeds identified in unaffected regions in comparison to regions of neurodegeneration was

required. As a result of the extensive analysis and overlap of the transcriptome in prion diseases in both animal models and human prion diseases, a microarray is the most appropriate tool to study the host response. To interpret the large data set to compare differentially expressed genes within and between brain regions, a network analysis tool, termed BioLayout *Express*^{3D}, was used [300]. This software allows the visualisation of biological data as a network. In contrast to a typical statistical approach to identify differentially expressed genes of interest, this software uses a correlation measure (pairwise Pearson) to gauge similarities between expression profiles of all transcripts. Data can then be subsequently divided into groups (clusters) using the Markov clustering algorithm (MCL) [302]. This means the software will cluster transcripts together without biasing data with assumptions on experimental design (questions being asked of the experiment) or microarray platform. As a result, this network analysis approach can result in clusters of genes which are co-expressed but not necessarily differentially expressed between the samples being compared. Examples of these are genes which are represented by multiple probe-sets on the microarray platform used [300]. Where clusters of genes are observed that show an interesting pattern of expression; analysis can be verified using statistical approach to test differentially expressed transcripts within a region (two-tailed t-test) or between regions (ANOVA).

6.2. Results

The left hemisphere brain stem, thalamus, cerebellum and cortex from six clinical stage GSS/101LL and aged matched NBH/101LL animals were dissected in artificial CSF followed by RNA extraction and purification (see chapter 2 for details). This

allows the RNA purification from regions of the brain which are undergoing neurodegeneration (brain stem and thalamus) or remain unaffected (cerebellum and cortex) in GSS/101LL animals. NBH/101LL samples are aged matched controls which received an i.c. injection of 1% uninfected brain homogenate at the same time as the GSS infection of 101LL experimental animals. Samples from each mouse were then paired and pooled to minimise individual sample variability, i.e. two GSS/101LL animals paired together and each brain region pooled. This resulted in three RNA samples per brain region for both GSS and NBH/101LL animals. The pooled RNA samples can be viewed in table 6.1. A microarray was then performed using the Affymetrix Mouse Gene 2.0 arrays and transcript intensity was scanned using the Affymetrix GeneTitan Instrument. Raw results were received in the Affymetrix .CEL file format. Overall probe intensity was initially analysed using Affymetrix Expression Console. 21 of 24 array samples used in this analysis exhibited relatively consistent probe intensities across all GSS and NBH brain regions (figure 6.1A). This allowed for normalisation of this data using the parameters outlined in chapter 2. The outlying samples in figure 6.1A do not appear to show any probe cell intensity in comparison to other arrays (figure 6.1B). The reason for this is unclear, but could be due to degraded or low quality RNA or a technical error when performing the microarray. As shown in table 6.1, the 260:280 ratio shows relatively high nucleic acid to protein contaminant proportions in the three samples of interest, similar to those other samples which exhibit good probe intensity on the arrays. This suggests the RNA quality of the three samples is not of a noticeably lower quality compared to other samples which successfully hybridised. Nevertheless, as a result these three array samples have been omitted from this study.

	GSS or NBH	Brain Region	260/280	ng/uL
	GSS	Brain stem (BS)	1.93	276.4
	GSS	Brain stem (BS)	1.92	309.8
	GSS	Brain stem (BS)	1.91	191.4
	GSS	Cerebellum (Cere)	1.94	549.2
	GSS	Cerebellum (Cere)	1.98	672.9
	GSS	Cerebellum (Cere)	1.94	465.5
*	GSS	Thalamus (Thal)	1.91	257.5
	GSS	Thalamus (Thal)	1.92	355
	GSS	Thalamus (Thal)	1.93	362.2
	GSS	Cortex (Cortx)	1.99	666.3
*	GSS	Cortex (Cortx)	2.01	762.8
*	GSS	Cortex (Cortx)	2.01	755.1
	NBH	Brain stem (BS)	1.89	772.4
	NBH	Brain stem (BS)	1.86	601.8
	NBH	Brain stem (BS)	1.78	161.3
	NBH	Cerebellum (Cere)	1.9	1186.2
	NBH	Cerebellum (Cere)	1.91	1266.5
	NBH	Cerebellum (Cere)	1.84	990.5
	NBH	Thalamus (Thal)	1.82	238.5
	NBH	Thalamus (Thal)	1.82	307.3
	NBH	Thalamus (Thal)	1.89	596.3
	NBH	Cortex (Cortx)	1.92	848.2
	NBH	Cortex (Cortx)	1.95	813.5
	NBH	Cortex (Cortx)	1.88	615.4

Table 6.1 - RNA purification from pooled brain regions of GSS/101LL (GSS) and NBH/101LL (NBH) animals

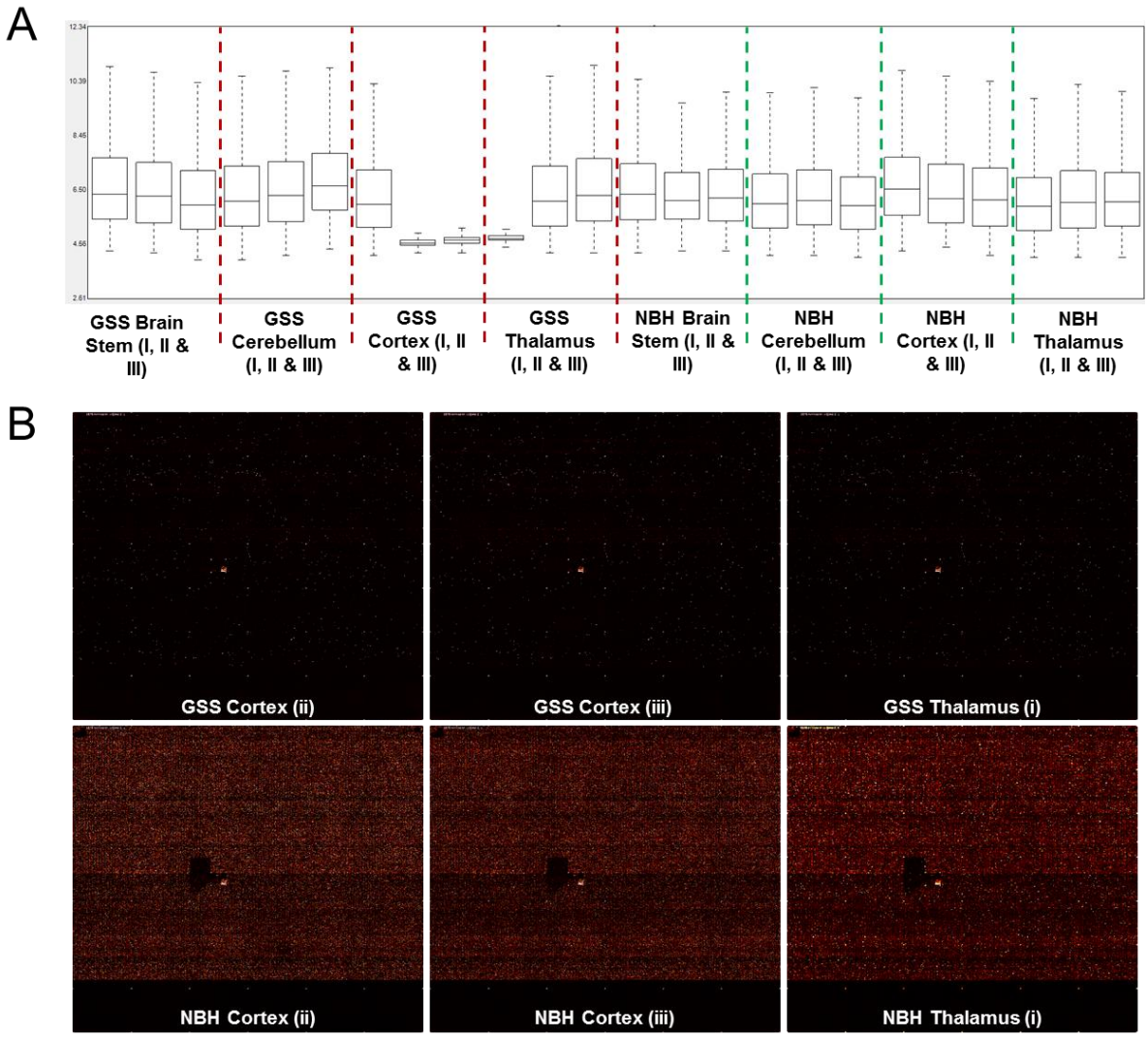

Figure 6.1 – (A) Sample variability in intensity read-out from microarray plate. Red dotted lines indicate GSS samples, green lines NBH. Samples generally show equivalent intensity values, however, three samples (GSS Cortex ii and iii and Thalamus i) exhibit intensity values far outside the general intensity probe. (B) Raw data from .CEL files shows that the three samples run by Edinburgh Genomics failed to adhere to the probe sets on the array chip.

The similarity of samples was assessed after normalisation of data. Figure 6.2 shows the principle component analysis (PCA) of each sample constructed using Pearson correlation coefficient. This type of plot allows the visualisation of sample similarity, whereby the nodes represent an individual sample and the edges represent their

correlation. Thus the closer two samples are together, the higher the sample similarity. This PCA shows an overall clustering of GSS/101LL samples (figure 6.2; red box) and NBH/101LL samples (figure 6.2; green box). The regions of the brain in GSS/101LL animals undergoing overt neurodegeneration (brain stem and thalamus) show relative similarity between NBH thalamus samples. The GSS brain stem however does not show any correlations with NBH brain stem. Similarly, the GSS cerebellum exhibits no correlation to NBH cerebellum. The GSS brain stem and cerebellum however do show sample correlation as do the NBH brain stem and cerebellum. The GSS and NBH cortex samples are clustered as a group, but also show high correlation between GSS and NBH thalamic samples.

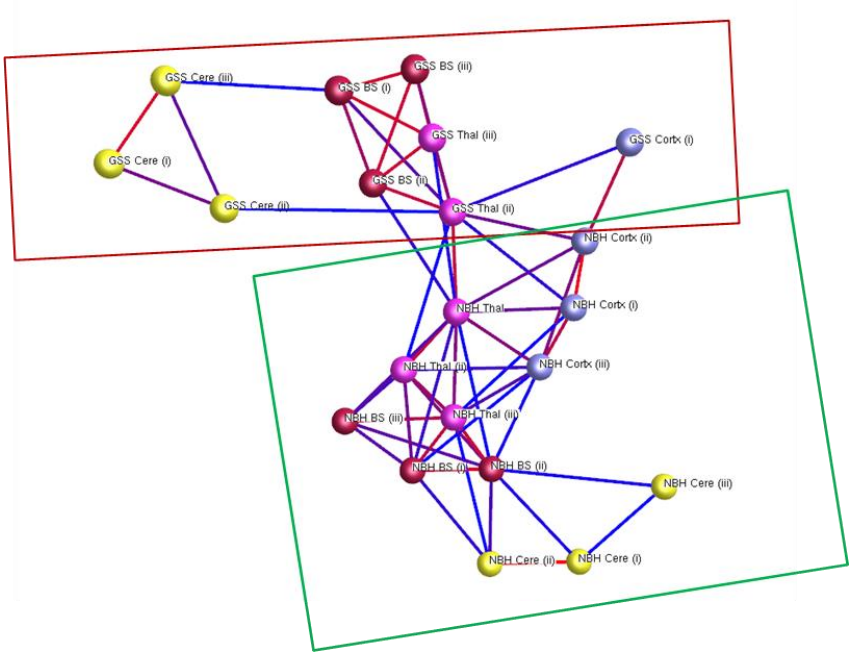

Figure 6.2 - Principle component analysis (PCA) constructed in Biolayout Express 3D representing sample variance. Each node represents a specific sample. Edges are colour coded to represent strength of correlation between samples ranging from red to purple to blue. No edge represents no significant correlation between samples. Red nodes = Brain stem. Pink nodes = Thalamus. Blue nodes = Cortex. Yellow nodes = Cerebellum. The widest variation in samples are the cerebellar samples. The GSS cerebellum clusters together with the closest similarity with GSS brain stem. NBH cerebellum clusters together but has closest similarity to NBH brain stem. The regions of neurodegeneration (GSS brain stem and thalamus) are clustered together also and show the highest similarity to their respective NBH control regions. The GSS and NBH cortex samples cluster together and also show high similarities to the thalamus samples – indicative of the neuroanatomical connections between these regions. Overall clusters of samples are highlighted in the red or green boxes to represent GSS/101LL samples (red) or NBH/101LL samples (green).

6.2.1. Network analysis of all array samples

Network topology showed three distinct major groups of clusters (figure 6.3) and using the MCL algorithm, groups of highly connected nodes were identified. Each cluster of nodes is colour coded and represents transcript expression patterns which are highly correlated. The edges show the correlation coefficient of individual nodes and thus are spatially ordered to show highly correlated samples closely arranged. These groups are defined by clusters of differentially expressed genes in GSS/101LL animals (Figure 6.3; groups B & C) and the non-disease related gene expression differences inherent to individual brain regions (Figure 6.3; group A). Figure 6.4 shows example clusters of each of these three major groups. Group A shows no expressional differences between GSS or NBH individual brain regions, but are identified in this network analysis due to the inherent differential gene expression between individual brain regions. Group B represents a number of highly related clusters showing down-regulated transcripts across all regions of GSS/101LL brains in comparison to NBH/101LL animals. Group C shows up-regulation of genes specifically in brain regions which have been shown to undergo neurodegeneration in chapters 3 and 4.

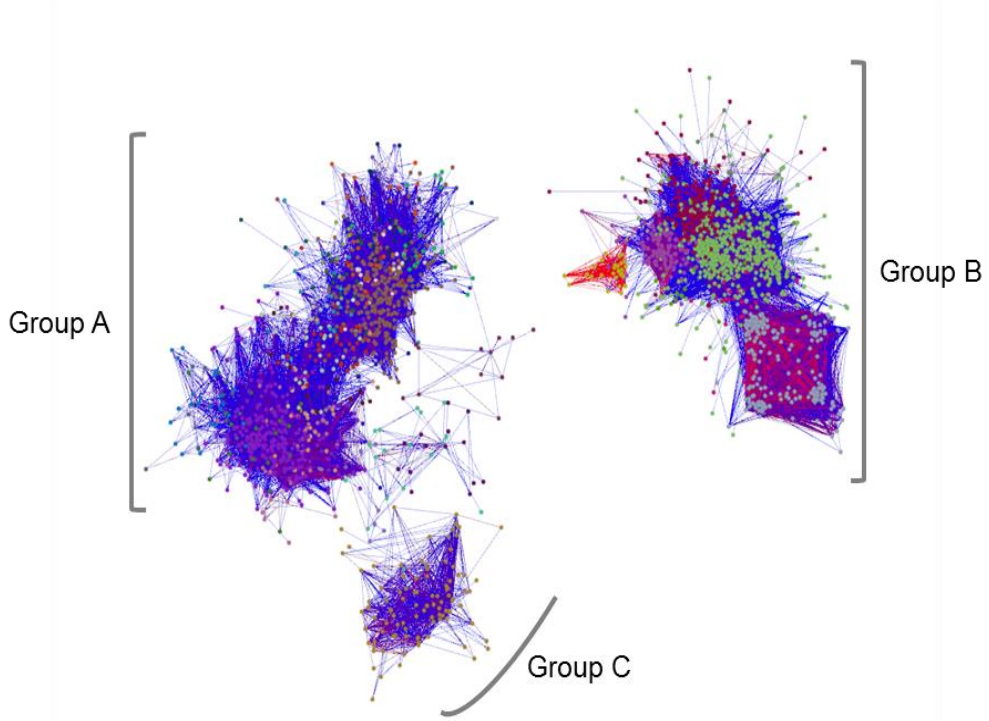

Figure 6.3 - Network graphs constructed by BioLayout *Express*^{3D}. Each node represents an individual transcript and each edge represents the correlation coefficient. Three major groups are defined in this network. Nodes are coloured according to individual clusters based on MCL algorithms.

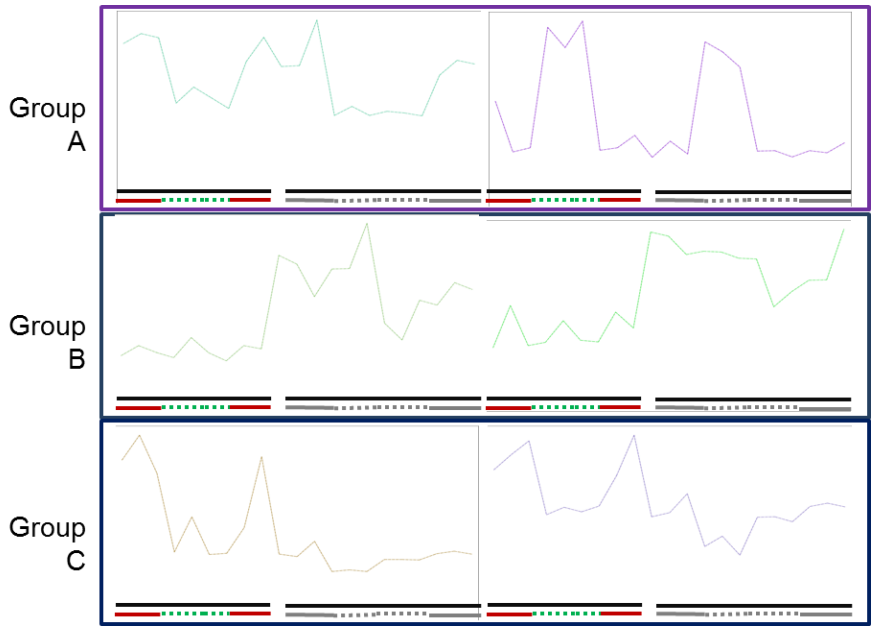

Figure 6.4 - Transcript expression changes in clusters arranged by the Markov algorithm. This data shows the mean expression levels of genes within a sample and shows the comparison to the mean expression levels of other samples. For instance, group B shows high expression in NBH/101LL brain regions in two distinct clusters identified by Biolayout *Express*^{3D} but comparatively lower expression in all brain regions tested within GSS/101LL mice. X-axis shows samples ranging from GSS/101LL brain regions undergoing neurodegeneration (red bars; brain stem and thalamus respectively); GSS/101LL brain regions which are unaffected (green dashed bars; cerebellum and cortex

respectively). Grey bars show NBH/101LL brain regions (solid grey bars; brain stem and thalamus respectively//dashed grey bars; cerebellum and cortex respectively.

6.2.2. Down-regulated transcripts across all brain regions of GSS/101LL animals

Group B exhibits a number of clusters which exhibit down-regulated transcripts across all regions of the GSS/101LL brain in comparison to NBH/101LL animals. These comprise 799 transcripts, of which 380 could be attributed to known or predicted genes, 11 encoded microRNAs, and 40 other non-coding RNAs and pseudogenes. A complete gene list can be found in Appendix 1. The remainder represented multiple transcripts for individual genes. Of the 380 genes identified in this group, 235 had a known function. Figure 6.5a shows a breakdown of functions attributed to the 235 genes, which include genes related with sensory function, immune function, genes involved in transcription, transcriptional regulation, pre-mRNA splicing, and translation. The largest proportion of genes is attributed to sensory function. These represent large families of vomeronasal receptors (42 genes) and olfactory receptors (41 genes), in addition to two taste receptor genes. Figure 6.6 shows examples of down-regulated sensory related genes across all regions tested.

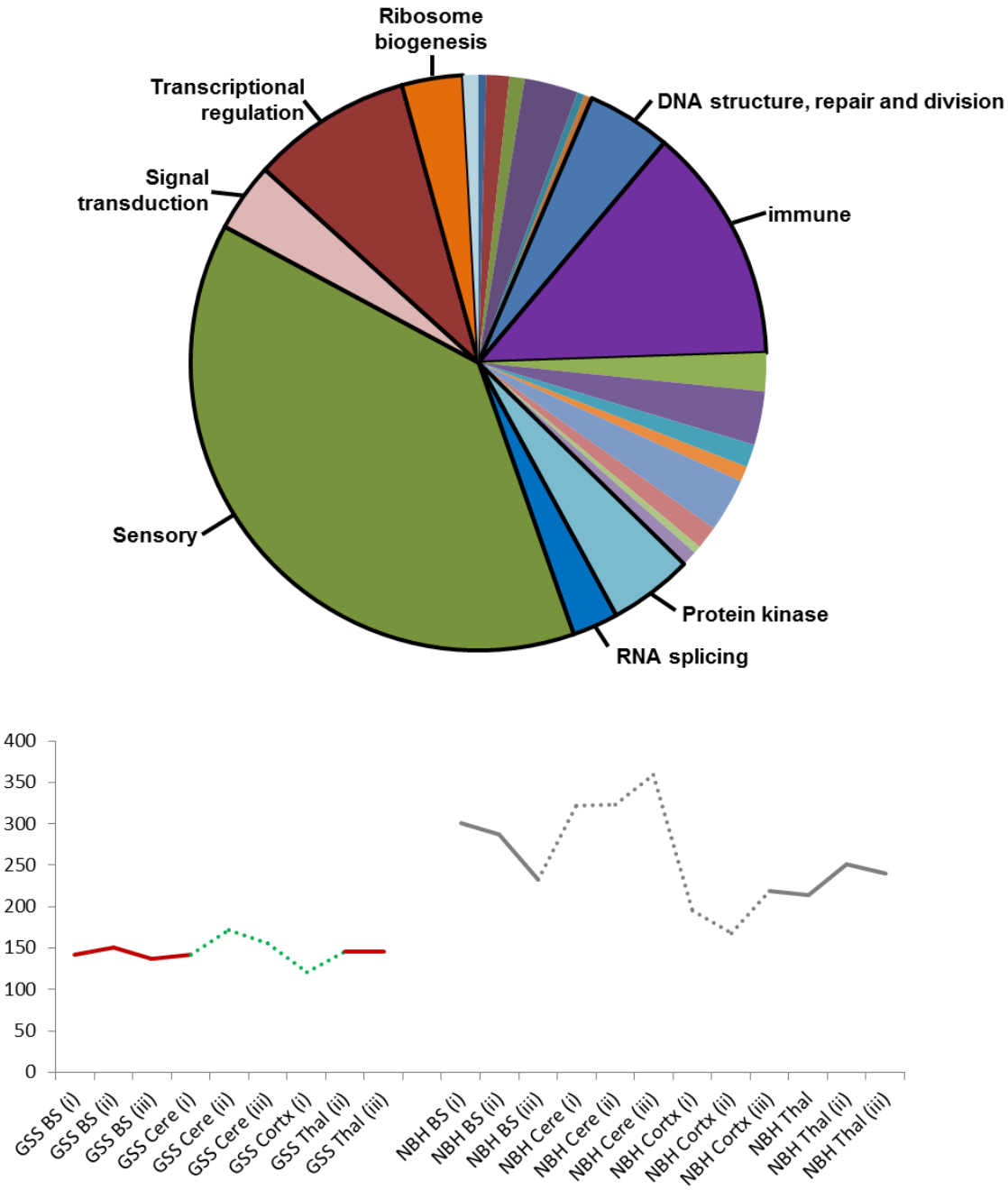

Figure 6.5 - (A) Breakdown of functions of genes identified in clusters assigned to group B. The largest proportion of genes belong to 3 families of sensory receptors; olfactory receptors, vormeronasal receptors and taste receptors (38%). Other general gene functions identified were immune related (13%) and transcriptional regulation (9%). (B) Average transcript intensity per sample found in all clusters of group B. (Red solid bars; GSS brain stem and thalamus, respectively. Green dashed bars; GSS cerebellum and cortex, respectively. Grey solid bars; NBH brain stem and thalamus, respectively. Grey dashed bars; NBH cerebellum and cortex, respectively.

A number of genes related to immune function have also been identified in this group. These consist of pro-inflammatory cytokines and receptors (e.g. interferon 1α

and TLR4), chemokines (e.g. CCL2) and genes related to neutrophil (e.g. Defensin-α 23) and Natural Killer cell (CD244) recruitment and function. Figure 6.7 shows the expression changes of some down-regulated immune related genes across all regions. A set of transcriptional regulatory proteins, Sp100/Sp110/Sp140, are also shown to be down-regulated (Figure 6.8). These form a complex, which is a constituent of the PML nuclear body (NB) [376] the expression of which is controlled by interferon levels [377]. Sp100 is most widely studied, and has been shown to play an important anti-viral function [378-380], through the transcriptional regulation of the transcription factor ETS1 [381, 382]. The ETS1 transcription factor directly controls the expression of a number of defensins, cytokines and chemokines [383]. The ETS1 gene, however, shows no evidence of changed expression in any region. Other functions of the Sp100/Sp110/Sp140 complex involve transcriptional control, as RNA polymerase II has been shown to co-localise with NBs [384-386] and nascent RNA has been identified in the periphery of NBs [387]. Indeed, genes involved in regulating RNA polymerase activity (e.g. CTDSPL [388] and Med7 [389]) and a subunit of RNA polymerase II (Polr2k) are found down-regulated (figure 6.9). A component of the Cullin-RING-based BCR E3 ubiquitin-protein ligase complex, Speckle-type POZ protein (SPOP), is also down-regulated in all brain regions (figure 6.10). This complex mediates ubiquitination and proteasomal degradation of target proteins, such as breast cancer metastasis suppressor 1 (BRMS1) and death-domain associated protein (DAXX) [390, 391], of which are repressors of NF-κB activation and constituents of the PML nuclear body, respectively [376, 392]. It was found that a general increase in expression of these down-stream genes occurred, although this is only statistically significant in brain stem and cerebellum for BRMS1 (t-test;

p<0.05) and only brain stem for DAXX (t-test; p=<0.05) (figure 6.10). The down-regulation of SPOP indicates that the protein products of such genes are likely to be increased during disease and the observation of an increase gene expression level supports this.

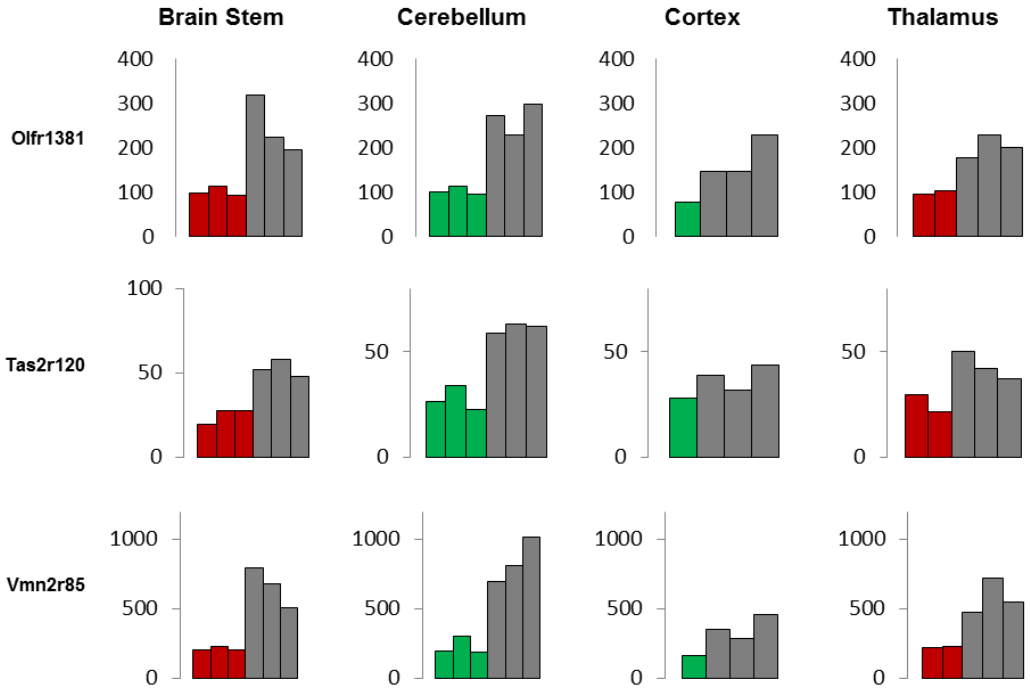

Figure 6.6 - Down-regulation of genes associated with sensory reception. Representative genes from the olfactory receptor family (Olfr1381), taste receptor family (Tas2r120) and vomeronasal receptor family (Vmn2r85) show down-regulation across all regions tested. Red bars; GSS brain stem and thalamus as assigned. Green bars; GSS cerebellum and cortex as assigned. Grey bars represent the respective NBH control.

A number of ribosomal proteins have also been shown to be down-regulated across all regions tested (figure 6.11). These include genes which encode components of the 40S (Rps12 and Rps18) and 60S (Rps7a) ribosomal subunits, suggesting loss of translation. Overall, the down-regulation of the Sp100/Sp110/Sp140 gene complex, possibly by the down-regulation of interferons, appears to be central to a large proportion of differentially regulated genes. The Sp100/Sp110/Sp140 complex is

commonly expressed in cells of the innate immune system, including macrophages [393]. As microglia represent the predominant macrophage population within the CNS, it is likely the substantial down-regulation of many of the genes identified in this group may be predominantly within microglia.

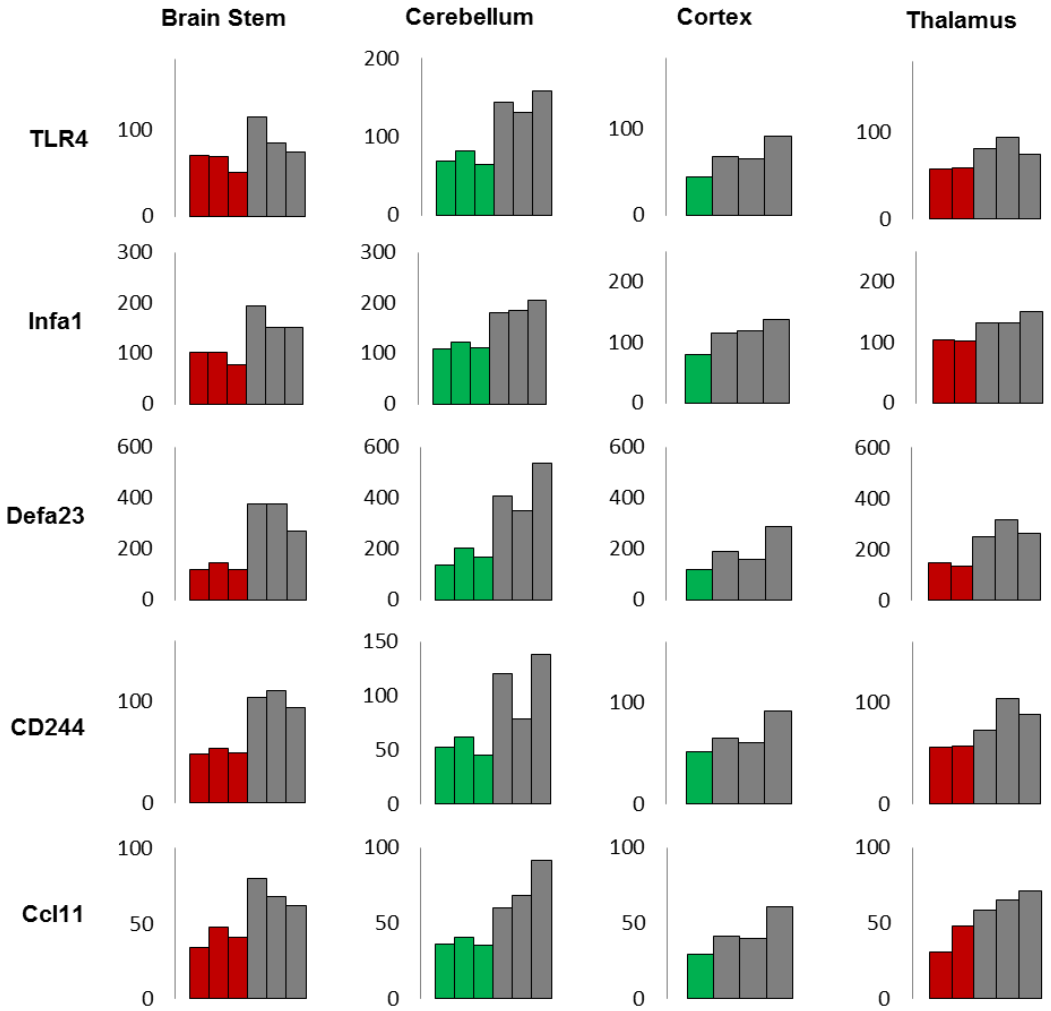

Figure 6.7 - Down-regulation of genes associated with the immune response, such as pro-inflammatory genes Toll-like receptor 4 (TLR4) and interferon1α (Infa1). Defa23 and CD244 are molecules expressed on neurophils and NK cells respectively and Ccl11 is a chemokine. All show down-regulation in every region tested.

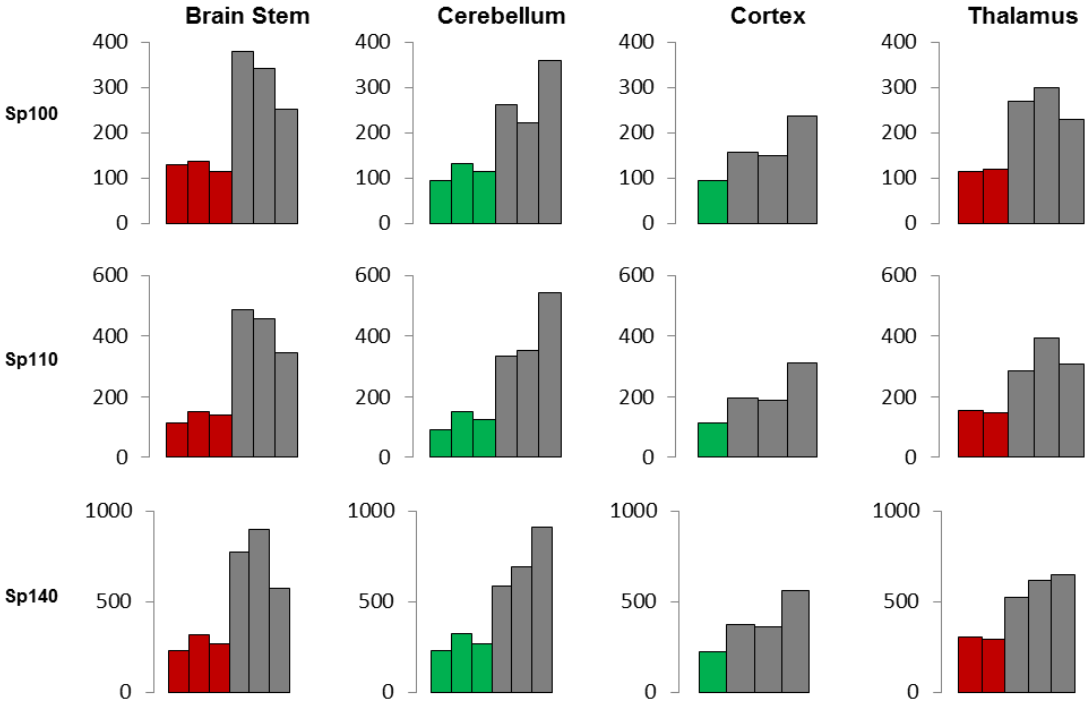

Figure 6.8 - Down-regulation of transcription regulatory genes involved in anti-viral responses. These genes also regulate transcription, via interaction with RNA polymerase II and translation via ribosome biogenesis. All regions show down-regulation of this complex.

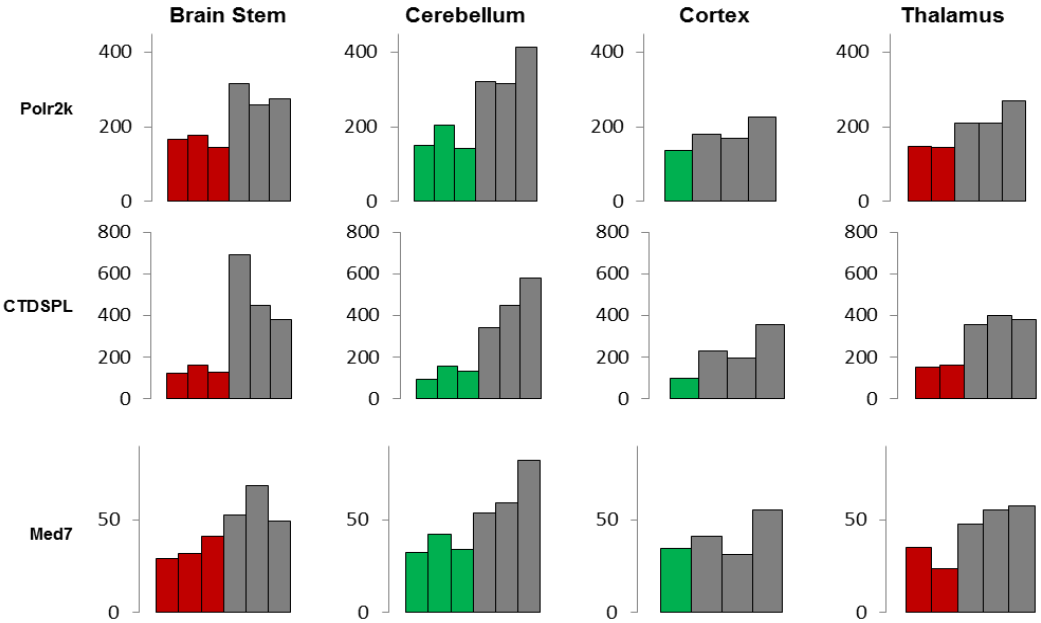

Figure 6.9 - Down-regulation of the RNA Polymerase II subunit, Polr2k, and other genes involved in mediating RNA Polymerase II activity. This is likely the result of the down-regulation of the Sp100/Sp110/Sp140 complex of genes in cells of the innate immune system, such as microglia. This therefore represents a possible loss of transcription of RNA Polymerase II targets in microglia and other CNS macrophages or potentially recruited blood leukocytes.

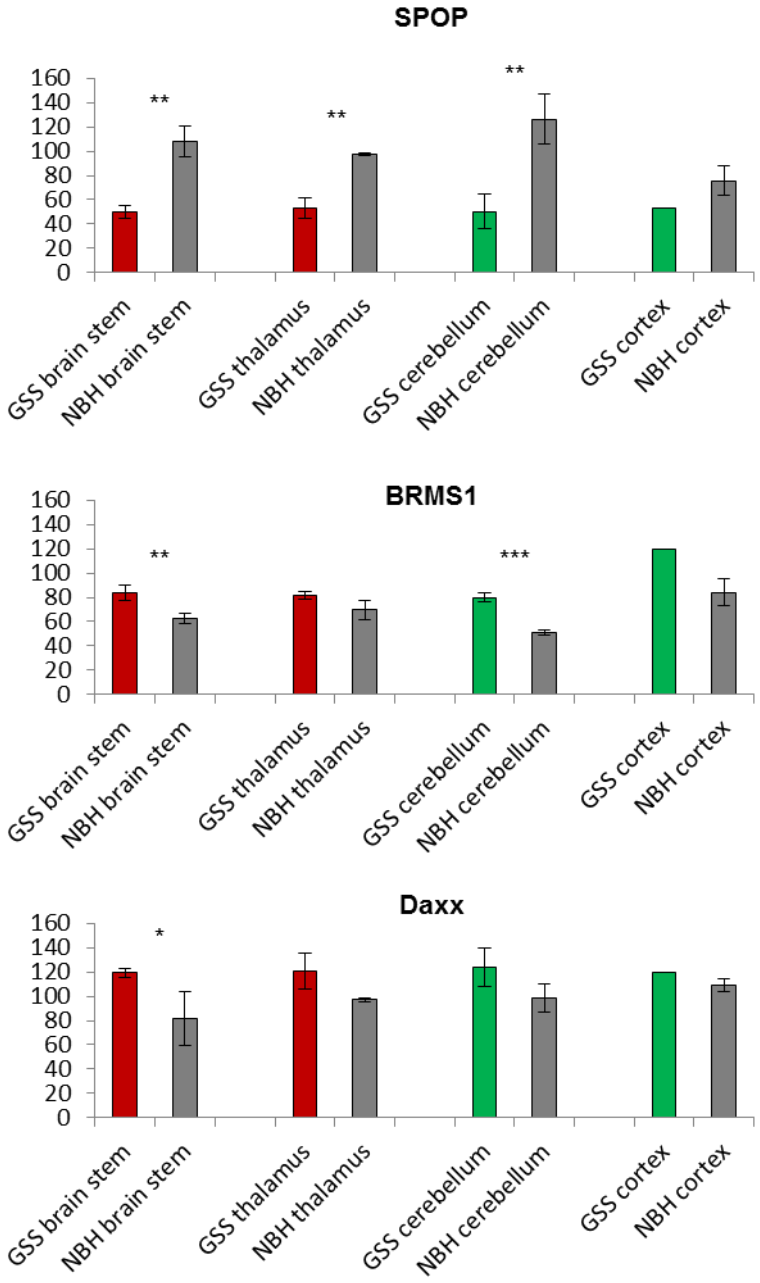

Figure 6.10 - Down-regulation of speckle-type POZ protein (SPOP) across all brain regions tested (t-test; p=<0.01). A increase in BRMS1 and DAXX, targets of SPOP-mediated ubiquitination, are also observed, although this is only significantly observed at the transcript level in brain stem and cerebellum for BRMS1 (t-test; p=<0.01 and <0.001 respectively) and only in brain stem for Daxx (t-test; p=<0.05).

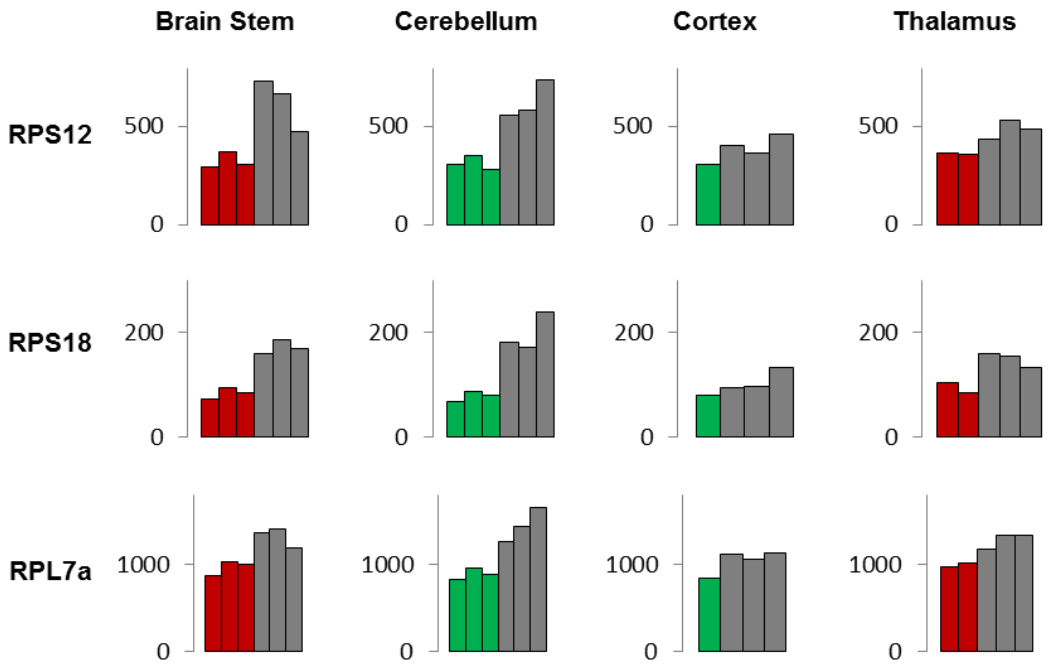

Figure 6.11 - Decreased expression of genes encoding ribosomal subunits. RPS12 and RPS18 encode subunits of the 40S ribosome, whereas RPL7a encodes a subunit of the 60S ribosome.

6.2.3. Neurodegeneration specific up-regulation of genes

In GSS/101LL animals, the brain stem and thalamus suffer neurodegeneration at clinical stages of disease. The cerebellum and cortex, however, appear unaffected using histopathological analysis. Figure 6.3 shows a separate group (Group C) which exhibits an up-regulation of genes specifically within regions of the brain which are undergoing overt neurodegeneration. This group comprises 117 transcripts which consist of 113 known or predicted genes (a complete gene list can be found in Appendix 2). The attributed functions of these genes are predominantly orientated around the immune response (figure 6.12 and figure 6.13). Cell proliferation and phagocytosis are also up-regulated (figure 6.14).

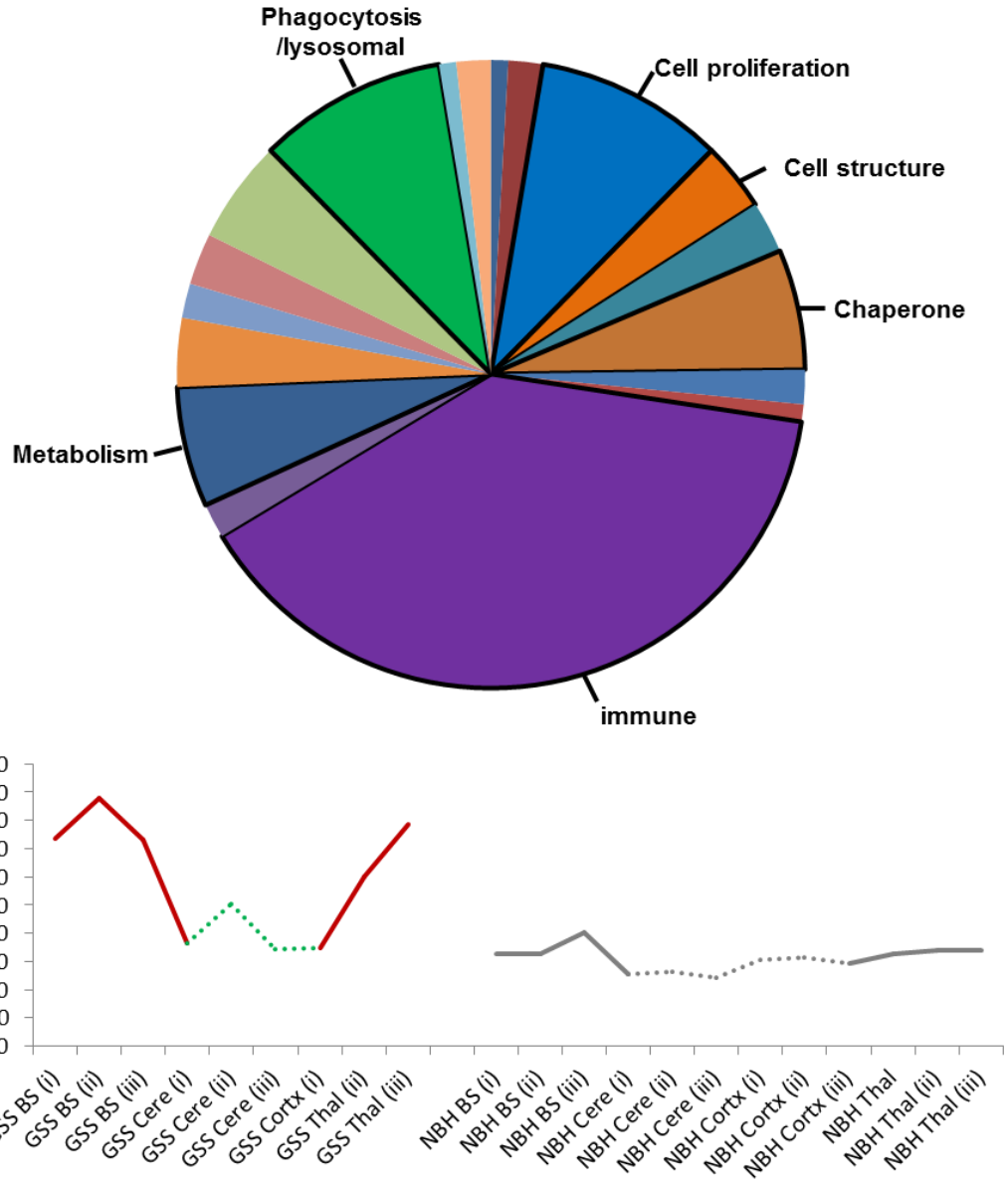

Figure 6.12 - (A) Breakdown of functions of genes identified in clusters assigned to group C. The largest proportion of genes are related to immune function (39%). Other general gene functions identified were genes related with cell proliferation (10%), phagocytosis and lysosomes (10%). (B) average transcript intensity per sample found in all clusters of group C. Red solid bars; GSS brain stem and thalamus, respectively. Green dashed bars; GSS cerebellum and cortex, respectively. Grey solid bars; NBH brain stem and thalamus, respectively. Grey dashed bars; NBH cerebellum and cortex, respectively.

Some astrocyte specific genes are also observed in this group, such as GFAP and major facilitator super family domain containing 2a (Mfsd2a) which are involved in reactive astrogliosis [248] and BBB [394] respectively. Due to the fact that GSS thalamus and GSS cortex samples had to be omitted, resulting in a loss of power of

analysis of these regions, analysis of group C genes will concentrate on a comparative analysis of the brain stem against the cerebellum. Figure 6.13 highlights a cohort of genes up-regulated specifically in the brain stem, which include TGFβ-1, components of the complement pathway, Relt, Toll-like receptors and TREM2. These indicate a hybrid pro- and anti-inflammatory response in these regions. There is some evidence of an increase of such genes within the cerebellum, such as TGFβ and Relt; however this is not statistically significant in comparison to the brain stem (ANOVA; p=<0.001).

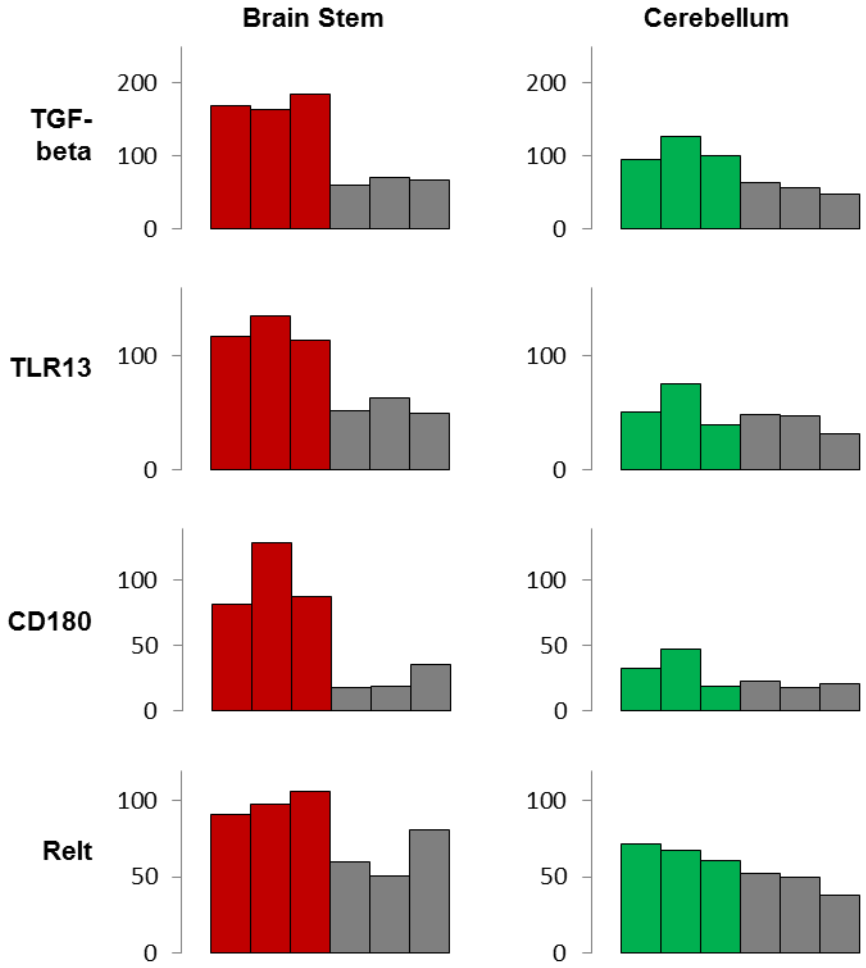

Figure 6.13 - Increased expression of genes related to immune function, particularly within the innate immune response. Some increase in TGF-beta and Relt are observed (t-test; p=<0.05) in the cerebellum, however the increased expression of these genes is more extensive in the brain stem compared to the cerebellum (ANOVA; p=<0.001).

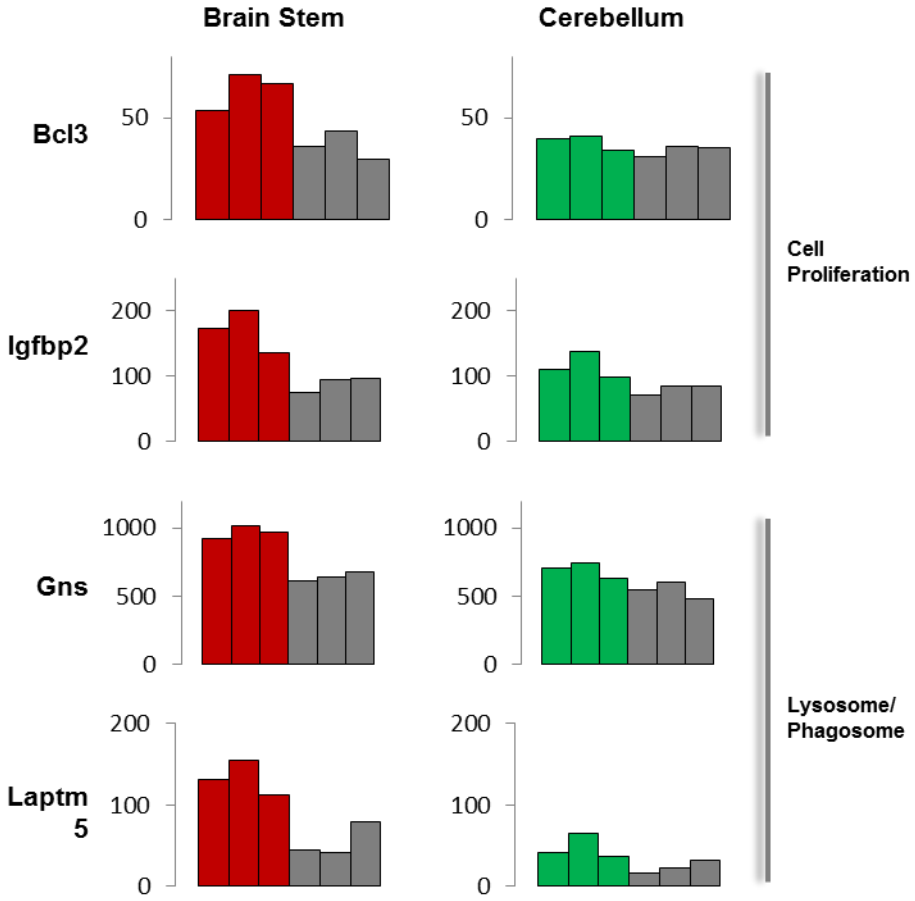

Figure 6.14 - Increased expression of genes related to cell proliferation (e.g. Bcl3 and Igfb2) and phagocytosis and lysosome specific genes (such as Gns or Laptm5). These genes are statistically significantly increased in GSS brain stem (t-test; p=<0.05) but no change is observed in the cerebellum.

Despite the expression of genes predominantly involved in the innate immune response, such as TGFβ1, no interleukins and only interleukin receptor 13α1 (IL13Ra) were identified in this group. Using transgenic mice which exhibit KO of cytokines or cytokine receptors, a number of studies have shown significant alterations of the incubation period of prion infected mice comparative to a WT prion infection. These include KO of genes which increase the incubation period, such as IL1r1 [395, 396], Ccl2 [397] and Cxcr3 [398] and KO or knock-down of genes which shorten the incubation period such as TGFβ1 [276], IL4 [399], IL10 [396, 399], IL13 [399] and Ccr1 [400]. In addition, KO of the CD14 surface antigen,

which is preferentially expressed on monocytes/macrophages and plays a role in activating the pro-inflammatory mediators TLR2 and TLR4, results in an increased incubation period [401]. It is important to note a number of other cytokine or cytokine receptor KO transgenic mice have been infected with prion diseases with little observable effect. These include Tnf, Tnfr1, Tnfr2, Ccr2, Ccr5 [396], and IL6 [402]. Table 6.2 shows the change in expression of these particular gene expression profiles in this study. Generally, KO genes from previous studies which show an increased incubation period are either up-regulated specifically in regions of neurodegeneration (e.g. CD14), or in both brain stem and cerebellum (e.g. IL1r1). Others do not show a change in expression comparative to NBH brain regions (e.g. Ccl2 and Cxcr3). Conversely, KO of genes which result in shortened incubation period are down-regulated in both brain stem and cerebellum (e.g. IL13) or only GSS cerebellum (Ccr1), whereas IL4 and IL10 show no change.

	Brain stem	t-test (p-value)	Cerebellum	t-test (p-value)
Il1r1	Up	0.0028	Up	0.0004
Ccl2	No change	>0.05	No change	>0.05
Cxcr3	No change	>0.05	No change	>0.05
CD14	Up	0.0414	No change	>0.05
IL4	No change	>0.05	No change	>0.05
IL10	No change	>0.05	No change	>0.05
IL13	Down	0.0409	Down	0.0218
Ccr1	No change	>0.05	Down	0.0487

Table 6.2 - Expression changes of genes in previously shown to impact incubation period of murine prion diseases when knocked out. Genes which confer an elongated incubation period when knocked out are Il1r1, Ccl2, Cxcr3 and CD14. All genes are comparative to the appropriate NBH brain stem or NBH cerebellum controls. Il1r1 and CD14 show an increase in expression in GSS brain stem and Il1r1 also shows an increased expression in GSS cerebellum. Genes which confer a shortened incubation period are IL4, IL10, IL13 and Ccr1. Ccr1 shows decreased expression in only the GSS cerebellum, but IL13 shows decreased expression in both GSS brain stem and GSS cerebellum. All other genes show no significant expression differences.

6.2.4. Up-regulation of genes specifically in cerebellum

In addition to the two major groups of genes which are differentially expressed either across all regions or in regions of neurodegeneration, a smaller group of up-regulated genes specifically in the cerebellum were identified (figure 6.15A). This cluster of genes is found in group A (figure 6.3; group A) due to the correlation with cerebellum-only expressed genes in GSS and NBH/101LL animals (figure 6.15B).

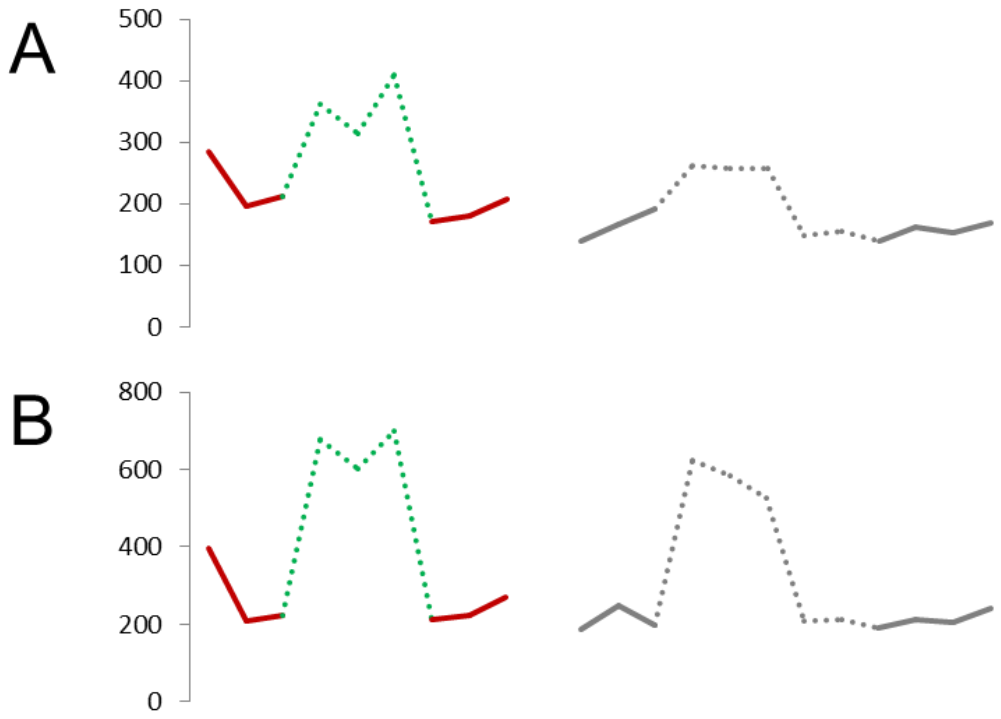

Figure 6.15 - (A) Average transcript intensity of a group of clusters which show increased transcript intensity in GSS cerebellum comparative to NBH cerebellum. (B) Average transcript intensity of a cluster of genes which show high expression specifically in cerebellum, independent of disease. Red bars, GSS brain stem and GSS thalamus respectively. Green dashed bars, GSS cerebellum and GSS cortex respectively. Grey bars, NBH brain stem and NBH thalamus respectively. Grey dashed bars, NBH cerebellum and NBH cortex respectively.

This group consists of 41 transcripts which can be assigned to 40 known or predicted genes. 31 genes have a known function. A complete gene list can be found in Appendix 3. The largest groups of these genes are involved within neuronal function

(6 genes) and transcriptional regulation (7 genes) (figure 6.16). As shown in chapter 3 of this thesis, brain regions which are pathologically unaffected (such as the cerebellum and cortex) appear to show an increased staining intensity of neuronal specific markers, such as MAP2. Figure 6.17A shows the increased expression of each gene associated with neuronal function in the cerebellum. Previous studies have identified an increased level of parvalbumin staining which precedes neurodegeneration in organotypic slice cultures of the cerebellum [403]. Although parvalbumin expression wasn't correlated with the six genes identified in this group; transcripts for parvalbumin are statistically significantly increased in the cerebellum also (figure 6.17B).

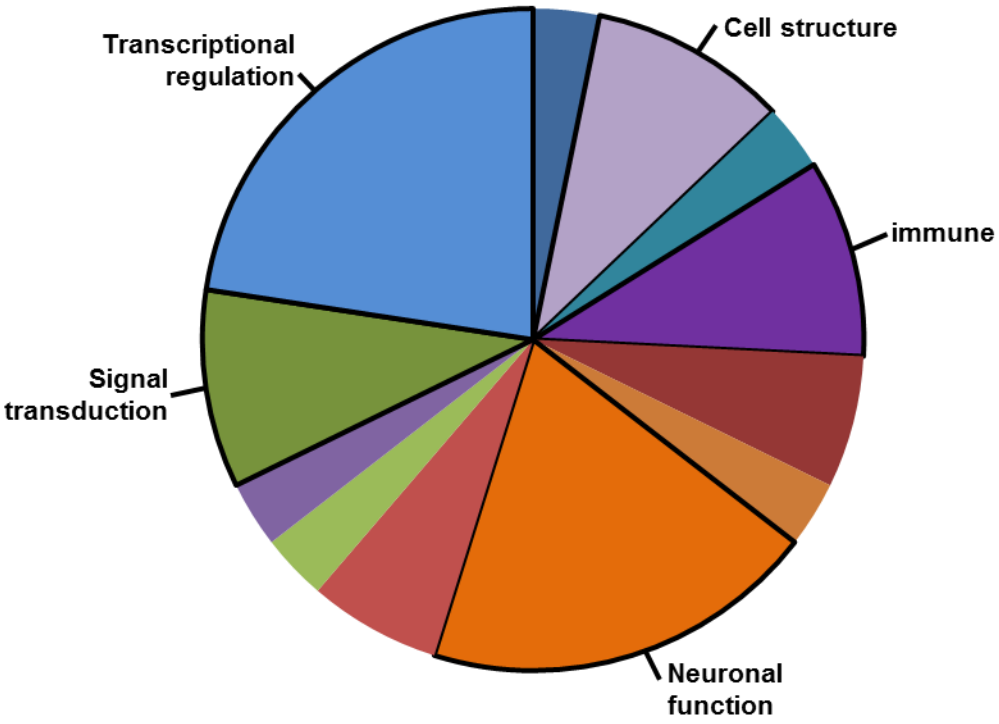

Figure 6.16 - Breakdown of functions of genes identified in clusters which show increased expression in GSS cerebellum comparative to NBH cerebellum. Genes attributed to neuronal function (6 genes) and transcriptional regulation (7 genes) represent the largest proportions of this cluster.

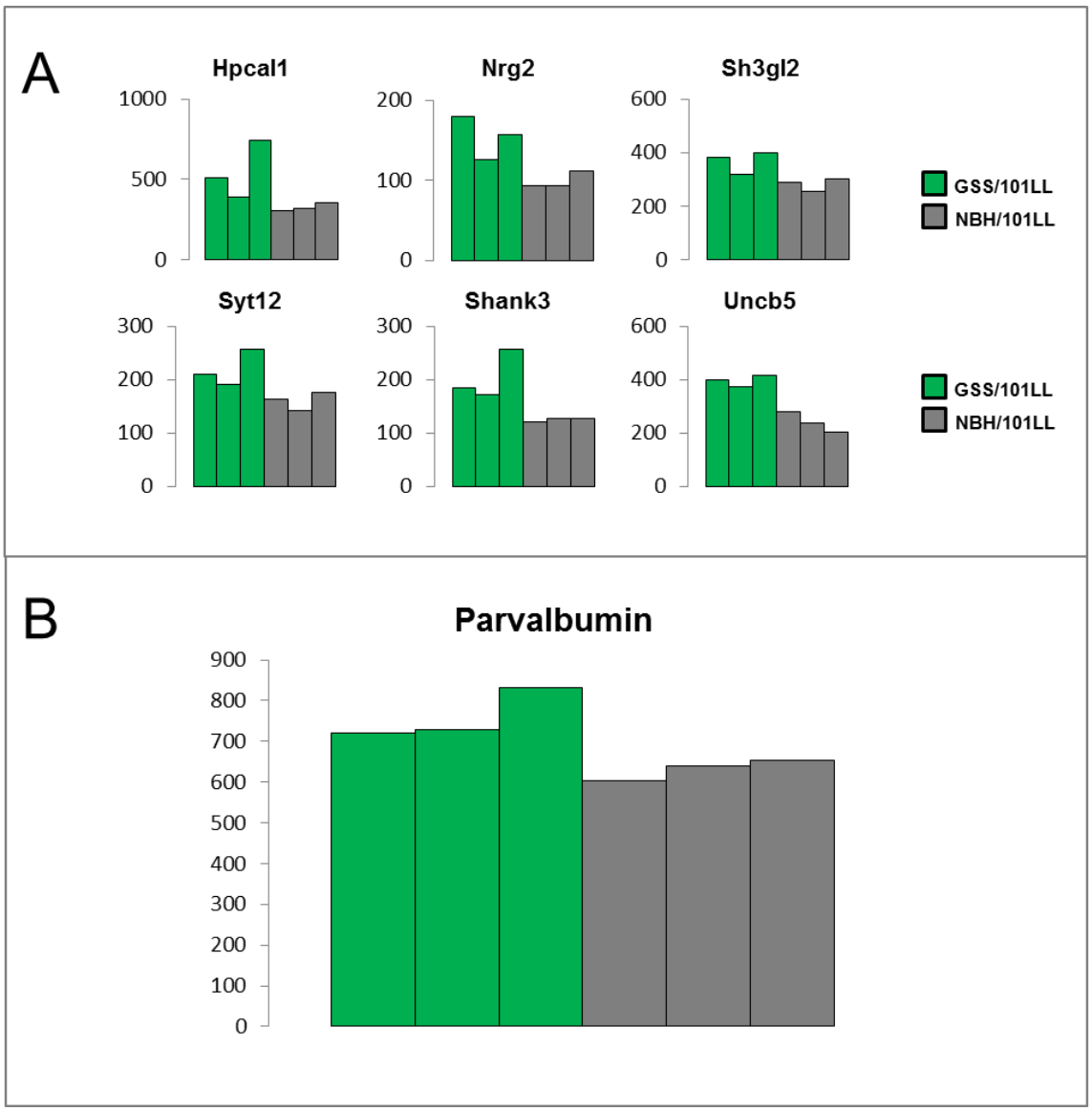

Figure 6.17 - (A) Increased expression of genes related to neuronal function in GSS cerebellum (green bars) comparative to NBH cerebellum (grey bars). (B) Increased expression of parvalbumin within GSS cerebellum comparative to NBH cerebellum (t-test; p=<0.05).

6.2.5. Differential stress responses in individual brain regions

Recent studies have suggested the involvement of ER stress and activation of the UPR in neurons as a potential neurotoxic mechanism in prion diseases [225-227]. Other studies have implicated oxidative DNA damage as a key mechanism of neurodegeneration in prion diseases [404]. The network analysis performed in this

study does not highlight the differential expression of such stress response pathways. However, to probe whether differential gene expression occurs in response to stresses, the activated transcription factors (ATFs) were assessed for differential expression. These are known to be activated as a result of various stresses, including cytokines [405], DNA damage [406] and misfolded proteins [407] and regulate the expression of stress response pathways [405-414]. Figure 6.18 shows the transcriptional changes of a number of transcripts assigned to the ATF transcription factors. As can be seen, the brain stem exhibits a statistically significant up-regulation of ATF2 (t-test; p=<0.05), ATF4 (t-test; p=<0.05), ATF6β (t-test; p=<0.01) and ATF7 (t-test; p=<0.05). The thalamus exhibits an up-regulation of ATF6 (t-test; p=<0.05) and ATF7 (t-test; p=<0.05). This data shows that in two anatomically distinct regions undergoing overt neurodegeneration, the specific stress response observed can differ. The cerebellum exhibits a statistically significant up-regulation of ATF1 (t-test; p=<0.05), ATF6 (t-test; p=<0.05) and ATF6β (t-test; p=<0.01). Due to omission of cortex samples, statistical analysis could not be performed on cortex, however up-regulation of ATF1 and ATF6β were prominent. In regions which appear pathologically unaffected, there appears to be a consistent stress response which differs only by the involvement of ATF6 in the cerebellum. ATF7 is consistently up-regulated in regions of neurodegeneration. Overall this data indicates the expression changes of transcription factors which have broad implications within stress response pathways in both regions of neurodegeneration and regions defined by pathological analysis as unaffected whilst exposed to prion seeds.

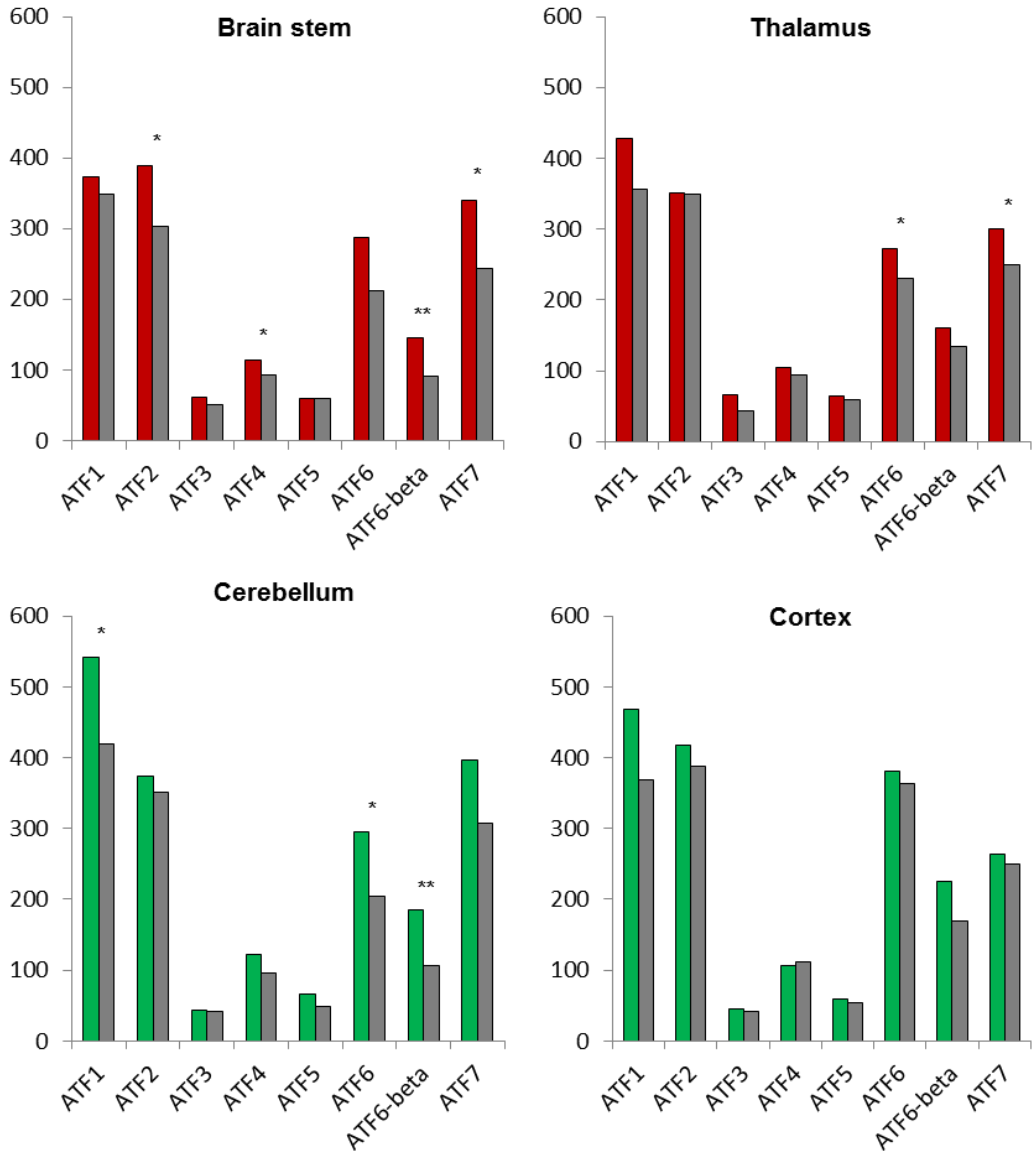

Figure 6.18 - Differential gene expression in activated transcription factors (ATFs). In GSS brain stem, an increase in ATF2 (t-test; p=<0.05), ATF4 (t-test; p=<0.05), ATF6-beta (t-test; p=<0.01) and ATF7 (t-test; p=<0.05) is observed. In GSS thalamus, an increase in ATF6 (t-test; p=<0.05) and ATF7 (t-test; p=<0.05) is observed. In GSS cerebellum, an increase in ATF1 (t-test; p=<0.05), ATF6 (t-test; p=<0.05) and ATF6-beta (t-test; p=<0.01) is observed. No statistical analysis can be performed in cortex due to omitted samples prior to analysis; however a large increase in ATF1 is observed in GSS cortex.

6.3. Results summary

- Two major groups of differentially regulated genes were observed; a down-regulation of genes across all regions tested and an up-regulation of genes specifically in regions of neurodegeneration. These can both be attributed to a microglial response
- Within regions of neurodegeneration, a hybrid pro- and anti-inflammatory response is observed
- A small up-regulation of genes specifically in the cerebellum which are partly involved in neuronal function (concurring with an up-regulation of neuronal specific proteins shown in chapter 3.
- Stress response pathways are suggested to be present across all regions, including cerebellum and cortex

6.4. Discussion

To test the hypothesis that different brain regions may protect/prevent neurodegeneration from occurring in pathologically unaffected regions exposed to prion seeds, a microarray analysis was performed. Two major groups of differentially expressed genes were identified. These consisted of a group of genes down-regulated across all brain regions tested and a group of genes up-regulated only in regions of overt neurodegeneration. A large proportion of genes which are down-regulated are related to sensory function, namely olfactory, vomeronasal and taste reception. What implications this has, if any, upon neurodegeneration is unclear and requires further studies to elucidate whether this is indeed an important mediator of disease or simply a consequence. The remaining genes in this group represented a down-regulation of

pro-inflammatory cytokines and anti-viral response genes. The down-regulation of this anti-viral response (orientated around the Sp100/Sp110/Sp140 complex) can thus have an impact upon transcription and ribosome biogenesis [377, 381, 382, 384-387]. Indeed, a large number of genes and non-coding RNA are down-regulated in a pattern correlating with the down-regulation of RNA polymerase II and other genes regulating its expression (e.g. CDTSPL and Med7). Additionally, a number of ribosomal genes encoding parts of the 40S and 60S ribosome subunits have also been shown to be down-regulated. The Sp100/Sp110/Sp140 complex is predominantly thought to function in the NB in cells of the innate immune system, including macrophages [377-380]. Therefore, this down-regulation of genes is most likely a microglial specific response, although this requires further verification. The down-regulation of pro-inflammatory cytokines observed in this group, such as interferons, has previously been shown to transcriptionally control the expression of the Sp100/Sp110/Sp140 complex of genes [377]. The down-regulation of Speckle-type POZ protein (SPOP) is likely having an additive effect to the overall down-regulation of many pro-inflammatory cytokines and receptors down-regulated in this group. SPOP is a component of the cullin-RING-based BCR ubiquitin-protein ligase complex [415] which mediates the proteasomal degradation of a number of target proteins, such as BRMS1 and DAXX. BRMS1 has previously been described to inhibit nuclear translocation of NF-κB [416]. This prevents the NF-κB transcriptional activation by cytokines shown to up-regulate in this study (e.g. Relt or IL1a) [417]. Therefore the decrease in SPOP levels, leading to an increase in BRMS1 results in the inhibition of the NF-κB pathway. This may act in competition to the activation of the NF-κB activation by pro-inflammatory cytokines which are up-regulated in this

study in regions of neurodegeneration. The down-regulation of SPOP can also lead to increased levels of DAXX, as mentioned above. DAXX has been shown to activate the Jun NH_2-terminal kinase (JNK) pathway through the mitogen-activated protein kinase, ASK1 [418]. ASK1 is activated as a result of cytokine [419] and/or other stress stimuli [420]. Therefore the increase in DAXX therefore represents a possible mediator of cell death in prion diseases, which is controlled by the signalling of pro-inflammatory cytokines to the neuron. Supporting this, studies in Parkinson's disease have shown mutations in the DJ-1 gene present in a monogenic form of human parkinsonism [421]. DJ-1 was subsequently shown to prevent DAXX binding to ASK1 and as a result, prevented apoptosis [422]. Therefore, it is hypothesised the loss of DJ-1 function in these patients leads to increased apoptosis which is a major contributor to disease in these patients.

In regions specifically undergoing neurodegeneration, pro-inflammatory cytokines (such as Relt, a member of the TNF superfamily) and anti-inflammatory or wound repair cytokines (such as TGFβ-1) are up-regulated. A number of genes involved in cell proliferation have also been identified in this group. Previous studies have shown that microglial proliferation can exacerbate prion disease but inhibition of this proliferation can lengthen prion disease incubation [280]. Further, genetic KO models of genes involved in the innate immune response have shown to influence the incubation period of prion disease. For example, KO of Il1r1, Ccl2, Cxcr3 and CD14 results in a prolonged incubation period [396-398, 401]. KO or knock-down of TGFβ-1, IL4, IL10, IL13 or Ccr1 on the other hand results in a shortened incubation period [276, 396, 399, 400]. Expression changes in the brain stem when assessing

these genes showed an increase of CD14, an activator of TLR2 and TLR4, and IL1r1 in both brain stem and cerebellum. A down-regulation of IL13 was observed in both brain stem and cerebellum and Ccr1 was also found decreased in cerebellum only. Broadly, genes which result in a shortened incubation period in KO animals infected with prion disease are shown here to be down-regulated in disease. Conversely, KO of genes resulting in a lengthened incubation period are shown here to be up-regulated. It is important to note however, other genes which impact incubation period (e.g. Ccl2, Cxcr3, IL4 and IL10) do not exhibit differential gene expression. Taken together, innate immune response and cell proliferation observed in regions undergoing neurodegeneration exemplify the importance of these factors within neurodegeneration.

The contradictory down-regulation of other pro-inflammatory cytokines and receptors, such as interferons and TLR4 (figure 6.3; group B) hints at the host's response to inhibit specific aspects of the innate immune response within an individual microglial cell. Alternatively, these differential responses may occur in different populations of microglia within the same brain region (represented in figure 6.19). Indeed, results in chapter 3 demonstrate this whereby, for example, thalamic degeneration appears to occur in the ventral-lateral parts of the thalamus however the dorsal thalamus does not show neurodegeneration. One possible explanation for this decrease of pro-inflammatory cytokines is the well-established interaction of macrophages with apoptotic cells, which results in a down-regulation of pro-inflammatory cytokines in surrounding cells [423, 424]. If this mechanism also

occurs here, the down-regulation of pro-inflammatory cytokines may act as a protective entity against the toxic effects of a pro-inflammatory event [273].

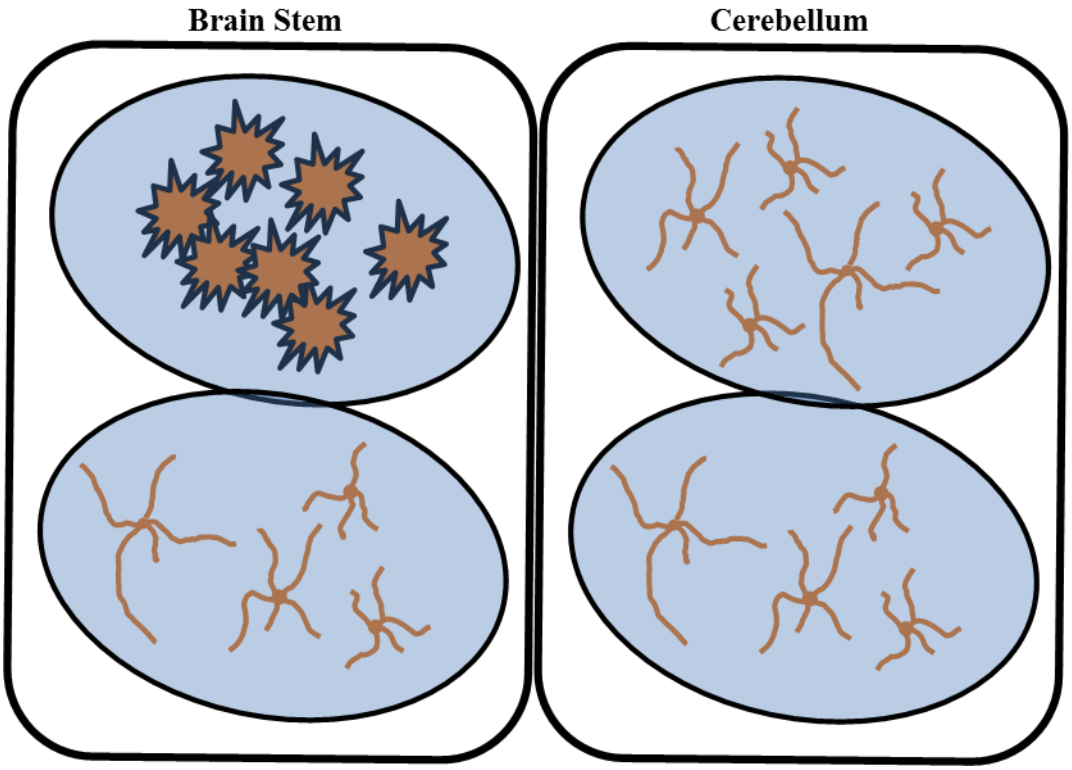

Figure 6.19 – Diagrammatic representation of microglial morphology within and between different brain regions of the same individual. The up- and down-regulated signal hypothesised to occur in microglia could occur in all microglia within a particular brain region, or could be the result of different populations of microglia which give different signals in different parts of a particular brain region.

Another small group of genes were found up-regulated specifically within the cerebellum. These encompassed genes related to neuronal function (such as synaptotagmin XII, parvalbumin and shank3). Results in chapter 3 show an up-regulation of neuronal specific proteins in pathologically unaffected regions, such as the cerebellum and cortex. Shank3 is a post-synaptic density protein found in the dendrites of neurons [425], whereas parvalbumin and MAP2 staining are localised to the cell body and dendrites of neurons. The increased expression of shank3 and parvalbumin therefore correlates with the observation of an increased MAP2 staining

(figure 3.6). Previous studies have shown an up-regulation of parvalbumin in neurons of the cerebellum at early stages of PrP^d accumulation, prior to neurodegeneration [403]. This could therefore suggest the increased gene (shank3 and parvalbumin) and protein (MAP2) levels in neurons may relate to disease events prior to overt neurodegeneration. An alternative explanation is that the pathologically unaffected regions are acting protectively by up-regulating neuronal specific genes in response to external cues present in a degenerative CNS. In order to test whether these regions are undergoing a potential pathological event, a host of ATF expression levels were assessed, which are known proteins to be activated in response to stress stimuli [405-407] and transcriptionally regulate genes associated with stress pathways [405-414]. Within regions of neurodegeneration, different subsets of ATF transcription factors were up-regulated. This indicates that each region undergoing neurodegeneration up-regulates ATF transcription factors in a regional-specific mechanism. The cerebellum and cortex, however exhibit a common up-regulation of ATF1 and ATF6β. Little work has been performed assessing the role of ATF1 in response to stress in mammals, however in yeast ATF1 has been shown to be activated by a stress-activated kinase in a similar fashion to ATF2 in mammals [426]. In the cerebellum, both ATF6 and ATF6β are shown to be significantly up-regulated. ATF6 is a transmembrane protein expressed predominantly on the surface of the ER and bound to the ER chaperone, immunoglobin binding protein (BiP). Upon ER stress BiP binding is disrupted and ATF6 is delivered to the Golgi [427], cleaved and imported into the nucleus [428]. ATF6 then is thought to activate a subset of genes involved in the UPR [411]. The combination of an up-regulation of neuronal genes and proteins in the cerebellum and up-regulation of ATF6 indicates that regions

defined via histopathological analysis as “pathologically unaffected” regions are in fact undergoing a possible stress response. The prion seeds may therefore be acting as a stress stimuli for the activation of such transcription factors, and hence having a detrimental effect on the tissue. However this is not sufficient to trigger overt neurodegeneration, as can be defined by histopathological analysis.

The presence of an innate immune response which encapsulates a hybrid pro- and anti-inflammatory response specifically in regions undergoing overt neurodegeneration highlights the importance of such a response in neurodegeneration. The down-regulation of other genes, most probably in microglia, including pro-inflammatory cytokines and receptors, could be explained by the interaction of activated microglia with degenerating neurons in neighbouring or connected tissue. Whether this phenomenon occurs only to directly neighbouring tissues or can be conferred along neuroanatomical pathways is unknown, but the latter could explain the widespread down-regulation of pro-inflammatory cytokines found in this study.

The results in this chapter detail the gene expression changes observed between brain regions in GSS/101LL and NBH/101LL mice. Microarray chips, including the Affymetrix chip used in this study, include numerous repeat transcripts and many genes are represented by a number of transcripts specific for different RNA segments in the gene. This allows an internal control to assess whether a transcript which shows differential expression levels in a sample of interest is indeed differentially

expressed or a technical error in the fluorescence read-out of that transcript. Of course, this is further controlled by using multiple array repeats. Nevertheless, the differential expression of genes which are identified require further work to validate expression changes. This can be done using other RNA quantifying techniques, such as real-time PCR. Of perhaps more importance, gene expression analysis only represents the transcriptional changes within a sample but not all transcripts produced are translated to protein. Therefore, testing whether the gene expression changes observed translate into protein expression is required to further understand the data output of this study.

The data in this chapter indicates that prion seeds are most likely having a detrimental impact in the cerebellum and cortex. As discussed in chapter 5, it is unclear whether specific toxic conformations are responsible for the presence or absence of neurodegeneration. However, this study indicates that prion seeds do exhibit some level of toxicity, resulting in increased expression of ATF1 and ATF6. Nevertheless, prion seeds, alone, do not appear sufficient to trigger overt neurodegeneration. The predominating innate immune response restricted to the brain stem and thalamus implicates the importance of glial cell responses, such as microglial activation, in neurodegeneration. It is possible the deficits caused by the accumulation of prion seeds results in microglial activation due to compromised neuronal homeostasis. This may lead to neurodegeneration, possibly resulting in apoptosis via the interaction of DAXX and ASK1, which is controlled by cytokine signalling. Why specific regions appear to be prevented from undergoing a glial cell response when exposed to compromising prion seeds is unknown. It can be

hypothesised that the interaction of activated microglia with degenerating neurons results in an inhibition of microglial activation in surrounding, or possibly neuronally connected tissue, thereby preventing a glial cell response. This may then prevent the toxic effects of a pro-inflammatory event in specific regions, thereby preventing neurodegeneration. An alternative explanation could be that glial cells, such as microglia, react to specific species of misfolded protein, thereby resulting in restricted microglial activation.

7. Discussion

Current perspectives in many chronic diseases of the CNS are that misfolded proteins are responsible for neurodegeneration. In prion diseases, the identification of an infectious, aberrantly folded protein [21], devoid of nucleic acids [16] is the underlying basis of the prion hypothesis [3, 6, 22-25]. This led to the hypothesis that the misfolded prion protein is required for the temporal and spatial lesions in prion diseases [260, 261, 429, 430], although some studies indicate that not all forms of misfolded prion protein are necessarily toxic [431, 432]. A similar ambiguity between misfolded protein and neurodegeneration is also suggested in other chronic neurodegenerative disease [163, 433-436]. Dose [437], spread [161, 162, 286, 288, 290-293, 438] and species of aggregate [168-176] are implicated as critical factors in determining toxicity of misfolded proteins.

7.1. Determining the correlation between misfolded prion protein and neurodegeneration

In this thesis, the relationship between the accumulation and spread of misfolded prion protein and neurodegeneration was studied. In contrast to previous studies, this study also took advantage of a highly sensitive assay, the QuIC assay, to detect the presence of prion seeds. Using IHC analysis, it was found that the spatial distribution of PrP^{d} is associated with neurodegeneration in a manner akin to previous studies [189, 191]. Further investigation showed the deposition of PrP^{d} coincided with the spread of neurodegeneration from one anatomically distinct region to another in a pattern resembling neuronal connectivity. This is conceptually identical to studies

assessing spread in other disease-associated misfolded proteins [161, 162, 286, 288, 290-293, 438] and pathological spread in humans [143, 144]. Microglial and astrocyte morphological cellular responses were also observed specifically in regions of IHC positive PrP^d prior to neurodegeneration. This progression of disease in GSS/101LL animals matched previous studies assessing disease progression in other models of murine scrapie [189, 191]. This data suggests morphological alterations in microglia and astrocytes are exquisitely sensitive biomarkers of neurodegeneration, but also highlight their functional role in prevention or induction of neurodegeneration. It has been shown the astrocyte can propagate PrP^d [263], but whether this has any impact upon disease is unknown. Microglia exhibit an innate immune response [275] which appears to be regulated by TGFβ-1 [276]. Inducing a systemic inflammatory response, by injection of LPS for example, results in exacerbation of disease [190]. Conversely, genetic KO of pro-inflammatory mediators results in amelioration of disease [401, 439]. Recent studies show that inhibiting the proliferation of microglia in prion disease ameliorates disease [280]. This indicates that the function and/or the oxidative stress of highly proliferative microglia represent a toxic entity. This data does not elucidate whether such microglial responses are a consequence of disease or play a significant role in neurodegeneration.

The detectable PrP^d via IHC was observed associated with the interpeduncular nuclei and SNc at early stages of disease, followed by accumulation in the dorsal and medial raphe nuclei of the brain stem or the SNr of the midbrain. Glial cell responses are observed associated with the spread of PrP^d and overt signs of neurodegeneration

can also be detected at this stage. This neurodegeneration can be characterised by the loss of neuronal structural integrity. It has been shown previously that neurons undergo atrophy prior to neuronal cell loss [191]. This implicates a loss of cell-structure integrity of neurons at early stages of disease in both GSS/101LL animals and other models of murine scrapie.

Using the QuIC assay as a tool to detect prion seeds, this study found no relationship between prion seeds and neurodegeneration. As mentioned earlier in this thesis, it is highly likely the QuIC assay detects misfolded prion protein; whether this represents species of PrP^{d} or different isoforms is as yet unknown. A recent study has shown the recPrP that aggregates/misfolds in the QuIC assay can recapitulate the prion strain characteristics of the sample that was used to seed the QuIC assay. For example, 22L murine prion strain used to seed the QuIC assay caused aggregation/misfolding of recPrP which consequently exhibited similar structural properties of 22L PrP^{d}. Furthermore, when inoculating into mice the recPrP seeded with 22L, the incubation period was comparative to the expected 22L incubation period [348]. A similar approach, sub-passaging GSS/101LL brain regions and/or the QuIC seeded product into mice could be useful to assess whether different species of misfolded prion protein exist between brain regions.

It is possible different misfolded prion protein conformations exist in different regions of the brain. Therefore a basic interpretation would be that toxic conformations exist in brain regions undergoing neurodegeneration, and non-toxic

conformations exist in unaffected regions. Conformational differences between brain regions of the same individual have been observed previously in human prion disease patients. The thalamus was shown to exhibit different aggregations of PrP^d to the cerebellum [350]. This however, draws attention to the fixed perspectives of "toxic" or "non-toxic" protein conformations alluded to in previous publications [432, 437]. These publications hypothesise that neurodegenerative diseases occur in a two-phase mechanism. The exponential increase in non-toxic conformations of misfolded protein. In the instance of prion diseases, these conformations of protein represent the infectious material [432, 437]. The levels of infectivity then plateau but overall misfolded prion protein levels continue to increase. The authors therefore propose that this plateau represents a 'switch' from infectious prion protein conformations to toxic conformations. If true, this would suggest infectivity levels in brain regions undergoing neurodegeneration have reached a plateau, whereas in brain regions without overt neurodegeneration but with accumulation of misfolded protein will be in the phase of increasing infectivity levels. Whether the infectivity plateau truly represents the switch from infectious to toxic protein isoforms has yet to be established. Nevertheless, the infectivity plateau is a well-known phenomenon in prion diseases [440-442]. Such a change in dynamics of disease must therefore be related to a significant alteration in host physiology. As the primary structure of the prion protein is the same across all brain regions tested in this study, differences in protein conformation must be represented at the secondary or tertiary protein structure levels. These can be influenced by a variety of conditions, including changes in environmental pH, temperature, nearby proteins/lipids/carbohydrates amongst many other factors. As a result, such a substantial change in host

physiology, represented by the plateau of infectivity, is likely having a major role in determining protein conformation and the role of the misfolded protein in neurodegeneration. An alternative argument can be made however. As misfolded protein accumulates, it aggregates into oligomers, fibrils and amyloid plaques. Whether this is a continuous pathway of aggregation or these protein constructs are observations of distinct pathways of aggregations is still unclear. As amyloid plaques form, some studies have shown that in the surrounding vicinity of the plaque, oligomers are formed [443]. This is associated with a concurrent glial cell response [444], but the burden of oligomers directly correlates with loss of excitatory synapses [443]. In this instance, it can be argued that the amyloid plaque generates an environment in its surrounding vicinity which is conducive to oligomer formation and neurodegeneration. Therefore rather than host environment impacting protein conformation, this would stipulate that misfolded protein aggregation can directly generate an environment for further protein misfolding which is correlated with toxicity. Overall, with only having the capability, at present, to detect prion seeds using the RT-QuIC assay, such studies on the impact of misfolded protein are limited. However, it is possible to define the host response to the accumulation to prion seeds and therefore determine the impact this may have on neurodegeneration.

7.2. Dose and spread of prion seeds play no discernible role in determining toxicity

As mentioned above, dose and spread of misfolded proteins have also been hypothesised to be factors determining misfolded protein toxicity. To answer whether these are indeed factors between brain regions in GSS/101LL animals, two

experiments were performed. Firstly a dilution series of each brain region was performed. The assumption being a region exposed to smaller quantities of prion seeds will not seed the QuIC assay at lower homogenate concentrations comparative to regions with larger quantities of prion seeds. Comparative quantities of prion seeds were found between brain regions in this study, suggesting no quantitative difference in prion seeds. Secondly, different brain regions were tested throughout the incubation period to determine whether prion seeds spread in a selective mechanism which would correlate with neurodegeneration. At earliest stages of disease (i.e. 150dpi), prion seeds were restricted to a small number of mice specifically within the brain stem. This is the point at which PrP^{d} detectable via IHC was observed in the midbrain. Due to the known connectivity between midbrain neurons associated with PrP^{d} and those of the brain stem [334, 335], this may indicate an early specific spread of prion seeds via neuronal connectivity. Further work is required to confirm this. After this stage, however, the prion seeds exponentially spread to all brain regions tested. The thalamus appears exposed to prion seeds at a similar stage to the cerebellum and cortex, yet the thalamus eventually undergoes neurodegeneration whereas the cerebellum and cortex do not. Why a specific region, such as the thalamus, would specifically undergo neurodegeneration when exposed to similar quantities of prion seed for the same time-frame as cerebellum or cortex is unknown. Taken together, this data demonstrates that prion seeds are present at equal quantities and are widespread at early stages of disease – ruling out the dose or spread as factors determining toxicity in this model. However, the early specific targeting to neurons of the midbrain, and potentially interconnected nuclei of the brain stem

could represent an important interplay between early targeting and spread of PrP^d and the subsequent host response to restrict/prevent neurodegeneration.

7.3. Host responses in determining prion seed toxicity

It was hypothesised that, due to the presence of prion seeds across all brain regions tested, the host must elicit a specific response to either protect against the toxic effects of prion seeds or aberrantly induce an environment which preferentially forms toxic isoforms of prion seeds in some regions and not others. A number of studies have used microarray to study genome-wide transcriptional changes during prion disease as a method to elucidate the mechanisms of neurodegeneration [218, 227, 228, 230, 351-356, 358-360, 362-368]. Earlier studies used whole brain analysis across a range of different strains either at clinical stages of disease [228, 230, 351-353] or throughout a time-course [228]. The major signature identified in these studies was a gene list related to gliosis [228, 230, 351-353], specifically an innate immune response which orientates around TGFβ-1 [228, 230, 351-353]. Later studies thus concentrated on the neuronal transcriptome in prion infected mice [218]. These studies indicate that degenerating neurons may elicit a protective response to prevent neuronal cell death prior to clinical onset of disease (reviewed in [445]).

The findings in this thesis allow a novel approach for the comparison of the host transcriptional profile in neurodegeneration against the host response to prion seeds, independent of neurodegeneration. Three major groups were identified as a result of the microarray; (i) a specific up-regulation of genes associated with gliosis in regions

of neurodegeneration, (ii) a down regulation of genes across all regions, also associated with a glial cell response and (iii) intrinsic gene expression differences between brain regions used in this study. A small cluster of genes which are specifically up-regulated only in cerebellum was also detected. Similarly, the activating transcription factors (ATFs), which are involved in active response pathways to stress stimuli, such as cytokines, misfolded proteins and DNA damage, have also been shown to be differentially regulated between brain regions in this study.

7.3.1. Up-regulation of genes in regions of neurodegeneration

The up-regulation of a gene expression profile in regions of neurodegeneration was an expected result. Results in chapters 3 and 4 in this thesis show glial cells undergo a substantial morphological response in regions of neurodegeneration. In addition, previous microarray studies have implicated a signature indicative of gliosis which is orientated around TGFβ-1 [228, 230, 351-353], a finding also observed in pathological and genetic analysis in previous studies [275, 276]. Indeed in this study, a hybrid pro- and anti-inflammatory response was identified, which included cellular proliferation, the complement pathway, pro-inflammatory cytokines and chemokines, TGFβ-1 and GFAP. This group of genes is therefore representative of a glial cell response, orientated predominantly around the innate immune response. Overall, this data indicates the importance of gliosis in neurodegeneration.

7.3.2. Down-regulation of genes across all brain regions tested

The down-regulation across all regions tested is also indicative of a glial cell response. The predominant signature appears to surround the down-regulation of the viral response transcription factors Sp100, Sp110 and Sp140. These are major constituents of a multi-protein matrix, termed nuclear bodies (NBs) [377]. The consequences of the down-regulation of such NB proteins are deficits in transcription and translation and also an inability to translocate CREB transcription factors to the nucleus [377, 381, 382, 384-387]. As shown in chapter 6, a sub-unit of RNA polymerase II is down-regulated, and a large set of transcripts also appear down-regulated in a pattern correlating with RNA polymerase II down-regulation. As discussed previously, the Sp100/110/140 nuclear body complex has previously been shown to co-localise with RNA polymerase II transcripts [384, 385]. This suggests this nuclear body complex may play a scaffold role in RNA polymerase II transcription. What causes the down-regulation of Sp100/110/140 nuclear body complex is unclear. It has been shown previously that interferons control the activation of this complex [377, 446-449]. Indeed, interferons are shown to be down-regulated across all regions in this study. Therefore, the down-regulation of interferons can lead to down-regulation of the Sp100/110/140 nuclear body complex, which thus has implications on transcription and translation in cells of the innate immune system, such as microglia.

Further work is required to understand why interferons are down-regulated across all regions tested. Some studies have demonstrated an important host protective response when apoptotic cells come into contact with macrophages [423, 424].

Specifically, surrounding connected tissue exhibits a down-regulation of pro-inflammatory cytokines to prevent an unnecessary inflammatory response or tissue damage in neighbouring cells. In this study, the appearance of a down-regulation of pro-inflammatory cytokines, such as interferons may indicate a protective response conferred in tissue neighbouring regions of neurodegeneration. This subsequent down-regulation of probable microglial specific genes thus hints at a protective response. It is clear from histopathological analysis that both microglia and astrocytes show no morphological alteration throughout disease in either the cortex or cerebellum, therefore it can be hypothesised that this down-regulation of innate immune response genes is possibly a host prevention of an activated microglial response. The pro-inflammatory response which may result from activated microglia (and which is observed as a hybrid pro- and anti-inflammatory response in brain stem and thalamus in this study) has previously been hypothesised to be toxic in neurodegenerative diseases [273]. Further work will thus be required to assess whether the macrophage-apoptotic cell interaction firstly occurs in the CNS, and secondly whether it impacts the (potentially toxic) function of an activated microglial cell.

7.3.3. Stress responses observed across all brain regions tested

To test whether prion seeds have an impact upon "unaffected" brain regions, the activating transcription factor (ATF) gene expression levels were assessed. This group of transcription factors are activated as a result of specific stress stimuli [405-407] and transcriptionally regulate genes associated with stress pathways, such as UPR [405-414]. Within the brain stem and thalamus, an up-regulation of ATFs was

observed, but these differed depending on region (e.g. brain stem exhibited up-regulation of ATF2, ATF4, ATF6β and ATF7, whereas the thalamus exhibited up-regulation in ATF6 and ATF7). This data suggests different brain regions may undergo specific stress response pathways during neurodegeneration. In regions of the brain previously defined as pathologically unaffected, however, ATF1 and ATF6 appeared up-regulated. Of particular relevance is ATF6, which is transcriptionally activated in instances of ER stress and is thought to regulate a subset of genes involved in the UPR [411]. Recent studies have indicated UPR activation as an important factor in mediating neurodegeneration [225, 226]. In these studies, rising levels of misfolded protein is proposed to be detected by BiP/Grp78 which leads to phosphorylation of PERK [225, 411]. This pathway leads to the activation of ATF4, which consequently activates the UPR pathway. ATF6 however is bound to BiP proteins on the surface of the ER. In instances of ER stress, this interaction is disrupted, resulting in translocation of ATF6 to the Golgi apparatus [427], where it is then cleaved and transported into the nucleus [428] and subsequently activates genes of the UPR pathway [411]. This data indicates that all brain regions tested exhibit stress responses. Whether this is a response restricted to neurons or found in other cell types has not been defined. Nevertheless, this profile suggests that the presence of prion seeds elicit a stress response across all brain regions. However, this response alone is not sufficient to trigger overt neurodegeneration.

Taken together, the data in this study indicates a complex relationship of different cell types in the CNS and the appearance and accumulation of PrP^{d}. The accumulation of prion seeds across all regions tested in this study appears to elicit a

cellular stress response. The context of the accumulation of PrP^d initially associated with neurons of the midbrain, followed by a specific neuronal spread to the brain stem suggests these stress pathways may be implicated early in disease. Indeed, this stress response is likely to elicit glial cell responses due to disrupted neuronal homeostasis, hence why glial cell responses are observed shortly after the initial accumulation of PrP^d. Microglial interactions with the stressed neurons of the midbrain and/or brain stem may thus elicit a protective anti-inflammatory response to surrounding tissue, including thalamus, cerebellum and cortex. Why the thalamus eventually results in overt neurodegeneration whereas the cerebellum and cortex appear unaffected is unknown. Further work is required to answer in more detail what the pathological processes occurring in the cerebellum and cortex are. Certainly, the stress responses occurring in these regions indicate a pathological event, but the reasons for an absence of the hybrid pro- and anti-inflammatory response and neurodegeneration (as seen in brain stem and thalamus) remain unanswered.

7.4. Concluding remarks

In summary, it appears the accumulation of misfolded prion protein, and the consequent stress responses associated with this, are not sufficient to trigger neurodegeneration. This could be due to the host down-regulation of pro-inflammatory cytokines, resulting in down-regulation of transcriptional and translational regulation in cells of the innate immune response, such as microglia. This may be indicative of a pathway inhibiting microglial activation and preventing toxicity, although this is highly speculative and requires further work. At early

stages, in the absence of a putative host protective response, gliosis may occur as a response to misfolded prion protein-mediated neuronal stress. The sustained and unresolved inflammation as a result of this, in conjunction with stress pathway activation, may therefore lead to neurodegeneration. These results lead to a "multi-hit" hypothesis, whereby two or more factors (e.g. accumulation of misfolded prion protein and microglial activation) are required to trigger neurodegeneration.

The results in this study therefore change our perspective on the progression of neurodegeneration and the putative role of the misfolded protein within this. The multi-hit hypothesis encapsulates the current perspectives regarding the importance of disease-associated misfolded proteins in neurodegeneration; however this study shows misfolded protein, alone, is not sufficient to trigger neurodegeneration. In conjunction with a growing understanding of the importance of the glial cell response in neurodegenerative diseases, the multi-hit hypothesis encapsulates how the interaction between misfolded protein and the glial cell responses may act additively to trigger neurodegeneration. Such an understanding changes our perception on disease progression and identifies new avenues to study this. Furthermore, future research into the multi-hit hypothesis may yield new therapeutic targets, for example, preventing the inflammatory response by understanding the host mechanism to potentially inhibit/restrict activated microglia.

References

1. Dauer, W. and S. Przedborski, *Parkinson's disease: Mechanisms and models.* Neuron, 2003. **39**(6): p. 889-909.
2. Hardy, J. and D.J. Selkoe, *Medicine - The amyloid hypothesis of Alzheimer's disease: Progress and problems on the road to therapeutics.* Science, 2002. **297**(5580): p. 353-356.
3. Prusiner, S.B., *Prions.* Proceedings of the National Academy of Sciences of the United States of America, 1998. **95**(23): p. 13363-13383.
4. Collinge, J., *Prion diseases of humans and animals: Their causes and molecular basis.* Annual Review of Neuroscience, 2001. **24**: p. 519-550.
5. Kimberlin, R.H., *Transmissible Encephalopathies in animals.* Canadian Journal of Veterinary Research-Revue Canadienne De Recherche Veterinaire, 1990. **54**(1): p. 30-37.
6. Prusiner, S.B., *Novel proteinaceous infectious particles cause scrapie.* Science, 1982. **216**(4542): p. 136-144.
7. Collins, S.J., V.A. Lawson, and C.L. Masters, *Transmissible spongiform encephalopathies.* Lancet, 2004. **363**(9402): p. 51-61.
8. Johnson, R.T., *Prion diseases.* Lancet Neurology, 2005. **4**(10): p. 635-642.
9. Greig, J.R., *Scrapie. Observations on the transmission of the disease by mediate contact.* Vet Jour, 1940. **96**((5)): p. 203-206.
10. Hornabro.Rw, *Kuru - a subactue cerebellar degeneration - natural history and clinical features.* Brain, 1968. **91**: p. 53-&.
11. Gajdusek, D.C. and V. Zigas, *Degenerative disease of the central nervous system in New Guinea - the endemic occurance of Kuru in the native population.* New England Journal of Medicine, 1957. **257**(20): p. 974-978.
12. Hadlow, W.J., *Scrapie and Kuru.* Lancet, 1959. **2**(SEP5): p. 289-290.
13. Gajdusek, D.C., C.J. Gibbs, and M. Alpers, *Experimental transmission of a Kuru-like syndrome to chimpanzees.* Nature, 1966. **209**(5025): p. 794-&.
14. Gajdusek, D.C., C.J. Gibbs, and M. Alpers, *Transmission and passage of experimental Kuru to chimpanzees.* Science, 1967. **155**(3759): p. 212-&.
15. Bruce, M.E., et al., *Transmissions to mice indicate that 'new variant' CJD is caused by the BSE agent.* Nature, 1997. **389**(6650): p. 498-501.
16. Alper, T., et al., *Does agent of scrapie replicate without nuclei acid.* Nature, 1967. **214**(5090): p. 764-&.
17. Dickinson, A.G. and V.M.H. Meikle, *Host-genotype and agent effects in scrapie incubation - change in allelic interaction with different strains of the agent.* Molecular and General Genetics, 1971. **112**(1): p. 73-&.
18. Bruce, M.E., *Scrapie strain variation and mutation.* British Medical Bulletin, 1993. **49**(4): p. 822-838.

19. Bruce, M.E. and H. Fraser, *Scrapie strain variation and its implications.* Current topics in microbiology and immunology, 1991. **172**: p. 125-38.

20. Bruce, M.E., *TSE strain variation.* British Medical Bulletin, 2003. **66**: p. 99-108.

21. McKinley, M.P., D.C. Bolton, and S.B. Prusiner, *A protease-resistant protein is a structural component of the scrapie prion.* Cell, 1983. **35**(1): p. 57-62.

22. McKinley, M.P., D.C. Bolton, and S.B. Prusiner, *A protease-resistant protein is a structural component of the scrapie prion.* Cell, 2004. **S116**(2): p. 57-62.

23. Oesch, B., et al., *A cellular gene encodes scrapie PrP 27-30 protein.* Cell, 1985. **40**(4): p. 735-746.

24. Stahl, N., et al., *Structural studies of the scrapie prion protein using mass-spectrometry and amino-acid sequencing.* Biochemistry, 1993. **32**(8): p. 1991-2002.

25. Basler, K., et al., *Scrapie and cellular PrP isoforms are encoded by the same chromosomal gene.* Cell, 1986. **46**(3): p. 417-428.

26. Prusiner, S.B., et al., *Transgenetic studies implicate interactions between homologous PrP isoforms in scrapie prion replication.* Cell, 1990. **63**(4): p. 673-686.

27. Scott, M., et al., *Transgenic mice expressing hamster prion protein produce species-specific scrapie infectivity and amyloid plaques.* Cell, 1989. **59**(5): p. 847-857.

28. Manson, J.C., et al., *A single amino acid alteration (101L) introduced into murine PrP dramatically alters incubation time of transmissible spongiform encephalopathy.* EMBO J, 1999. **18**(23): p. 6855-6864.

29. Barron, R.M., et al., *Transmission of murine scrapie to P101L transgenic mice.* Journal of General Virology, 2003. **84**: p. 3165-3172.

30. Bueler, H., et al., *Mice devoid of PrP are resistant to scrapie.* Cell, 1993. **73**(7): p. 1339-1347.

31. Manson, J.C., et al., *129/Ola mice carrying a null mutation in PrP that abolishes messenger RNA production are developmentally normal.* Molecular Neurobiology, 1994. **8**(2-3): p. 121-127.

32. Safar, J., et al., *Eight prion strains have PrP(Sc) molecules with different conformations.* Nat Med, 1998. **4**(10): p. 1157-65.

33. Tremblay, P., et al., *Mutant PrPSc conformers induced by a synthetic peptide and several prion strains.* J Virol, 2004. **78**(4): p. 2088-99.

34. Chiesa, R., et al., *Neurological illness in transgenic mice expressing a prion protein with an insertional mutation.* Neuron, 1998. **21**(6): p. 1339-51.

35. Ma, J., R. Wollmann, and S. Lindquist, *Neurotoxicity and neurodegeneration when PrP accumulates in the cytosol.* Science, 2002. **298**(5599): p. 1781-5.

36. Stewart, R.S. and D.A. Harris, *A transmembrane form of the prion protein is localized in the Golgi apparatus of neurons.* J Biol Chem, 2005. **280**(16): p. 15855-64.

37. Diringer, H., et al., *Scrapie infectivity, fibrils and low-molecular weight proteins.* Nature, 1983. **306**(5942): p. 476-478.

38. Multhaup, G., et al., *The protein-component of scrapie-associated fibrils is a glycosylated low-molecular weight protein.* Embo Journal, 1985. **4**(6): p. 1495-1501.

39. Lasmezas, C.I., et al., *Transmission of the BSE agent to mice in the absence of detectable abnormal prion protein.* Science, 1997. **275**(5298): p. 402-405.

40. Piccardo, P., et al., *Accumulation of prion protein in the brain that is not associated with transmissible disease.* Proc Natl Acad Sci U S A, 2007. **104**(11): p. 4712-7.

41. Barron, R.M., et al., *High titers of transmissible spongiform encephalopathy infectivity associated with extremely low levels of PrPSc in vivo.* J Biol Chem, 2007. **282**(49): p. 35878-86.

42. Manuelidis, L., T. Sklaviadis, and E.E. Manuelidis, *Evidence suggesting that PrP is not the infectious agent in Creutzfeldt-Jakob disease.* EMBO J, 1987. **6**(2): p. 341-7.

43. Shaked, G.M., et al., *Protease-resistant and detergent-insoluble prion protein is not necessarily associated with prion infectivity.* J Biol Chem, 1999. **274**(25): p. 17981-6.

44. Wille, H., S.B. Prusiner, and F.E. Cohen, *Scrapie infectivity is independent of amyloid staining properties of the N-terminally truncated prion protein.* Journal of Structural Biology, 2000. **130**(2-3): p. 323-338.

45. Somerville, R.A., et al., *Characterisation of thermodynamic diversity between TSE agent strains.* Biochemical Society Transactions, 2002. **30**(3): p. A79.

46. Weissmann, C., *A unified theory of prion propagation.* Nature, 1991. **352**(6337): p. 679-683.

47. Apetri, A.C. and W.K. Surewicz, *Kinetic intermediate in the folding of human prion protein.* Journal of Biological Chemistry, 2002. **277**(47): p. 44589-44592.

48. Gabizon, R., M.P. McKinley, and S.B. Prusiner, *Purified prion proteins and scrapie infectivity copartition into liposomes.* Proceedings of the National Academy of Sciences of the United States of America, 1987. **84**(12): p. 4017-4021.

49. McKinley, M.P., et al., *Scrapie prion rod formation in vitro requires both detergent extraction and limited proteolysis.* Journal of Virology, 1991. **65**(3): p. 1340-1351.

50. Pan, K.M., et al., *Conversion of alpha-helices into beta-sheets features in the formation of the scrapie prion proteins.* Proceedings of the National Academy of Sciences of the United States of America, 1993. **90**(23): p. 10962-10966.

51. Silveira, J.R., et al., *The most infectious prion protein particles.* Nature, 2005. **437**(7056): p. 257-261.

52. Harper, J.D. and P.T. Lansbury, *Models of amyloid seeding in Alzheimier's disease and scrapie: Mechanistic truths and physiological consequences of the time-dependent solubility of amyloid proteins.* Annual Review of Biochemistry, 1997. **66**: p. 385-407.

53. Somerville, R.A., *TSE agent strains and PrP: reconciling structure and function.* Trends Biochem Sci, 2002. **27**(12): p. 606-12.

54. Somerville, R.A. and N. Gentles, *Characterization of the effect of heat on agent strains of the transmissible spongiform encephalopathies.* Journal of General Virology, 2011. **92**: p. 1738-1748.

55. Diringer, H., M. Beekes, and U. Oberdieck, *The nature of the scrapie agent - the virus theory*, in *Slow Infections of the Central Nervous System: The Legacy of Dr Bjorn Sigurdsson*, J. Bjornsson, et al., Editors. 1994, New York Acad Sciences: New York. p. 246-258.

56. Adams, D.H., *Scrapie agent - small deoxyribonucleic acid-mediated virus.* Biochemical Journal, 1972. **127**(5): p. P82-&.

57. Hunter, G.D., *Nature of the scrapie virus.* Pathologie Biologie, 1973. **21**(3): p. 282-283.

58. Adams, D.H. and E.A. Caspary, *Nature of scrapie virus.* British Medical Journal, 1967. **3**(5558): p. 173-&.

59. Diener, T.O., *Is scrapie agent a viroid.* Nature-New Biology, 1972. **235**(59): p. 218-&.

60. Marx, J.L., *Scrapie agent - is it a viroid.* Science, 1979. **203**(4380): p. 532-532.

61. Hope, J., *The nature of the scrapie agent - the evolution of the virino*, in *Slow Infections of the Central Nervous System: The Legacy of Dr Bjorn Sigurdsson*, J. Bjornsson, et al., Editors. 1994, New York Acad Sciences: New York. p. 282-289.

62. Kimberlin, R.H., *Scrapie agent - prions or virinos.* Nature, 1982. **297**(5862): p. 107-108.

63. Manuelidis, L., et al., *Cells infected with scrapie and Creutzfeldt-Jakob disease agents produce intracellular 25-nm virus-like particles.* Proceedings of the National Academy of Sciences of the United States of America, 2007. **104**(6): p. 1965-1970.

64. Manuelidis, L., *A 25 nm virion is the likely cause of transmissible spongiform encephalopathies.* Journal of Cellular Biochemistry, 2007. **100**(4): p. 897-915.

65. Manuelidis, L., *Nuclease resistant circular DNAs copurify with infectivity in scrapie and CJD.* Journal of Neurovirology, 2011. **17**(2): p. 131-145.

66. Dron, M. and L. Manuelidis, *Visualization of viral candidate cDNAs in infectious brain fractions from Creutzfeldt-Jakob disease by representational difference analysis.* Journal of Neurovirology, 1996. **2**(4): p. 240-248.

67. Akowitz, A., T. Sklaviadis, and L. Manuelidis, *Endogenous viral complexes with long RNA cosediment with the agent of Creutzfeldt-Jakob disease.* Nucleic Acids Research, 1994. **22**(6): p. 1101-1107.

68. Ozel, M. and H. Diringer, *Small virus-like structure in fractions from scrapie hamster brain.* Lancet, 1994. **343**(8902): p. 894-895.

69. Akowitz, A., E.E. Manuelidis, and L. Manuelidis, *Protected endogenous retroviral sequences copurify with infectivity in experimental Creutzfeldt-Jakob disease.* Archives of Virology, 1993. **130**(3-4): p. 301-316.

70. Lewis, V. and N.M. Hooper, *The role of lipid rafts in prion protein biology.* Frontiers in Bioscience-Landmark, 2011. **16**: p. 151-168.

71. Taylor, D.R. and N.M. Hooper, *The prion protein and lipid rafts (Review).* Molecular Membrane Biology, 2006. **23**(1): p. 89-99.

72. Walmsley, A.R., F. Zeng, and N.M. Hooper, *The N-terminal region of the prion protein ectodomain contains a lipid raft targeting determinant.* Journal of Biological Chemistry, 2003. **278**(39): p. 37241-37248.

73. Naslavsky, N., et al., *Characterization of detergent-insoluble complexes containing the cellular prion protein and its scrapie isoform.* Journal of Biological Chemistry, 1997. **272**(10): p. 6324-6331.

74. Calzolai, L., et al., *Prion protein NMR structures of chickens, turtles, and frogs.* Proceedings of the National Academy of Sciences of the United States of America, 2005. **102**(3): p. 651-655.

75. Wuthrich, K. and R. Riek, *Three-dimensional structures of prion proteins.* Advances in Protein Chemistry, Vol 57, 2001. **57**: p. 55-82.

76. Perez, D.R., F.F. Damberger, and K. Wuthrich, *Horse Prion Protein NMR Structure and Comparisons with Related Variants of the Mouse Prion Protein.* Journal of Molecular Biology, 2010. **400**(2): p. 121-128.

77. Christen, B., et al., *NMR Structure of the Bank Vole Prion Protein at 20 degrees C Contains a Structured Loop of Residues 165-171.* Journal of Molecular Biology, 2008. **383**(2): p. 306-312.

78. Gossert, A.D., et al., *Prion protein NMR structures of elk and of mouse/elk hybrids.* Proceedings of the National Academy of Sciences of the United States of America, 2005. **102**(3): p. 646-650.

79. Lysek, D.A., et al., *Prion protein NMR structures of cats, dogs, pigs, and sheep.* Proceedings of the National Academy of Sciences of the United States of America, 2005. **102**(3): p. 640-645.

80. Zahn, R., et al., *NMR solution structure of the human prion protein.* Proceedings of the National Academy of Sciences of the United States of America, 2000. **97**(1): p. 145-150.

81. Haire, L.F., et al., *The crystal structure of the globular domain of sheep prion protein.* Journal of Molecular Biology, 2004. **336**(5): p. 1175-1183.

82. Knaus, K.J., et al., *Crystal structure of the human prion protein reveals a mechanism for oligomerization.* Nature Structural Biology, 2001. **8**(9): p. 770-774.

83. Whittal, R.M., et al., *Copper binding to octarepeat peptides of the prion protein monitored by mass spectrometry.* Protein Science, 2000. **9**(2): p. 332-343.

84. Brimacombe, D.B., et al., *Characterization and polyanion-binding properties ef purified recombinant recombinant protein.* Biochemical Journal, 1999. **342**: p. 605-613.

85. Hope, J., et al., *The major polypeptide of scrapie-associated fibrils (SAF) has the same size, charge distribution and N-terminal protein sequence as predicted for the normal brain protein (PrP).* EMBO J, 1986. **5**(10): p. 2591-7.

86. Fischer, M., et al., *Prion protein (PrP) with amino-proximal deletions restoring susceptibility of PrP knockout mice to scrapie.* Embo Journal, 1996. **15**(6): p. 1255-1264.

87. Somerville, R.A., et al., *Biochemical typing of scrapie strains.* Nature, 1997. **386**(6625): p. 564-564.

88. Hill, A.F., et al., *Investigation of variant Creutzfeldt-Jakob disease and other human prion diseases with tonsil biopsy samples.* Lancet, 1999. **353**(9148): p. 183-189.

89. Caughey, B.W., et al., *Secondary structure-analysis of the scrapie-associated protein PrP 27-30 in water by intrared-spectroscopy.* Biochemistry, 1991. **30**(31): p. 7672-7680.

90. Peretz, D., et al., *A conformational transition at the N terminus of the prion protein features in formation of the scrapie isoform.* Journal of Molecular Biology, 1997. **273**(3): p. 614-622.

91. Guest, W.C., S.S. Plotkin, and N.R. Cashman, *Toward a Mechanism of Prion Misfolding and Structural Models of PrPSc: Current Knowledge and Future Directions.* Journal of Toxicology and Environmental Health-Part a-Current Issues, 2011. **74**(2-4): p. 154-160.

92. Wille, H., et al., *Structural studies of the scrapie prion protein by electron crystallography.* Proceedings of the National Academy of Sciences of the United States of America, 2002. **99**(6): p. 3563-3568.

93. Smirnovas, V., et al., *Structural organization of brain-derived mammalian prions examined by hydrogen-deuterium exchange.* Nature Structural & Molecular Biology, 2011. **18**(4): p. 504-506.

94. Kocisko, D.A., et al., *Cell-free formation of protease-resistant prion protein.* Nature, 1994. **370**(6489): p. 471-474.

95. Kirby, L., et al., *In vitro cell-free conversion of bacterial recombinant PrP to Prp(res) as a model for conversion.* Journal of General Virology, 2003. **84**: p. 1013-1020.

96. Kocisko, D.A., et al., *Species-specificity in the cell-free conversion of prion protein to protease-resistant forms - a model for the scrapie species barrier.* Proceedings of the National Academy of Sciences of the United States of America, 1995. **92**(9): p. 3923-3927.

97. Saborio, G.P., B. Permanne, and C. Soto, *Sensitive detection of pathological prion protein by cyclic amplification of protein misfolding.* Nature, 2001. **411**(6839): p. 810-813.

98. Barria, M.A., et al., *De Novo Generation of Infectious Prions In Vitro Produces a New Disease Phenotype.* Plos Pathogens, 2009. **5**(5).

99. Deleault, N.R., et al., *Formation of native prions from minimal components in vitro.* Proceedings of the National Academy of Sciences of the United States of America, 2007. **104**(23): p. 9741-9746.

100. Castilla, J., et al., *In vitro generation of infectious scrapie prions.* Cell, 2005. **121**(2): p. 195-206.

101. Atarashi, R., et al., *Simplified ultrasensitive prion detection by recombinant PrP conversion with shaking.* Nature Methods, 2008. **5**(3): p. 211-212.

102. Orru, C.D., et al., *Human variant Creutzfeldt-Jakob disease and sheep scrapie PrPres detection using seeded conversion of recombinant prion protein.* Protein Engineering Design & Selection, 2009. **22**(8): p. 515-521.

103. Atarashi, R., et al., *Ultrasensitive human prion detection in cerebrospinal fluid by real-time quaking-induced conversion.* Nature Medicine, 2011. **17**(2): p. 175-178.

104. Atarashi, R., et al., *Real-time quaking-induced conversion A highly sensitive assay for prion detection.* Prion, 2011. **5**(3): p. 150-153.

105. Orru, C.D., et al., *Prion Disease Blood Test Using Immunoprecipitation and Improved Quaking-Induced Conversion.* Mbio, 2011. **2**(3).

106. Scott, M.R., et al., *Chimeric prion protein expression in cultured cells and transgenic mice.* Protein Sci, 1992. **1**(8): p. 986-97.

107. Scott, M., et al., *Propagation of prions with artificial properties in transgenic mice expressing chimeric PrP genes.* Cell, 1993. **73**(5): p. 979-88.

108. Bossers, A., et al., *PrP genotype contributes to determining survival times of sheep with natural scrapie.* J Gen Virol, 1996. **77 (Pt 10)**: p. 2669-73.

109. Baylis, M. and W. Goldmann, *The genetics of scrapie in sheep and goats.* Curr Mol Med, 2004. **4**(4): p. 385-96.

110. Goldmann, W., et al., *Two alleles of a neural protein gene linked to scrapie in sheep.* Proc Natl Acad Sci U S A, 1990. **87**(7): p. 2476-80.

111. Hsiao, K., et al., *Mutation of the prion protein in Libyan Jews with Creutzfeldt-Jakob disease.* N Engl J Med, 1991. **324**(16): p. 1091-7.

112. Goldfarb, L.G., et al., *An insert mutation in the chromosome 20 amyloid precursor gene in a Gerstmann-Straussler-Scheinker family.* J Neurol Sci, 1992. **111**(2): p. 189-94.

113. Brown, P., et al., *Familial Creutzfeldt-Jakob disease in Chile is associated with the codon 200 mutation of the PRNP amyloid precursor gene on chromosome 20.* J Neurol Sci, 1992. **112**(1-2): p. 65-7.

114. Goldfarb, L.G., et al., *Creutzfeldt-Jakob disease cosegregates with the codon 178Asn PRNP mutation in families of European origin.* Ann Neurol, 1992. **31**(3): p. 274-81.

115. Goldfarb, L.G., et al., *Fatal familial insomnia and familial Creutzfeldt-Jakob disease: disease phenotype determined by a DNA polymorphism.* Science, 1992. **258**(5083): p. 806-8.

116. Ghetti, B., et al., *Gerstmann-Straussler-Scheinker disease and the Indiana kindred.* Brain Pathol, 1995. **5**(1): p. 61-75.

117. Furukawa, H., et al., *New variant prion protein in a Japanese family with Gerstmann-Straussler syndrome.* Brain Res Mol Brain Res, 1995. **30**(2): p. 385-8.

118. Turk, E., et al., *Purification and properties of the cellular and scrapie hamster prion proteins.* Eur J Biochem, 1988. **176**(1): p. 21-30.

119. Jackson, G.S., et al., *Reversible conversion of monomeric human prion protein between native and fibrilogenic conformations.* Science, 1999. **283**(5409): p. 1935-7.

120. Welker, E., et al., *Intramolecular versus intermolecular disulfide bonds in prion proteins.* J Biol Chem, 2002. **277**(36): p. 33477-81.

121. Rudd, P.M., et al., *Glycosylation and prion protein.* Curr Opin Struct Biol, 2002. **12**(5): p. 578-86.

122. Priola, S.A. and V.A. Lawson, *Glycosylation influences cross-species formation of protease-resistant prion protein.* EMBO J, 2001. **20**(23): p. 6692-9.

123. Cancellotti, E., et al., *Altered glycosylated PrP proteins can have different neuronal trafficking in brain but do not acquire scrapie-like properties.* J Biol Chem, 2005. **280**(52): p. 42909-18.

124. DeArmond, S.J., et al., *Selective neuronal targeting in prion disease.* Neuron, 1997. **19**(6): p. 1337-48.

125. Tuzi, N.L., et al., *Host PrP glycosylation: a major factor determining the outcome of prion infection.* PLoS Biol, 2008. **6**(4): p. e100.

126. Ritchie, M.A., et al., *Precursor ion scanning for detection and structural characterization of heterogeneous glycopeptide mixtures.* J Am Soc Mass Spectrom, 2002. **13**(9): p. 1065-77.

127. Chesebro, B., et al., *Anchorless prion protein results in infectious amyloid disease without clinical scrapie.* Science, 2005. **308**(5727): p. 1435-9.

128. Deleault, N.R., et al., *Formation of native prions from minimal components in vitro.* Proc Natl Acad Sci U S A, 2007. **104**(23): p. 9741-6.

129. Edgeworth, J.A., et al., *Spontaneous generation of mammalian prions.* Proc Natl Acad Sci U S A, 2010. **107**(32): p. 14402-6.

130. Weber, P., et al., *Generation of genuine prion infectivity by serial PMCA.* Vet Microbiol, 2007. **123**(4): p. 346-57.

131. Wang, F., et al., *Generating a prion with bacterially expressed recombinant prion protein.* Science, 2010. **327**(5969): p. 1132-5.

132. Giorgi, A., et al., *Proteomic profiling of PrP27-30-enriched preparations extracted from the brain of hamsters with experimental scrapie.* Proteomics, 2009. **9**(15): p. 3802-14.

133. Moore, R.A., et al., *Comparative profiling of highly enriched 22L and Chandler mouse scrapie prion protein preparations.* Proteomics, 2010. **10**(15): p. 2858-69.

134. Graham, J.F., et al., *Na+/K+-ATPase is present in scrapie-associated fibrils, modulates PrP misfolding in vitro and links PrP function and dysfunction.* PLoS One, 2011. **6**(11): p. e26813.

135. Hooper, N.M., D.R. Taylor, and N.T. Watt, *Mechanism of the metal-mediated endocytosis of the prion protein.* Biochem Soc Trans, 2008. **36**(Pt 6): p. 1272-6.

136. Peters, P.J., et al., *Trafficking of prion proteins through a caveolae-mediated endosomal pathway.* J Cell Biol, 2003. **162**(4): p. 703-17.

137. Shyng, S.L., M.T. Huber, and D.A. Harris, *A prion protein cycles between the cell surface and an endocytic compartment in cultured neuroblastoma cells.* J Biol Chem, 1993. **268**(21): p. 15922-8.

138. Graham, J.F., et al., *Low density subcellular fractions enhance disease-specific prion protein misfolding.* J Biol Chem, 2010. **285**(13): p. 9868-80.

139. Borchelt, D.R., A. Taraboulos, and S.B. Prusiner, *Evidence for synthesis of scrapie prion proteins in the endocytic pathway.* J Biol Chem, 1992. **267**(23): p. 16188-99.

140. Abid, K., R. Morales, and C. Soto, *Cellular factors implicated in prion replication.* FEBS Lett, 2010. **584**(11): p. 2409-14.

141. Hooper, N.M., *Glypican-1 facilitates prion conversion in lipid rafts.* J Neurochem, 2011. **116**(5): p. 721-5.

142. Goold, R., et al., *Alternative fates of newly formed PrPSc upon prion conversion on the plasma membrane.* J Cell Sci, 2013. **126**(Pt 16): p. 3552-62.

143. Braak, H. and E. Braak, *Neuropathological stageing of Alzheimer-related changes.* Acta Neuropathol, 1991. **82**(4): p. 239-59.

144. Braak, H., et al., *Stages in the development of Parkinson's disease-related pathology.* Cell Tissue Res, 2004. **318**(1): p. 121-34.

145. Lundmark, K., et al., *Transmissibility of systemic amyloidosis by a prion-like mechanism.* Proc Natl Acad Sci U S A, 2002. **99**(10): p. 6979-84.

146. Meyer-Luehmann, M., et al., *Exogenous induction of cerebral beta-amyloidogenesis is governed by agent and host.* Science, 2006. **313**(5794): p. 1781-4.

147. Bolmont, T., et al., *Induction of tau pathology by intracerebral infusion of amyloid-beta -containing brain extract and by amyloid-beta deposition in APP x Tau transgenic mice.* Am J Pathol, 2007. **171**(6): p. 2012-20.

148. Kordower, J.H., et al., *Lewy body-like pathology in long-term embryonic nigral transplants in Parkinson's disease.* Nat Med, 2008. **14**(5): p. 504-6.

149. Li, J.Y., et al., *Lewy bodies in grafted neurons in subjects with Parkinson's disease suggest host-to-graft disease propagation.* Nat Med, 2008. **14**(5): p. 501-3.

150. Desplats, P., et al., *Inclusion formation and neuronal cell death through neuron-to-neuron transmission of alpha-synuclein.* Proc Natl Acad Sci U S A, 2009. **106**(31): p. 13010-5.

151. Eisele, Y.S., et al., *Induction of cerebral beta-amyloidosis: intracerebral versus systemic Abeta inoculation.* Proc Natl Acad Sci U S A, 2009. **106**(31): p. 12926-31.

152. Sydow, A. and E.M. Mandelkow, *'Prion-like' propagation of mouse and human tau aggregates in an inducible mouse model of tauopathy.* Neurodegener Dis, 2010. **7**(1-3): p. 28-31.

153. Guo, J.L. and V.M. Lee, *Seeding of normal Tau by pathological Tau conformers drives pathogenesis of Alzheimer-like tangles.* J Biol Chem, 2011. **286**(17): p. 15317-31.

154. Munch, C., J. O'Brien, and A. Bertolotti, *Prion-like propagation of mutant superoxide dismutase-1 misfolding in neuronal cells.* Proc Natl Acad Sci U S A, 2011. **108**(9): p. 3548-53.

155. Grad, L.I., et al., *Intermolecular transmission of superoxide dismutase 1 misfolding in living cells.* Proc Natl Acad Sci U S A, 2011. **108**(39): p. 16398-403.

156. Frost, B. and M.I. Diamond, *Prion-like mechanisms in neurodegenerative diseases.* Nat Rev Neurosci, 2010. **11**(3): p. 155-9.

157. Sanders, D.W., et al., *Distinct tau prion strains propagate in cells and mice and define different tauopathies.* Neuron, 2014. **82**(6): p. 1271-88.

158. Stohr, J., et al., *Distinct synthetic Abeta prion strains producing different amyloid deposits in bigenic mice.* Proc Natl Acad Sci U S A, 2014. **111**(28): p. 10329-34.

159. Watts, J.C., et al., *Serial propagation of distinct strains of Abeta prions from Alzheimer's disease patients.* Proc Natl Acad Sci U S A, 2014. **111**(28): p. 10323-8.

160. Guo, J.L. and V.M. Lee, *Cell-to-cell transmission of pathogenic proteins in neurodegenerative diseases.* Nat Med, 2014. **20**(2): p. 130-8.

161. Clavaguera, F., et al., *Transmission and spreading of tauopathy in transgenic mouse brain.* Nat Cell Biol, 2009. **11**(7): p. 909-13.

162. Clavaguera, F., et al., *Brain homogenates from human tauopathies induce tau inclusions in mouse brain.* Proc Natl Acad Sci U S A, 2013. **110**(23): p. 9535-40.

163. Petkova, A.T., et al., *Self-propagating, molecular-level polymorphism in Alzheimer's beta-amyloid fibrils.* Science, 2005. **307**(5707): p. 262-5.

164. Kayed, R., et al., *Conformation dependent monoclonal antibodies distinguish different replicating strains or conformers of prefibrillar Abeta oligomers.* Mol Neurodegener, 2010. **5**: p. 57.

165. Yonetani, M., et al., *Conversion of wild-type alpha-synuclein into mutant-type fibrils and its propagation in the presence of A30P mutant.* J Biol Chem, 2009. **284**(12): p. 7940-50.

166. Brandner, S., et al., *Normal host prion protein necessary for scrapie-induced neurotoxicity.* Nature, 1996. **379**(6563): p. 339-43.

167. Stohr, J., et al., *Spontaneous generation of anchorless prions in transgenic mice.* Proc Natl Acad Sci U S A, 2011. **108**(52): p. 21223-8.

168. Bucciantini, M., et al., *Inherent toxicity of aggregates implies a common mechanism for protein misfolding diseases.* Nature, 2002. **416**(6880): p. 507-11.

169. Caughey, B. and P.T. Lansbury, *Protofibrils, pores, fibrils, and neurodegeneration: separating the responsible protein aggregates from the innocent bystanders.* Annu Rev Neurosci, 2003. **26**: p. 267-98.

170. Novitskaya, V., et al., *Amyloid fibrils of mammalian prion protein are highly toxic to cultured cells and primary neurons.* J Biol Chem, 2006. **281**(19): p. 13828-36.

171. Simoneau, S., et al., *In vitro and in vivo neurotoxicity of prion protein oligomers.* PLoS Pathog, 2007. **3**(8): p. e125.

172. Zhang, C., et al., *Amyloid-like aggregates of the yeast prion protein ure2 enter vertebrate cells by specific endocytotic pathways and induce apoptosis.* PLoS One, 2010. **5**(9).

173. Sanghera, N., et al., *Globular and pre-fibrillar prion aggregates are toxic to neuronal cells and perturb their electrophysiology.* Biochim Biophys Acta, 2008. **1784**(6): p. 873-81.

174. Kayed, R., et al., *Permeabilization of lipid bilayers is a common conformation-dependent activity of soluble amyloid oligomers in protein misfolding diseases.* J Biol Chem, 2004. **279**(45): p. 46363-6.

175. Quist, A., et al., *Amyloid ion channels: a common structural link for protein-misfolding disease.* Proc Natl Acad Sci U S A, 2005. **102**(30): p. 10427-32.

176. Martins, I.C., et al., *Lipids revert inert Abeta amyloid fibrils to neurotoxic protofibrils that affect learning in mice.* EMBO J, 2008. **27**(1): p. 224-33.

177. Haass, C. and D.J. Selkoe, *Soluble protein oligomers in neurodegeneration: lessons from the Alzheimer's amyloid beta-peptide.* Nat Rev Mol Cell Biol, 2007. **8**(2): p. 101-12.

178. Bueler, H., et al., *Normal development and behaviour of mice lacking the neuronal cell-surface PrP protein.* Nature, 1992. **356**(6370): p. 577-82.

179. Miele, G., et al., *Ablation of cellular prion protein expression affects mitochondrial numbers and morphology.* Biochem Biophys Res Commun, 2002. **291**(2): p. 372-7.

180. Curtis, J., et al., *Age-dependent loss of PTP and LTP in the hippocampus of PrP-null mice.* Neurobiol Dis, 2003. **13**(1): p. 55-62.

181. Maglio, L.E., et al., *Role of cellular prion protein on LTP expression in aged mice.* Brain Res, 2006. **1097**(1): p. 11-8.

182. Tobler, I., et al., *Altered circadian activity rhythms and sleep in mice devoid of prion protein.* Nature, 1996. **380**(6575): p. 639-42.

183. Bremer, J., et al., *Axonal prion protein is required for peripheral myelin maintenance.* Nat Neurosci, 2010. **13**(3): p. 310-8.

184. Resenberger, U.K., K.F. Winklhofer, and J. Tatzelt, *Neuroprotective and neurotoxic signaling by the prion protein.* Top Curr Chem, 2011. **305**: p. 101-19.

185. Mallucci, G., et al., *Depleting neuronal PrP in prion infection prevents disease and reverses spongiosis.* Science, 2003. **302**(5646): p. 871-4.

186. Mallucci, G.R., et al., *Targeting cellular prion protein reverses early cognitive deficits and neurophysiological dysfunction in prion-infected mice.* Neuron, 2007. **53**(3): p. 325-35.

187. Raeber, A.J., et al., *Astrocyte-specific expression of hamster prion protein (PrP) renders PrP knockout mice susceptible to hamster scrapie.* EMBO J, 1997. **16**(20): p. 6057-65.

188. Guenther, K., et al., *Early behavioural changes in scrapie-affected mice and the influence of dapsone.* Eur J Neurosci, 2001. **14**(2): p. 401-9.

189. Cunningham, C., et al., *Synaptic changes characterize early behavioural signs in the ME7 model of murine prion disease.* Eur J Neurosci, 2003. **17**(10): p. 2147-55.

190. Cunningham, C., et al., *Central and systemic endotoxin challenges exacerbate the local inflammatory response and increase neuronal death during chronic neurodegeneration.* J Neurosci, 2005. **25**(40): p. 9275-84.

191. Gray, B.C., et al., *Selective presynaptic degeneration in the synaptopathy associated with ME7-induced hippocampal pathology.* Neurobiol Dis, 2009. **35**(1): p. 63-74.

192. Siskova, Z., et al., *Degenerating synaptic boutons in prion disease: microglia activation without synaptic stripping.* Am J Pathol, 2009. **175**(4): p. 1610-21.

193. Belichenko, P.V., et al., *Dendritic and synaptic alterations of hippocampal pyramidal neurones in scrapie-infected mice.* Neuropathol Appl Neurobiol, 2000. **26**(2): p. 143-9.

194. Seelig, D.M., et al., *Chronic wasting disease prion trafficking via the autonomic nervous system.* Am J Pathol, 2011. **179**(3): p. 1319-28.

195. Kaatz, M., et al., *Spread of classic BSE prions from the gut via the peripheral nervous system to the brain.* Am J Pathol, 2012. **181**(2): p. 515-24.

196. Hoffmann, C., et al., *Prions spread via the autonomic nervous system from the gut to the central nervous system in cattle incubating bovine spongiform encephalopathy.* J Gen Virol, 2007. **88**(Pt 3): p. 1048-55.

197. Montagna, P., et al., *Familial and sporadic fatal insomnia.* Lancet Neurol, 2003. **2**(3): p. 167-76.

198. Mead, S., et al., *A novel prion disease associated with diarrhea and autonomic neuropathy.* N Engl J Med, 2013. **369**(20): p. 1904-14.

199. Cortelli, P., et al., *Cardiovascular dysautonomia in fatal familial insomnia.* Clin Auton Res, 1991. **1**(1): p. 15-21.

200. Portaluppi, F., et al., *Diurnal blood pressure variation and hormonal correlates in fatal familial insomnia.* Hypertension, 1994. **23**(5): p. 569-76.

201. Collinge, J., et al., *Prion dementia without characteristic pathology.* Lancet, 1990. **336**(8706): p. 7-9.

202. Budka, H., et al., *Neuropathological diagnostic criteria for Creutzfeldt-Jakob disease (CJD) and other human spongiform encephalopathies (prion diseases).* Brain Pathol, 1995. **5**(4): p. 459-66.

203. Chiti, Z., et al., *An integrated, temporal study of the behavioural, electrophysiological and neuropathological consequences of murine prion disease.* Neurobiol Dis, 2006. **22**(2): p. 363-73.

204. Siskova, Z., et al., *Reactive hypertrophy of synaptic varicosities within the hippocampus of prion-infected mice.* Biochem Soc Trans, 2010. **38**(2): p. 471-5.

205. Mallucci, G.R., *Prion neurodegeneration: starts and stops at the synapse.* Prion, 2009. **3**(4): p. 195-201.

206. Marcello, E., et al., *Synaptic dysfunction in Alzheimer's disease.* Adv Exp Med Biol, 2012. **970**: p. 573-601.

207. Picconi, B., G. Piccoli, and P. Calabresi, *Synaptic dysfunction in Parkinson's disease.* Adv Exp Med Biol, 2012. **970**: p. 553-72.

208. Yin, D.M., et al., *Synaptic dysfunction in schizophrenia.* Adv Exp Med Biol, 2012. **970**: p. 493-516.

209. Herms, J., et al., *Evidence of presynaptic location and function of the prion protein.* J Neurosci, 1999. **19**(20): p. 8866-75.

210. Mironov, A., Jr., et al., *Cytosolic prion protein in neurons.* J Neurosci, 2003. **23**(18): p. 7183-93.

211. Sharma, M., et al., *CSPalpha knockout causes neurodegeneration by impairing SNAP-25 function.* EMBO J, 2012. **31**(4): p. 829-41.

212. Caleo, M., et al., *The role of activity in synaptic degeneration in a protein misfolding disease, prion disease.* PLoS One, 2012. **7**(7): p. e41182.

213. Mallucci, G., et al., *Depleting neuronal PrP in prion infection prevents disease and reverses spongiosis.* Science, 2003. **302**(5646): p. 871-874.

214. Brown, D., et al., *Early loss of dendritic spines in murine scrapie revealed by confocal analysis.* Neuroreport, 2001. **12**(1): p. 179-83.

215. Fuhrmann, M., et al., *Dendritic pathology in prion disease starts at the synaptic spine.* J Neurosci, 2007. **27**(23): p. 6224-33.

216. Barrow, P.A., et al., *Intrinsic physiological and morphological properties of principal cells of the hippocampus and neocortex in hamsters infected with scrapie.* Neurobiol Dis, 1999. **6**(5): p. 406-23.

217. Jeffrey, M., et al., *Synapse loss associated with abnormal PrP precedes neuronal degeneration in the scrapie-infected murine hippocampus.* Neuropathol Appl Neurobiol, 2000. **26**(1): p. 41-54.

218. Majer, A., et al., *Early mechanisms of pathobiology are revealed by transcriptional temporal dynamics in hippocampal CA1 neurons of prion infected mice.* PLoS Pathog, 2012. **8**(11): p. e1003002.

219. Sitia, R. and I. Braakman, *Quality control in the endoplasmic reticulum protein factory.* Nature, 2003. **426**(6968): p. 891-4.

220. Galehdar, Z., et al., *Neuronal apoptosis induced by endoplasmic reticulum stress is regulated by ATF4-CHOP-mediated induction of the Bcl-2 homology 3-only member PUMA.* J Neurosci, 2010. **30**(50): p. 16938-48.

221. Brown, A.R., et al., *Gene expression profiling of the preclinical scrapie-infected hippocampus.* Biochem Biophys Res Commun, 2005. **334**(1): p. 86-95.

222. Mukherjee, A., et al., *Calcineurin inhibition at the clinical phase of prion disease reduces neurodegeneration, improves behavioral alterations and increases animal survival.* PLoS Pathog, 2010. **6**(10): p. e1001138.

223. Torres, M., et al., *Abnormal calcium homeostasis and protein folding stress at the ER: A common factor in familial and infectious prion disorders.* Commun Integr Biol, 2011. **4**(3): p. 258-61.

224. Torres, M., et al., *Prion protein misfolding affects calcium homeostasis and sensitizes cells to endoplasmic reticulum stress.* PLoS One, 2010. **5**(12): p. e15658.

225. Moreno, J.A., et al., *Sustained translational repression by eIF2alpha-P mediates prion neurodegeneration.* Nature, 2012. **485**(7399): p. 507-11.

226. Moreno, J.A., et al., *Oral treatment targeting the unfolded protein response prevents neurodegeneration and clinical disease in prion-infected mice.* Sci Transl Med, 2013. **5**(206): p. 206ra138.

227. Tang, Y., et al., *Transcriptional analysis implicates endoplasmic reticulum stress in bovine spongiform encephalopathy.* PLoS One, 2010. **5**(12): p. e14207.

228. Hwang, D., et al., *A systems approach to prion disease.* Mol Syst Biol, 2009. **5**: p. 252.

229. Martinez, T. and A. Pascual, *Identification of genes differentially expressed in SH-SY5Y neuroblastoma cells exposed to the prion peptide 106-126.* Eur J Neurosci, 2007. **26**(1): p. 51-9.

230. Sorensen, G., et al., *Comprehensive transcriptional profiling of prion infection in mouse models reveals networks of responsive genes.* BMC Genomics, 2008. **9**: p. 114.

231. Unterberger, U., et al., *Endoplasmic reticulum stress features are prominent in Alzheimer disease but not in prion diseases in vivo.* J Neuropathol Exp Neurol, 2006. **65**(4): p. 348-57.

232. Senatore, A., E. Restelli, and R. Chiesa, *Synaptic Dysfunction in Prion Diseases: A Trafficking Problem?* Int J Cell Biol, 2013. **2013**: p. 543803.

233. Mansuy, I.M., *Calcineurin in memory and bidirectional plasticity.* Biochem Biophys Res Commun, 2003. **311**(4): p. 1195-208.

234. Wang, H.G., et al., *Ca2+-induced apoptosis through calcineurin dephosphorylation of BAD.* Science, 1999. **284**(5412): p. 339-43.

235. Groth, R.D., R.L. Dunbar, and P.G. Mermelstein, *Calcineurin regulation of neuronal plasticity.* Biochem Biophys Res Commun, 2003. **311**(4): p. 1159-71.

236. Lonze, B.E. and D.D. Ginty, *Function and regulation of CREB family transcription factors in the nervous system.* Neuron, 2002. **35**(4): p. 605-23.

237. Franklin, S.L., et al., *Loss of Perineuronal Net in ME7 Prion Disease.* J Neuropathol Exp Neurol, 2008. **67**(3): p. 189-99.

238. Siskova, Z., et al., *Brain Region Specific Pre-Synaptic and Post-Synaptic Degeneration Are Early Components of Neuropathology in Prion Disease.* PLoS One, 2013. **8**(1).

239. Kovacs, G.G., et al., *Rapidly progressive dementia with thalamic degeneration and peculiar cortical prion protein immunoreactivity, but absence of proteinase K resistant PrP: a new disease entity?* Acta Neuropathol Commun, 2013. **1**(1): p. 72.

240. Spreafico, R., N.L. Hayes, and A. Rustioni, *Thalamic projections to the primary and secondary somatosensory cortices in cat: single and double retrograde tracer studies.* J Comp Neurol, 1981. **203**(1): p. 67-90.

241. Friedman, D.P. and E.A. Murray, *Thalamic connectivity of the second somatosensory area and neighboring somatosensory fields of the lateral sulcus of the macaque.* J Comp Neurol, 1986. **252**(3): p. 348-73.

242. Araque, A., et al., *Tripartite synapses: glia, the unacknowledged partner.* Trends Neurosci, 1999. **22**(5): p. 208-215.

243. Clarke, L.E. and B.A. Barres, *Emerging roles of astrocytes in neural circuit development.* Nat Rev Neurosci, 2013. **14**(5): p. 311-21.

244. Allen, N.J. and B.A. Barres, *Neuroscience: Glia - more than just brain glue.* Nature, 2009. **457**(7230): p. 675-7.

245. Matyash, V. and H. Kettenmann, *Heterogeneity in astrocyte morphology and physiology.* Brain Res Rev, 2010. **63**(1-2): p. 2-10.

246. Sofroniew, M.V., *Reactive astrocytes in neural repair and protection.* Neuroscientist, 2005. **11**(5): p. 400-7.

247. Sofroniew, M.V., *Molecular dissection of reactive astrogliosis and glial scar formation.* Trends Neurosci, 2009. **32**(12): p. 638-47.

248. Eng, L.F. and R.S. Ghirnikar, *GFAP and astrogliosis.* Brain Pathol, 1994. **4**(3): p. 229-237.

249. Brosius Lutz, A. and B.A. Barres, *Contrasting the glial response to axon injury in the central and peripheral nervous systems.* Dev Cell, 2014. **28**(1): p. 7-17.

250. Alvarez, J.I., T. Katayama, and A. Prat, *Glial influence on the blood brain barrier.* Glia, 2013. **61**(12): p. 1939-58.

251. Alves, J.L., *Blood-brain barrier and traumatic brain injury.* J Neurosci Res, 2014. **92**(2): p. 141-7.

252. Fitch, M.T. and J. Silver, *CNS injury, glial scars, and inflammation: Inhibitory extracellular matrices and regeneration failure.* Exp Neurol, 2008. **209**(2): p. 294-301.

253. Garthwaite, J., *Glutamate, nitric-oxide and cell cell signalling in the nervous-system.* Trends Neurosci, 1991. **14**(2): p. 60-67.

254. Rothstein, J.D., et al., *Knockout of glutamate transporters reveals a major role for astroglial transport in excitotoxicity and clearance of glutamate.* Neuron, 1996. **16**(3): p. 675-686.

255. Parpura, V. and P.G. Haydon, *Physiological astrocytic calcium levels stimulate glutamate release to modulate adjacent neurons.* Proceedings of the National Academy of Sciences of the United States of America, 2000. **97**(15): p. 8629-8634.

256. Burnstock, G., *Physiology and pathophysiology of purinergic neurotransmission.* Physiological Reviews, 2007. **87**(2): p. 659-797.

257. Zonta, M., et al., *Neuron-to-astrocyte signaling is central to the dynamic control of brain microcirculation.* Nat Neurosci, 2003. **6**(1): p. 43-50.

258. Stone, J., et al., *Development of retinal vasculature is mediated by hypoxia-induced vascular endothelial growth-factor (VEGF) expression by neuroglia.* Journal of Neuroscience, 1995. **15**(7): p. 4738-4747.

259. Schenk, D., et al., *Immunization with amyloid-beta attenuates Alzheimer disease-like pathology in the PDAPP mouse.* Nature, 1999. **400**(6740): p. 173-177.

260. Parchi, P., et al., *Regional distribution of protease-resistant prion protein in Fatal Familial Insomnia.* Annals of Neurology, 1995. **38**(1): p. 21-29.

261. Hainfellner, J.A., et al., *Pathology and immunocytochemistry of a Kuru Brain.* Brain Pathol, 1997. **7**(1): p. 547-553.

262. Diedrich, J., et al., *The molecular pathogenesis of astrogliosis in scrapie and Alzheimer's disease.* Microbial Pathogenesis, 1987. **2**(6): p. 435-442.

263. Diedrich, J.F., et al., *Scrapie-associated prion protein accumulates in astrocytes during scrapie infections.* Proceedings of the National Academy of Sciences of the United States of America, 1991. **88**(2): p. 375-379.

264. Gomi, H., et al., *Mice devoid of the glial fibrillary acidic protein develop normally and are susceptible to scrapie prions.* Neuron, 1995. **14**(1): p. 29-41.

265. Nimmerjahn, A., F. Kirchhoff, and F. Helmchen, *Resting microglial cells are highly dynamic surveillants of brain parenchyma in vivo.* Science, 2005. **308**(5726): p. 1314-8.

266. Davalos, D., et al., *ATP mediates rapid microglial response to local brain injury in vivo.* Nat Neurosci, 2005. **8**(6): p. 752-758.

267. Paolicelli, R.C., et al., *Synaptic pruning by microglia is necessary for normal brain development.* Science, 2011. **333**(6048): p. 1456-8.

268. Schafer, D.P., et al., *Microglia sculpt postnatal neural circuits in an activity and complement-dependent manner.* Neuron, 2012. **74**(4): p. 691-705.

269. Wake, H., et al., *Resting microglia directly monitor the functional state of synapses in vivo and determine the fate of ischemic terminals.* J Neurosci, 2009. **29**(13): p. 3974-80.

270. Marker, D.F., et al., *A thin-skull window technique for chronic two-photon in vivo imaging of murine microglia in models of neuroinflammation.* J Vis Exp, 2010(43).

271. Parkhurst, C.N., et al., *Microglia promote learning-dependent synapse formation through brain-derived neurotrophic factor.* Cell, 2013. **155**(7): p. 1596-609.

272. Schafer, D.P., E.K. Lehrman, and B. Stevens, *The "quad-partite" synapse: microglia-synapse interactions in the developing and mature CNS.* Glia, 2013. **61**(1): p. 24-36.

273. Block, M.L., L. Zecca, and J.S. Hong, *Microglia-mediated neurotoxicity: uncovering the molecular mechanisms.* Nat Rev Neurosci, 2007. **8**(1): p. 57-69.

274. Polazzi, E. and B. Monti, *Microglia and neuroprotection: from in vitro studies to therapeutic applications.* Prog Neurobiol, 2010. **92**(3): p. 293-315.

275. Perry, V.H., C. Cunningham, and D. Boche, *Atypical inflammation in the central nervous system in prion disease.* Curr Opin Neurol, 2002. **15**(3): p. 349-54.

276. Boche, D., et al., *TGFbeta1 regulates the inflammatory response during chronic neurodegeneration.* Neurobiol Dis, 2006. **22**(3): p. 638-50.

277. Perry, V.H., C. Cunningham, and C. Holmes, *Systemic infections and inflammation affect chronic neurodegeneration.* Nat Rev Immunol, 2007. **7**(2): p. 161-7.

278. Combrinck, M.I., V.H. Perry, and C. Cunningham, *Peripheral infection evokes exaggerated sickness behaviour in pre-clinical murine prion disease.* Neuroscience, 2002. **112**(1): p. 7-11.

279. Murray, C., et al., *Systemic inflammation induces acute working memory deficits in the primed brain: relevance for delirium.* Neurobiology of Aging, 2012. **33**(3): p. 603-616 e3.

280. Gomez-Nicola, D., et al., *Regulation of microglial proliferation during chronic neurodegeneration.* J Neurosci, 2013. **33**(6): p. 2481-93.

281. Harris, J.A., et al., *Transsynaptic progression of amyloid-beta-induced neuronal dysfunction within the entorhinal-hippocampal network.* Neuron, 2010. **68**(3): p. 428-41.

282. Drager, U.C. and J.F. Olsen, *Ganglion cell distribution in the retina of the mouse.* Invest Ophthalmol Vis Sci, 1981. **20**(3): p. 285-93.

283. Fraser, H., *Neuronal spread of scrapie agent and targeting of lesions within the retino-tectal pathway.* Nature, 1982. **295**(5845): p. 149-50.

284. Russelakis-Carneiro, M., S. Betmouni, and V.H. Perry, *Inflammatory response and retinal ganglion cell degeneration following intraocular injection of ME7.* Neuropathol Appl Neurobiol, 1999. **25**(3): p. 196-206.

285. Borchelt, D.R., et al., *Rapid anterograde axonal transport of the cellular prion glycoprotein in the peripheral and central nervous systems.* J Biol Chem, 1994. **269**(20): p. 14711-4.

286. Stohr, J., et al., *Purified and synthetic Alzheimer's amyloid beta (Abeta) prions.* Proc Natl Acad Sci U S A, 2012. **109**(27): p. 11025-30.

287. Eisele, Y.S., et al., *Peripherally applied Abeta-containing inoculates induce cerebral beta-amyloidosis.* Science, 2010. **330**(6006): p. 980-2.

288. Iba, M., et al., *Synthetic tau fibrils mediate transmission of neurofibrillary tangles in a transgenic mouse model of Alzheimer's-like tauopathy.* J Neurosci, 2013. **33**(3): p. 1024-37.

289. Lasagna-Reeves, C.A., et al., *Alzheimer brain-derived tau oligomers propagate pathology from endogenous tau.* Sci Rep, 2012. **2**: p. 700.

290. Luk, K.C., et al., *Pathological alpha-synuclein transmission initiates Parkinson-like neurodegeneration in nontransgenic mice.* Science, 2012. **338**(6109): p. 949-53.

291. Luk, K.C., et al., *Intracerebral inoculation of pathological alpha-synuclein initiates a rapidly progressive neurodegenerative alpha-synucleinopathy in mice.* J Exp Med, 2012. **209**(5): p. 975-86.

292. Masuda-Suzukake, M., et al., *Prion-like spreading of pathological alpha-synuclein in brain.* Brain, 2013. **136**(Pt 4): p. 1128-38.

293. Nonaka, T., et al., *Prion-like properties of pathological TDP-43 aggregates from diseased brains.* Cell Rep, 2013. **4**(1): p. 124-34.

294. Collins, S., C.A. McLean, and C.L. Masters, *Gerstmann-Straussler-Scheinker syndrome,fatal familial insomnia, and kuru: a review of these less common human transmissible spongiform encephalopathies.* J Clin Neurosci, 2001. **8**(5): p. 387-97.

295. Dickinson, A.G., V.M. Meikle, and H. Fraser, *Identification of a gene which controls the incubation period of some strains of scrapie agent in mice.* J Comp Pathol, 1968. **78**(3): p. 293-9.

296. Fraser, H. and A.G. Dickinson, *Distribution of experimentally induced scrapie lesions in the brain.* Nature, 1967. **216**(5122): p. 1310-1.

297. McCutcheon, S., et al., *Prion Protein-Specific Antibodies that Detect Multiple TSE Agents with High Sensitivity.* PLoS One, 2014. **9**(3): p. e91143.

298. Wilham, J.M., et al., *Rapid End-Point Quantitation of Prion Seeding Activity with Sensitivity Comparable to Bioassays.* Plos Pathogens, 2010. **6**(12).

299. Vascellari, S., et al., *Prion seeding activities of mouse scrapie strains with divergent PrPSc protease sensitivities and amyloid plaque content using RT-QuIC and eQuIC.* PLoS One, 2012. **7**(11): p. e48969.

300. Theocharidis, A., et al., *Network visualization and analysis of gene expression data using BioLayout Express(3D).* Nat Protoc, 2009. **4**(10): p. 1535-50.

301. Fruchterman, T.M.J. and E.M. Reingold, *Graph Drawing by Force-Directed Placement.* Software-Practice & Experience, 1991. **21**(11): p. 1129-1164.

302. Brohee, S. and J. van Helden, *Evaluation of clustering algorithms for protein-protein interaction networks.* BMC Bioinformatics, 2006. **7**: p. 488.

303. Fraser, H. and A.G. Dickinson, *The sequential development of the brain lesion of scrapie in three strains of mice.* J Comp Pathol, 1968. **78**(3): p. 301-11.

304. Cunningham, C., *Microglia and neurodegeneration: the role of systemic inflammation.* Glia, 2013. **61**(1): p. 71-90.

305. Fraser, J.R., *What is the basis of transmissible spongiform encephalopathy induced neurodegeneration and can it be repaired?* Neuropathol Appl Neurobiol, 2002. **28**(1): p. 1-11.

306. Dorandeu, A., et al., *Neuronal apoptosis in fatal familial insomnia.* Brain Pathol, 1998. **8**(3): p. 531-7.

307. Budka, H., *Neuropathology of prion diseases.* Br Med Bull, 2003. **66**: p. 121-30.

308. D'Castro, L., et al., *Isolation of proteinase K-sensitive prions using pronase E and phosphotungstic acid.* PLoS One, 2010. **5**(12): p. e15679.

309. West, M.J., *Introduction to stereology.* Cold Spring Harb Protoc, 2012. **2012**(8).

310. Barlow, R.M., *Transmissible mink encephalopathy: pathogenesis and nature of the aetiological agent.* J Clin Pathol Suppl (R Coll Pathol), 1972. **6**: p. 102-9.

311. Jackson, W.S., *Selective vulnerability to neurodegenerative disease: the curious case of Prion Protein.* Dis Model Mech, 2014. **7**(1): p. 21-9.

312. Swaab, D.F., et al., *Neuronal atrophy, not cell death, is the main hallmark of Alzheimer's disease.* Neurobiology of Aging, 1994. **15**(3): p. 369-71; discussion 379-80.

313. Gemmell, E., et al., *Hippocampal neuronal atrophy and cognitive function in delayed poststroke and aging-related dementias.* Stroke, 2012. **43**(3): p. 808-14.

314. Ito, D., et al., *Microglia-specific localisation of a novel calcium binding protein, Iba1.* Brain Res Mol Brain Res, 1998. **57**(1): p. 1-9.

315. Eddleston, M. and L. Mucke, *Molecular profile of reactive astrocytes - implications for their role in neurologic disease.* Neuroscience, 1993. **54**(1): p. 15-36.

316. Capucchio, M.T., et al., *Parenchymal and vascular lesions in ageing equine brains: histological and immunohistochemical studies.* J Comp Pathol, 2010. **142**(1): p. 61-73.

317. Fraser, H. and A.G. Dickinson, *Scrapie in mice. Agent-strain differences in the distribution and intensity of grey matter vacuolation.* J Comp Pathol, 1973. **83**(1): p. 29-40.

318. Collinge, J., et al., *Kuru in the 21st century--an acquired human prion disease with very long incubation periods.* Lancet, 2006. **367**(9528): p. 2068-74.

319. Kimberlin, R.H., *Transmissible encephalopathies in animals.* Can J Vet Res, 1990. **54**(1): p. 30-7.

320. Hilton, K.J., et al., *Early Hippocampal Synaptic Loss Precedes Neuronal Loss and Associates with Early Behavioural Deficits in Three Distinct Strains of Prion Disease.* PLoS One, 2013. **8**(6): p. e68062.

321. Beach, T.G., R. Walker, and E.G. McGeer, *Patterns of gliosis in Alzheimer's disease and aging cerebrum.* Glia, 1989. **2**(6): p. 420-36.

322. Itagaki, S., et al., *Relationship of microglia and astrocytes to amyloid deposits of Alzheimer disease.* J Neuroimmunol, 1989. **24**(3): p. 173-82.

323. Rogers, J., et al., *Expression of immune system-associated antigens by cells of the human central nervous system: relationship to the pathology of Alzheimer's disease.* Neurobiology of Aging, 1988. **9**(4): p. 339-49.

324. Masliah, E., et al., *Immunoreactivity of CD45, a protein phosphotyrosine phosphatase, in Alzheimer's disease.* Acta Neuropathol, 1991. **83**(1): p. 12-20.

325. Betmouni, S., V.H. Perry, and J.L. Gordon, *Evidence for an early inflammatory response in the central nervous system of mice with scrapie.* Neuroscience, 1996. **74**(1): p. 1-5.

326. Siskova, Z., et al., *Morphological and functional abnormalities in mitochondria associated with synaptic degeneration in prion disease.* Am J Pathol, 2010. **177**(3): p. 1411-21.

327. Scheff, S.W., S.T. DeKosky, and D.A. Price, *Quantitative assessment of cortical synaptic density in Alzheimer's disease.* Neurobiology of Aging, 1990. **11**(1): p. 29-37.

328. Scheff, S.W., et al., *Hippocampal synaptic loss in early Alzheimer's disease and mild cognitive impairment.* Neurobiology of Aging, 2006. **27**(10): p. 1372-84.

329. Scheff, S.W., et al., *Synaptic alterations in CA1 in mild Alzheimer disease and mild cognitive impairment.* Neurology, 2007. **68**(18): p. 1501-8.

330. DeKosky, S.T. and S.W. Scheff, *Synapse loss in frontal cortex biopsies in Alzheimer's disease: correlation with cognitive severity.* Ann Neurol, 1990. **27**(5): p. 457-64.

331. Terry, R.D., et al., *Physical basis of cognitive alterations in Alzheimer's disease: synapse loss is the major correlate of cognitive impairment.* Ann Neurol, 1991. **30**(4): p. 572-80.

332. Kaufman, S.K. and M.I. Diamond, *Prion-like propagation of protein aggregation and related therapeutic strategies.* Neurotherapeutics, 2013. **10**(3): p. 371-82.

333. Hajos, M. and S.A. Greenfield, *Synaptic connections between pars compacta and pars reticulata neurones: electrophysiological evidence for functional modules within the substantia nigra.* Brain Res, 1994. **660**(2): p. 216-24.

334. Shibata, H., T. Suzuki, and M. Matsushita, *Afferent projections to the interpeduncular nucleus in the rat, as studied by retrograde and anterograde transport of wheat germ agglutinin conjugated to horseradish peroxidase.* J Comp Neurol, 1986. **248**(2): p. 272-84.

335. Vertes, R.P., W.J. Fortin, and A.M. Crane, *Projections of the median raphe nucleus in the rat.* J Comp Neurol, 1999. **407**(4): p. 555-82.

336. Waselus, M., et al., *Differential projections of dorsal raphe nucleus neurons to the lateral septum and striatum.* J Chem Neuroanat, 2006. **31**(4): p. 233-42.

337. Del Cid-Pellitero, E. and M. Garzon, *Medial prefrontal cortex receives input from dorsal raphe nucleus neurons targeted by hypocretin1/orexinA-containing axons.* Neuroscience, 2011. **172**: p. 30-43.

338. Chen, W.Y., J.J. Wang, and Q.X. Yu, *[Effects of dorsal raphe stimulation on activities of cerebellar nuclear neurons in the rat].* Sheng Li Xue Bao, 1996. **48**(2): p. 132-40.

339. Pierce, E.T., G.H. Hoddevik, and F. Walberg, *The cerebellar projection from the raphe nuclei in the cat as studied with the method of retrograde transport of horseradish peroxidase.* Anat Embryol (Berl), 1977. **152**(1): p. 73-87.

340. Hsu, D.T. and J.L. Price, *Paraventricular thalamic nucleus: subcortical connections and innervation by serotonin, orexin, and corticotropin-releasing hormone in macaque monkeys.* J Comp Neurol, 2009. **512**(6): p. 825-48.

341. Hikosaka, O., *The habenula: from stress evasion to value-based decision-making.* Nat Rev Neurosci, 2010. **11**(7): p. 503-13.

342. Iribe, Y., et al., *Subthalamic stimulation-induced synaptic responses in substantia nigra pars compacta dopaminergic neurons in vitro.* J Neurophysiol, 1999. **82**(2): p. 925-33.

343. Chowdhury, R., et al., *Parcellation of the human substantia nigra based on anatomical connectivity to the striatum.* Neuroimage, 2013. **81**: p. 191-8.

344. Millson, G.C., et al., *Early Distribution of Radioactive Liposomes and Scrapie Infectivity in Mouse-Tissues Following Administration by Different Routes.* Vet Microbiol, 1979. **4**(2): p. 89-99.

345. Geoghegan, J.C., et al., *Selective incorporation of polyanionic molecules into hamster prions.* J Biol Chem, 2007. **282**(50): p. 36341-53.

346. Saa, P., J. Castilla, and C. Soto, *Ultra-efficient replication of infectious prions by automated protein misfolding cyclic amplification.* J Biol Chem, 2006. **281**(46): p. 35245-52.

347. Biancalana, M. and S. Koide, *Molecular mechanism of Thioflavin-T binding to amyloid fibrils.* Biochim Biophys Acta, 2010. **1804**(7): p. 1405-12.

348. Sano, K., et al., *Conformational properties of prion strains can be transmitted to recombinant prion protein fibrils in real-time quaking-induced conversion.* J Virol, 2014.

349. Somerville, R.A., S. Hamilton, and K. Fernie, *Transmissible spongiform encephalopathy strain, PrP genotype and brain region all affect the degree of glycosylation of PrPSc.* J Gen Virol, 2005. **86**(Pt 1): p. 241-6.

350. Choi, Y.P., et al., *Correlation of polydispersed prion protein and characteristic pathology in the thalamus in variant Creutzfeldt-Jakob disease: implication of small oligomeric species.* Brain Pathol, 2011. **21**(3): p. 298-307.

351. Booth, S., et al., *Identification of central nervous system genes involved in the host response to the scrapie agent during preclinical and clinical infection.* J Gen Virol, 2004. **85**(Pt 11): p. 3459-71.

352. Xiang, W., et al., *Identification of differentially expressed genes in scrapie-infected mouse brains by using global gene expression technology.* J Virol, 2004. **78**(20): p. 11051-60.

353. Skinner, P.J., et al., *Gene expression alterations in brains of mice infected with three strains of scrapie.* BMC Genomics, 2006. **7**: p. 114.

354. Riemer, C., et al., *Gene expression profiling of scrapie-infected brain tissue.* Biochem Biophys Res Commun, 2004. **323**(2): p. 556-64.

355. Filali, H., et al., *Gene expression profiling and association with prion-related lesions in the medulla oblongata of symptomatic natural scrapie animals.* PLoS One, 2011. **6**(5): p. e19909.

356. Filali, H., et al., *Medulla oblongata transcriptome changes during presymptomatic natural scrapie and their association with prion-related lesions.* BMC Genomics, 2012. **13**: p. 399.

357. Khaniya, B., et al., *Microarray analysis of differentially expressed genes from Peyer's patches of cattle orally challenged with bovine spongiform encephalopathy.* J Toxicol Environ Health A, 2009. **72**(17-18): p. 1008-13.

358. Almeida, L.M., et al., *Gene expression in the medulla following oral infection of cattle with bovine spongiform encephalopathy.* J Toxicol Environ Health A, 2011. **74**(2-4): p. 110-26.

359. Almeida, L.M., et al., *Microarray analysis in caudal medulla of cattle orally challenged with bovine spongiform encephalopathy.* Genet Mol Res, 2011. **10**(4): p. 3948-62.

360. Basu, U., et al., *Transcriptome analysis of the medulla tissue from cattle in response to bovine spongiform encephalopathy using digital gene expression tag profiling.* J Toxicol Environ Health A, 2011. **74**(2-4): p. 127-37.

361. Panelli, S., et al., *Analysis of gene expression in white blood cells of cattle orally challenged with bovine amyloidotic spongiform encephalopathy.* J Toxicol Environ Health A, 2011. **74**(2-4): p. 96-102.

362. Race, B., et al., *Susceptibilities of nonhuman primates to chronic wasting disease.* Emerg Infect Dis, 2009. **15**(9): p. 1366-76.

363. Barbisin, M., et al., *Gene expression profiling of brains from bovine spongiform encephalopathy (BSE)-infected cynomolgus macaques.* BMC Genomics, 2014. **15**: p. 434.

364. Tian, C., et al., *Comparative analysis of gene expression profiles between cortex and thalamus in Chinese fatal familial insomnia patients.* Mol Neurobiol, 2013. **48**(1): p. 36-48.

365. Xiang, W., et al., *Cerebral gene expression profiles in sporadic Creutzfeldt-Jakob disease.* Ann Neurol, 2005. **58**(2): p. 242-57.

366. Tian, C., et al., *Global transcriptional profiling of the postmortem brain of a patient with G114V genetic Creutzfeldt-Jakob disease.* Int J Mol Med, 2013. **31**(3): p. 676-88.

367. Tian, C., et al., *Analyses of the Similarity and Difference of Global Gene Expression Profiles in Cortex Regions of Three Neurodegenerative Diseases: Sporadic*

Creutzfeldt-Jakob Disease (sCJD), Fatal Familial Insomnia (FFI), and Alzheimer's Disease (AD). Mol Neurobiol, 2014.

368. Greenwood, A.D., et al., *Cell line dependent RNA expression profiles of prion-infected mouse neuronal cells.* J Mol Biol, 2005. **349**(3): p. 487-500.

369. Zhang, S.J., et al., *Decoding NMDA receptor signaling: identification of genomic programs specifying neuronal survival and death.* Neuron, 2007. **53**(4): p. 549-62.

370. Herbst, A., et al., *Prion disease diagnosis by proteomic profiling.* J Proteome Res, 2009. **8**(2): p. 1030-6.

371. Wei, X., et al., *A quantitative proteomic approach to prion disease biomarker research: delving into the glycoproteome.* J Proteome Res, 2011. **10**(6): p. 2687-702.

372. Asuni, A.A., et al., *Analysis of the Hippocampal Proteome in ME7 Prion Disease Reveals a Predominant Astrocytic Signature and Highlights the Brain-restricted Production of Clusterin in Chronic Neurodegeneration.* J Biol Chem, 2014. **289**(7): p. 4532-45.

373. Wagner, W., et al., *Quantitative phosphoproteomic analysis of prion-infected neuronal cells.* Cell Commun Signal, 2010. **8**: p. 28.

374. Pushie, M.J., et al., *An NMR metabolomics study of elk inoculated with chronic wasting disease.* J Toxicol Environ Health A, 2011. **74**(22-24): p. 1476-92.

375. Inoue, K., et al., *Metabolic profiling of Alzheimer's disease brains.* Sci Rep, 2013. **3**: p. 2364.

376. Lallemand-Breitenbach, V. and H. de The, *PML nuclear bodies.* Cold Spring Harb Perspect Biol, 2010. **2**(5): p. a000661.

377. Regad, T. and M.K. Chelbi-Alix, *Role and fate of PML nuclear bodies in response to interferon and viral infections.* Oncogene, 2001. **20**(49): p. 7274-86.

378. Ling, P.D., et al., *Mediation of Epstein-Barr virus EBNA-LP transcriptional coactivation by Sp100.* EMBO J, 2005. **24**(20): p. 3565-75.

379. Tavalai, N., et al., *Evidence for a dual antiviral role of the major nuclear domain 10 component Sp100 during the immediate-early and late phases of the human cytomegalovirus replication cycle.* J Virol, 2011. **85**(18): p. 9447-58.

380. Kim, Y.E., et al., *Human cytomegalovirus infection causes degradation of Sp100 proteins that suppress viral gene expression.* J Virol, 2011. **85**(22): p. 11928-37.

381. Wasylyk, C., et al., *Sp100 interacts with ETS-1 and stimulates its transcriptional activity.* Mol Cell Biol, 2002. **22**(8): p. 2687-702.

382. Yordy, J.S., et al., *SP100 expression modulates ETS1 transcriptional activity and inhibits cell invasion.* Oncogene, 2004. **23**(39): p. 6654-65.

383. Nagarajan, P., et al., *Ets1 blocks terminal differentiation of keratinocytes and induces expression of matrix metalloproteases and innate immune mediators.* J Cell Sci, 2010. **123**(Pt 20): p. 3566-75.

384. Doucas, V., et al., *Adenovirus replication is coupled with the dynamic properties of the PML nuclear structure.* Genes Dev, 1996. **10**(2): p. 196-207.

385. LaMorte, V.J., et al., *Localization of nascent RNA and CREB binding protein with the PML-containing nuclear body.* Proc Natl Acad Sci U S A, 1998. **95**(9): p. 4991-6.

386. Fuchsova, B., et al., *Nuclear DNA helicase II is recruited to IFN-alpha-activated transcription sites at PML nuclear bodies.* J Cell Biol, 2002. **158**(3): p. 463-73.

387. Boisvert, F.M., M.J. Hendzel, and D.P. Bazett-Jones, *Promyelocytic leukemia (PML) nuclear bodies are protein structures that do not accumulate RNA.* J Cell Biol, 2000. **148**(2): p. 283-92.

388. Yeo, M., et al., *A novel RNA polymerase II C-terminal domain phosphatase that preferentially dephosphorylates serine 5.* J Biol Chem, 2003. **278**(28): p. 26078-85.

389. Blazek, E., G. Mittler, and M. Meisterernst, *The mediator of RNA polymerase II.* Chromosoma, 2005. **113**(8): p. 399-408.

390. Kim, B., et al., *Breast cancer metastasis suppressor 1 (BRMS1) is destabilized by the Cul3-SPOP E3 ubiquitin ligase complex.* Biochem Biophys Res Commun, 2011. **415**(4): p. 720-6.

391. Kwon, J.E., et al., *BTB domain-containing speckle-type POZ protein (SPOP) serves as an adaptor of Daxx for ubiquitination by Cul3-based ubiquitin ligase.* J Biol Chem, 2006. **281**(18): p. 12664-72.

392. Liu, Y., P.W. Smith, and D.R. Jones, *Breast cancer metastasis suppressor 1 functions as a corepressor by enhancing histone deacetylase 1-mediated deacetylation of RelA/p65 and promoting apoptosis.* Mol Cell Biol, 2006. **26**(23): p. 8683-96.

393. Dror, N., et al., *Interferon regulatory factor-8 is indispensable for the expression of promyelocytic leukemia and the formation of nuclear bodies in myeloid cells.* J Biol Chem, 2007. **282**(8): p. 5633-40.

394. Ben-Zvi, A., et al., *Mfsd2a is critical for the formation and function of the blood-brain barrier.* Nature, 2014. **509**(7501): p. 507-11.

395. Schultz, J., et al., *Role of interleukin-1 in prion disease-associated astrocyte activation.* Am J Pathol, 2004. **165**(2): p. 671-8.

396. Tamguney, G., et al., *Genes contributing to prion pathogenesis.* J Gen Virol, 2008. **89**(Pt 7): p. 1777-88.

397. Felton, L.M., et al., *MCP-1 and murine prion disease: separation of early behavioural dysfunction from overt clinical disease.* Neurobiol Dis, 2005. **20**(2): p. 283-95.

398. Riemer, C., et al., *Accelerated prion replication in, but prolonged survival times of, prion-infected CXCR3-/- mice.* J Virol, 2008. **82**(24): p. 12464-71.

399. Thackray, A.M., et al., *Accelerated prion disease in the absence of interleukin-10.* J Virol, 2004. **78**(24): p. 13697-707.

400. LaCasse, R.A., et al., *Role of Erk1/2 activation in prion disease pathogenesis: absence of CCR1 leads to increased Erk1/2 activation and accelerated disease progression.* J Neuroimmunol, 2008. **196**(1-2): p. 16-26.

401. Sakai, K., et al., *Absence of CD14 delays progression of prion diseases accompanied by increased microglial activation.* J Virol, 2013. **87**(24): p. 13433-45.

402. Mabbott, N.A., et al., *Tumor necrosis factor alpha-deficient, but not interleukin-6-deficient, mice resist peripheral infection with scrapie.* J Virol, 2000. **74**(7): p. 3338-44.

403. Campeau, J.L., et al., *Early increase and late decrease of purkinje cell dendritic spine density in prion-infected organotypic mouse cerebellar cultures.* PLoS One, 2013. **8**(12): p. e81776.

404. Jalland, C.M., et al., *Accelerated clinical course of prion disease in mice compromised in repair of oxidative DNA damage.* Free Radic Biol Med, 2014. **68**: p. 1-7.

405. Davis, R.J., *Signal transduction by the JNK group of MAP kinases.* Cell, 2000. **103**(2): p. 239-52.

406. Bhoumik, A., et al., *ATM-dependent phosphorylation of ATF2 is required for the DNA damage response.* Mol Cell, 2005. **18**(5): p. 577-87.

407. Taylor, R.C., K.M. Berendzen, and A. Dillin, *Systemic stress signalling: understanding the cell non-autonomous control of proteostasis.* Nat Rev Mol Cell Biol, 2014. **15**(3): p. 211-7.

408. Hai, T., et al., *ATF3 and stress responses.* Gene Expr, 1999. **7**(4-6): p. 321-35.

409. Whitney, M.L., L.S. Jefferson, and S.R. Kimball, *ATF4 is necessary and sufficient for ER stress-induced upregulation of REDD1 expression.* Biochem Biophys Res Commun, 2009. **379**(2): p. 451-5.

410. Han, J., et al., *ER-stress-induced transcriptional regulation increases protein synthesis leading to cell death.* Nat Cell Biol, 2013. **15**(5): p. 481-90.

411. Ron, D. and P. Walter, *Signal integration in the endoplasmic reticulum unfolded protein response.* Nat Rev Mol Cell Biol, 2007. **8**(7): p. 519-29.

412. Wek, R.C. and D.R. Cavener, *Translational control and the unfolded protein response.* Antioxid Redox Signal, 2007. **9**(12): p. 2357-71.

413. De Graeve, F., et al., *Role of the ATFa/JNK2 complex in Jun activation.* Oncogene, 1999. **18**(23): p. 3491-500.

414. Maekawa, T., et al., *Social isolation stress induces ATF-7 phosphorylation and impairs silencing of the 5-HT 5B receptor gene.* EMBO J, 2010. **29**(1): p. 196-208.

415. Petroski, M.D. and R.J. Deshaies, *Function and regulation of cullin-RING ubiquitin ligases.* Nat Rev Mol Cell Biol, 2005. **6**(1): p. 9-20.

416. Cicek, M., et al., *Breast cancer metastasis suppressor 1 inhibits gene expression by targeting nuclear factor-kappaB activity.* Cancer Res, 2005. **65**(9): p. 3586-95.

417. Lawrence, T., *The nuclear factor NF-kappaB pathway in inflammation.* Cold Spring Harb Perspect Biol, 2009. **1**(6): p. a001651.

418. Chang, H.Y., et al., *Activation of apoptosis signal-regulating kinase 1 (ASK1) by the adapter protein Daxx.* Science, 1998. **281**(5384): p. 1860-3.

419. Ichijo, H., et al., *Induction of apoptosis by ASK1, a mammalian MAPKKK that activates SAPK/JNK and p38 signaling pathways.* Science, 1997. **275**(5296): p. 90-4.

420. Dhanasekaran, D.N. and E.P. Reddy, *JNK signaling in apoptosis.* Oncogene, 2008. **27**(48): p. 6245-51.

421. Bonifati, V., et al., *Mutations in the DJ-1 gene associated with autosomal recessive early-onset parkinsonism.* Science, 2003. **299**(5604): p. 256-9.

422. Junn, E., et al., *Interaction of DJ-1 with Daxx inhibits apoptosis signal-regulating kinase 1 activity and cell death.* Proc Natl Acad Sci U S A, 2005. **102**(27): p. 9691-6.

423. Voll, R.E., et al., *Immunosuppressive effects of apoptotic cells.* Nature, 1997. **390**(6658): p. 350-1.

424. Fadok, V.A., et al., *Macrophages that have ingested apoptotic cells in vitro inhibit proinflammatory cytokine production through autocrine/paracrine mechanisms involving TGF-beta, PGE2, and PAF.* J Clin Invest, 1998. **101**(4): p. 890-8.

425. Sheng, M. and E. Kim, *The Shank family of scaffold proteins.* J Cell Sci, 2000. **113 (Pt 11)**: p. 1851-6.

426. Wilkinson, M.G., et al., *The Atf1 transcription factor is a target for the Sty1 stress-activated MAP kinase pathway in fission yeast.* Genes Dev, 1996. **10**(18): p. 2289-301.

427. Shen, J., et al., *ER stress regulation of ATF6 localization by dissociation of BiP/GRP78 binding and unmasking of Golgi localization signals.* Dev Cell, 2002. **3**(1): p. 99-111.

428. Ye, J., et al., *ER stress induces cleavage of membrane-bound ATF6 by the same proteases that process SREBPs.* Mol Cell, 2000. **6**(6): p. 1355-64.

429. Stewart, R.S., et al., *Neurodegenerative illness in transgenic mice expressing a transmembrane form of the prion protein.* J Neurosci, 2005. **25**(13): p. 3469-77.

430. Chiesa, R., et al., *Accumulation of protease-resistant prion protein (PrP) and apoptosis of cerebellar granule cells in transgenic mice expressing a PrP insertional mutation.* Proc Natl Acad Sci U S A, 2000. **97**(10): p. 5574-9.

431. Chiesa, R., et al., *Molecular distinction between pathogenic and infectious properties of the prion protein.* J Virol, 2003. **77**(13): p. 7611-22.

432. Sandberg, M.K., et al., *Prion neuropathology follows the accumulation of alternate prion protein isoforms after infective titre has peaked.* Nat Commun, 2014. **5**: p. 4347.

433. Spillantini, M.G. and M. Goedert, *Tau pathology and neurodegeneration.* Lancet Neurol, 2013. **12**(6): p. 609-22.

434. Iovino, M., et al., *The novel MAPT mutation K298E: mechanisms of mutant tau toxicity, brain pathology and tau expression in induced fibroblast-derived neurons.* Acta Neuropathol, 2014. **127**(2): p. 283-95.

435. Forno, L.S., *Neuropathology of Parkinson's disease.* J Neuropathol Exp Neurol, 1996. **55**(3): p. 259-72.

436. Spillantini, M.G., et al., *alpha-Synuclein in filamentous inclusions of Lewy bodies from Parkinson's disease and dementia with lewy bodies.* Proc Natl Acad Sci U S A, 1998. **95**(11): p. 6469-73.

437. Sandberg, M.K., et al., *Prion propagation and toxicity in vivo occur in two distinct mechanistic phases.* Nature, 2011. **470**(7335): p. 540-2.

438. Clavaguera, F., et al., *"Prion-like" templated misfolding in tauopathies.* Brain Pathol, 2013. **23**(3): p. 342-9.

439. Reed-Geaghan, E.G., et al., *Deletion of CD14 attenuates Alzheimer's disease pathology by influencing the brain's inflammatory milieu.* J Neurosci, 2010. **30**(46): p. 15369-73.

440. Eklund, C.M., R.C. Kennedy, and W.J. Hadlow, *Pathogenesis of scrapie virus infection in the mouse.* J Infect Dis, 1967. **117**(1): p. 15-22.

441. Dickinson, A.G. and H. Fraser, *Genetical control of the concentration of ME7 scrapie agent in mouse spleen.* J Comp Pathol, 1969. **79**(3): p. 363-6.

442. Kimberlin, R.H. and C.A. Walker, *Pathogenesis of mouse scrapie: dynamics of agent replication in spleen, spinal cord and brain after infection by different routes.* J Comp Pathol, 1979. **89**(4): p. 551-62.

443. Koffie, R.M., et al., *Oligomeric amyloid beta associates with postsynaptic densities and correlates with excitatory synapse loss near senile plaques.* Proc Natl Acad Sci U S A, 2009. **106**(10): p. 4012-7.

444. Meyer-Luehmann, M., et al., *Rapid appearance and local toxicity of amyloid-beta plaques in a mouse model of Alzheimer's disease.* Nature, 2008. **451**(7179): p. 720-4.

445. Majer, A. and S.A. Booth, *Microdissection and transcriptional profiling: a window into the pathobiology of preclinical prion disease.* Prion, 2014. **8**(1): p. 67-74.

446. Grotzinger, T., K. Jensen, and H. Will, *The interferon (IFN)-stimulated gene Sp100 promoter contains an IFN-gamma activation site and an imperfect IFN-stimulated response element which mediate type I IFN inducibility.* J Biol Chem, 1996. **271**(41): p. 25253-60.

447. Grotzinger, T., et al., *Interferon-modulated expression of genes encoding the nuclear-dot-associated proteins Sp100 and promyelocytic leukemia protein (PML).* Eur J Biochem, 1996. **238**(2): p. 554-60.

448. Korioth, F., et al., *Molecular characterization of NDP52, a novel protein of the nuclear domain 10, which is redistributed upon virus infection and interferon treatment.* J Cell Biol, 1995. **130**(1): p. 1-13.

449. Guldner, H.H., et al., *IFN enhance expression of Sp100, an autoantigen in primary biliary cirrhosis.* J Immunol, 1992. **149**(12): p. 4067-73.

Appendix 1

Down regulation of genes associated with group B (figure 6.3)

Function	Count	Genes
Autophagy	1	Gm10377
Cell adhesion	3	Cdh11; Crisp1; Spam1
Cell proliferation	2	Dbf4; Ttk
Cell structure	7	Capza1; Gm19924; Grxcr1; Dlg5; Rp1; Sptlc3; Tcte3
Production of CSF	1	Car1
DNA structure, repair and division	12	Aspm; H2-T3; H3f3a; Hmgb1; Hmgb2; Ncapg; Ott; Rad54b; Sfi1; Slx; Sly; Top2a
Immune related	31	Pla2g10os; Ccl11; Cd244; COX2; Csprs; Defa17; Defa20; Defa23; Defa5; Defb12; Fam60a; Cd194; SPOP; Ifna1; Ighg3; Ighv1-72; Igh-VJ558; Igkv4-70; Igkv5-43; Il12b; Sp140-l; Mgst2; Ms4a2; Nlrp4e; Slamf6; Sp100; Sp110; Sp140; Tlr4; Trav12-2; Trav7-4;
Intracellular trafficking	5	Atp6v1g1; Rab11b; Rab19; Slc30a8; Slco1a6
Metabolism	7	Acbd7; Amy2a5; Arg1; Mptx; Lipm; Mgam; Mup1
Metal ion homeostasis	3	Caps2; Ftl1; Gm15421
Misfolded protein regulation	2	Sel1l2; Ugt2b1
Mitochondrial function	7	Atp5l; ATP6; Cps1; Cyp3a25; Cyp3a41a; Cyp3a41b; Gm10921
Neuronal function	3	Gabrr3; Gm3002; Gm3591
Other	1	Uts2d
Protease inhibitor	2	Cst8; Cst9
Protein kinase	4	AU018829; Gm10324; Itln1; Lrriq3
RNA splicing	6	Cwc22; Ear14; Esrp1; Hnrnpf; Lsm5; Rbmy1a1
Sensory function	90	Vmn1r102; Mup17; Olfr1036; Olfr1162; Olfr1234; Olfr1252; Olfr1289; Olfr1294; Olfr1330; Olfr1362; Olfr1368; Olfr1373; Olfr1381; Olfr1467; Olfr1477; Olfr177; Olfr205; Olfr247; Olfr347; Olfr355; Olfr43; Olfr447; Olfr452; Olfr485; Olfr559; Olfr568; Olfr575; Olfr591; Olfr594; Olfr6; Olfr656; Olfr671;

		Olfr728; Olfr749; Olfr796; Olfr8; Olfr810; Olfr819; Olfr890; Olfr901; Olfr917; Olfr968; Olfr974; Olfr983; Tas2r118; Tas2r120; Trpa1; Vmn1r100; Vmn1r101; Vmn1r104; Vmn1r107; Vmn1r111; Vmn1r112; Vmn1r114; Vmn1r117; Vmn1r118; Vmn1r119; Vmn1r120; Vmn1r126; Vmn1r127; Vmn1r129; Vmn1r130; Vmn1r132; Vmn1r135; Vmn1r142; Vmn1r143; Vmn1r151; Vmn1r152; Vmn1r159; Vmn1r174; Vmn1r196; Vmn1r218; Vmn1r32; Vmn1r43; Vmn1r77; Vmn1r91; Vmn1r93; Vmn1r94; Vmn1r-ps79; Vmn2r21; Vmn2r29; Vmn2r32; Vmn2r33; Vmn2r34; Vmn2r38; Vmn2r42; Vmn2r43; Vmn2r44; Vmn2r51; Vmn2r85
Signal transduction	9	Arhgap15os; Abca13; Abcb11; Gm10375; Gm14482; Mcoln2; Sirpb1b; Gm14484; Gm14850
Transcriptional regulation	40	Dppa2; Dppa3; Gcl1; 1700020N01Rik; 1700029I01Rik; Zbed4ps; Zfp30; CTDSPL; Med7; Polr2k; Tdpoz5; Zbed4; Zfp600; Zfp772; Zfp808; Zscan4a; Zscan4b; Zscan4e; Zscan4f;
Translational regulation	8	Nop16; eIF2a; Alyref1; Alyref2; Rpl23al; Rpl7a; Rps12; Rps18;
Ubiquitination	3	Gmcl1l; Ube2d2b; SPOP

Appendix 2

Up-regulation of genes associated with group C (figure 6.3)

Function	Count	Gene
Apoptosis	1	Rassf4
Astrocyte function	2	Gfap; Mfsd2a
Cell proliferation	11	Axl; Csf3r; Emp3; Fgf18; Fstl1; Gata2; Gpnmb; Igfbp2; Inpp5d; S1pr3; Timp1
Cell structure	4	Abi3; Arpc1b; Dock2; Rhoj
ECM	3	Adamtsl5; Fxyd5; Sh3pxd2b
Protease	7	Ctsb; Ctsc; Ctsd; Ctse; Ctsh; Ctss; Ctsz
Fatty acid biosyntesis	2	Soat1; Anxa3
Golgi function	1	Gltpd1
Immune related	44	Vista; Asb13; Bcl3; C1qa; C1qb; C1qc; C3; C3ar1; C4b; Ccl3; Cd109; Cd180; Cd52; Cd53; Cd63; Cd9; Clec7a; Csk; Cst7; Cxcl13; Cxcl16; Dap; Emr1; Eng; Fcer1g; Fcgr1; Grn; H2-Ab1; Il13ra1; Irf8; Itgax; Itgb2; Ly86; Mpeg1; Osmr; P2ry6; Relt; Tapbp; Tgfb1; Tlr13; Tlr7; Trem2; Tyrobp; Unc93b1
Intracellular trafficking	2	Rab31; Rin2
Metabolism	7	Cyba; Cybb; Dhrs1; Gpt2; Hsd17b11; Man2b1; Nnt
Metal ion homeostasis	4	Crip1; Cybrd1; S100a1; Slc11a1

mRNA degradation	2	Zfp36l2; Apobec1
Neuronal function	3	Nfasc; Rgma; Tmem176b
Other	7	Acy3; Flnc; Gusb; Slc43a3; Smoc1; Tagln2; Plek
Phagocytosis/Lysosomal	11	Cd68; Cyth4; Gns; Hexb; Ifi30; Laptm5; Lipa; Lyz2; Pld4; Plin3; Vps33b
Signal transduction	2	Hvcn1; Kcnab3

Appendix 3

Up-regulated genes of the GSS/101LL cerebellum in group A (figure 6.3)

Function	Count	Gene
Cell adhesion	1	Clmp
Cell structure	3	Ttll3; Mtss1; Rhod
DNA structure, repair and division	1	Cep120
Immune related	3	Darc; Stk10; Rorc
Intracellular trafficking	2	Git2; Pard6g
mRNA degradation	1	Pan2
Neuronal function	6	Hpcal1; Nrg2; Sh3gl2; Syt12; Shank3; Unc5b
other	2	Ece1; Hs3st1
Ubiquitination	1	Rnf123
Protein kinase	1	Ubash3b
Signal transduction	3	Kcnk1; Kcnk3; Spag1
Transcriptional regulation	7	Gabpb2; Kank2; Max; Ppargc1b; Baz2b; Nfia; Phxr4

Publications

Work presented in this thesis is currently being formatted for publication. Other publications to have arisen during the PhD training are shown below:

- McCutcheon S, Langveld J, Tan BC, Gill A, de Wolf C, Martin S, Gonzalez L, **Alibhai J**, Alejo Blanco R, Campbell L, Hunter N, Houston F. *Prion protein-specific antibodies that detect multiple TSE agents with High Sensitivity*. PLoS ONE, 2014. **9**(3): p. e91143.

- Lane F*, **Alibhai J***, Manson J, Gill A. *Mechanisms of cell death in the Transmissible Spongiform Encephalopathies*. Book Chapter in Miscellanea on Encephalopathies. 2012. Eds: Tanasescu R. InTech

- Gill A, Lane F, **Alibhai J**, Manson J, McCutcheon S. *The mechanisms of prion disease*. CAB Reviews: Perspectives in Agriculture, Veterinary Science, Nutrition and Natural Resources, 2011. **6**(55): p. 1-34